Chem Soc Rev

REVIEW ARTICLE

View Article Online
View Journal | View Issue

Cite this: *Chem. Soc. Rev.*, 2025, **54**, 1453

Surface-enhanced Raman spectroscopy: a half-century historical perspective†

Jun Yi, ‡[a] En-Ming You,‡[b] Ren Hu, ‡[a] De-Yin Wu, [a] Guo-Kun Liu, [a] Zhi-Lin Yang, [a] Hua Zhang, [a] Yu Gu,[a] Yao-Hui Wang,[a] Xiang Wang,[a] Hao Ma, [a] Yang Yang, [a] Jun-Yang Liu, [a] Feng Ru Fan, [a] Chao Zhan,[a] Jing-Hua Tian,[a] Yu Qiao, [a] Hailong Wang,[a] Si-Heng Luo,[a] Zhao-Dong Meng,[a] Bing-Wei Mao, [a] Jian-Feng Li, [a] Bin Ren, [a] Javier Aizpurua,[c] Vartkess Ara Apkarian,[d] Philip N. Bartlett, [e] Jeremy Baumberg, [f] Steven E. J. Bell, [g] Alexandre G. Brolo, [hi] Louis E. Brus,[j] Jaebum Choo, [k] Li Cui, [l] Volker Deckert,[mn] Katrin F. Domke,[o] Zhen-Chao Dong, [pq] Sai Duan, [r] Karen Faulds, [s] Renee Frontiera, [t] Naomi Halas, [u] Christy Haynes, [t] Tamitake Itoh, [v] Janina Kneipp, [w] Katrin Kneipp,[w] Eric C. Le Ru,[x] Zhi-Peng Li, [y] Xing Yi Ling, [zaa] Jacek Lipkowski,[ab] Luis M. Liz-Marzán, [acadae] Jwa-Min Nam, [af] Shuming Nie, [ag] Peter Nordlander, [u] Yukihiro Ozaki, [ah] Rajapandiyan Panneerselvam, [ai] Jürgen Popp, [mn] Andrea E. Russell, [e] Sebastian Schlücker, [aj] Yang Tian, [ak] Lianming Tong, [al] Hongxing Xu, [amanao] Yikai Xu, [ap] Liangbao Yang, [aq] Jianlin Yao, [ar] Jin Zhang, [ar] Yang Zhang,[pq] Yao Zhang,[pq] Bing Zhao, [as] Renato Zenobi, [at] George C. Schatz, [au] Duncan Graham [s] and Zhong-Qun Tian *[a]

Surface-enhanced Raman spectroscopy (SERS) has evolved significantly over fifty years into a powerful analytical technique. This review aims to achieve five main goals. (1) Providing a comprehensive history of SERS's discovery, its experimental and theoretical foundations, its connections to advances in nanoscience and plasmonics, and highlighting collective contributions of key pioneers. (2) Classifying four pivotal phases from the view of innovative methodologies in the fifty-year progression: initial development (mid-1970s to mid-1980s), downturn (mid-1980s to mid-1990s), nano-driven transformation (mid-1990s to mid-2010s), and recent boom (mid-2010s onwards). (3) Illuminating the entire journey and framework of SERS and its family members such as tip-enhanced Raman spectroscopy (TERS) and shell-isolated nanoparticle-enhanced Raman spectroscopy (SHINERS) and highlighting the trajectory. (4) Emphasizing the importance of innovative methods to overcome developmental bottlenecks, thereby expanding the material, morphology, and molecule generalities to leverage SERS as a versatile technique for broad applications. (5) Extracting the invaluable spirit of groundbreaking discovery and perseverant innovations from the pioneers and trailblazers. These key inspirations include proactively embracing and leveraging emerging scientific technologies, fostering interdisciplinary cooperation to transform the impossible into reality, and persistently searching to break bottlenecks even during low-tide periods, as luck is what happens when preparation meets opportunity.

Received 10th September 2024

DOI: 10.1039/d4cs00883a

rsc.li/chem-soc-rev

[a] *State Key Laboratory of Physical Chemistry of Solid Surfaces, College of Chemistry and Chemical Engineering, School of Electronic Science and Engineering, College of Environment and Ecology, State Key Laboratory of Marine Environmental Science, Department of Physics, iChEM, IKKEM, Xiamen University, Xiamen 361005, China. E-mail: zqtian@xmu.edu.cn*

[b] *School of Ocean Information Engineering, Fujian Provincial Key Laboratory of Oceanic Information Perception and Intelligent Processing, Jimei University, Xiamen 361021, China*

[c] *Donostia International Physics Center, DIPC, and Ikerbasque, Basque Agency for Research, and University of the Basque Country (UPV/EHU), San Sebastian, Spain*

[d] *Department of Chemistry, University of California Irvine, Irvine, California 92697, USA*

[e] *School of Chemistry and Chemical Engineering, University of Southampton, Highfield, Southampton SO17 1BJ, UK*

[f] *NanoPhotonics Centre, Cavendish Laboratory, Department of Physics, University of Cambridge, JJ Thompson Avenue, Cambridge, UK*

† Electronic supplementary information (ESI) available. See DOI: **https://doi.org/10.1039/d4cs00883a**

‡ These authors contributed equally to this work.

1. Introduction

Half a century ago, in 1974, M. Fleischmann, P. J. Hendra, and A. J. McQuillan of the University of Southampton reported unexpected and high-quality potential-dependent surface Raman spectra from pyridine adsorbed on a silver (Ag) electrode roughened by an electrochemical method.[1] Stunned by the results, R. P. Van Duyne and D. L. Jeanmaire of Northwestern University meticulously reproduced the experiments, and determined that the effective Raman scattering cross-section from adsorbed pyridine was enhanced by 10^5–10^6 times. Their paper was published at the end of 1977 after a multi-year and multiple journal review process, as the so-called surface enhancement effect was initially met with strong skepticism.[2] In the same year, J. A. Creighton and M. G. Albrecht of the University of Kent independently reported a similar result.[3] Following these discoveries, several mechanisms were proposed to explain the abnormally intense Raman scattering on the surface. The widely accepted surface plasmon mechanism was put forward by M. Moskovits of the University of Toronto in 1978.[4] Subsequently, the effect was officially named surface-enhanced Raman scattering (SERS) in 1979 by Van Duyne.[5]

[g] School of Chemistry and Chemical Engineering, Queen's University Belfast, David Keir Building, BT9 5AG Belfast, UK
[h] Department of Chemistry, University of Victoria, Victoria, BC, V8N 4Y3, Canada
[i] Centre for Advanced Materials and Related Technologies (CAMTEC), University of Victoria, Victoria, BC V8P 5C2, Canada
[j] Department of Chemistry, Columbia University, New York, 10027, USA
[k] Department of Chemistry, Chung-Ang University, Seoul 06974, South Korea
[l] Xiamen Key Laboratory of Indoor Air and Health, Key Lab of Urban Environment and Health, Institute of Urban Environment, Chinese Academy of Sciences, Xiamen 361021, China
[m] Leibniz Institute of Photonic Technology, Albert-Einstein-Str. 9, 07745 Jena, Germany
[n] Institute of Physical Chemistry and Abbe Center of Photonics, Friedrich Schiller University Jena, Helmholtzweg 4, 07743 Jena, Germany
[o] Faculty of Chemistry, University of Duisburg-Essen, Universitätsstr. 5, 45141 Essen, Germany
[p] Hefei National Research Center for Physical Sciences at the Microscale and Synergetic Innovation Center of Quantum Information and Quantum Physics, School of Physics and Department of Chemical Physics, University of Science and Technology of China, Hefei 230026, China
[q] Hefei National Laboratory, University of Science and Technology of China, Hefei 230088, China
[r] Collaborative Innovation Center of Chemistry for Energy Materials, Shanghai Key Laboratory of Molecular Catalysis and Innovative Materials, MOE Key Laboratory of Computational Physical Sciences, Department of Chemistry, Fudan University, Shanghai 200433, China
[s] Centre for Nanometrology, Department of Pure and Applied Chemistry, Technology and Innovation Centre, University of Strathclyde, Glasgow G1 1RD, UK
[t] Department of Chemistry, University of Minnesota, 207 Pleasant St SE, Minneapolis, Minnesota 55455, USA
[u] Department of Chemistry, Department of Electrical and Computer Engineering, Department of Physics & Astronomy, Department of Materials Science and Nanoengineering, Laboratory for Nanophotonics Rice University, Houston, Texas 77005, USA
[v] Health and Medical Research Institute (HRI), National Institute of Advanced Industrial Science and Technology (AIST), Takamatsu, Kagawa 761-0395, Japan
[w] Department of Chemistry, Humboldt-Universität zu Berlin, Brook-Taylor-Straße 2, 12489 Berlin, Germany
[x] The MacDiarmid Institute for Advanced Materials and Nanotechnology, School of Chemical and Physical Sciences, Victoria University of Wellington, P.O. Box 600, Wellington 6140, New Zealand
[y] Beijing Key Laboratory for Nano-Photonics and Nano-Structure (NPNS), Department of Physics, Capital Normal University, Beijing 100048, China
[z] School of Chemistry, Chemical Engineering and Biotechnology, Nanyang Technological University, 21 Nanyang Link, Singapore, 637371, Singapore
[aa] School of Chemical and Material Engineering, Jiangnan University, Wuxi 214122, China
[ab] Electrochemical Technology Center, Department of Chemistry, University of Guelph, Guelph, Ontario N1G 2W1, Canada
[ac] CIC biomaGUNE, Basque Research and Technology Alliance (BRTA), 20014 Donostia-San Sebastián, Spain
[ad] Ikerbasque, Basque Foundation for Science, 48009 Bilbao, Spain
[ae] Cinbio, University of Vigo, 36310 Vigo, Spain
[af] Department of Chemistry, Seoul National University, Seoul 08826, South Korea
[ag] Department of Bioengineering, Department of Electrical and Computer Engineering, Department of Materials Science and Engineering and Department of Chemistry, University of Illinois at Urbana – Champaign, Champaign, Illinois 61801, USA
[ah] School of Biological and Environmental Sciences, Kwansei Gakuin University, 1 Gakuen-Uegahara, Sanda, Hyogo 669-1330, Japan
[ai] Department of Chemistry, SRM University AP, Amaravati, Andhra Pradesh 522502, India
[aj] Physical Chemistry I, Department of Chemistry, and Center of Nanointegration Duisburg-Essen (CENIDE) & Center of Medical Biotechnology (ZMB), University of Duisburg-Essen (UDE), 45141 Essen, Germany
[ak] Shanghai Key Laboratory of Green Chemistry and Chemical Processes, School of Chemistry and Molecular Engineering, East China Normal University, Dongchuan Road 500, Shanghai 200241, P. R. China
[al] Center for Nanochemistry, Beijing Science and Engineering Center for Nanocarbons, Beijing National Laboratory for Molecular Sciences, College of Chemistry and Molecular Engineering, Peking University, 100871 Beijing, China
[am] School of Physics and Technology and Key Laboratory of Artificial Micro- and Nano-structures of Ministry of Education and School of Microelectronics, Wuhan University, Wuhan 430072, China
[an] Wuhan Institute of Quantum Technology, Wuhan 430206, China
[ao] Henan Academy of Sciences, Zhengzhou 450046, China
[ap] Key Laboratory for Advanced Materials and Feringa Nobel Prize Scientist Joint Research Center, Frontiers Science Center for Materiobiology and Dynamic Chemistry, School of Chemistry and Molecular Engineering, East China University of Science and Technology, 130 Meilong Road, Shanghai 200237, P. R. China
[aq] Anhui Province Key Laboratory of Medical Physics and Technology, Institute of Health and Medical Technology, Hefei Institutes of Physical Science, Chinese Academy of Sciences, Hefei 230031, China
[ar] College of Chemistry, Chemical Engineering and Materials Science, Soochow University, China
[as] State Key Laboratory of Supramolecular Structure and Materials, College of Chemistry, Jilin University, 2699 Qianjin Street, Changchun 130012, P. R. China
[at] Department of Chemistry and Applied Biosciences, ETH Zürich, 8093 Zürich, Switzerland
[au] Department of Chemistry, Northwestern University, Evanston, Illinois 60208-3113, USA

The process of making a groundbreaking discovery by these key pioneers that open a new scientific field was intricate and challenging. It often involved pushing the boundaries of existing beliefs and theories, requiring individuals to think outside the box and challenge conventional understanding. Four critical elements in the process including experiments, new concepts, theoretical explanations, and naming of the observed effect are vital for significant scientific breakthroughs such as SERS, as illustrated in Fig. 1.

1. A new phenomenon is observed in experiments and documented faithfully: by conducting experiments and carefully observing unexpected phenomena, scientists can uncover new information that challenges existing knowledge or reveals previously unknown patterns or behaviors. The experimental observation was the starting point of the discovery journey to SERS.

2. Novel concepts are introduced: once unexpected phenomena are observed, scientists must develop new concepts or ideas to explain these observations. This often involves thinking creatively and outside the box to propose novel theories that can account for observed data.

3. Theoretical models/explanations are developed to support these concepts: after introducing new concepts, scientists must then develop theoretical explanations to support these ideas. This involves creating models, equations, or frameworks that can explain the underlying mechanisms behind the observed phenomena and predict future outcomes.

4. An appropriate name is provided for the observed effect: naming the observed effects is an important step in solidifying scientific discovery and communicating it to the wider scientific community. The name should accurately reflect the nature of the effect and make it easier for other researchers to reference and build upon the discovery.

In the scientific community, every individual who contributes to these key steps plays a vital role. Without the collective efforts of these pioneers, the emergence of new research areas and the expansion of scientific knowledge would not have been possible.

Jun Yi

Jun Yi is an associate professor of Electronic Science and Engineering at Xiamen University. He obtained his BSc in Physics from University of Science and Technology of China in 2012 and completed his PhD in Physical Chemistry from Xiamen University in 2019 under the supervision of Prof. Zhong-Qun Tian. He conducted postdoctoral research at the University of California, Berkeley, with Prof. Xiang Zhang from 2019 to 2021, and joined Xiamen University as a faculty member in 2021. His research focuses on SERS, plasmonics and nano-spectroscopy.

En-Ming You

En-Ming You is an associate professor at the School of Ocean Information Engineering at Jimei University. He earned his BSc in Physics from Nanjing University and obtained his PhD in Physical Chemistry at Xiamen University in 2020, under the supervision of Prof. Zhong-Qun Tian. Following this, he conducted postdoctoral research in Prof. Tian's group. He joined Jimei University in 2023, and his research interests include plasmon-enhanced Raman spectroscopy, plasmon-enhanced infrared spectroscopy, and infrared nanospectroscopy and imaging.

Ren Hu

Ren Hu is a senior engineer of State Key Laboratory of Physical Chemistry of Solid Surfaces, Xiamen University. She obtained her PhD in Physical Chemistry at Xiamen University in 2005. She conducted postdoctoral research in LIA CNRS XiamENS (with Professor Christian Amatore's group at École Normale Supérieure, Paris and Professor Zhong-Qun Tian in Xiamen University). She joined Xiamen University as a senior engineer in 2011. Her current research interest focuses on micro-/nano-electrochemistry and spectroelectrochemistry.

De-Yin Wu

De-Yin Wu received his BSc at Shaanxi's Normal University in 1992 and his PhD in Physical Chemistry at Sichuan University in 1998. Then he worked as a postdoc fellow with Professor Zhong-Qun Tian on theories of SERS. Now he is a full professor of Department of Chemistry, College of Chemistry and Chemical Engineering (2006-), Xiamen University. His research area focuses on theories of surface-enhanced Raman spectroscopy, spectroelectrochemistry and plasmon-mediated chemical reactions. He has published about 250 papers.

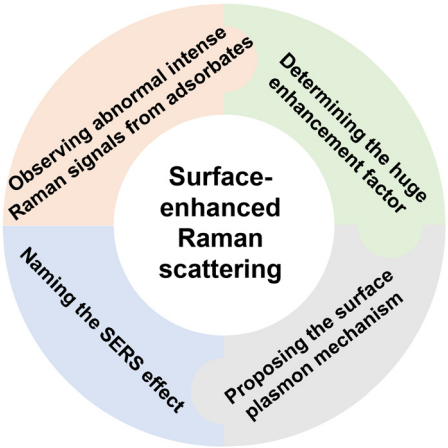

Fig. 1 Four key elements in the process of discovering the surface-enhanced Raman scattering effect.

Similar to that of SERS, the discovery of the Raman effect about a century ago was not accomplished in one stroke. Smekal predicted the inelastic scattering of light after interactions with molecules utilizing classical quantum theory in 1923.[6] However, the experimentalists at that time did not take note of the theory, probably because the concepts of quantum mechanics were not completely understood. In 1928, Raman and Krishnan observed the scattered secondary radiation with degraded frequency in 60 liquids and vapors and later named the inelastic scattering the Raman effect.[7,8] In the same year, Landsberg and Mandelstam accidentally observed a similar effect in quartz and Iceland spar while studying the change of wavelength in scattering based on the Debye's theory of specific heat in solids.[9,10] Generally, the publications by Raman[7] and Landsberg[9] are considered landmarks in the discovery of the Raman effect.[11] The discovery not only promoted the development of quantum theory, but also fostered an important method for qualitative and quantitative chemical analysis. Two years later, Raman was awarded the Nobel Prize in physics for his work on the scattering of light and the discovery of the Raman effect. However, Raman scattering is a weak effect, with a typical cross-section of about 10^6 and 10^{14} times lower than that of the infrared absorption and fluorescence processes, respectively.[12] Since the birth of Raman spectroscopy, detection sensitivity has always been a major challenge hindering the smooth development and broad application of Raman spectroscopy.

Breaking developmental bottlenecks in a scientific field often requires the introduction of new science and technology. In the 1960s, the invention and introduction of lasers had greatly improved sensitivity and expanded applications of Raman spectroscopy. However, it was still extremely difficult to apply Raman spectroscopy in the study of surface science until the discovery of SERS (Fig. 2). The emergence of SERS revolutionized surface spectroscopy and analytical science by eliminating the inherent limitation of low detection sensitivity in surface Raman spectroscopy. Nevertheless, the upsurge following the discovery of SERS was regrettably short-lived. From the mid-1970s to the mid-1980s, SERS could only be realized on roughened substrates and colloids composed of "free-electron-like" metals, mainly Ag, Au and Cu. The lack of substrate and surface generalities severely limited the acceptance of SERS by the community of surface science, electrochemistry, corrosion, catalysis and other industries. Many research groups were gradually exiting the field, causing a low-tide from the mid-1980s to the mid-1990s.

Similar to the reactivation of Raman spectroscopy by SERS, the rapid advancements in nanoscience since the 1990s

Guo-Kun Liu

Guo-Kun Liu is a professor at the College of Environment and Ecology at Xiamen University. He earned his BSc in Chemical Education from Soochow University and obtained his PhD in Physical Chemistry at Xiamen University in 2006, under the supervision of Prof. Zhong-Qun Tian. He conducted postdoctoral research with Prof. Ru-Qin Yu at Hunan University, then Prof. Peng Chen at Cornell University and finally Dr Thomas Moffat at NIST USA. He joined Xiamen University in 2015, and his research interest focuses on various applications of SERS.

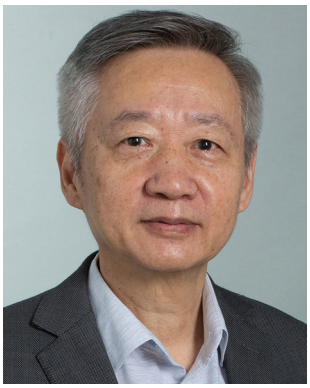

Zhong-Qun Tian

Zhong-Qun Tian received his BSc from Xiamen University in 1982 and completed a PhD in Electrochemical SERS under Prof. Martin Fleischmann (FRS) at the University of Southampton in 1987. He became a full professor at Xiamen University in 1991, and Member of the Chinese Academy of Sciences and Fellow of the Royal Society of Chemistry in 2005. He served as President of the International Society of Electrochemistry (2019–2020), associate editor of Chem. Soc. Rev. (2012–2024), and is on the advisory boards of 16 international journals. He received several scientific awards, including the Raman lifetime award. His research focuses on SERS and SHINERS, spectroelectrochemistry, nanochemistry, plasmonics, and catalytic assembly.

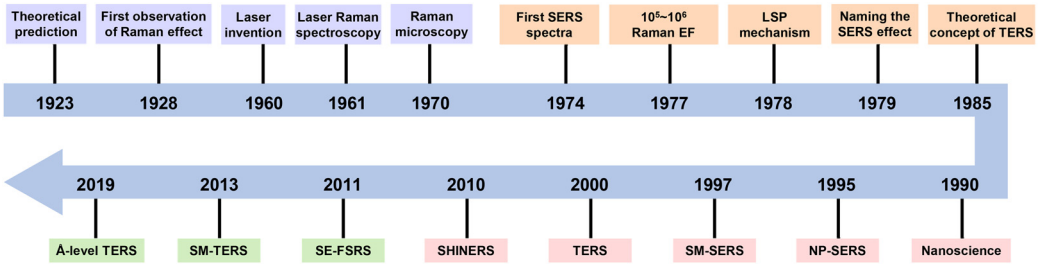

Fig. 2 A timeline of historical advances in Raman effect, SERS, and related revolutionizing science and technologies. The invention and introduction of the lasers in the 1960s expanded the applications of Raman spectroscopy. Advancements in nanoscience in the 1990s boosted the second upsurge of the SERS field. EF: enhancement factor; LSP: localized surface plasmon; NP: nanoparticle; SM: single-molecule; TERS: tip-enhanced Raman spectroscopy; SHINERS, shell-isolated nanoparticle-enhanced Raman spectroscopy; SE-FSRS: surface-enhanced femtosecond stimulated Raman spectroscopy.

provided a boost for SERS, which regained widespread interest in the mid-1990s and thereafter experienced a resurgence until today. In this period, innovative nanomaterial synthesis, nanofabrication and characterization techniques enabled the evolution of SERS substrates from micrometer-scale ill-defined rough electrodes to tens of nanometer-scale well-defined nanoparticles.[13] High-quality SERS spectra from a single molecule adsorbed on Ag and Au nanoparticles had been obtained, marking SERS as one of the most promising tools for single-molecule science and trace analysis.[14,15]

In parallel, the urgent need to develop high-spatial resolution techniques and characterize atomically flat single-crystals in surface science gave rise to two important variants of SERS: tip-enhanced Raman spectroscopy (TERS)[16–19] and shell-isolated nanoparticle-enhanced Raman spectroscopy (SHINERS).[20] Both methods produced intense Raman signals from undisturbed surfaces of general materials, breaking the bottlenecks of surface and material generalities of SERS.[21] Thereafter, the application fields of SERS have been expanded from surface chemistry to material characterization, bioanalysis, drug analysis, food safety, and environmental monitoring, *etc.*,[21–34] which have enormously increased the impact and promise of SERS.

In the past 50 years, SERS has gone through a tortuous path to develop into a powerful diagnostic method. Due to the length of the review, this retrospect describes four important stages of the SERS field from the view of experimental and theoretical methods in the fifty-year progression. First, we recall the history of the birth of SERS and discuss the milestone works in the initial 10 years, *i.e.*, from 1974 to the ~mid-1980s, during which the main experimental and theoretical foundations of SERS were established. Then we discuss the low-tide period (mid-1980s to mid-1990s) and the second upsurge of SERS research profoundly boosted by nanoscience (nano-driven SERS), which laid the key foundation and triggered an exponential increase in interest in the SERS field for the subsequent 2 decades. We conclude by presenting the notable methods of recent decades, which have significantly pushed the boundaries in terms of detection sensitivity and spatial resolution of SERS, TERS, and SHINERS.

We believe that a deep analysis of the discovery and breakthroughs of SERS highlights the invaluable spirit of groundbreaking innovation and perseverance demonstrated by the pioneers and trailblazers over the past 50 years. The lessons contemporary researchers can draw from this history are rich and profound: they involve not blindly believing in authority but being willing to challenge established knowledge to break developmental bottlenecks; proactively embracing and leveraging emerging scientific technologies to lead to revolutionary advancements; encouraging interdisciplinary cooperation to transform the seemingly impossible into reality; and bravely recognizing that great discoveries and observations are often achieved even with incomplete or incorrect explanations.

There have been over 800 reviews and books on SERS from different perspectives, so it is impossible for us to comprehensively present the whole story of the birth and advancement of SERS in all its details. Instead, we focus on innovative experimental and theoretical methods, as they form the core of this new field and continuously break developmental bottlenecks. We hope this review serves as a treasured reminder of the importance of innovation, perseverance, and collaboration in any scientific research, offering invaluable insights and inspiration for future generations of researchers.

2. The foundation of surface-enhanced Raman spectroscopy (mid-1970s–mid-1980s)

SERS has become one of the most important branches of Raman spectroscopy and vibrational spectroscopy in the past two decades, providing "molecular fingerprint" information with exceptionally high sensitivity.[35] It greatly transformed the capabilities and applications of Raman spectroscopy. Thus, we briefly recall the early days of the Raman effect before reviewing the discovery of SERS, drawing inspiration by comparing the discovery history of these great scientific fields.

2.1 Theoretical prediction and experimental discovery of the Raman effect

About a century ago, the Austrian physicist A. G. Smekal, whose scientific interests were focused on applying new quantum theories to different areas of physics, theoretically predicted the inelastic scattering of light from gases, liquids, or solids at

wavelengths different from those of the usual monochromatic incident radiation. Smekal utilized the classical quantum theory, by which he assumed that light had a quantum structure and showed that scattered monochromatic light would consist of its original wavelength as well as higher and lower wavelengths. The related paper was subsequently published in a German-language journal in 1923.[6] The key equations are shown as followed,

$$h\upsilon + \frac{Mv^2}{2} + E_m = \frac{Mv'^2}{2} + E_n \quad (E_n > E_m) \tag{1}$$

$$\frac{Mv^2}{2} + E_m = \frac{Mv'^2}{2} + E_n + h\upsilon' \quad (E_n < E_m) \tag{2}$$

where h is the Planck constant, υ is the frequency of the monochromatic radiation, M is the mass of the atom or the molecule, v and v' are the velocities of the atom or the molecule before and after the interaction with the incident radiation. E_m and E_n are the energies of every atom or molecule that is in their mth or nth quantum state with the energy E_m and E_n.

Five years later, the phenomenon was first discovered experimentally by the Indian scientist C. V. Raman. In the paper published in the *Indian J. Phys.*, Raman described the experimental phenomenon of scattered secondary radiation and gave spectroscopic evidences.[8] The paper was delivered on March 16, 1928, and published on March 31, 1928. Meanwhile, Raman and Krishnan's article "A New type of secondary radiation", published in *Nature*,[7] reported the observation of frequency-varying secondary scattering radiation in 60 solutions and vapors. The work was sent out on February 16, 1928, and published on March 31. They pointed out that the scattered light was polarized and of great intensity to rule out the possibility of fluorescence. The effect was then named after Raman as the Raman effect, which was also known as the Smekal-Raman effect in some German-speaking districts.[36]

Almost at the same time, the former Soviet Union (now Russian) scientists G. S. Landsberg and L. I. Mandelstam, accidentally observed the similar effect in quartz and Iceland spars while studying the Brillouin scattering in solids.[9] The work was first published in the French-language journal *Comptes Rendus* on July 9, 1928,[10] and then in the German-language journal *Die Naturwissenschaften* four days later,[9] which were the earliest articles reporting Raman effects in solids. In some reviews,[11] these two pieces of work by Raman and Landsberg are considered as the landmark of the discovery of the Raman effect. The discovery of the Raman effect had far-reaching consequences for scientific research in physics and chemistry. Two years after the experimental discovery, C. V. Raman was awarded the 1930 Nobel Prize in Physics "*for his work on the scattering of light and for the discovery of the effect named after him.*"

Anything that is strong and excellent often also has its weaknesses and less favorable aspects. Raman scattering, classified as a two-photon process, exhibits a scattering cross-section for molecules that is approximately 10^6 to 10^{14} times smaller than that associated with infrared and fluorescence processes,[35] respectively. As a result, Raman spectroscopy is fundamentally limited by its low detection sensitivity.

In the early experiments, scientists used filtered sunlight or mercury lamps as the light source and the eye or photographic film as the detector, with very long exposure times, often up to several days. Because of the very low intensity of the Raman scattering signals and the lack of monochromatic and high-brightness light sources, the efficiency of the technique remained quite low until the 1960s. The invention of laser in 1960 and its rapid introduction to Raman spectroscopy therefore really revolutionized the field. The first laser-based Raman scattering experiment was realized in 1962.[37] Thereafter, Raman spectroscopy became a more versatile technique that utilizes lasers ranging from ultraviolet (UV) to near-infrared (IR) to analyze samples at the molecular level. This flexibility allows for the examination of various materials, including lunar rocks, ocean ore, silicon chips, plastic, proteins, and drugs.[38–43]

2.2 Why was surface Raman spectroscopic research initiated in the 1970s?

In the 1970s, two of the main challenges for Raman spectroscopy were its potential application in surface science and trace analysis. They involved studying a much smaller number of probe molecules compared to the bulk materials or solutions typically used in Raman measurements. For instance, even if a flat surface was fully covered with sample molecules like pyridine, there would only be between 10^{11} and 10^{13} molecules within the 1 mm diameter of the laser spot. This was the typical illuminated area before the widespread use of the confocal microscope in the mid-1990s. Given that usually one Raman photon is produced by approximately 10^6–10^9 incident photons for the surface adsorbates of with monolayer coverage,[12] it remained difficult to detect it using even the most advanced Raman instruments available at that time. Moreover, increasing the power of the laser cannot be of great help because it will ultimately damage the probed sample. Increasing the sample concentration is a common way to enhance the intensity, which proved effective for studying bulk signals in liquid phases and transparent samples. However, this approach had limitations when it came to surface adsorption, where only one monolayer of molecules is typically present. At this concentration level, the signals for most adsorbates without a resonance Raman effect fell below the detection limit. Consequently, due to the inherent weakness of the scattering mechanism, Raman spectroscopy was rarely used for characterizing surface species, with only a few papers addressing highly powdered oxide catalysts (which have surface areas many orders of magnitude larger than those of flat surface samples) before the mid-1970s.[44–46]

Nevertheless, Raman spectroscopy held great appeal for surface scientists as it had the potential to provide valuable insights into various chemical, physical, and biological surfaces and interfaces at the molecular level.[35] It could determine surface bonding, molecular conformation, and adsorption orientation. Additionally, Raman spectroscopy could be employed for *in situ* investigations of various interfaces, including but not limited to solid–liquid, solid–gas, and solid–solid

interfaces. It is particularly useful in scenarios where many other surface techniques are not applicable. These significant advantages strongly motivated some researchers to challenge established knowledge and explore ways to enhance the applicability of Raman spectroscopy in surface science and related analytical fields, ultimately leading to the birth of surface-enhanced Raman spectroscopy (SERS).[21]

2.3 Why was the birth of SERS rooted in an electrochemical system?

Between the mid-1960s and 1970s, electrochemistry was undergoing a significant transition from a macroscopic to a microscopic level. During this period, spectro-electrochemistry emerged to provide mechanistic and dynamic insights into electrochemical interfaces at a molecular level.[47–52] Several leading electrochemists seized the opportunity provided by the rapid development of spectroscopy at that time, introducing several optical spectroscopy techniques to electrochemical systems in sequence, including ellipsometry, UV-vis absorption spectroscopy, and IR spectroscopy.[52] The university of Southampton was one of the leading institutes of spectro-electrochemistry. Nevertheless, Raman spectroscopy appeared to be the most promising optical techniques for analyzing the chemical structure of species on the most commonly used metal electrode surfaces,[48] given that the widely used aqueous solutions in electrochemistry do not significantly interfere with the surface signal compared to IR spectroscopy.[51]

However, initiating interdisciplinary collaboration between Raman spectroscopy and electrochemistry was challenging. The primary obstacle was designing an electrochemical cell that could effectively measure both Raman scattering signals and electrochemical signals simultaneously and efficiently. A significant challenge was the Raman process's inherent low detection sensitivity. In an electrochemical cell, the deflection of the optical path by the liquid phase further reduced Raman spectroscopy's detection efficiency. These issues made electrochemical Raman experiments impractical and unfeasible. It took the bravery of a small group with diverse expertise in electrochemistry and Raman spectroscopy. Their expert cross-disciplinary cooperation, courageous efforts, and methodological advancements ultimately transformed what was once considered impossible into reality.

Fleischmann, a very creative scientist in electrochemistry in the 1970s, played a key role in establishing electrochemical Raman spectroscopy. According to the formula for Raman intensity in textbooks, it was not possible to detect a surface adsorbate with monolayer coverage even with state-of-the-art Raman instruments. However, he was highly eager to break through this limitation by developing a new method that utilizes Raman spectroscopy to measure the signals of molecules that are adsorbed on electrode surfaces. However, bravery alone is not sufficient to achieve breakthroughs in science; rational design, a detailed scientific plan, and finding the best collaborators are also essential. Encouraged by Graham Hills, the Chair of Physical Chemistry at the University of Southampton, Fleischmann initiated a successful collaboration with Hendra, an expert in Raman spectroscopy who had pioneered the study of adsorption on oxide powder catalysts with much larger surface areas than electrodes, and with McQuillan, a young and energetic postdoc.

McQuillan documented the collaboration between the two scientists in his note,[53] "*Both were innovative scientists, enjoyed competing with each other in scientific brainstorming sessions, and were excited by the prospect of audacious experiments.*" Recalling the history, Hendra wrote that[54] "*Back in 1972 we discussed and argued over the possibility of recording Raman spectra from an electrode surface. Problem, of course, is that the amount of material present is minimal. So what system to use?*" "*My ears duly flapped because Calomel (Hg_2Cl_2) is nearly the strongest Raman scatterer known to man (C_{60} is better!), Martin came up with the idea of generating a high area mercury surface – so we were hopefully 'in business'.*" Fleischmann and McQuillan generated a surface coated with micro globular mercury, which increased the surface area to ten times that of a smooth surface. Then they successfully recorded Raman spectra from multiple layers of Hg_2Cl_2, Hg_2Br_2 and HgO on small mercury droplets formed by nucleation onto a platinum disc electrode. This work was reported in early 1973 in a brief paper without figures in *Chemical Communications*.[55] Hg_2Cl_2 has a very strong Hg–Hg stretch Raman signal, but detection limits for Hg_2Cl_2 multilayers were still significantly above the more intriguing monolayer level. Nevertheless, this approach was a logical first step in scientific exploration, particularly in venturing into the unknown. The authors successfully demonstrated that Raman signals could be obtained from their designed electrochemical cell.

Encouraged by these results, they continued to advance their methods to achieve detection at the monolayer level. As noted by McQuillan,[53] "*Thus, the focus of work turned to methods of enhancing the Raman signal. The possibilities of using phase-sensitive detection, resonance Raman, and large-surface-area electrodes were considered. As Pat had pioneered the use of Raman to study species adsorbed on large-area oxide catalysts, so large surface area became the favoured direction.*" The collaboration between the electrochemist and the Raman spectroscopist facilitated the combination of Ag electrodes and pyridine molecules. McQuillan wrote down the words about the choice of pyridine,[53] "*Pyridine had long been used as a probe molecule for infrared spectroscopic studies of acidic sites on metal oxide catalysts and had also found use in corresponding Raman studies that Pat's group had conducted.*" Fleischmann and McQuillan prepared various roughed electrodes by an electrochemical oxidation reduction cycle (ORC) method, as written by Hendra,[56] "*Martin's Group came up with many roughened surfaces – platinum, palladium, iron, lead, you name it – and studied them in electrodes containing good Raman scattering prospects. Among numerous ideas, it was decided to try silver using an electrolyte containing pyridine.*"

2.4 First observation of SERS spectra of molecules adsorbed on electrode

On 15 May 1974, the first potential-dependent surface Raman spectra of pyridine adsorbed on an electrochemically

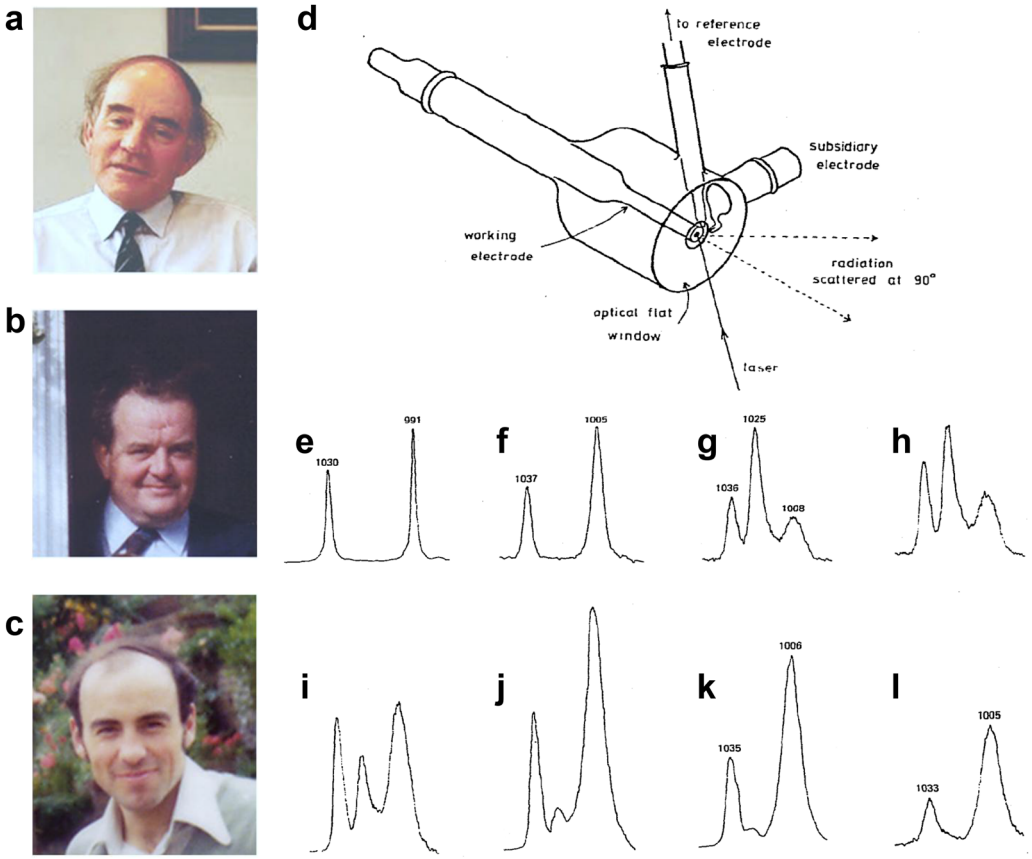

Fig. 3 (a)–(c) Photographs of Martin Fleischmann, Patrick Hendra and Jim McQuillan, respectively. (d) Illustration of the electrochemical cell used for the Raman detection of pyridine adsorbed on Ag electrode. And Raman spectra of pyridine in solution and on the Ag electrode at different potentials: (e) liquid pyridine; (f) 0.05 M aqueous pyridine; (g) Ag electrode 0 V *vs.* saturated calomel electrode (S.C.E.); (h) −0.2 V; (i) −0.4 V; (j) −0.6 V; (k) −0.8 V; (l) −1.0 V. (a)–(c) are reproduced from ref. 56 with permission. Copyright 2016 Royal Society of Chemistry. (d)–(l) are reproduced from ref. 1 with permission. Copyright 1974 Elsevier B.V.

roughened Ag electrode were reported by Fleischmann, Hendra and McQuillan (Fig. 3a–c) in *Chem. Phys. Lett.*, 1974, **26**(2), 163–166.[1] The abstract of the article states that,[1] "*Raman spectroscopy has been employed for the first time to study the role of adsorption at electrodes. It has been possible to distinguish two types of pyridine adsorption at a silver electrode. The variation in intensity and frequency of some of the bands with potential in the region of the point of zero charge has given further evidence as to the structure of the electrical double layer; it is shown that the interaction of adsorbed pyridine and water must be taken into account.*" Ahead of this publication, McQuillan gave a very brief report and presented a single Raman spectrum of pyridine adsorbed at Ag electrode in the Faraday Discussions of the Chemical Society on Intermediates in Electrochemical Reactions at Oxford on 19 September, 1973.[57]

The experiments were conducted in a specially designed electrochemical cell (Fig. 3d), well-matched with the spectrometer.[53] The collecting window for both the incident and scattered light was optically flat, ensuring optimal efficiency. The surface consisted of a Ag rod electrode sheathed in Teflon, which could be easily adjusted in position relative to the window. Additionally, the focused argon ion laser beam could be incident at variable angles. The obtained Raman spectra were of very high quality and clearly indicated the presence of a surface species, as evidenced by the distinctive dependence of spectral features, particularly the relative intensity, on the electrode potential, as shown in Fig. 3g–l.

According to McQuillan's note,[53] "*the first really significant evidence which could well be due to adsorbed pyridine*" ... "*a shoulder about 1008 cm^{-1} under the 1003 cm^{-1} (solution) band.*" ... "*On 4 July I spent a day on the Cary 82 using the 5145 Å laser line looking at Ag deposited onto Pt and included some cyclic voltammetry of system containing pyridine. Once again evidence for adsorbed (?) pyridine as on 22 June ... quite a distinct variation in the size of the adsorbed species peak with potential.*" ... "*Short discussion with Martin about results. Quite enthusiastic.*"

Fleischmann and McQuillan attended the Faraday Discussions on Intermediates in Electrochemical Reactions at Oxford on 19 September 1973. During the discussion session, McQuillan gave a very brief report with a single spectrum about their observations.[57] Then the paper was prepared for publication at the end of 1973, as noted by McQuillan.[53] "..., *and began putting a paper together for Chemical Physics Letters. This was finally sent to David Buckingham on 21 February 1974 after considerable discussion over unresolved aspects, such as the unusually high observed Raman intensities. In the end no comment*

was included on the intensities. The response from David Buckingham less than a week later was to say that the paper had been accepted and that 'you appear to have found an interesting phenomenon'.''

In retrospect, this was indeed the first SERS measurement, and the roughened electrode can be considered the first SERS-active nanostructure (albeit mixed with microstructures), although it was not recognized as such at the time. They initially believed that the electrochemical roughening procedure had significantly increased the electrode's surface area and, consequently, the number of adsorbed molecules. This increase was thought to be responsible for the intense surface Raman signal of pyridine, a molecule with a very large Raman cross-section.

Through persistent and broad searching, logically followed by a focus on the pyridine/Ag system, the high-level collaboration between electrochemists and Raman spectroscopists led to the first Raman measurements of adsorbed molecules on electrode surfaces. This initial experimental observation marked the right entrance door, *i.e.*, the beginning of the discovery journey of SERS.

2.5 First determination of the surface enhanced Raman effect

The deep understanding of the essence of phenomena is crucial for further transforming a preliminary phenomenon observation into a scientific progress and even a new field. The abnormally intense Raman spectra of pyridine adsorbed on a roughened Ag electrode had garnered significant attention from Van Duyne. This was not only due to its capability to measure surface-adsorbed monolayers of molecules, but primarily because their intensities were about a million times stronger than the same species in solution, an astonishing claim first made by Van Duyne when he was a young assistant professor (Fig. 4a).

He described how he was surprised when he first read the paper by Fleischmann *et al.*,[59] *''Imagine my surprise in early May 1974 when I opened the May 4th issue of Chemical Physics Letters and found the report by Fleishmann et al. describing their observation of normal Raman signals from a monolayer of pyridine adsorbed on a roughened silver electrode immersed in a simple aqueous electrolyte solution in an electrochemical cell. I was stunned! They observed count rates of ~500–1000 counts per second using 100 mW of 514.5 nm argon ion laser light.''*

Van Duyne's big surprise stemmed from his own interest in using Raman spectroscopy to study electrochemical systems since 1973.[60] He had estimated that the Raman signals of monolayer molecules adsorbed on surfaces could not be measured using the state-of-art instrument of the time.[59] *''I estimated that for 1 monolayer of a non-resonant adsorbate such as pyridine adsorbed in a vertical orientation on a platinum (111) single crystal and excited with 1 watt of argon ion laser light at 488.0 nm, the total Raman signal for the 991 cm^{-1} fundamental integrated over the vibrational band would be something like 25 counts per second on a (then) state-of-the-art scanning double monochromator with a cooled photomultiplier tube as a detector. I concluded that this experiment was just barely possible and therefore was of limited practicality.''* Subsequently, he just focused on improving the Raman sensitivity by several methods, especially by taking advantages of the resonance Raman effect of dye molecules.[59]

To resolve the confusion in his mind, Van Duyne then visited Fleischmann's laboratory at the University of Southampton after the International Society of Electrochemistry meeting in Brighton, England in September 1974. As written in ref. 59, *''I was very keen to understand how it was possible to observe surface Raman signals from pyridine because I had just calculated how unlikely this experiment was to succeed. I learned from Jim that surface roughness was likely to be the key factor.''*

Although Fleischmann's article attributed the enhancement of the pyridine Raman signal on the surface of rough Ag electrodes to the increased surface area of the rough electrodes, Van Duyne still raised several questions about the renowned electrochemist's interpretation upon his return to Northwestern:[59] *''1. Why was the Raman intensity of 500–1000 counts s^{-1} so high? 2. If the surface area was made ~1000 times greater, should not the double-layer capacitance of the electrode/solution interface*

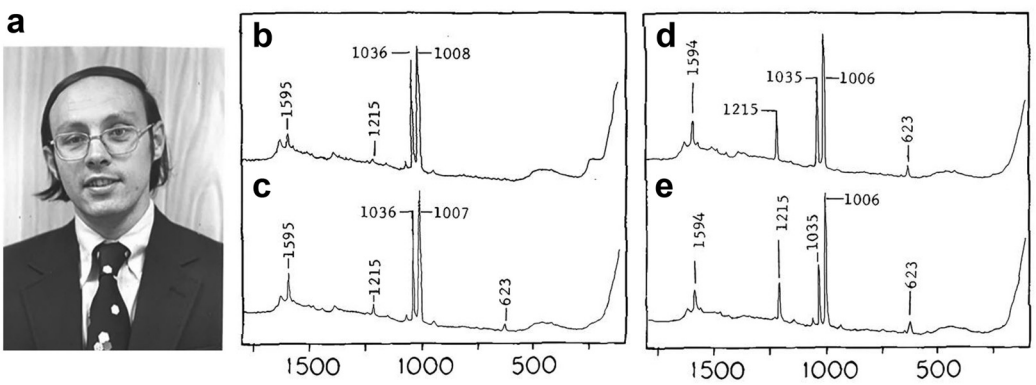

Fig. 4 (a) Photograph of Richard P. Van Duyne. Reproduced from ref. 58 with permission. Copyright 2020 Wiley. (b)–(e) Raman spectra of pyridine adsorbed on a Ag electrode. The solution contained 50 mM pyridine and 0.1 M KCl. Electrode potentials are −0.2 V, −0.4 V, −0.6 V and −0.8 V for (b)–(e). The Raman spectra were enhanced by image processing methods as the original spectra were blurry. Reproduced from ref. 2 with permission. Copyright 1977 Elsevier B.V.

have increased in proportion to the area, yielding a huge, easily measurable value of ~40 000 μF cm^{-2}?''

He persuaded his graduate student David Jeanmaire to check the questions *via* scrutinizing the Fleischmann experiments, and they successfully repeated, and largely extended the experiments over the next two years. As surface roughness was speculated to be a key factor, they started with the surface roughness dependence of Raman intensity and found unexpected results. As written in ref. 59, ''*To test the surface area hypothesis, we repeated the Fleischmann electrochemical roughening procedure and carefully measured pyridine surface Raman intensity vs. the number of coulombs of charge passed. Surprisingly, we found that, starting from roughness conditions used by Fleischmann, the surface Raman signals increased as the surface roughness decreased! Eventually, we found that the 'optimum' level of roughness corresponded to the oxidation and re-reduction of approximately 100 monolayers of silver.*''

The surface roughening procedure for Ag electrodes was modified by using a slightly treated electrode that underwent a few cycles of electrochemical oxidation–reduction. This electrode displayed a yellowish surface and produced Raman signals that were either equivalent to or even stronger than those obtained from deeply roughened Ag electrodes used in the Fleischmann experiments. The latter electrodes, subjected to over a hundred cycles of treatment, exhibited a very dark color. This observation suggests that the unexpectedly intense Raman signals were likely attributed to specific surface properties of the roughened electrode, rather than an increase in surface area.

Chance favors the prepared mind. Utilizing his previous research experience on electrochemical Raman spectroscopy based on the resonance Raman effect, Van Duyne and Jeanmaire calculated the enhancement factor.[59] ''*Subsequently, David and I devised a procedure to measure the surface enhancement factor which compared the signal intensity per molecule on the surface to the signal intensity per molecule for the same molecule in free solution and discovered the 10^5–10^6 enhancement factor associated with SERS.*'' This result led them to propose the surface enhancement effect, as stated in their article published in *J. Electroanal. Chem.*, 1977, **84**(1), 1–20:[2] ''*Given that the experimentally observed intensities of NR scattering from adsorbed pyridine in our laboratory are 5–6 orders of magnitude greater than expected, we felt that some property of the electrode surface or the electrode/solution interface is acting to enhance the effective Raman scattering cross section for these adsorbed amines.*''

They compiled the results and sent it out for publication in 1976. However, their paper underwent a multi-year, multi-journal review process, as the so-called surface enhancement was initially met with strong skepticism. How could the Raman signal from molecules adsorbed on rough metal surfaces be dramatically and substantially increased compared to their solution state? This notion was indeed too surprising and difficult for the scientific community to accept. Their paper was submitted to *J. Electroanal. Chem.* (received 7 October 1976) and accepted on 12 May 1977. Subsequently, the paper was published on November 1977.[2]

Independently, Creighton and Albrecht reported a similar result in *J. Am. Chem. Soc.*, 1977, **99**(15), 5215–5217,[3] which was submitted 6 months later than Van Duyne's. Both papers presented compelling evidence indicating that the enormously intense surface Raman signal is attributable to a true enhancement in the efficiency of Raman scattering itself.[35]

The effect was then designated as surface-enhanced Raman scattering (SERS) in 1979 by Van Duyne.[5] ''*Such enormous enhancements of the normal Raman (NR) scattering process completely overcome the traditional limitation of SRS – its low sensitivity. The experimental context in which surface enhanced Raman scattering (SERS) was first recognized was that of an electrochemical cell.*''

After five decades, it may be essential to draw inspiration by delving deep into the starting point and asking three correlated questions. Why was the discovery of the SERS effect first made in pyridine that was adsorbed on an electrochemically roughened Ag electrode? Why did Van Duyne and other colleagues continue their investigations in the same Ag–pyridine system? More surprisingly, why does the combination of Ag and pyridine, proposed half a century ago, remain one of the best electrochemical SERS systems with the strongest signal among all non-resonance Raman molecules? Nowadays, every newcomer to this electrochemical SERS may be asked to first repeat this model system (but do not blindly follow, be careful about the 1025 cm^{-1} peak, see Section 4.8 for detailed discussions) to ensure the correct experimental procedure.

Upon closer examination, it becomes clear that this was not just a coincidence or a stroke of luck, but a result of a very successful and high-quality collaboration, including mutual brainstorming by experts in different fields: an electrochemist well-versed in electrochemical cells and roughening electrode procedures and a Raman spectroscopist knowledgeable about the instrument and the best probe molecules with large Raman cross sections.

The birth of SERS sparked enthusiastic interests from scientists and engineers, and attracted researchers from various fields such as physics, analytical chemistry, electrochemistry, heterogeneous catalysis, materials science, *etc.* Compared with the exploration on the various materials and feasible systems meeting recurrent obstacles, the advancement of mechanisms was more fruitful in the early days of SERS.

2.6 Foundation of enhancement mechanisms of SERS

From the late 1970s to the mid-1980s, research into theoretical mechanisms saw remarkable growth. Many active groups in physics and physical chemistry were fully captivated by the serendipitous discovery, eager to unravel the mysteries of this new phenomenon. Such was the excitement that some viewed SERS as a divine gift to surface spectroscopy. The field thrived with an abundance of innovative ideas, diverse models, and lively, constructive debates.

2.6.1 Initial understandings of SERS. To explain the abnormal enhancement process observed for pyridine on Ag electrode, Van Duyne and Jeanmaire postulated a static electric field enhancement mechanism based on electrochemical

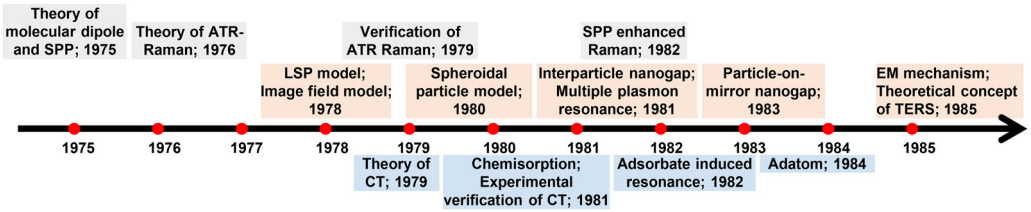

Fig. 5 The timeline of the mechanistic studies on SERS in the first decade. SPP: surface plasmon polariton; ATR: attenuated total reflectance; LSP: localized surface plasmon; EM: electromagnetic; CT: charge transfer.

double-layer.[2] "*Electric field gradients in the vicinity of the electrode can attain values of 10^6 V cm^{-1} which are well within the range needed to observe electric field enhanced scattering.*" Creighton and Albrecht attributed the intensity enhancement to the resonance Raman scattering through the broadening of the electronic energy levels of molecules at roughened metal surfaces.[3] "*It has been suggested by Philpott that broadening of the electronic energy levels of molecules at roughened metal surfaces may induce resonant Raman scattering from molecules adsorbed on metals through interaction with surface plasmons. Resonant Raman enhancements of the order of 10^5 and above are certainly known for some conjugated chromophores, and it may prove that this is the explanation of the intensity enhancement reported here.*"

Meanwhile, as shown in Fig. 5, a number of mechanisms were proposed and developed in the late 1970s and the mid-1980s to account for SERS.[4,61–69] It should be noted that, according to the current understanding, surface plasmons can be categorized into two types: propagating surface plasmon polaritons (SPPs) and localized surface plasmons (LSPs). The "surface plasmons" mentioned in earlier works largely refer to what is now recognized as SPPs.

As we can see, Fleishmann and colleagues observed the first SERS spectrum on a rough Ag electrode, while they misattributed it to an increased surface adsorption area. Van Duyne and Creighton discovered the significant enhancement effect of SERS, nevertheless, their interpretations concerning the origin of this colossal enhancement remained erroneous. In fact, recalling the whole history of modern natural sciences, a common phenomenon is that of "*Great discoveries/observations with incorrect/incomplete explanations*", especially in the early stages of establishing disciplines across many fields. This is because great discoveries are often about making the impossible possible and extending the boundaries of the knowledge, and thus, explanations based on past established knowledge are usually wrong or incomplete. In fact, this phenomenon has been recurring throughout the history of SERS, particularly when significant breakthroughs were achieved. Over the subsequent decades, almost every new milestone in SERS research was followed by a period of confusion and debate as the scientific community grapples with understanding the true implications and underlying mechanisms of the discovery.

2.6.2 Localized surface plasmon resonance mechanism. A localized surface plasmon resonance (LSPR) mechanism based on free-electron like metals was introduced by Moskovits[4] (Fig. 6a) and independently by Creighton[70] (Fig. 7a) *et al.*, both in 1978. Moskovits and Dignam proposed that the optical characteristics of rough metal films could be explained by considering the roughness layer as an effective medium with optical homogeneity in 1973. This concept proved particularly relevant for metals like Cu and Ag, as they exhibited plasmonic resonances.[71] In 1978, Moskovits applied this concept to

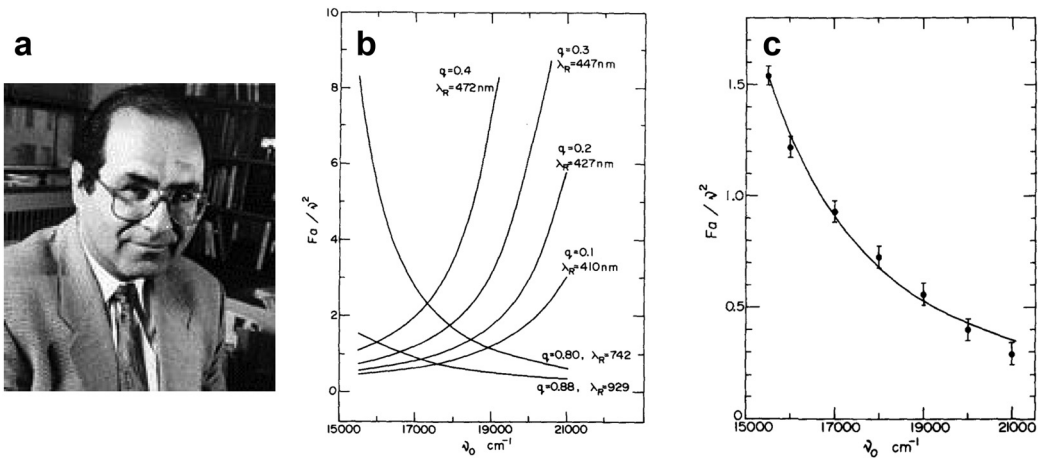

Fig. 6 (a) Photograph of Martin Moskovits. (b) The dependence of the quantity F_a/v^2 on exciting frequency v_0 for various values of λ_R, which is the resonance wavelength. The Raman intensity is proportional to F_a/v^2. q is the volume fraction of the metal within a dielectric of dielectric constant ε_0. The quantity plotted is actually $6.69 \times 10^7 F_a/v^2$. (c) The solid line is the one of λ_R = 929 nm in (b). Points are taken from ref. 72 and refer to the 1008 cm^{-1} ring vibration of pyridine. Reproduced from ref. 4 with permission. Copyright 1978 AIP publishing.

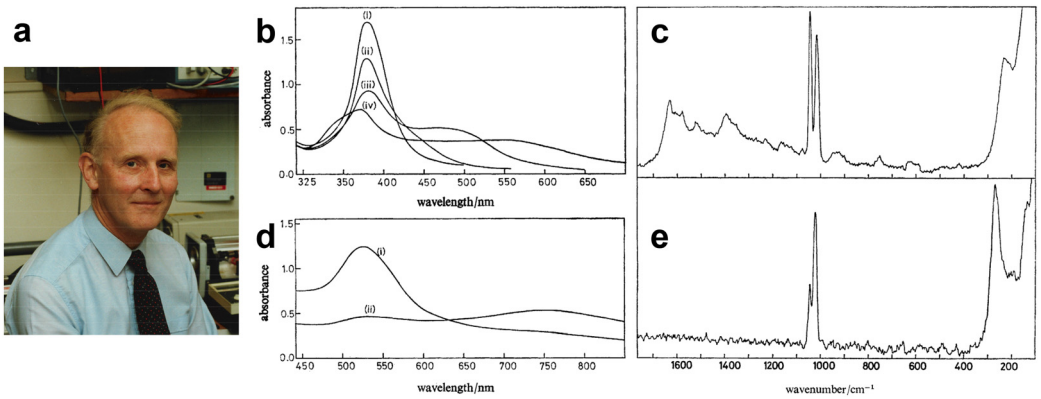

Fig. 7 (a) Photograph of J. Alan Creighton, taken in his laboratory in the early 1980s. (b)–(e) Extinction spectra and Raman spectra of Ag and Au colloids with added pyridine. (b) Extinction spectrum of Ag sol (1.5 cm^3) (i) freshly prepared; (ii) 5 min after adding 0.25 cm^3 0.01 mol dm^{-3} pyridine; (iii) 1 min and (iv) 5 min after adding 0.1 cm^3 10^{-1} mol dm^{-3} pyridine. (c) Raman spectra of Ag sol with added pyridine. (d) Extinction spectrum of Au sol (1.5 cm^3) (i) freshly prepared; (ii) 3 h after adding 0.05 cm^3 0.1 mol dm^{-3} pyridine. (e) Raman spectra of Au sol with added pyridine. Figures are reproduced from ref. 70 with permission. Copyright 1979 Royal Society of Chemistry.

explain the contrasting trends in SERS intensity reported by Van Duyne and Creighton, attributing the discrepancy to the distinct methods employed in roughening the Ag electrodes. As shown in Fig. 6b and written in ref. 4, "*With small values of q, λ_R is at high frequencies and the intensity rises with increasing exciting frequency. This is what Van Duyne reports, and indeed his surface pretreatment is mild, resulting in small q values. For large values of q, λ_R is in the red and the opposite trend is observed, as reported by Creighton et al. Again, their surface treatment is more severe; consequently, q is expected to be large in their case.*" The paper was submitted to *J. Chem. Phys.* on 12th June 1978 and published on 1st November 1978. (*J. Chem. Phys.*, 1978, **69**(9), 4159–4161) As written in the abstract, "*I propose that the anomalous intensity arises from preresonant or resonant excitations of conduction electron resonances in adsorbate covered metal bumps on the surface.*"[4]

Recalling that history, Moskovits wrote that:[73] "*In the spring of 1978 I wrote a paper in which I jotted down my early ideas regarding the relationship between SERS and the excitation of localized surface plasmons (LSPs) in microrough silver. Focusing on the original reports on SERS from electrochemically roughened silver, I suggested that the submicroscopic silver roughness features (nano-features in today's idiom) were subwavelength and sustained plasmons, and it was the plasmon resonance that was responsible for the enhancement.*"

Based on the mechanism, Moskovits also proposed several forecasts including that similar enhancements would be observed in Ag and Cu colloids covered with adsorbates, as described in his Note published in 2012:[73] "*I also made several predictions: (i) that intense SERS would be observed primarily with nanostructured systems composed of the coinage metals (and the alkalis) because only nanoparticles of those metals would possess the high-Q LSP resonances required for large enhancement; (ii) that subwavelength nanostructure was an essential ingredient for observing SERS; and (iii) that true colloids of those metals should also produce SERS.*"

At about the same time, in March 1978, and unaware of Moskovits' predictions, Creighton *et al.* for the first time demonstrated SERS from Ag and Au colloids experimentally (Fig. 7a). This pioneering experimental work was submitted to *J. Chem. Soc.* on 19th July 1978 and published in 1979. (*J. Chem. Soc., Faraday Trans., 2*, 1979, **75**, 790–798).[70] Their work on this began with the synthesis of Ag and Au colloids. In his Note published on 2009,[74] he recalled that: "*Working together one afternoon, having done no previous literature work on metal colloids, we tried adding a solution of sodium borohydride, the only reducing agent that happened to be on our reagent shelves, to a silver nitrate solution. We found that provided that the silver nitrate solution was sufficiently dilute (less than about 10^{-3} mol dm^{-3}) this gave a beautifully clear yellow silver colloid. When we then added pyridine to this yellow colloid (to a concentration of about 10^{-2} mol dm^{-3}, the same concentration as in the pyridine silver electrode experiments) the colour slowly changed through various greenish shades, finally becoming blue-grey before silver was deposited as a black precipitate. A similar procedure using $Na[AuCl_4]$ in place of $AgNO_3$ gave a wine-red gold colloid that also changed colour gradually when pyridine was added.*"

And then they tried Raman measurements in the colloid system and obtained enhanced Raman signals from pyridine, as shown in Fig. 7b–e.[74] Creighton wrote that:[74] "*We straight away put these pyridine-containing colloids into the Raman spectrometer and observed the same 1008 and 1036 cm^{-1} Raman bands of adsorbed pyridine that we had previously seen from the roughened silver electrodes. Although the bands were not as intense as in the spectra from roughened silver electrodes, it was clear that they were nevertheless considerably enhanced, because with the same spectrometer settings we could scarcely see the ca. 1000 cm^{-1} bands from a pyridine solution of the same concentration in the absence of the colloidal metal particles. The Raman bands were also substantially depolarized, a characteristic of SERS bands, whereas for pyridine in solution the strong bands around 1000 cm^{-1} are very strongly polarized.*"

The first experimental correlation between the optimized excitation wavelength for SERS and the wavelength of the surface plasmon resonance (SPR) was also reported in the same paper,[70] and it was from this correlation that it was independently proposed that plasmon resonances in metal nanoparticles or roughened electrodes are responsible for SERS. ''*During that most productive weekend, the moment when we realized that the SERS excitation profiles were sharply peaked and that the SERS excitation profile maximum was tracking the absorption maximum as the colloid slowly changed colour was the most exciting research moment I can recall.*''

Moskovits and Creighton's pioneering works extended the concept of SERS active substrates from roughened electrodes or island films to metal colloid systems. Colloidal substrates offered several advantages over electrodes: they were easy to prepare, and their particle size, shape, and aggregation could be adjusted during preparation. Although it was very challenging to control and characterize them during that time, this variability allowed for the exploration of the relationship between surface morphology and SERS enhancement. Also, at that time there was already a good theoretical understanding of elastic light scattering by colloidal dispersions, and the introduction of colloidal SERS substrates therefore quickly stimulated theoretical work on the SERS of metallic nanoparticles. It's worthy to note that their pioneering works in colloidal SERS[4,70] also inferred the close relationship between SERS and nanoscience, heralding its second upsurge in the era of nanoscience.

2.6.3 Other contributions to electromagnetic mechanisms. The foundation of EM mechanism also laid on the contributions by Schatz,[67,75,76] Metiu,[65,77,78] Kerker,[64,79,80] Gersten and Nitzan,[81] Weber and Ford,[82] and McCall[83,84] and their coworkers. An image field model, initially proposed by King, Van Duyne, and Schatz (also named as the KVS model) in 1978,[85] then independently by Efrima and Metiu in 1979,[86–88] suggesting that the considerable enhancement observed may be linked to the substantial polarizability that emerges for specific parameter selections when the Raman-emitting system is viewed as a composite of the molecule and its reflected charge distribution in the metal. This model, recognized as the ''image field model'', was further refined by Weber and Ford in 1980,[82] who improved the model by removing the local assumption and introducing a spherical representation for the adsorbed molecule, thereby removing the limitation to a point dipole. The image field model predicts a Raman enhancement factor (EF) of 16 for perfect conductors;[86–88] however, calculations conducted with real metals, as indicated by Moskovits in 1982,[89] suggest that a factor of 5 or 6 may be a more reasonable approximation. While the image field theory was not considered the primary electromagnetic mechanism for SERS, it holds historical significance as the first comprehensive model to include the intricate interactions between molecules and electrodes, which laid the groundwork for understanding the complex interplay at the molecular–electrode interface.

Kerker and coworkers employed a molecular dipole and spherical nanoparticle mutual polarization model (Fig. 8a and b),[80,90] and comprehensively calculated the influence of particle size, molecular dipole location, and incident light wavelength on the SERS EF. It is noteworthy that Kerker simplified the geometry to a sphere, thus the results were analytically solved with high accuracy by deriving the Lorenz–Mie theory.

Gersten and Nitzan simplified the metallic rough surface as hemispheroid protruding from a conducting plane, and employed a molecular induced dipole model to investigate the mirror field effect of molecular dipoles on the semi-ellipsoid (Fig. 8c and d).[81] They revealed that in addition to the excitation of surface plasmons, the image dipole enhancement effect as well as the ''lightning rod'' effect at the tip of the ellipsoid also contributes to the Raman enhancement.[77,81] McCall *et al.* developed a spheroidal model of the rough metallic surface and revealed the EM interactions between spheroidal metals and molecular dipoles.[84] It is worth noting that Gersten and Nitzan, along with Kerker independently, were the first show *via* calculations that the SERS enhancement is proportional to the fourth power of the local electromagnetic field.

Subsequently, Metiu and coworkers were the first to study the electromagnetic (EM) coupling of a nanosphere dimer[77] (Fig. 9a). The electromagnetic interaction between the two spheres significantly amplifies the local field in the space between them (Fig. 9b). Later on, the calculation based on electrostatic field theory for nanosphere-on-plane coupled structure[78] demonstrated the production of very large local enhancements of the electric fields exceeding those obtained from the isolated sphere or isolated flat surface (Fig. 9c–e). The importance of colloidal dimers was not fully recognized until the discovery of single-molecule SERS.[14,15] And the nanoparticles on mirror configuration set the early theoretical foundation of TERS and SHINERS. Laor and Schatz examined clusters of metal hemispheroids on a perfectly conducting flat surface and found significant SERS enhancement arising from the electromagnetic coupling between the random distributed metal hemispheroids, which was termed as the multiple plasmon resonance effect.[75,76]

2.6.4 Surface plasmon polariton mechanism. Another analytically solvable model used in that period involved SPP excitation at a flat metallic surface. Though a SPP can confine the local optical field at metal/dielectric interfaces, it should be noted that the Raman enhancement generated by exciting SPP is only 10–100 times, which is much lower than the enhancement of over 10^6 generated by exciting LSP. SPP at the metal/dielectric interface can be excited through prism coupling (attenuated total reflection, ATR) at an optimized incident angle. The seminal work on the Kretschmann–Raether (Fig. 10a) and Otto configurations (Fig. 10b) for optically exciting propagating surface plasmons at metal/air interfaces was published in 1968.[91,92] The Kretschmann–Raether configuration is comparatively straightforward, yet it is limited to measuring signals exclusively on the surface of metal thin films. In contrast, the Otto configuration demands more stringent structural requirements for measurement but enables the detection of signals on bulk single-crystal surfaces.

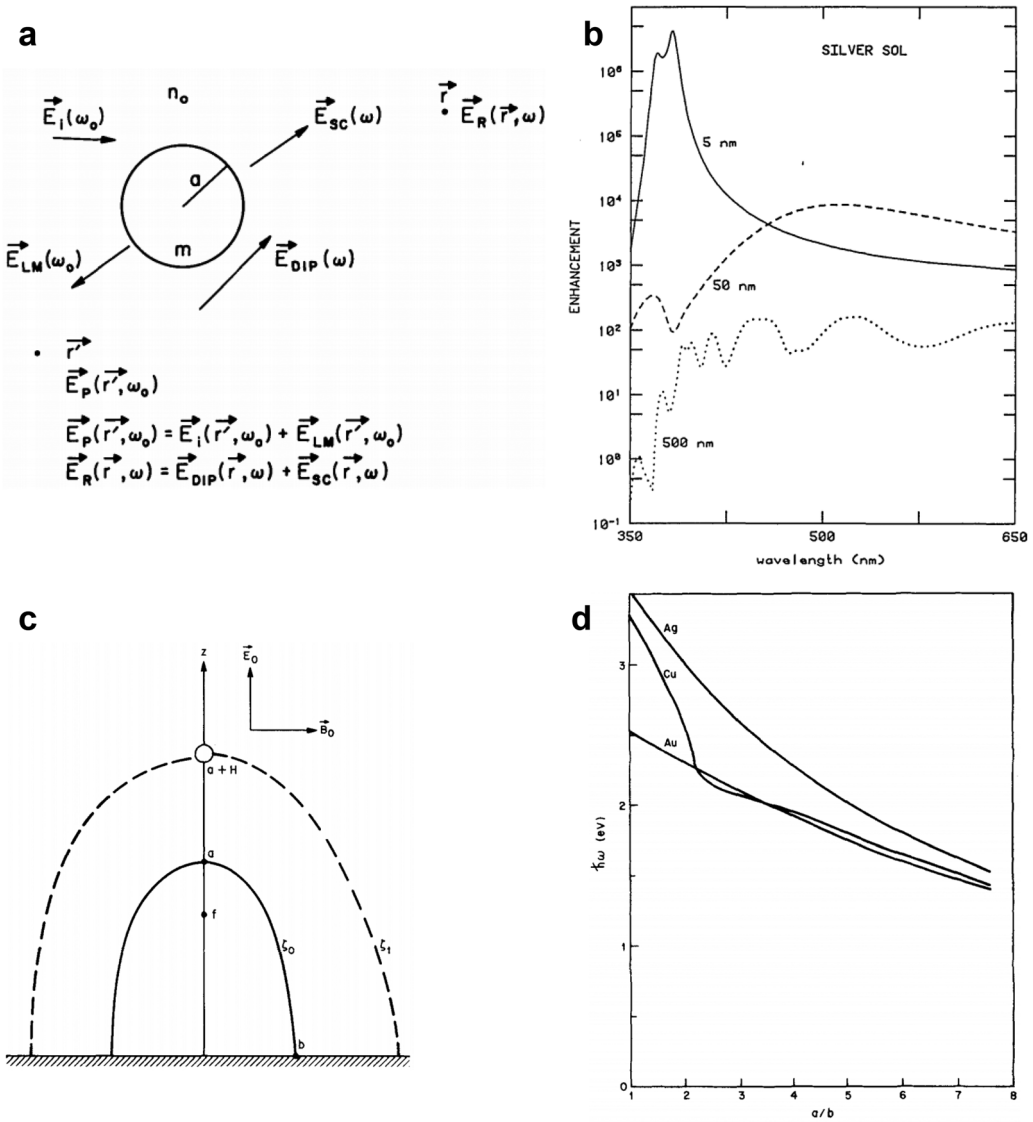

Fig. 8 (a) Schematic view of electric fields near sphere of radius a and refractive index m. At the incident frequency ω_0 there are the incident, Lorenz–Mie, and primary fields, $E_i(\omega_0)$, $E_{LM}(\omega_0)$, and $E_p(r, \omega_0)$. At the shifted frequency ω there are the dipole, scattered, and Raman fields, $E_{DIP}(\omega)$, $E_{sc}(\omega)$, and $E_R(r, \omega)$, where r' and r are the positions of the dipole and observer, respectively. (b) Calculated enhancement for a 1010 cm^{-1} Raman band of molecules that are adsorbed on Ag spheres of radii 5, 50, and 500 nm. Reproduced from ref. 80 with permission. Copyright 1980 Optica publishing. (c) Geometry of surface protrusion. The semimajor axis is a and the semi minor axis is b. The spheroid surface is $\xi = \xi_0$ and that passing through the molecule is $\xi = \xi_1$. (d) Energy of surface plasmons for Ag, Cu, and Au as a function of the aspect ratio of the spheroid. Reproduced from ref. 81 with permission. Copyright 1980 AIP publishing.

Burstein and coworkers theoretically predicted a substantial hundred-fold enhancement for ATR-Raman and ATR-coherent anti-Stokes Raman spectroscopy (CARS) in 1976.[95] Building on this theoretical framework, Pettinger *et al.* experimentally demonstrated the excitation of surface plasmons at Ag electrodes through ATR[94] in 1979 (Fig. 10c), resulting in an enhanced Raman signal from adsorbed pyridine (Fig. 10d). Subsequent research underscored the significant influence of excitation frequency and incident light angle on surface Raman intensity for roughened Au, Ag, and Cu electrodes.[96] Subsequently, Dornhaus *et al.* performed a comparative investigation of attenuated total reflection Raman spectroscopy (ATR-Raman) using hemicylindrical prisms coated with silver films, alongside surface Raman spectra obtained from silver islands. Their findings highlighted the pivotal role of surface plasmon excitation in SERS in 1980.[97] Furthermore, in 1982, Shen and coworkers investigated SERS of pyridine adsorbed onto weakly roughened Ag films using a well-characterized SPP excitation.[98] They demonstrated that the SPP was the primary contributing factor contributing to the additional enhancement in the Raman signal.

Smooth metal films can also be excited by metallic gratings or molecular dipoles to generate surface plasmons. In 1975, Philpott investigated the interaction of excited molecules with

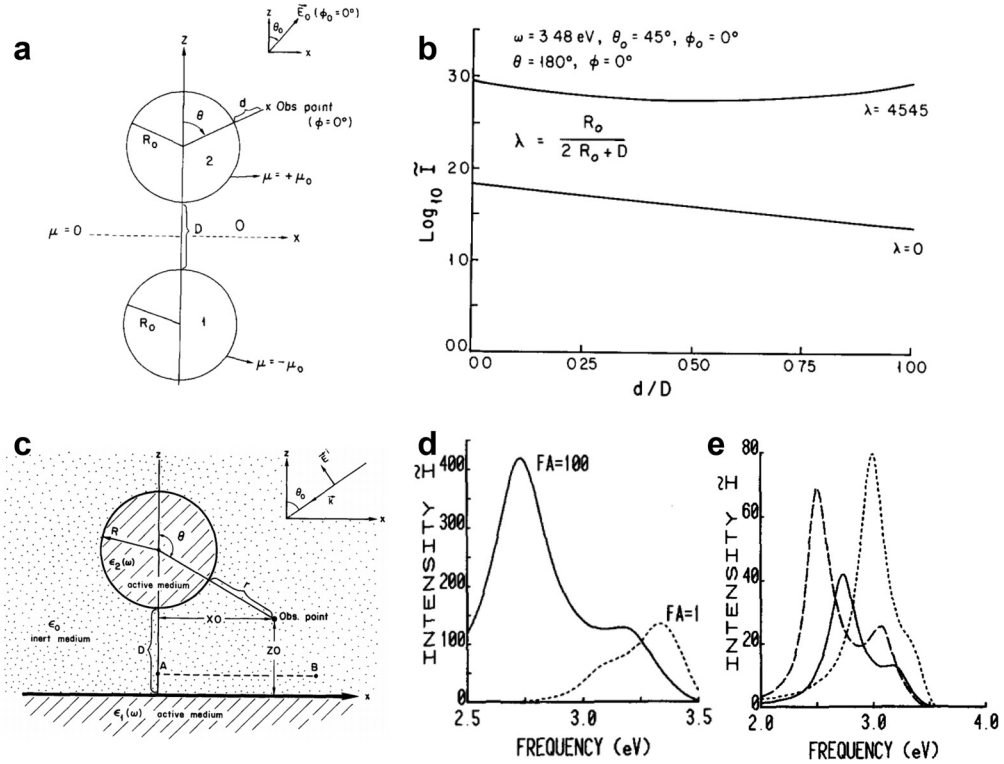

Fig. 9 (a) Schematic of the 2-sphere system. Shown here are the relative positions of the two spheres, the orientation of the external field E_0 and the observation point at which the field enhancement is calculated. (b) The upper curve is for the 2-sphere system $\lambda = 0.4545$, is a plot of I (on a log scale) *versus* distance d/D as one proceeds from the surface of one sphere to the other along their common axis. The lower curve is for the isolated sphere $\lambda = 0$ and the abscissa for this case should be read $5d/R_0$ rather than d/D as shown. The external frequency $\omega = 3.48$ eV is the resonance of the isolated sphere. Reproduced from ref. 77 with permission. Copyright 1981 Elsevier. (c) Schematic of the particle on substrate system. (d) Resonance spectrum of the Ag–Ag system (*i.e.,* Ag substrate with Ag sphere on top) with parameters $R = 10$ nm, $D = 0.5$ nm. The intensity enhancement ratio I is plotted as a function of the incident laser frequency in eV. The laser beam is incident at an angle of 45°. The solid curve is for p-polarized incident light and the dotted curve for s-polarized light. The value of FA indicated for each curve is the factor by which the vertical axis must be multiplied to obtain the value of I for that curve. (e) The variation of the resonance frequencies with system geometry (λ) for the Ag–Ag system. Dashed curve: $\lambda = 0.03$, FA = 2000; solid curve: $\lambda = 0.05$, FA = 1000; dotted curve: $\lambda = 0.1$, FA = 100. In each case the light beam is incident at 45° and is p-polarized. Reproduced from ref. 78 with permission. Copyright 1983 Elsevier.

the surface plasmon of metallic film and developed a theoretical framework for explaining the effect of surface plasmons on molecular electronic transition.[99] Tsang *et al.* and Girlando *et al.* reported the Raman spectra enhanced by the SPP on a Ag grating in 1979[100] and 1980.[101,102] The EF provided by surface plasmons is quite limited compared to the LSP mechanism, primarily due to the minor electric field enhancement of SPP.

2.6.5 Theoretical concept of TERS based on the EM mechanism. Although SERS allowed for the measurement of adsorbed species, its spatial resolution was previously limited by the diffraction limit. In 1985, John Wessel introduced the concept of an optical probe capable of achieving spatial resolution beyond the diffraction limits. This approach utilized optical field confinement through surface plasmons generated by a submicrometer-sized metallic particle, with projections indicating the potential for spatial resolution nearing 1 nanometer.[103] By studying the excitation of LSP, Wessel suggested that the probe particle/tip could provide both enhanced electric fields and spatial confinement, as shown in Fig. 11a. An improved optical spatial resolution was predicted through calculation using an electrostatic model (Fig. 11b). Through theoretical calculations, Wessel predicted a high level of detection sensitivity through this approach.[103] "*Detection sensitivity approaching one molecule is projected.*" The technique proposed in this work is now widely known as TERS. The research laid the theoretical foundation for the development of TERS,[16–19] and several predictions made in the article were confirmed in subsequent experiments two or three decades later.[104]

2.6.6 The chemical enhancement mechanism. When considering the scientific concept of surface enhancement in a rigorous and comprehensive manner, it must encompass any molecule–surface system where the signal enhancement of molecules on the surface (referred to as the surface state) occurs compared to their behavior in liquid or gas states.

The electromagnetic mechanism, represented by the LSPR, contributes dominantly to the anomalous enhancement in SERS, which constitutes a distinctive feature of SERS distinguishing it unambiguously from the previous surface Raman spectroscopy and the surface resonance Raman spectroscopy. The surface plasmon enhancement mechanism, however, fails to account for modifications such as shifts in peak positions or changes in relative intensities in the SERS spectrum.

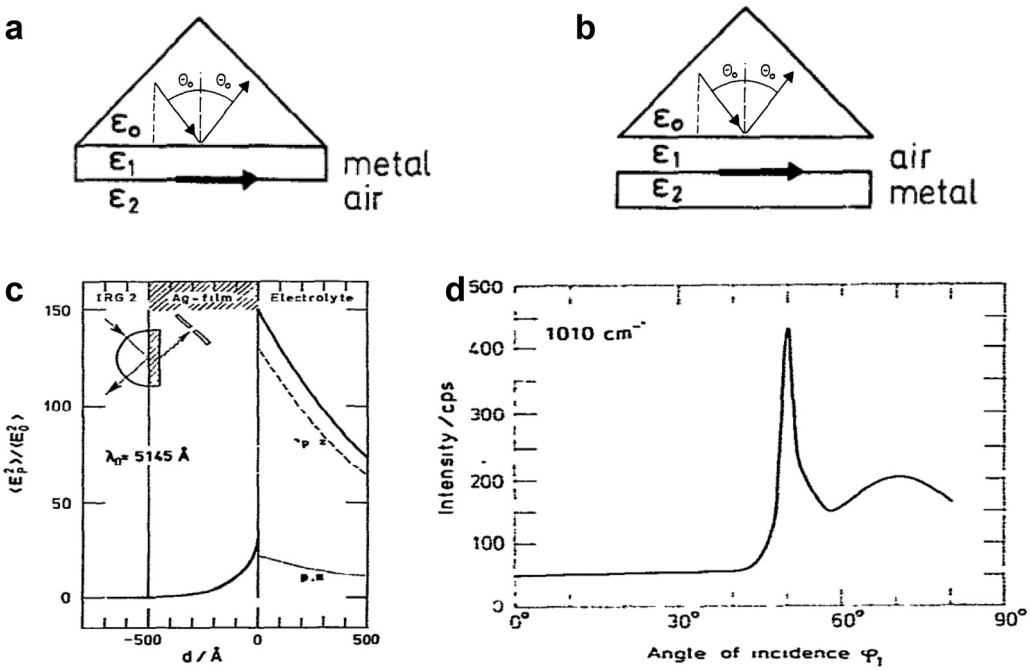

Fig. 10 (a) and (b) Configuration of the ATR method. (a) The metal contacts the prism and couples the SPPs with the evanescent field of the totally reflected light wave, Kretschmann–Raether configuration. (b) The dielectric (air) lies between the prism and the metal surface, Otto configuration. Reproduced from ref. 93 with permission. Copyright 1988 Springer Nature. (c) Time-averaged and normalized square of the electric field strength as a function of distance d from the electrode–electrolyte interface under surface plasmon resonance conditions. λ_0 = 514.5 nm; φ_1 = 50°; d_{Ag} = 50 nm, n_{hemi} = l.906; n_{H_2O} = 1.336; the components in x- and z-direction of the enhanced field are also shown. The insert shows the geometry for the observation of Raman scattered light. (d) Angle dependence of the Raman intensity at 1010 cm^{-1} from pyridine on Ag electrode with ATR excitation by a Kretschmann configuration. λ_0 = 514.5 nm. Reproduced from ref. 94 with permission. Copyright 1979 Elsevier.

These feature was first observed in Fleischmann's experiment.[1] Subsequently, in 1977, Van Duyne and Jeanmaire[2] documented in detail that the Raman intensities of the adsorbed pyridine are a function of electrode potential with a laser excitation wavelength of 514.5 nm, which presented a resonance shaped profile as shown in Fig. 12a. Since no known molecular transition existed in that spectral region, it was speculated that when considering the molecule and metal system as a whole, the reason for the spectral features was probably due to the surface structure, applied potential as well as charge transfer (CT). Similar potential/photon dependence phenomena of SERS were also observed by Otto,[105–107] Ueba,[108,109] Furtak,[110,111] Lombardi,[112] Weaver[113] and coauthors in pyridine and other SERS molecular probes on Ag electrode systems under different excitation wavelengths of laser, which elicited a surge of studies on chemical enhancement (CE) mechanisms in early years of SERS.[106–109,113–120]

The CE mechanism mainly focused on the increase or change of spectral intensity from chemical active site properties on the surface such as the bonding and molecular adsorption orientation between probe molecules and surfaces. The CE mechanism developed in the early years of SERS centered essentially in the CT resonance Raman enhancement. The CT processes necessitate the association of the CT state between the metal and the molecule. When the CT processes are resonant with the exciting radiation, it resembles an electronic resonance of the normal resonance Raman effect, which could partially explain the observed Raman scattering cross sections on the order of resonance Raman spectra.

In 1979, Gersten, Birke and Lombardi adopted a model involving CT process between adsorbed molecule and Fermi level of metal (Fig. 12b) and proposed a theory predicting that the CT between surface molecule and metal would induce a resonance in the vicinity of Fermi surface and lead to an enhancement of Raman scattering.[115] Lombardi and coauthors in 1986 re-investigated the model (Fig. 12c) and presented a comprehensive development of the CT theory of SERS on the basis of direct CT mechanism.[118] Based on the theory of Tang and Albrecht[121] and the work of Adrian,[120] they incorporated the Herzberg–Teller mixing of zero-order Born–Oppenheimer electronic states by using of vibronic interaction terms in the Hamiltonian. Considering both Franck–Condon and Herzberg–Teller contributions, they predicted the potential dependent Raman intensity profiles that fit very well to the observed intensity *vs.* voltage profile for pyridine adsorbed on a Ag electrode as shown in Fig. 12d, although the surface coverage was not strictly considered.

Aside from the previously studied enhancement by collective (surface plasmon) excitations, Burstein *et al.* in 1979 emphasized the role of electron–hole excitations which, due to their localized nature, coupled strongly with the adsorbed molecules.[114] They further proposed the four types of electron–hole excitations related enhancement mechanisms, including the three-step Frohlich scattering (Fig. 13a-i) and

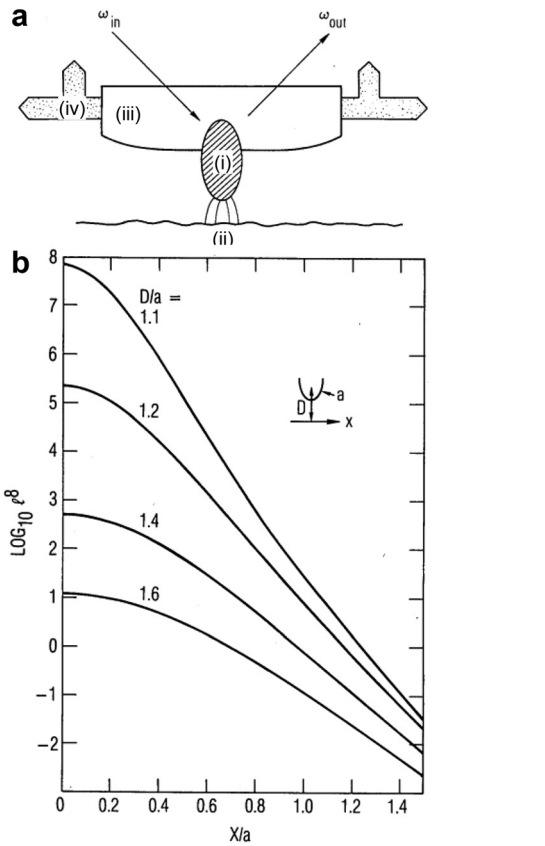

Fig. 11 (a) The optical probe particle (i) intercepts an incident laser beam, of frequency ω_{in}, and concentrates the field in a region adjacent to the sample surface (ii). The Raman signal from the sample surface is reradiated into the scattered field at frequency ω_{out}. The surface is scanned by moving the optically transparent probe-tip holder (iii) by piezoelectric translators (iv). (b) Transverse dependence of coherent Raman enhancement for several values of D/a, where D is the distance from the sample to the center of curvature of the probe tip and a is the radius of curvature at the probe tip. Figures are reproduced from ref. 103 with permission. Copyright 1985 Optica publishing.

the four-step CT mechanism (Fig. 13a-ii).[114] The former energy transfer Frohlich mechanism was developed later by Pettinger.[122] While the latter four-step CT mechanism was integrated to the adatom model proposed by Otto *et al.*[107] Burstein *et al.* in their work[114] depicted a relatively comprehensive physical picture of CE mechanism, despite that the quantitative estimation was not given, since at the time the theory of the radiative excitation of electron–hole pairs was not complete as well as precise information of interface energy level alignment was missing.

In 1981, Persson proposed a model for Raman scattering from molecules chemisorbed on surfaces and found that CT excitations between the Ag and the adsorbed pyridine molecules could produce an EF of up to 10^2.[117] In the same year, CT states were experimentally observed for pyridine chemisorbed on Ag(111) by Demuth and Sanda utilizing high-resolution electron energy loss spectroscopy, which bolstered the CT mechanism.[116] Later, Adrian[120] used the semiempirical Wolfsberg–Helmholz method to treat the molecule–surface interactions and showed that CT Raman enhancements were of the order of 10 to 1000 for the ethylene adsorbed on silver model system. In this work, both Franck–Condon and Herzberg–Teller terms were derived, despite that the Herzberg–Teller term was considerably smaller than the Franck–Condon term for this model system.

Interfacial energy level alignment plays an important role in the CT enhancement mechanism. Ueba *et al.*[108,109] conducted a detailed re-examination on the pyridine–silver system and constructed an energy diagram of pyridine adsorbed on Ag. They explained SERS as adsorbate-induced resonance Raman scattering through CT excitations and used the Newns–Anderson model of chemisorption to obtain a large EF about 10^3 when an extremely narrower CT state were assumed.

Following the CT mechanism proposed by Burstein *et al.*,[114] Otto and coauthors further proposed the four-step CT mechanism based on the adatom model for pyridine and cyanide anion adsorbed on Ag surfaces in electrochemical interfaces,[107] which predicted resonant-like Raman scattering by adsorbate vibrations facilitated by photon-excited charge-transfer transitions from localized electronic states at atomic-scale roughness sites (*e.g.*, ''adatoms'') on Ag surfaces to the affinity levels of the adsorbates (Fig. 13b). For pyridine adsorbed on a Ag electrode (Fig. 13b-i), they considered that the CT process proceeds in four steps, such as the generation of the surface plasmon excitation, the formation of the negative ionic molecule, electron transfer back to metal equal to the energy and final emission as radiating photons. The CT took place from the Ag to the unoccupied molecular orbital of pyridine. While for cyanide anions adsorbed on Ag electrode (Fig. 13b-ii), the CT took place from adsorbed cyanide anion to the unoccupied state above the Fermi level in Ag.

Although the CE, represented by the CT, processes typically provide EFs about one to three orders of magnitude for non-resonance Raman molecules, this phenomenon involves intricate interactions between surfaces, photons and molecules. Thus, it plays a crucial role in investigating molecular adsorption and chemical reactions on surfaces and cannot be overlooked. Furthermore, to accurately quantify the SERS intensity, a profound understanding of the CE effects arising from surface interactions at the molecular level is essential.

In 1982, Chang and Furtak edited and published the first book on SERS, which for the first time collected representative theoretical and experimental contributions in the development of the SERS field.[62] There were some experimental exploration of various SERS active substrates by chemical and physical means.[123–128] In 1985, after nearly a decade of exploration and competition, the electromagnetic theory represented by surface plasmon mechanism became the dominant SERS mechanism in the academic community, marked by the famous review article by Moskovits.[69]

Overall, in the initial decade of its foundation, the theoretical framework of SERS gradually took shape, laying robust groundwork for the field. Though it fell short of precisely quantifying the SERS effect or fully unveiling the nature of SERS-active structures, this foundational science served as the

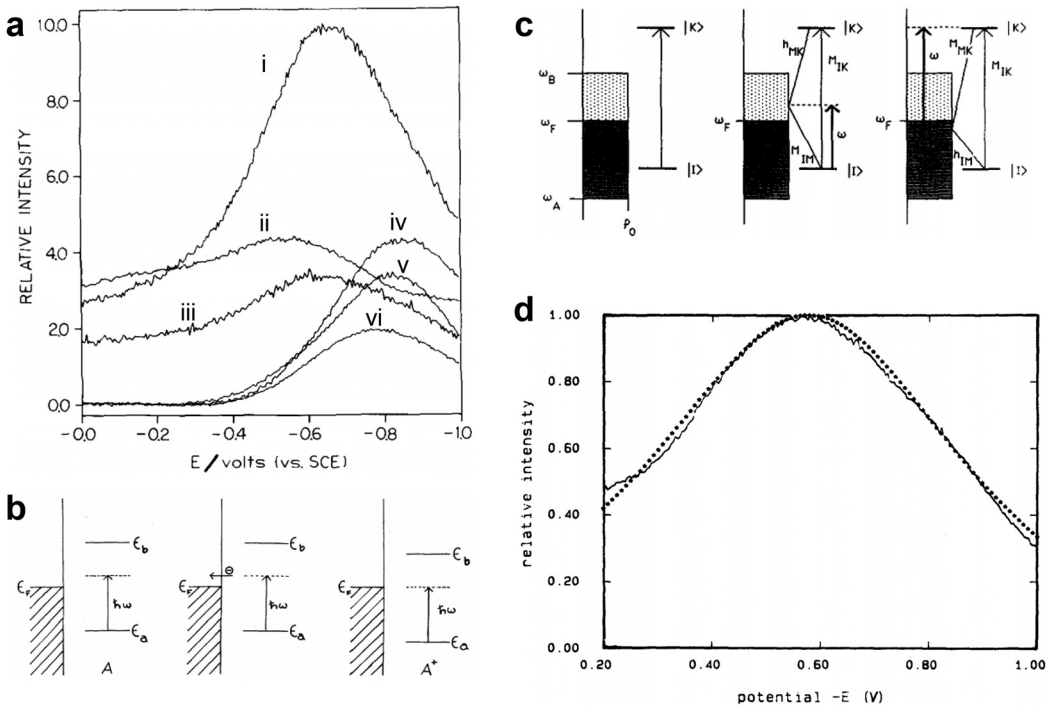

Fig. 12 (a) The SERS intensity of the adsorbed pyridine on Ag as a function of the electrode potential, (i) 1006 cm^{-1}, (ii) 1035 cm^{-1}, (iii) 3056 cm^{-1}, (iv) 1215 cm^{-1}, (v) 1594 cm^{-1}, (vi) 623 cm^{-1}. (b) Conceptual model of the energy levels changing with the electrode potential in the CT process from molecule to metal in the metal–molecule system: metal–neutral molecule A on illumination immediately before tunneling (left), electron tunneling to the metal (middle), and adjustment of energy levels on formation of A^+ for the resonant tunneling case (right). (c) The relevant energy states and the vibronic coupling involved in the Franck–Condon term and the Herzberg–Teller terms in the CT process. (d) The potential-intensity profile fitting from the CT enhancement mechanism for pyridine adsorbed on a Ag electrode. Figures are reproduced from ref. 2, 115 and 118 with permissions. Copyright 1977 Elsevier. Copyright 1979 American Physical Society. Copyright 1986 AIP publishing.

bedrock upon which the next four decades of progress would stand, guiding its evolution and inspiring further exploration.

3. The decade of persistent exploration (mid-1980s–mid-1990s)

The journey of SERS had been fraught with significant challenges and limitations during its second decade. The generality and versatility of SERS have been frequently questioned by the broader scientific community beyond the communities of Raman spectroscopy, materials and surface science.

According to the electromagnetic mechanism, the SERS effect mainly arises from the excitation of surface plasmons in free-electron-like metals with subwavelength structures.[21,69] Nevertheless, only a few metals like Ag, Au, and Cu, along with some alkali metals can provide the significant enhancement required for strong Raman signal amplification.[4,69] The limitation, that SERS rely on specific metals for giant enhancement, severely restricts the breadth of practical applications involving other materials, thus curtailing the versatility of SERS in various scientific and industrial contexts.

Even these ''free electron metals'' require specific surface morphologies to achieve the significant enhancement characteristic of SERS. Surfaces must possess roughness, island-like structure, or contain metal colloids in the sub-micrometer size range.[62,69] In contrast, the atomically flat and structurally well-defined surfaces commonly used in fundamental research in surface science and interface engineering could not support the necessary localized surface plasmon resonances.[69] As a result, SERS could not be effectively applied to these structurally well-defined surfaces, further limiting its adoption and utility. This was especially awkward for SERS, given its name emphasizes ''surface-enhanced,'' yet it struggled to gain acceptance and make itself a useful tool across the scientific and industrial communities.

Consequently, many research groups gradually abandoned the field from the late 1980s to the mid-1990s, primarily due to difficulties in securing research funding. Some young researchers even faced the risk of being dismissed. However, a few scientists persisted in their efforts to break through the seemingly impossible barriers. The SERS effect, though incompletely understood, remained an incredibly attractive phenomenon due to its extremely high surface sensitivity. Those who persevered in exploring new approaches believed that SERS shouldn't be so easily sentenced to death or exile. The breakthrough might eventually occur, even though no one could predict when.

3.1 The ''borrowing SERS activity'' strategy

During the mid-1980s and early 1990s, several research groups tried to overcome the key limitations of generality. They aimed

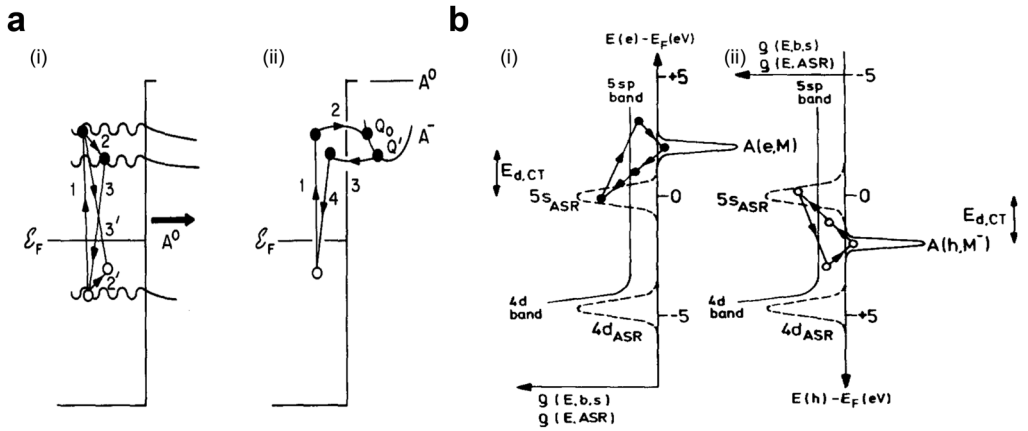

Fig. 13 Chemical enhancement mechanisms of SERS. (a) Schemes of (i) the three-step Frohlich Raman scattering mechanism and (ii) the CT mechanism. (i) Step 1, and step 3 and 3′ correspond to the radiation excitation and recombination, of the electron–hole pairs, respectively. Steps 2 and 2′ correspond to the scattering of excited electrons and excited holes by the vibrations of adsorbed molecule, respectively. (ii) Steps 1 and 4 correspond to the radiative excitation and recombination of an electron–hole pair, respectively. Steps 2 and 3 correspond to the hopping of the excited electron to and back from the virtual bound state of adsorbed molecule, respectively. An energy *versus* configuration curve for the virtual bound state, in which Q_0 and Q' are the equilibrium and perturbated configuration of the molecule, is also shown. (b) the four-step CT processes for pyridine adsorbed on a Ag electrode (i) and cyanide anion adsorbed on a Ag electrode (ii). Figures are reproduced from ref. 107 and 114 with permissions. Copyright 1979 & 1984 Elsevier.

to create SERS activity from metallic substrates beyond the traditional materials of Ag, Au, and Cu, and to obtain Raman signals from atomically flat single-crystal surfaces. Some researchers have reported achieving both unenhanced[129–131] and enhanced[132–134] Raman signals from adsorbates on either roughened or mechanically polished Rh and Pt electrodes and, thereafter, on porous Pt, Pd, Ni, Co and Ti films.[135] Nonetheless, the SERS spectra documented in these studies have either proven challenging to replicate or exhibited minimal detectability.

As a result, these efforts were largely unacknowledged by the Raman spectroscopy and surface science communities, casting a bleak outlook on the potential of SERS. The mainstream consensus was that SERS was not as important as initially expected when it was discovered, and it seemed unlikely to evolve into a generalized and powerful analytical tool.

Fortunately, a few determined groups continued their efforts during this low period. They believed that the discovery of SERS, which made highly surface-sensitive analysis possible, suggested that finding ways to transform SERS into a versatile tool was achievable,[21,35,136] because when one door closes, another window of opportunity often opens, revealing new paths and possibilities. While the electromagnetic mechanism of the SERS effect defined the limitations of substrates and surfaces, it also left room for potential solutions to circumvent these obstacles.

One of the highlights in that dark period is an innovative strategy with long-term significance, *i.e.*, exploring SERS signals of adsorbates on semiconductor or transition metal surfaces, see Fig. 14. This strategy utilized the long-range effect of the electromagnetic field and deposited small Au or Ag islands on the SERS-inactive substrate.[137–142] The probed molecules on the non-SERS-active surface can still experience the electromagnetic field from the SERS-active-islands thus their Raman signals were enhanced accordingly. This strategy allowed researchers to exploit the SERS effect on the traditionally non-SERS-active surfaces, which was later referred to as ''borrowing SERS activity'' strategy.[143]

The first investigation that introduced the concept of ''borrowing SERS activity'' strategy was conducted and reported by Van Duyne group in 1983.[137] They deposited discontinuous Ag overlayers or islands on non-SERS-active semiconductor surfaces pre-adsorbed with the molecules of interest, as illustrated in Fig. 14a. Despite their poor nanostructure aggregate, the SERS-active Ag islands created the long-range effect of strong electromagnetic fields, enhancing the resonance Raman scattering of adsorbates on the nearby semiconductor surface. Consequently, surface-enhanced resonance Raman signals of the adsorbed transition metal complexes molecules on n-GaAs electrodes (Fig. 14c) were observed.[137,140]

In this preliminary trial of the ''borrowing SERS activity'' strategy, it was challenging to ensure that the species of interest were selectively adsorbed only on the non-SERS-active substrate other than on the high-SERS-active Ag islands. In most cases, molecules tend to undergo surface diffusion and eventually adsorb on the high-SERS-active materials, which generate stronger signals. The signals overshadowed the smaller signals from the non-SERS-active surfaces of interest, thus complicating the analysis and reducing the effectiveness of the ''borrowing SERS activity'' strategy.

A more effective and reliable approach, which involved electrochemical deposition of an ultrathin layer of weak or non-SERS-active metal materials on Ag and Au roughened substrates (Fig. 14b), was independently developed in 1987 by Fleischmann group[138,141] and Weaver group.[139,142,144] By borrowing the strong electromagnetic field generated by inner Ag or Au nanostructures, Raman signals of target molecules in vicinity of their surfaces are enhanced even if the molecules are

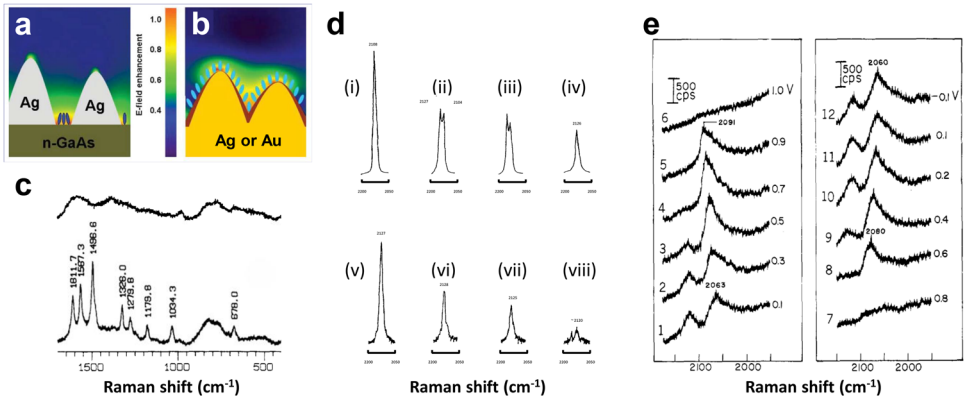

Fig. 14 Schematic illustrations of the two strategies for borrowing SERS activity: (a) deposit discontinuous SERS-active metal islands on the substrate to study the molecules adsorbed on the non-SERS-active substrate; (b) coat an ultrathin non- or weak-SERS-active layer on the SERS-active substrate to study the molecules adsorbed on the layers. (c) Surface-enhanced resonance Raman spectra of $Ru(bpy)_3^{2+}$-treated n-GaAs: without (upper) and with (lower) discontinuous Ag islands overlayer by strategy illustrated in (a). (d) Raman spectra in the C–N stretching region before and after zinc deposition onto a Ag electrode at the potentials (i) −1.2 V, (ii) −1.25 V, (iii) −1.25 V, after 3 min, (iv) −1.30 V, (v) −1.4 V, (vi) −1.4 V after 1 min, (vii) − 1.4 V after 3 min, (viii) − 1.4 V after 16 min. (e) Potential-dependent SER spectra in C–O stretching region for CO adsorbed on a platinum-coated Au electrode. (d) and (e) were obtained by the strategy illustrated in (b). Panel a and b are reproduced from ref. 35. Copyright 2007 Royal Society of Chemistry. Panel c is reproduced from ref. 137, copyright 1983 American Chemical Society. Panel d is reproduced from ref. 138, copyright 1987 Elsevier. Panel e is reproduced from ref. 139, copyright 1987 American Chemical Society.

not contact with the SERS active substrate directly. For example, as shown in Fig. 14d(i)–(iv), the peak ascribed to CN^- adsorbed on Ag was gradually replaced by a new peak ascribed to CN^- adsorbed on zinc during the process of underpotential deposition of zinc. Subsequently the peak intensity of CN^- adsorbed on zinc gradually decreased upon the further progress of overpotential deposition of the thick film as shown in Fig. 14d(v)–(viii).[138] Fig. 14e illustrates that using an ultrathin Pt film over roughened Au surfaces effectively reveals SER spectra for carbon monoxide adsorbed on Pt thin film (*ca.* one to three monolayers) with potential-dependence. Since the enhancement decreases exponentially with increased distance from the SERS-active substrate, the transition metal layer must be ultrathin, typically only a few atomic layers, to effectively borrow/experience the electromagnetic field. Meanwhile, the ultrathin metal film must be pinhole-free to prevent direct molecule adsorption on the underlying SERS-active Ag or Au substate, which could lead to misleading spectral interpretations.

It is worth noting that preparing ultrathin and pinhole-free metal layers was quite challenging due to the irregular and undulating surface of electrochemically roughened electrodes. Despite their clear limitations at the time, these early efforts in exploring the "borrowing SERS activity" strategy set a foundation for solving generality problems and challenging seemingly impossible boundaries.

3.2 Explorations on bio-SERS and electrochemical-SERS

During these challenging times, it is widely recognized that the standard benchmarks and reproducibility are lacking in SERS studies without extending the research to weak- or non-SERS-active material, even with the use of roughened Ag and Au electrodes or colloids. Furthermore, the messy and disorderly SERS-active sites, which include various ad-atoms, ad-clusters, and surface complexes, undermines the rigorous scientific standards required for systematic and reproducible studies. Therefore, the coherent recognition and full support from spectroscopy, analytical chemistry, biology, electrochemistry and other fields were lacked in the SERS studies.

Fortunately, some researchers persisted in exploring various research methods and application areas to enhance the advantages and mitigate the disadvantages of SERS-active metals like Ag and Au. Cu, being highly reactive and prone to forming copper oxide, complicates the establishment of a reliable benchmark. One approach is to focus on the detection sensitivity for probing surfaces species because normally only monolayer or even sub-monolayer species (10^{13}–10^{15} per cm^2) are presented, especially for some weak Raman scatterers.[145–147] They developed several ways to improve the detection sensitivity: (1) employing a high numerical aperture lens to optimize collection efficiency; (2) increasing laser power to the maximum permissible level without exceeding the damage threshold; (3) utilizing the potential difference method to isolate the faint interfacial signal from the stronger bulk signal; (4) selecting an appropriate excitation wavelength to leverage the resonance Raman effect; and (5) maximizing the SERS effect through appropriate modifications of the electrode surfaces.[148–150]

Another crucial approach is to develop various methods for creating new substrates that produce strong and stable SERS signals. These methods include: roughening of electrode surfaces through multiple oxidation–reduction cycles (ORCs),[141,151–154] chemical etching of surfaces in acidic solutions,[155–157] deposition of island films on substrates at elevated temperatures,[158] as well as the preparation of films *via* evaporation or sputtering in a vacuum onto cryogenic

substrates (100 K),[159] and electrochemical deposition.[141,160] Additionally, colloids—particularly aggregated ones, can be generated through chemical methods[161] or laser ablation.[162] Sub-microstructure can also be prepared using lithographic, self-assembly, or template techniques.[163]

A highlight was the development of a highly stable SERS-active Au substrate using an asymmetric ORC process, which was proposed by Weaver and his colleagues.[164] The Au surface showed a distinct brown color after repeating the process for about 15 minutes, contrasting with the yellowish hue of highly SERS-active Ag electrodes. Although the nanostructured surfaces were poorly defined at the time, their effectiveness was evident, and the differences could be distinguished by the naked eye, which often provides quicker and more sensitive detection than a simple visible spectrometer in that time.

From methodologic view, SERS research could be broadly divided into two trends: species identification from an analytical perspective and structure/process characterization from a physicochemical perspective.[165] The analytically oriented studies primarily focused on whether SERS could detect and identify the target species in complex systems such as the biologic systems. In contrast, physicochemical-oriented studies require a more comprehensive understanding of the way and the reason that target species interact with surfaces and their surroundings by analyzing spectral features. To achieve this, more systematic characterizations are needed to estimate all the physical and chemical mechanisms involved, while considering surface selection rules. Additionally, it is necessary to develop preparation methods for simpler SERS-active surface, as the spectral features of the same probed molecules, whether tightly trapped in a gap or freely adsorbed on a surface, can differ significantly. These efforts are essential for providing meaningful insights into adsorption configurations or reaction mechanisms, such as in electrochemistry.[49,50,130,166,167]

During the 1980s, there was an increasing interest in the utilization of the "SERS reporter" technique, which significantly enhances the weak signals from targeted species by employing reporters exhibiting strong (resonant) Raman signals. This approach has been demonstrated to be effective for the trace detection of molecules in solutions, as well as for the identification of specific molecules within live cells or animal models. With the effort of Cotton *et al.*,[168,169] Koglin and Sequaris,[170] Nabiev *et al.*[171] and other groups,[172–175] SERS was also extended to biological systems, including DNA (from base to mononucleotide, double-stranded polynucleotides and modified DNA, as shown in Fig. 15), chromosomes, amino acid and protein (*e.g.*, lysozyme and BSA) and various porphyrin chromophores. Although there are some criticisms of SERS or surface enhanced resonance Raman spectroscopy (SERRS) as a technique for biological systems regarding the possibility of denaturation by the interaction with the SERS substrate surface, the *in vivo* applicability of SERS was promisingly anticipated with the further improvements in SERS substrates and instrumentation.[168,170]

This perseverance and creative problem-solving kept the field of SERS research alive, eventually leading to its resurgence and broader acceptance as a powerful analytical tool for various branches of SERS.

3.3 Interfacial water as an unusual target by SERS

Regarding molecular generality and electrochemical application, SERS also underwent a slow and intricate journey. In the early exploration of molecules chemically or physically adsorbed at surfaces, which can be probed by SERS, the surface water molecules on electrodes stood out as one of the most surprising and unique systems. Since water is one of the most important molecules and the most essential solvent, playing significant roles in interfacial processes such as

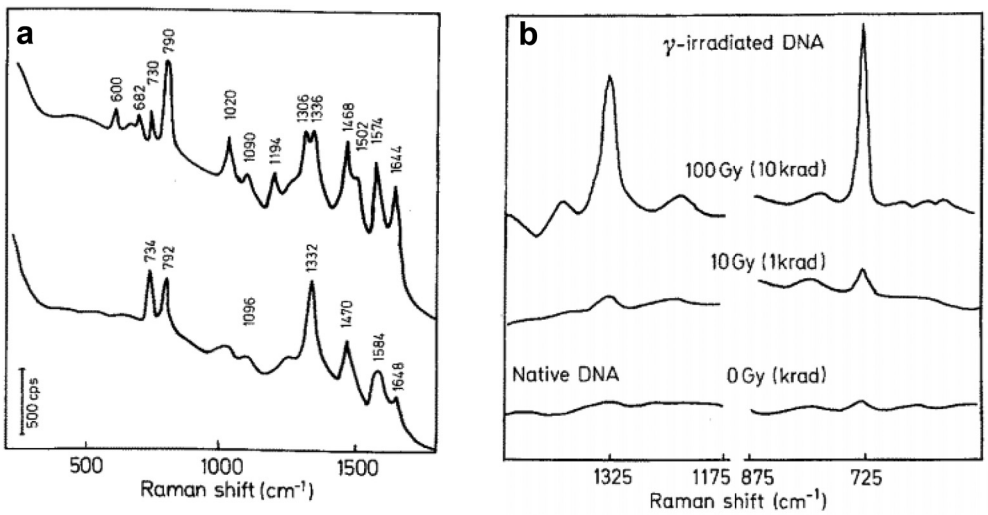

Fig. 15 (a) SERS spectra of native DNA (top) and of poly(dA-dT)·poly(dA-dT) (bottom). DNA concentration 50 μg ml^{-1} and 80 μg ml^{-1}, respectively; 0.15 M KCl, 10^{-3} M Tris pH 8; adsorption potential −0.6 V *vs.* Ag/AgCl. (b) SERS spectra of native and γ-irradiated DNA. 0.1 M KCl + 2 × 10^{-3} M Na_2HPO_4; DNA concentration: 300 μg ml^{-1}; pH 8.0; irradiated with γ-rays from a ^{60}Co-source. Figures are reproduced from ref. 170 with permissions. Copyright 1986 Springer Nature.

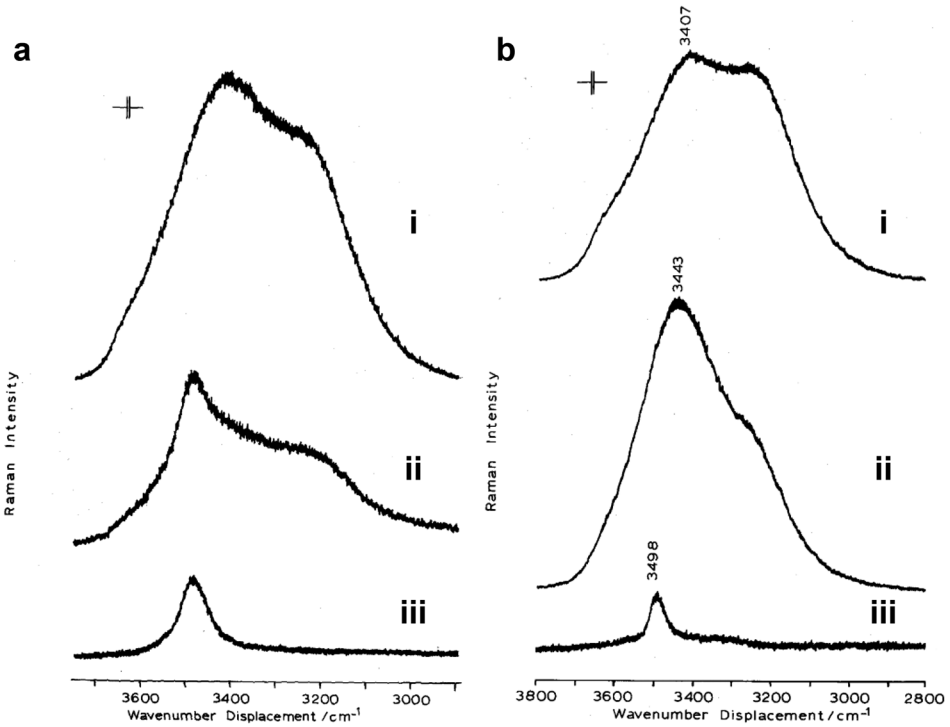

Fig. 16 (a) The Raman spectra in the OH stretching frequency region of molar KCl/H_2O with the laser focused on a polished Ag electrode. All spectra were measured at a potential of −0.2 V. (i) Polished electrode; (ii) roughened electrode; (iii) roughened electrode pushed up against the cell window; (b) a comparison of the Raman spectra in the OH stretching region and using the same intensity scale of: (i) pure H_2O; (ii) 4 M KCl; (iii) a Ag electrode roughened in 1 M KCl, with the electrode pushed up against the cell window. Figures are reproduced from ref. 176 with permission. Copyright 1981 Elsevier B.V.

electrocatalysis, researchers were eager to obtain the SERS of water after discovering the SERS effect. Although water is naturally a very weak Raman scatterer, the presence of multiple layers of water molecules at the interface often results in a significant Raman signal. It can be reasonably assumed that the SERS signal from the total amount of water molecules should not be too weak. However, surface/interfacial water gave no detectable SERS signals despite its universal presence at most interfaces, which remained a puzzle.

In 1981 Fleischmann and coworkers were the first to obtain SERS of water with a paper entitled "*Enhanced Raman spectra from species formed by the coadsorption of halide ions and water molecules on silver electrodes*".[176] For this they adopted a special experimental condition with a high concentration halide salt aqueous solution, such as 1 mol dm^{-3} KCl, to obtain the SERS signal from water, as shown in Fig. 16. In the experiment, the Ag electrode underwent electrochemical oxidation–reduction treatment in a KCl aqueous solution, and *in situ* observation was immediately conducted in the same solution under controlled electrochemical potentials. This procedure is effective in avoiding the influence of surface contaminants. It was later identified as a typical SERS-detectable coadsorption system containing halide anions and water molecules.

In the same year, Pettinger *et al.* attributed SERS of water and halide ions in a similar solution to the formation of surface complexes involving Ag adatoms, halide ions, and water molecules.[177] The further experimental results provided a strong evidence that the SERS signal of water was irreversibly diminished when the applied potential was moved to highly negative potentials. The desorption of halide ions from the negatively charged surface led to decomposition of the SERS-active site.[178] Therefore, the SERS of water in surface complex forms is most likely related to chemical enhancement. These water molecules are atypical in the double layer of ordinary electrolytes and this aspect of the SERS of water undermined the utility of SERS for characterizing the water molecules typically present in the double layer, dealing a heavy blow to researchers' confidence in using SERS as a powerful tool to study electrochemical interfaces.

This great difficulty, however, only fueled the determination of a small group of researchers to persistently unravel this mystery. They thought that if we cannot understand SERS of water, no one can claim SERS is truly useful and the SERS mechanism is fully understood. In 1987, Funtikov *et al.* reported an intriguing and atypical finding regarding the surface-enhanced Raman scattering (SERS) of water at silver electrodes immersed in sodium sulfate solutions devoid of (pseudo-)halide ions.[179] They asserted that detection was limited to the SERS signal associated with the bending vibration of water, while the characteristic stretching mode remained undetectable. Furthermore, the study was confined to a narrow potential range of −1.1 V to −1.45 V (with reference to a saturated silver chloride electrode) owing to the interference caused by hydrogen evolution at more negative potentials.

After seven years, progress was made through the cooperation of Tian group and Funtikov group in 1994. They employed

a special ORC procedure to achieve a highly SERS-active surface and obtain high quality SERS spectra of both the stretching and bending vibration modes of water at Ag electrodes.[180] Additionally, by positioning the electrode as close as possible to the optical window of the Raman spectroscopic cell to form a thin layer cell, the interference of hydrogen bubbles and Raman signal from bulk water was efficiently minimized. This allowed for the investigation of the potential dependence of the SERS intensity and frequency over a much wider potential range from −0.5 V to −2.0 V (referred to saturated calomel electrode, SCE), including potentials with severe hydrogen evolution. However, to obtain high-quality SERS signals, a highly concentrated electrolyte, such as 8 mol dm^{-3} of $NaClO_4$, was needed, leaving some aspects of the puzzle unsolved.

Because of the efforts of these dedicated researchers through the mid-1990s, the interfacial water systems probing by SERS were systematically expanded to various transition metal surfaces in different dilute electrolytes by Tian group, *via* the several approaches including special ORC roughening procedure, the use of a thin layer cell, as well as the difference spectrum method when confocal Raman microscopy with much higher detection sensitivity at surfaces was invented and commercialized.[181] These works provided basic methods for the later and wider exploration of interfacial water structures on single-crystal surfaces of different metals in the past decade.

Looking backward to the first two decades of SERS, the journey of SERS was fraught with significant challenges and limitations. A broader historical and fundamental view is needed to understand the reason why SERS had such a challenging growth and took a difficult and intricate journey. It is now much clearer that SERS is truly a branch of nanoscience, as its sensitivity and spectral features critically depend on the interaction between nanostructures and incident light. However, SERS was discovered about two decades before the advent of nanoscience, thus lacking suitable experimental and theoretical methods that were finally developed in the 1990s and beyond.

The first and second chapters of the SERS story are thus unique and encouraging compared to many other scientific fields because it would have been much easier to get started in the mid-1990s when nanoscience was booming. However, the early hard exploration was worthy as it marks SERS as one of the oldest branches of plasmon-enhanced spectroscopy, plasmonics, and even the broader field of nanoscience. The pioneers who laid the foundation of SERS and their persevering spirits in those early decades deserve great respect.

4. SERS breakthroughs enabled by advancements in nanoscience (mid-1990s–mid-2010s)

Undoubtedly, the significant advances and breakthroughs in the SERS field were driven by nanoscience. To understand this further, we need to examine why nanoscience gained momentum in the 1990s rather than in the 1960s. In 1959, Richard Feynman had laid the conceptual foundation of nanoscience with his famous lecture, "*There's Plenty of Room at the Bottom*".[182] He proposed the potential for manipulating and controlling matter at atomic and molecular scales, laying the intellectual groundwork for what would later become nanotechnology. However, despite his groundbreaking vision, Feynman was unable to develop nanotechnology tools or devices directly, leaving the field open for further exploration and advancement in the 1990s.

The three decades' delay in opening the field of nanoscience is mainly due to lack of adequate characterization methods. From the perspective of the history of scientific development and methodology, to precisely control and manipulate matter at any scale, it is essential first to develop methods and tools capable of observing that scale. The starting point could be the 1986 Nobel Prize in Physics awarded jointly to Ernst Ruska, Gerd Binnig, and Heinrich Rohrer for their groundbreaking contributions to microscopy techniques at the nano- and atomic scales. These revolutionary methods provided unprecedented resolution, enabling scientists to image and manipulate matter, effectively opening the door to nanotechnology. The widespread recognition of any new field and its integration into various scientific branches typically took 5 to 10 years, driven by the development of in-house solutions or the commercialization of new instruments.

For the younger generation today, it may be hard to imagine that in the 1980s, obtaining a nanometer-level scanning electron microscope (SEM) image was far more difficult for most research groups worldwide than achieving a sub-angström resolution with a transmission electron microscope (TEM) is today. Scanning probe microscopes (SPM), such as the scanning tunneling microscope (STM) and atomic force microscope (AFM), were still in their infancy, with no commercial products available. At that time, experimental techniques and theoretical capabilities were inadequate to overcome the obstacles hindering SERS development. Highly active and stable SERS substrates could not be rationally prepared or accurately characterized at the nanoscale, leading to challenges in quantitatively analyzing and establishing mechanical models of SERS. These challenges illustrate just how early researchers were in the field, highlighting the crucial role of developing new methods and instruments in emerging areas like nanoscience and its one of the oldest branches, SERS.

4.1 The significant rise in SERS

The rapid development of nanoscience served as a booster for SERS,[35] which rose like a phoenix from the ashes in the mid-1990s to 2000s, as evidenced by the significant increase in annual publications (Fig. 17). A series of new synthesis methods for SERS-active nanoparticles (NPs), nanofabrication techniques for structured surfaces, and advanced analysis methods for characterizing the prepared nanostructures in the 1990s contributed significantly to the progress of SERS substrates, which evolved from roughened Au and Ag electrodes, island films deposited on cold surfaces in the ultrahigh vacuum, and colloidal aggregates,[1–3,5,62,70,183,184] to Au, Ag and Cu[185,186]

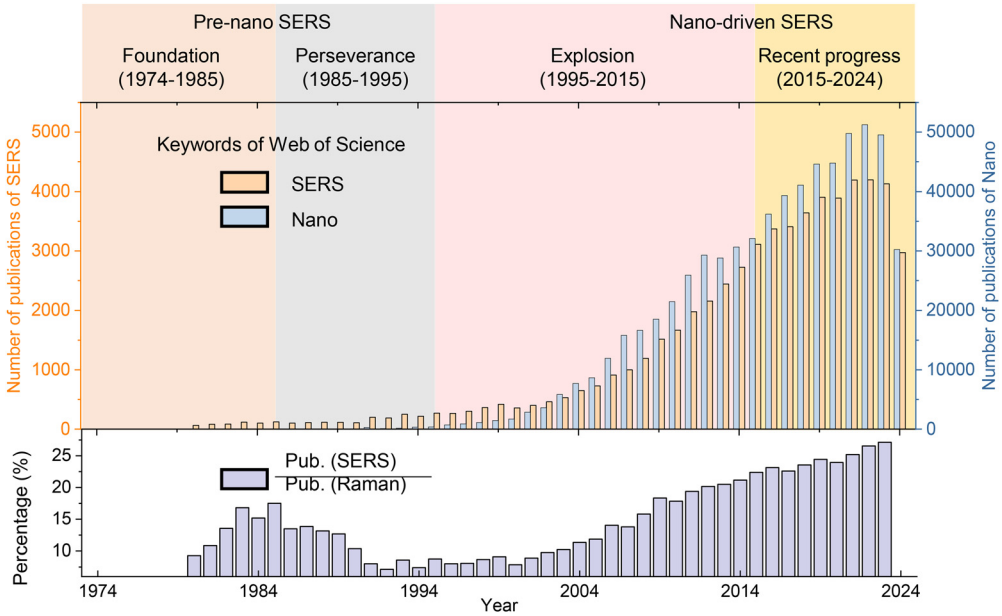

Fig. 17 The number of publications in the 1974–2024 period searched through the ISI Web of Sciences (top panel) and the ratio of the number of publications (bottom panel). The keywords used for SERS include "Surface-enhanced Raman", "SERS", "Surface-enhanced Resonance Raman" and "SERRS". The keyword used for nano is "Nano". The 50-years history of SERS was divided into four periods: 1974–1985: the foundation period; 1985–1995: the perseverance period; 1995–2015: the explosive increase period; 2015–2024: the recent progresses.

nanoparticles featuring nanometer-sized gaps, shells, tips, edges, and structured surfaces with nanometer-sized holes, voids, bumps, grooves, or ridges.[14,15,20,22,26,35,187–198] The characteristic dimensions of the above structures are progressively decrease from the ill-defined and disordered micrometer and sub-micrometer scale to the defined and ordered tens of nanometers scale structure, as shown in Fig. 18. The landmark work marking the entry of SERS into the nano era was the demonstration of SERS using monodisperse Au and Ag nanospheres by Natan and coworkers in 1995,[187] heralding the phase when SERS substrates transitioned into a well-defined structural stage.

4.2 Demonstration of single-molecule sensitivity in SERS

A significant milestone in the advancements of SERS in nano era was the achievement of single-molecule SERS (SM-SERS) detection. In 1997, Nie and Emory[14] and Kneipp and colleagues[15] independently reported experimental evidence observing SERS from single dye molecules on Ag nanoparticle colloids (Fig. 19). This breakthrough not only pioneered a new single-molecule spectroscopic method beyond single-molecule fluorescence but also provided high energy-resolved molecular vibrational fingerprint information while avoiding the common photobleaching issues in single-molecule fluorescence.

At that moment, Nie had already noted that achieving SM-SERS required suitable nanostructures and excitation conditions, and he estimated a SERS EF of 10^{14}–10^{15} in their experiments. (Note that these were wrongly referenced against non-resonance Raman cross-section and were likely closer to 10^{10} when using the corrected single-molecule EF definition.[203] see Section 4.7) Nie wrote,[14] "*An unexpected finding during this work was that a very small number of nanoparticles exhibited unusually high enhancement efficiencies. These particles emitted bright, Stokes-shifted (toward longer wavelengths) light and are called hot particles.*" While Nie performed resonant SERS experiments, Kneipp applied near infrared (NIR) excitation non-resonant to the target molecules and explained their single molecule experiments by very strong electromagnetic enhancement, related to Ag clusters (aggregates of Ag nanoparticles), which is particularly effective at NIR excitation.[15]

The specific structure of these hot particles seems to be a key to unveil the unexpected signal enhancement observed in SM-SERS experiments. Nie investigated the morphology of these hot particles using High-resolution AFM and found that "*High-resolution AFM images of selected hot Ag nanoparticles show that the majority of them are well-separated, single particles with a narrow size range of 110 to 120 nm in diameter, indicating a strong correlation between enhancement efficiency and particle size.*"[14] Experiments by Kneipp and colleagues showed that huge SERS enhancement is related to colloidal clusters and NIR excitation.[15,204,205] This observation was in agreement with computations by Stockman *et al.* which showed that electromagnetic enhancement increases with longer excitation wavelengths in the fractal clusters.[206] By using electron microscopy, Kneipp found that "*Electron micrographs of the sol… show that the colloidal solution is slightly aggregated and consists of small 100–150 nm sized clusters*".[15] However, it was not clear how the clusters/single particles cause the efficient Raman enhancement, and such SM level enhancement were not widely accepted by the community at that time.

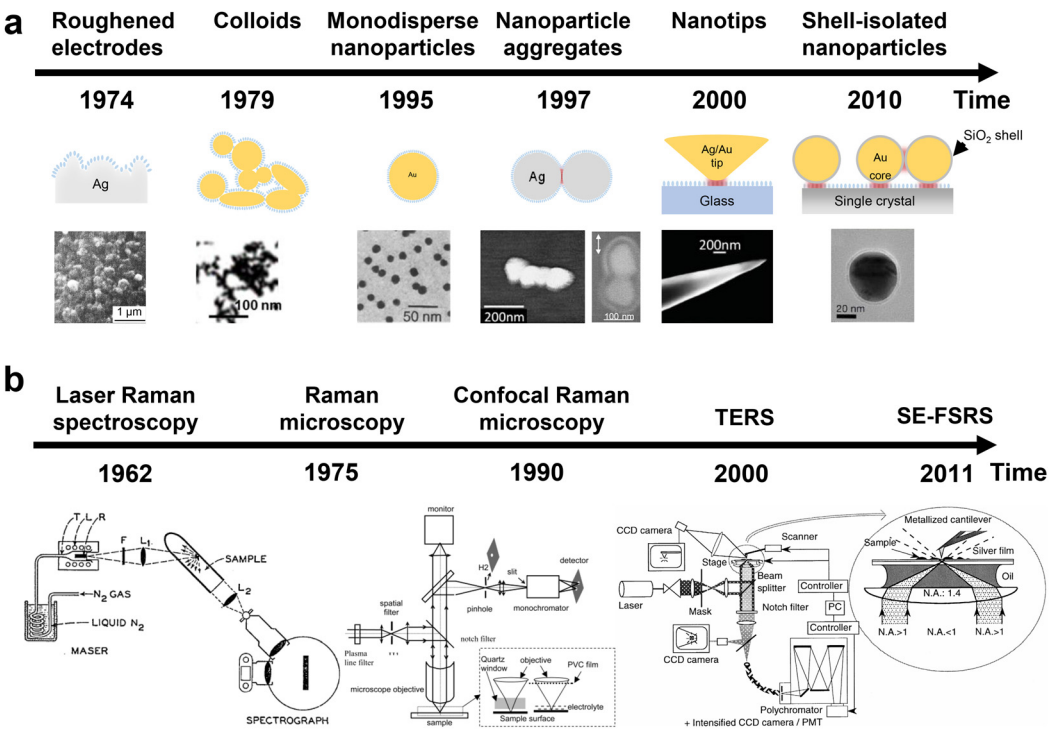

Fig. 18 The evolution and milestones related to (a) representative SERS-active substrates and (b) development of Raman instrument. Figures of panel a are reproduced from ref. 14, 20, 35, 187 and 199–201 with permissions. Copyright 1981 & 1982 Elsevier B.V. Copyright 1995 & 1997 AAAS. Copyright 1999 APS. Copyright 2007 Royal Society of Chemistry. Copyright 2010 Springer Nature. Figures of panel b are reproduced from ref. 18, 165 and 202 with permissions. Copyright 1962 Optica publishing. Copyright 2002 American Chemical Society. Copyright 2000 Elsevier.

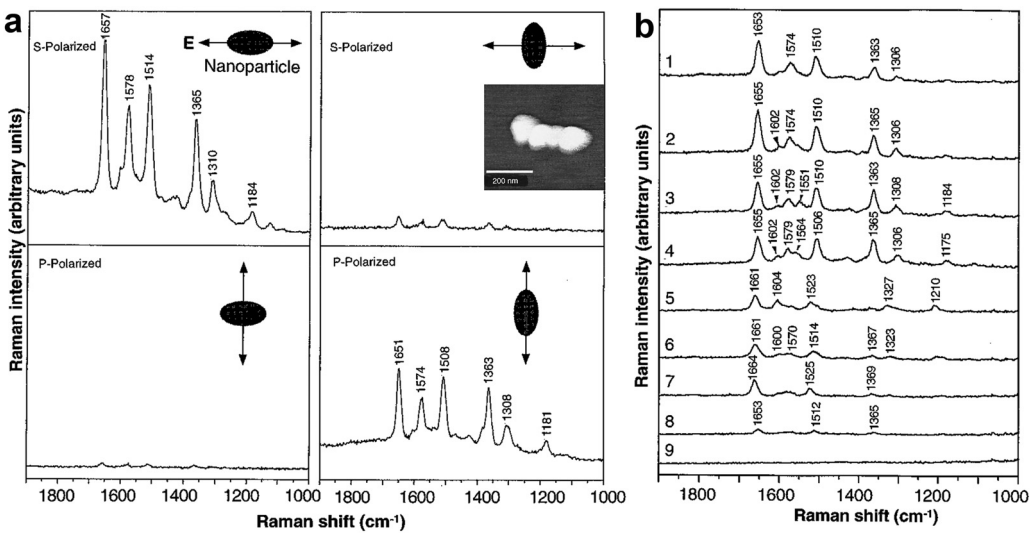

Fig. 19 Experimental demonstration of single-molecules SERS. (a) SERS of rhodamine 6G (R6G) obtained with a linearly polarized confocal laser beam from Ag nanoparticles. (b) Time-resolved surface-enhanced Raman spectra of a single R6G molecule recorded at 1-s intervals. The Raman signals abruptly changed in both frequency and intensity three times, as shown in spectra 2, 5, and 8. Figures are adapted from ref. 14 with permission. Copyright 1997 AAAS.

Aiming to understanding the SM-SERS mechanism, in 1999, detailed electromagnetic calculations and experiments by Käll and coworkers[201,207] and Brus and coworkers[208,209] proved that it's the giant electromagnetic field enhancement in the nanogaps between coupled Ag nanoparticles that are essential for achieving SM-SERS. As shown in Fig. 20, the Raman spectra of single hemoglobin in Ag nanoparticle dimer show significant temporal fluctuation, which is consider as the direct evidence of SM-SERS event. Fig. 20b and c confirmed the giant electromagnetic field enhancement (E^4) in the nanogap of

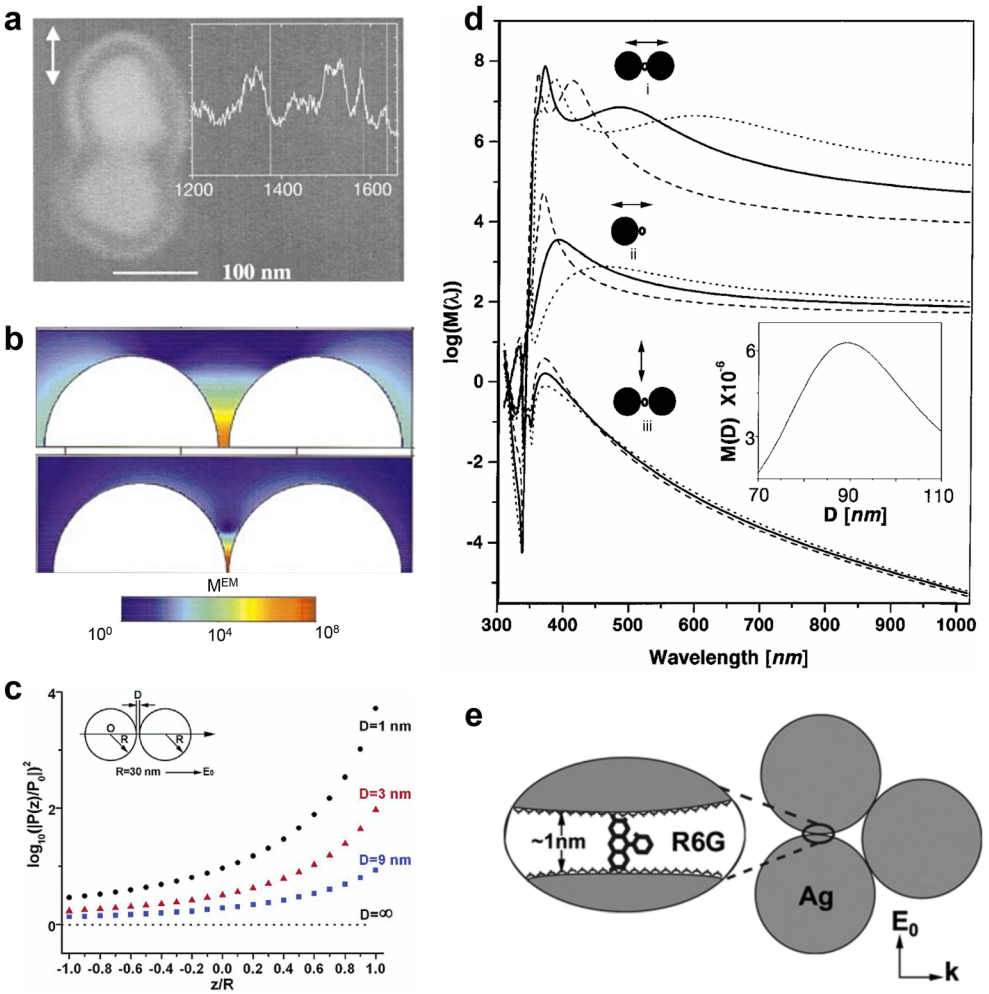

Fig. 20 (a) SEM image of a hot dimers and corresponding single Hb molecule spectra in the inset. The double arrow indicates the polarization of the incident laser field. (b) EM enhancement for nanoparticle dimers with separations from top to bottom 5.5 nm and 1 nm, respectively. (c) Calculated enhancement of the two-particle system (configuration shown in the inset) compared to the single-particle case, as a function of particle coupling. (z/R) 0 is at one particle center, and (z/R) + 1 is on the particle surface at the particle–particle interface side. (d) Calculated electromagnetic EF for the midpoint between two Ag spheres separated by d = 5.5 nm and for a point $d/2$ outside a single sphere. Diameters of spheres D = 60 nm (dashed curves), 90 nm (solid curves) and 120 nm (dotted curves). Double arrows indicate the incident polarizations. Inset shows the enhancement *versus* D for λ = 514.5 nm. (e) Schematic representation of SERS active aggregate geometry. A single R6G molecule adsorbed on the Ag particle covered with a citrate layer. The xanthene plane is aligned along the local field direction. Panel a and d are reproduced from ref. 201. Copyright 1999 American Physical Society. Panel b is reproduced from ref. 207. Copyright 2000 American Physical Society. Panel c and e are adapted from ref. 209. Copyright 2003 American Chemical Society.

nanoparticle dimer, which is highly sensitive to the gap distance as well as the incident polarizations (Fig. 20d and e). These results clearly elucidated the observations from the 1997 SM-SERS experiments by Nie and Emory, and Kneipp and colleagues, revealing the electromagnetic mechanism underlying the SM-SERS, which also initiated the field of nanogap plasmonics.

It is important to mention that actually Metiu and coworkers[77] had pointed out in 1981 that the gap between nanostructures could lead to significant electromagnetic interactions and produce enormous SERS enhancement inside the gap. These ''rare sites'' were further conceptualized by Shalaev *et al.* as the hotspots.[210] However, due to the limitations in precise fabrication and characterization of such nanostructures at that time, the significance of gap mode in SERS was not widely recognized until after the seminal single-molecule experiments in 1997. *Via* rigorous theoretical analysis, Käll and Xu further proposed that the gap between nanoparticle dimers can generate significant optical trapping forces.[211] The optical forces create an optical trap for molecules in the hotspots, thereby make the SM-SERS detection possible.

It is noteworthy that the initial SM-SERS studies were based on ultra-low concentration of analytes, whereby the concentration was diluted to the extent that only a single molecule was present in the detection area. However, for a molecule to contribute a signal, it must adsorb onto the ''rare hot particles/sites,'' making it challenging to accurately estimate the number of adsorbed molecules. The convolution of ''rare sites''

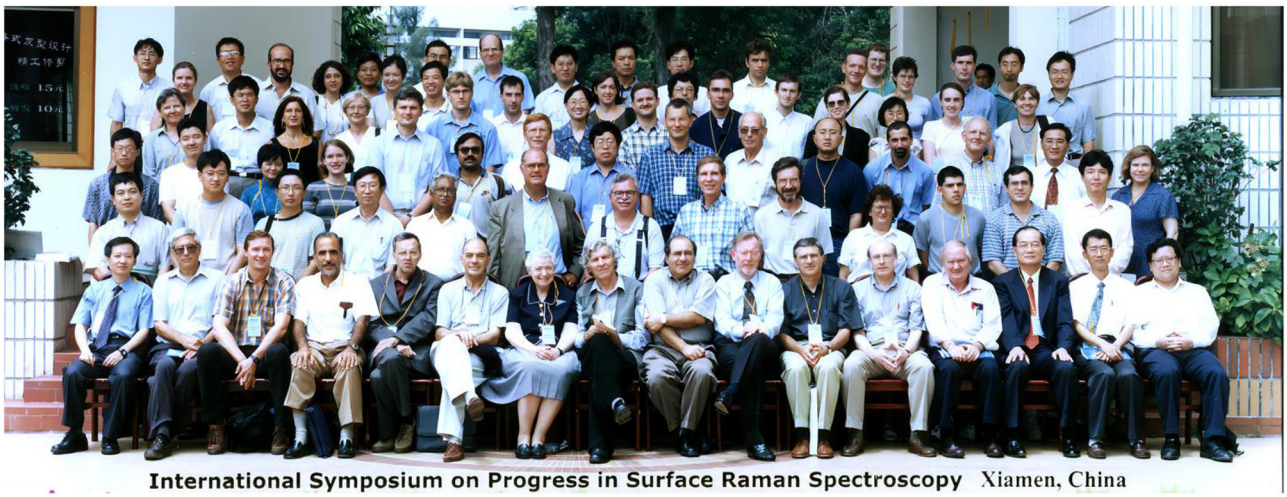

Fig. 21 Group photo of International Symposium on Progress in Surface Raman Spectroscopy, held in Xiamen University, Xiamen, China during Aug. 14–17, 2000. Attendees include (from the front row to the back row, counting from right to left): 1st row: Shu-Ming Nie (1st), Nai-Teng Yu (3rd), James Durig (4th), Richard Van Duyne (5th), Martin Moskovits (8th), Andreas Otto (9th), Mildred Dresselhaus (10th), Aleksey Polubotko (12th), Ricardo Aroca (13th), Vladimir Shalaev (14th), John Lombardi (15th), Zhong-Qun Tian (16th); 2nd row: Linda Prinsloo (1st), Alexandre Brolo (3rd), Joel Rubim (8th), Kwan Kim (11th); 3rd row: Alan Creighton (2nd), Bernhard Schrader (5th), Wieland Hill (6th), Andrzej Kudelski (10th), Christy Haynes (11th); 4th row: Katrin Kneipp (1st), Yan-Xia Chen (3rd), Marek Prochazska (5th), Jürgen Popp (6th), Ralf Gessner (7th), Kiki Gessner (8th), Volker Deckert (11th), Wei-Qing Xu (15st); 5th row: Andreas Emge (6th), Jörg Kottmann (8th), Jian-Lin Yao (9th), Louis Brus (11th), Bin Ren (13th), Juan Otero (17th), Bing Zhao (18st).

(or hotspots) with ultra-low concentrations results in poor statistical reliability and soundness, thus aroused numerous doubts and led to debates regarding the interpretation and even the reality of the observations of SM-SERS.[14,15] These debates were only fully settled with the development of the bi-analyte SERS technique for an unambiguous demonstration of single-molecule SERS detection.[212–214]

While the electromagnetic theories developed in the first phase of SERS history by numerous pioneers provided a solid foundation for the resurgence of SERS,[4,62,64,65,67,69,75–90] it is essential to recognize that the substantial advancements in nanostructure preparation, characterization, and theoretical and computational methods during the mid-1990s to 2000s contributed to the beginning of the resurgence of SERS.[14,15,187,201,207–210,212–215] Subsequently a substantial amount of research further propelled the revival of SERS in the nanotechnology era.[21,32]

An international symposium on Progress in Surface Raman Spectroscopy was held in Xiamen University, Xiamen, China during Aug. 14–17, 2000. The symposium brought together approximately 80% of the most active and leading researchers in SERS worldwide, as depicted in the group photo in Fig. 21 and the symposium program, to present cutting-edge methods and advancements. This symposium provided a dynamic platform for discussing and even debating SERS mechanisms, SM-SERS, the newly invented TERS, and their applicability to broader systems. The detailed topics can be found in the program as shown in Table 1.

In 1997, skepticism regarding the 10^{14} EF claimed for SM-SERS from the mainstream community was quite similar to the strong doubts about the 6th power EF claimed for SERS in 1977. Therefore, validations and mechanisms of SM-SERS became a major focus of the symposium. To delve deeply into this theme, round table discussion 1 was arranged immediately following the presentations by Kneipp and Nie, to examine and discuss the challenges and opportunities within SM-SERS. Round table discussion 2 was held after presentations by Campion, Shalaev, Otero, and Kottman to highlight the latest progress in physical and chemical enhancement mechanisms. These heated discussions and debates were instrumental in exchanging various views and advancing theoretical methods.

Notably, the symposium coincided with newly reported TERS results, and Deckert, one of the inventors, delivered an acclaimed plenary presentation despite being an early-career researcher at that time. Coincidently, the dual advances of SM-SERS and TERS methods have collectively captured significant attention from experimenters and theorists, focusing on the same 'hotspot'—the singular behavior of molecules, nanoparticles, and nano-tips with profoundly high local electromagnetic fields. This focus has ultimately positioned SERS as a new scientific Frontier, extending the boundaries of knowledge beyond traditional surface spectroscopy.

Moreover, efforts to broaden the materials generality of SERS, such as transition metal SERS using confocal microscopy reported by Ren and semiconductor SERS by Quagliano, also invoked some interests. Many topics have continued to evolve over the subsequent decades of SERS research. The collective contribution by all participants reinvigorated research momentum in the field, marking a shift from a low-tide phase to a dynamic, nano-driven SERS era.

4.3 Key methods of SERS since the mid-1990s

SM-SERS demonstrated the astonishing sensitivity of SERS, fueling the belief that SERS, when combined with well-defined

Table 1 The timetable and program of the 2000 liternational symposium on progress in surface Raman spectroscopy in Xiamen University

Tuesday, 15 August

	Session A	Session B
8:30-8:55	**Z.-Q. Tian** Opening Ceremony	
8:55-9:20	**R. P. Van Duyne** Surface-enhanced Spectroscopy: It's 2000-What Do We Know Now?	
9:20-9:45		
10:00-10:15	**M. Moskovits** Surface Enhanced Raman: A Report from the Near Field	
10:15-10:40		
10:40-11:05	**A. Creighton** The SERS of Pyridine into the New Millennium	
11:05-11:30		
13:30-13:55	**J. Lombardi** Time Resolved Surface Enhanced Raman Scattering Studies of Proton Transferring 3-hydroxyflavone	
13:55-14:20	**L. Brus** Electromagnetic Field Enhancement and the Raman Spectra of Single R6G Dye Molecules	
14:20-14:45	**N.-T. Yu** Efficient Surface-enhanced Raman Scattering from a Nanocrystals-on-electrode Setting	
14:45-15:10	**V. Deckert** Vibrational Spectroscopy Beyond the Diffraction Limit: Tip Enhanced Raman Scattering	
15:30-15:55	**M. Weaver** The Interfacial Versatility of SERS: New Applications in Surface Chemistry and Materials Science	**K. Kim** Adsorption and Reaction Characteristics of Thiols and Sulfides on Noble Metals
15:55-16:20	**L. G. Quagliano** Surface Enhanced Raman Spectroscopy on Semiconductor Surfaces	**R. Aroca** Surface-enhanced Raman Scattering Imaging of Langmuir-Blodgett Monolayers
16:20-16:45	**B. Ren** Confocal Microprobe Raman Spectroscopy for Investigating the Electrochemical Interfaces	**B. Zhao** Comparison in Surface Enhanced Raman Scattering on Salicylideneamine Between Silver and Gold Colloid and Silver Mirror Substrate

Wednesday, 16 August

	Session A	Session B
8:30-8:55	**M. Dresselhaus** Resonant Surface Enhanced Raman Spectra of Carbon Nanotubes	**R. Cooney** Vibrational Spectroscopic and EPR Studies of Doped Polyisothianaphthene
8:55-9:20	**J. C. Rubim** Raman Spectroscopy of Surface Modified Magnetic Nanoparticles Based on Ferrites	**P. W. Jagodzinski** Surface-enhanced Raman Spectroscopy using Metal Colloids
9:20-9:45	**Y. Lu** Applications of SERS in Polymer/Metal Interface and Polymer Surface Structure Research	**T. N. Misra** Surface Enhanced Raman Spectroscopy: Some Applications in Surface Chemistry
9:45-10:00	**S. Lefrant (o)** SERS Studies on Conducting Polymers and Carbon Nanotubes	**P. Rosch (o)** The Use of Silver Colloids for the Analysis of Mentha
10:15-10:40	**W. Hill** Fiber Optic SERS Sensor	**J. Popp** SERS on Biological Systems
10:40-11:05	**N. Felidj** SERS Studies on Lithographically Designed Metal Nanoparticles	**I. Nabiev** SERS Monitoring of Molecular Interactions within the Supramolecular Complexes: Impact in the Design and Screening of New Anticancer Compounds
11:05-11:30	**M. Futamata** Highly-sensitive ATR-SPP Raman Spectroscopy Beyond Diffraction Limit	**M. Prochazska** Metalation Kineties of Free-base Porphyrins as a Probe of Ag Colloid/porphyrin SERS-active Systems
11:30-11:45	**Y. X. Chen (o)** ATR-Raman Spectroscopic Studies of Water on Single Crystalline Cu Electrodes	**S. Lecomte (o)** Time Resolved Surface Enhanced Resonance Raman Spectroscopy for Probing the Heterogeneous Electron Transfer Reaction of Cytochrome c_{552}
13:30-13:55	**T. Lopez-Rios** Inelastic Light Scattering Investigation for Nanometric Spatial Resolution	**W. Richter** Raman Spectroscopy of Surface Phonons on Semiconductors
13:55-14:20	**J. I. Marcos** Analysis of a SERS Spectrum on the Basis of a Charge Transfer Mechanism Involving Three Electronic States	**G. Mattei** Vibrational Study of Surface Species in Porous Silicon
14:20-14:45	**J. Bukowska** SERS in a Study of a Copper Electrode Surface Modified by Adsorbed Nitrogen-containing Heterocyclic Molecules	**S. Miyajima** Raman Spectroscopy of Roughness-controlled Silicon Surfaces
14:45-15:10	**D.-Y. Wu** A Theoretical Study on the Raman properties of CO Adsorption on Platinum Surfaces	**H. D. Bist** Micro-Raman Studies on Film Surfaces Deposited on Silicon Substrate
15:30-15:55	**J. V. Garcia-Ramos** SERS Spectroscopy on Metal Colloids	**X. Zhang (o)** Use of in situ Confocal Microprobe Raman to Monitor the Active Surface Reconstruction over Ce-Ag-Mo-P-O Catalyst during Selective Oxidation of Propane
15:55-16:20	**K. Kneipp** Surface-enhanced Raman Scattering at Extremely High Enhancement Level - Application to Raman Studies of Single Molecules and of Single-walled Carbon Nanotubes	**J. Chowdhury (o)** Concentration Dependent Surface Enhanced Raman Scattering Study of 4-benzoylpyridine Adsorbed on Colloidal Silver Particles
16:20-16:45	**S.-M. Nie** Blinking Surface-enhanced Raman Scattering Observed in Single Colloidal Nanocrystals	**D. M. Chen (o)** Surface-enhanced Raman Spectroscopy of Metallo-tetraphenlyporphyrins Adsorbed on Ag2O and Hydroxyl-modified Silver Colloids
17:00-18:30	**Round Table Discussion 1: Prospectus of SERS** **Speakers: M. Moskovits & L. Brus**	

Thursday, 17 August 2000

	Session A	Session B
8:30-8:55	**A. Campion** Chemical-enhancement in SERS: Focusing on the Metal States	**C. Li** Advances in UV Resonance Raman Spectroscopic Studies on Highly Isolated Transition Metal Oxides
8:55-9:20	**V. Shalaev** SERS and SEHRS in Fractal and Fractal-microcavity Composites	**W. Z. Weng** In Situ Confocal Microprobe Raman and Time-resolved FTIR Investigation on the Active Phase and the Reaction Mechanism for the Partial Oxidation of Methane to Syngas over Supported Ru and Rh Catalysts
9:20-9:45	**J. Otero** Discussion on the Nature of the Charge Transfer Mechanism in SERS	**Y. Yang** The Applications of Confocal Raman Micro-Spectroscopy for Study of PracticalElectrode Materials
9:45-10:00	**J. P. Kottman (o)** Strong Raman Enhancement in Isolated and Coupled Non-Regularly Shaped Nanoparticles	**A. Kudelski (o)** Fluctuations and Dynamics of Raman Intensities Observed in SERS Micro-spectroscopy
10:15-11:45	**Round Table Discussion 2: SERS mechanism** **Speaker: A. Otto** Some Aspects of the Mechanisms of SERS	

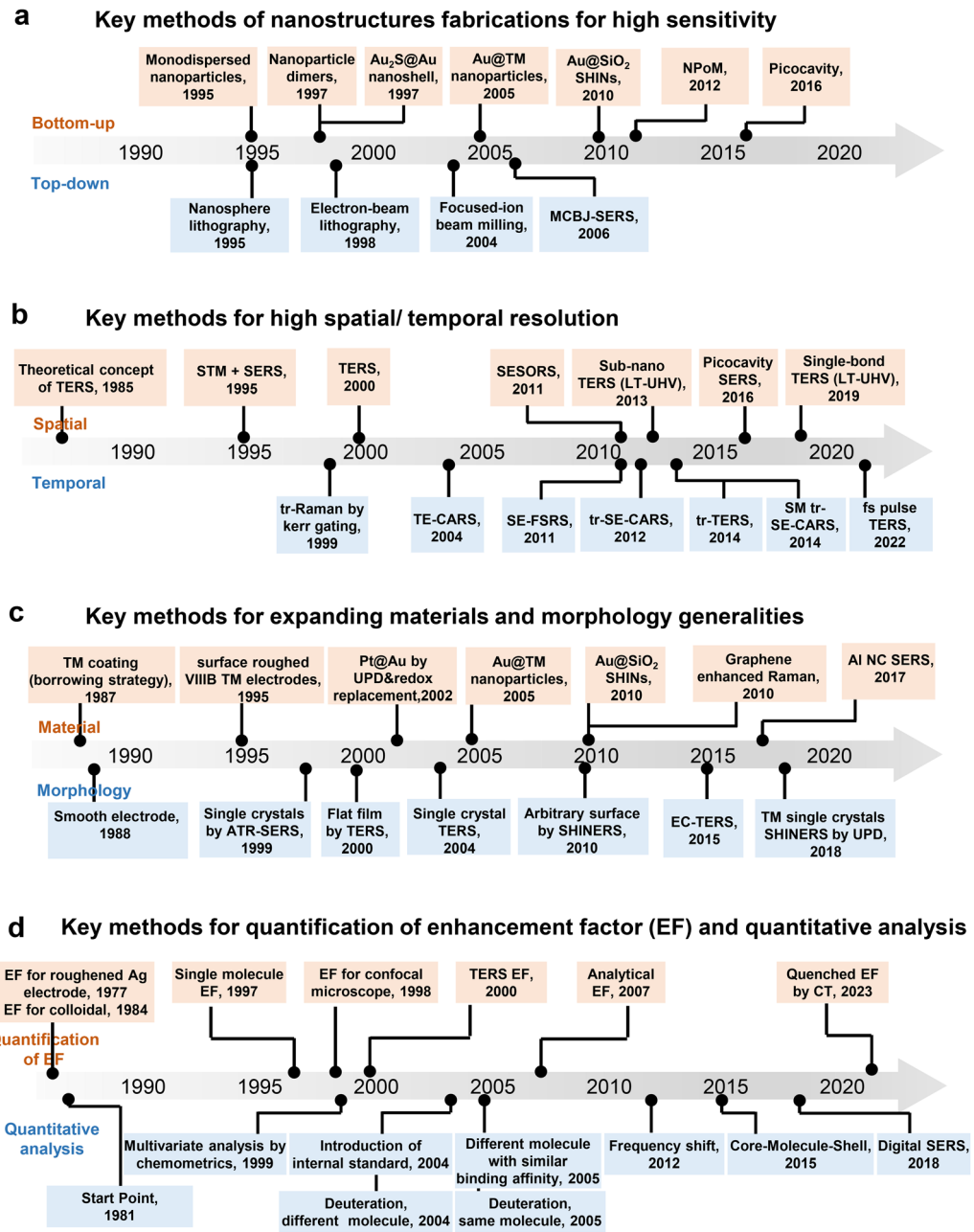

Fig. 22 The timeline of key methods since 1990s (a) toward well-ordered SERS-active micro-/nano-structures fabrication for high-sensitivity of SERS; (b) key methods for high spatial and temporal resolution; (c) key methods for expanding the generalities of SERS substrate materials and morphology. (d) key methods for quantification of SERS EF and quantitative analysis. The abbreviations: TM: transition metals; SHINs: shell-isolated nanoparticles; NPoM: nanoparticle on mirror; MCBJ: mechanically controllable break junction; STM: scanning tunneling microscope; SESORS: surface-enhanced spatially offset Raman spectroscopy; LT-UHV: low temperature-ultrahigh vacuum; tr: time-resolved; TE-CARS: tip enhanced coherent anti-Stokes Raman spectroscopy; SE-FSRS: surface enhanced femtosecond stimulated Raman spectroscopy; tr-SE-CARS: time-resolved surface enhanced CARS; tr-TERS: time-resolved TERS; SM tr-SE-CARS: single molecule tr-CARS; fs-tr-TERS: femtosecond time-resolved TERS; UPD: underpotential deposition; ATR-SERS: attenuated total reflection-SERS; EC-TERS: electrochemical TERS; NC: nanocrystal; EF: enhancement factor; CT: charge transfer.

nanostructures and characterization techniques, can usher in a new era of development opportunities. This realization sparked widely renewed interest among researchers in the field of SERS. Leveraging rapid advancements in nanotechnology, numerous methods in SERS research have flourished, creating a vibrant and dynamic landscape. We meticulously and comprehensively organize these methods from the past decades in a matrix format, covering aspects such as detection sensitivity, spatial and temporal resolution, materials and morphology generalities for SERS, and quantitative analysis of SERS (see Fig. 22). These achievements have greatly propelled the three decades of continuous explosive growth of SERS.

Nano-driven SERS has also opened new avenues for pushing the limits of capability, reliability, and applicability. With the

ability to precisely engineer and control nanostructures at the atomic level, researchers can now tailor the plasmonic properties of SERS substrates to enhance the signal, improve reproducibility, and expand the range of analytes that can be detected.[21,30] Moreover, the integration of SERS with spatial-resolved and time-resolved spectroscopic techniques, such as TERS and ultrafast spectroscopy, has enabled the investigation of chemical and biological processes with unprecedented spatial and temporal resolution.[104,216,217] These developments have not only deepened our understanding of the fundamental mechanisms underlying SERS but have also paved the way for its widespread adoption in various fields.[21,32]

It is important to highlight that SERS is the eldest member of the broader family of nanostructure-based plasmon-enhanced spectroscopy techniques.[21] By harnessing the plasmon enhancement effect of nanostructures, other spectroscopic methods such as surface-enhanced infrared absorption,[218] surface-enhanced fluorescence spectroscopy,[219] and surface-enhanced nonlinear spectroscopy[217] (including surface-enhanced second harmonic generation,[220] sum frequency generation,[221] third harmonic generation,[222] four wave mixing,[223] and coherent anti-Stokes Raman scattering[224]) were also realized. These advancements clearly demonstrate the tremendous progress and boundless possibilities that the field of surface-enhanced spectroscopy has experienced and driven by the development of nanoscience and technology.

In the development of SERS, the researchers have enjoyed exchanging ideas and establishing deep cooperation *via* international meetings including two Faraday discussions on SERS (held in 2005,[225] 2017[226]), the biennial International Conference on Raman Spectroscopy (ICORS) (of which, SERS is the largest branch), and other SERS or TERS symposia. Readers are referred to these proceeding papers especially the records of two Faraday discussions to witness the full collision of ideas.[225–227]

4.4 Key methods for high sensitivity

4.4.1 Concept of SERS hotspots. The mechanism behind the hotspots in SM-SERS is the electromagnetic field enhancement in gap mode SERS. Fig. 23a shows three typical nanostructures that exhibit gap mode SERS/TERS, which includes the nanoparticle dimer, nanoparticle on substrate and tip on substrate. The electromagnetic enhancement in SERS involves a two-step process, as shown in Fig. 23b. The first step involves a localized enhancement of the electromagnetic field near plasmonic nanoparticles (NPs) at the incident frequency (ω_0). In this stage, the plasmonic NPs serve as optical antennas, transforming the incident far-field light into a concentrated near-field. In the subsequent step, the enhancement is influenced by the derivatives of the Raman polarizability of the molecule–NP system, which arise from the significant interaction between the induced dipoles of the molecules and the dipoles or multipoles of the NPs. Here, the plasmonic NPs function as transmitting optical antennas, retransmitting the near-field back to the far-field at the Raman scattered frequency (ω_R). The EF at this stage is directly related to the square of the local electric field (E_{loc}) at ω_R. For vibrational modes of adsorbed molecules at the low-frequencies, the incident and Raman scattered frequencies are usually similar, leading to comparable EFs in the first and second steps ($G_1(\omega_0)$ and $G_2(\omega_R)$, respectively). Consequently, the SERS EF is proportional to the fourth power of the enhancement of the local electric field:[12,21]

$$\begin{aligned} G_{SERS} &= G_1(\omega_0)G_2(\omega_R) \\ &= (|E_{loc}(\omega_0)|^2|E_{loc}(\omega_R)|^2)/(|E_0(\omega_0)|^2|E_0(\omega_R)|^2) \\ &\approx |E_{loc}(\omega_0)|^4/|E_0(\omega_0)|^4 \end{aligned} \quad (3)$$

The electromagnetic field surrounding such nanostructures is highly localized in specific areas referred to as SERS hotspots (Fig. 23). These hotspots can include configurations such as nanotips, interparticle nanogaps, or gaps between particles and substrates.[21,77,78,209,210,228–237] The local electromagnetic field in the nanogaps between Au or Ag nanoparticle dimers with nanogaps is extremely intense and highly sensitive to the interparticle gap distance. For instance, when the gap size of a dimer composed of gold nanospheres is decreased from 10 nm to 1 nm, the SERS EF improves dramatically from 10^4 to 10^9 (Fig. 23c). Consequently, the SERS signals are significantly amplified from these hotspots, even enabling single-molecule detection.[14,15,201,215,238–240]

4.4.2 Development of SERS-active nanostructures by bottom-up synthesis. As the electromagnetic field near the nanostructures is closely associated with surface plasmon resonances, which can be tuned to enhance the SERS activity by precisely controlling the nanostructures, particularly their optical couplings. For example, the position and scattering attributes of plasmon resonance peaks in nanostructures are influenced by factors such as the size, shape, and arrangement of the nanoparticles. During this period, driven by the rise of nanotechnology, various nanoscale characterization techniques, such as high-resolution scanning electron microscopy (SEM), transmission electron microscopy (TEM), and AFM, were progressively developed. This advancement, in turn, facilitated progress for controllable nanostructures in synthesis and fabrication techniques. Consequently, numerous methods for the controlled synthesis of nanoparticles and more complex nanostructures have emerged.[13,35,198,241–243]

In 2006, Xia and coworkers developed a method for synthesizing monodisperse single-crystalline Ag nanocubes (Fig. 24a).[244,245] García de Abajo, Liz-Marzán, and coworkers introduced a simple synthetic method for zeptomol SERS detection of non-resonant molecule by sandwiching the analyte between the tips of Au nanostar nanoparticles and a flat Au surface (Fig. 24b).[246] This was accomplished by exploiting the lightning rod effect of individual nanostars and the plasmonic coupling between the nanostars and the Au film.

In addition to nanostructures with varying morphologies, core–shell nanoparticles represent a significant category of SERS substrates due to the wide range of possible combinations of core and shell materials, different shell thicknesses, and

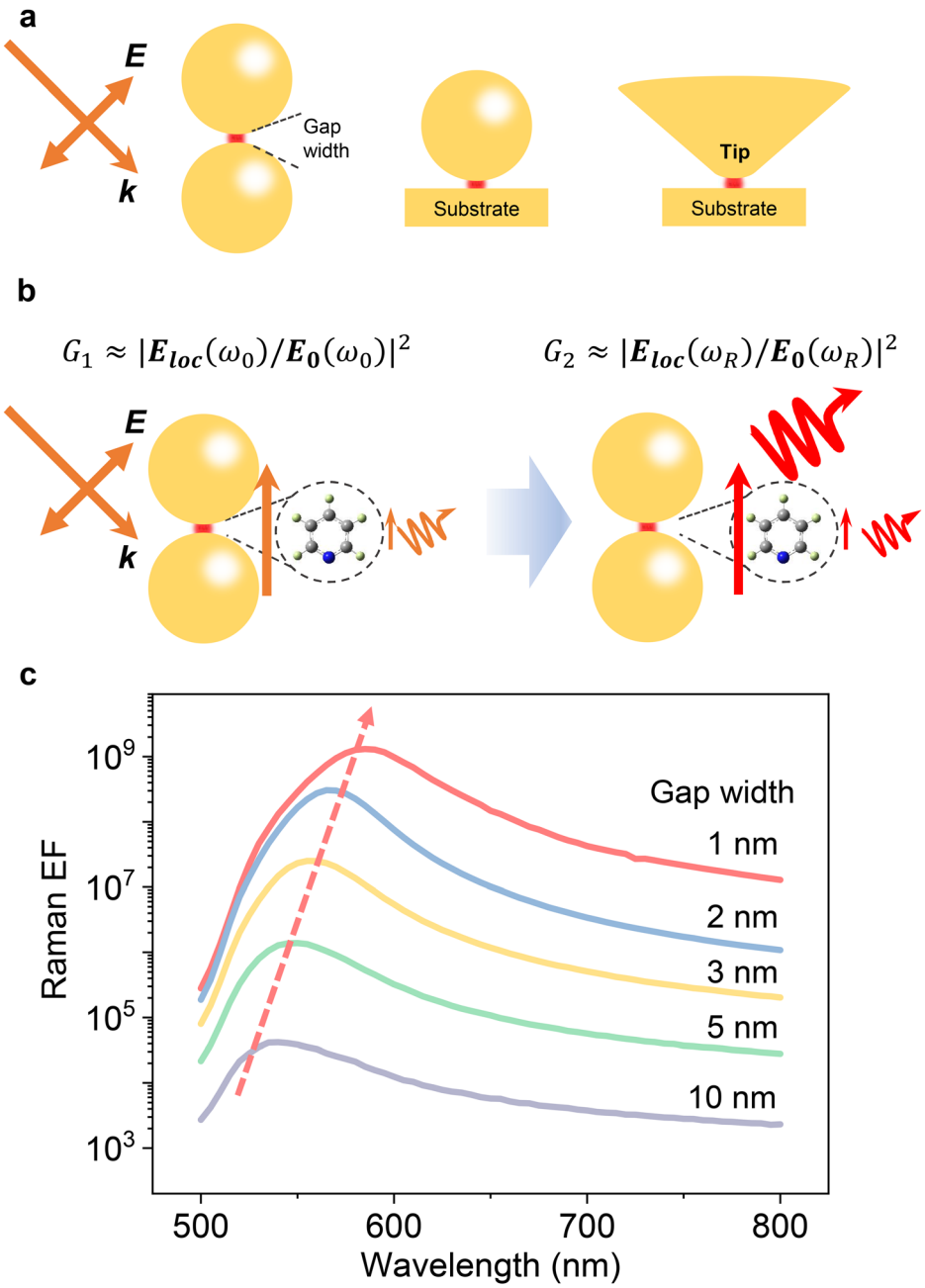

Fig. 23 (a) Representative nanostructures for gap-mode SERS/TERS, including nanoparticle dimer, nanoparticle on substrate and tip on substrate (b) The two-step process of enhancement of the electromagnetic field in SERS for nanoparticle dimer. (c) The spectra of the maximum Raman EFs for nanoparticle dimers with different gap widths.

distinct optical properties (see Fig. 25), which offers a new degree of freedom to modify the optical properties of nanostructures. These variations, particularly in dielectric indices, can lead to diverse SERS activities and novel applications, which play the a key role in overcoming the limitations of the material and morphology generality of traditional SERS.

In 1997, Halas and colleagues pioneered the development of nanoshells, consisting of a dielectric core and a metallic shell.[256,257] By manipulating the dimensions of the core and shell, the resonance wavelength of the structure can be tailored across the visible to near-infrared spectrum (Fig. 24c and 25c). Subsequently, Nordlander, Halas, and coworkers introduced the plasmon hybridization theory,[258] drew from molecular orbital theory, which effectively explained and predicted the optical properties of nanoshell and other plasmonic structures.[198] Nanoshells offer two key advantages as SERS substrates: (1) the plasmon resonance can be easily tuned to match the wavelength of the pump laser, and (2) nanoshells exhibit significantly larger field enhancements compared to solid metal cores due to hybridized plasmon resonances, which we will discuss in detail in Section 4.4.10.

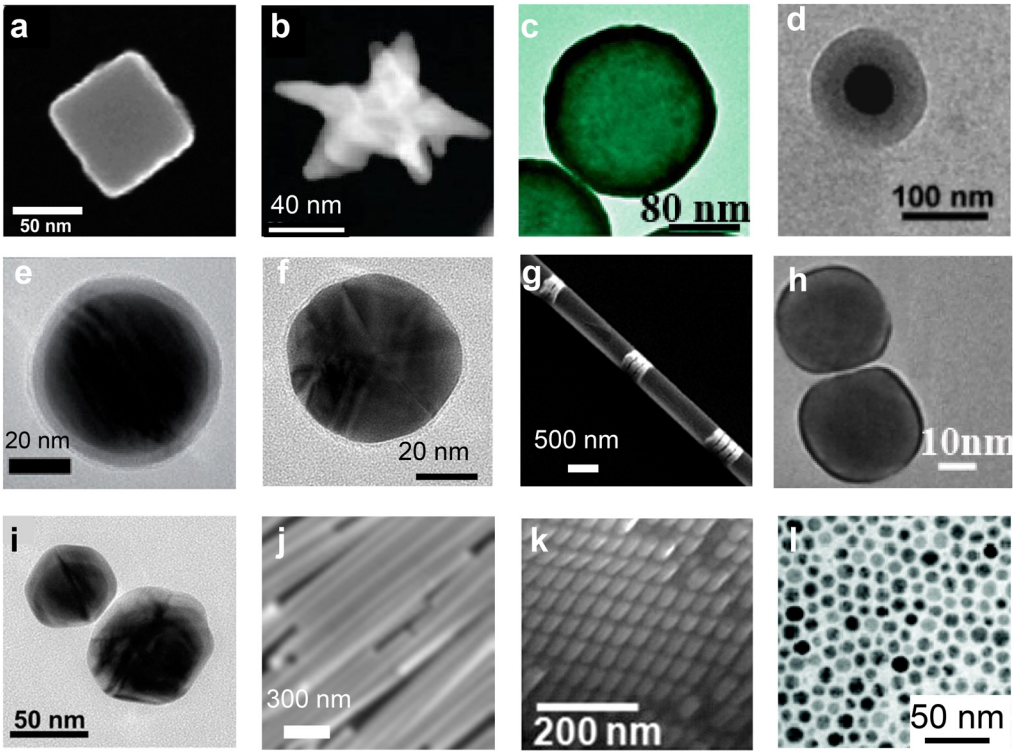

Fig. 24 SERS-active nanoparticles synthesized using bottom-up method. (a) SEM image of a Ag nanocube. Reproduced from ref. 245 with permission. Copyright 2007 American Chemical Society. (b) High-resolution STEM dark-field image of a single Au nanostar. Reproduced from ref. 246 with permission. Copyright 2009 American Chemical Society. (c) A TEM image of SiO_2@Au nanoshells. Reproduced from ref. 198 with permission. Copyright 2007 American Chemical Society. (d) TEM image of a SERS-active Au nanoparticle coated with a 40 nm thick silica shell. Reproduced from ref. 247 with permission. Copyright 2003 American Chemical Society. (e) TEM image of the Au core-molecular tag-Ag shell nanoparticles. Reproduced from ref. 248 with permission. Copyright 2015 Wiley. (f) TEM image of a SiO_2 shell-isolated nanoparticle. Reproduced from ref. 20 with permission. Copyright 2010 Springer Nature. (g) SEM image of gapped nanowire structures with dimers, trimers and tetramers. Reproduced from ref. 197 with permission. Copyright 2006 by The National Academy of Sciences of the USA. (h) SEM image of a dimer of Ag nanospheres. Reproduced from ref. 191 with permission. Copyright 2009 American Chemical Society. (i) High-resolution TEM image of a single-DNA-tethered Au–Ag core–shell dimer. Reproduced from ref. 249 with permission. Copyright 2013 American Chemical Society. (j) SEM image of a Langmuir–Blodgett Ag nanowire monolayer deposited on a silicon wafer. Reproduced from ref. 250 with permission. Copyright 2003 American Chemical Society. (k) SEM image of Au nanorods 3D-supercrystals. Reproduced from ref. 193 with permission. Copyright 2011 by The National Academy of Sciences of the USA. (l) TEM image showing the size distribution of the 20 nm Ag nanoparticles. Reproduced from ref. 251 with permission. Copyright 2005 American Chemical Society.

Another breakthrough was made in 1999 by Porter and coworkers,[259] which employed dielectric shell coated Au nanoparticles with embedded molecules (Raman tag) that possess a high Raman scattering cross-section in the shell as Raman labels for bioanalysis. They[259] and Mirkin and coworkers[260] developed a Raman tag system, known as extrinsic Raman labels (ERLs) by functionalizing Au nanoparticles with a Raman reporter molecule. The ERLs are applied in sandwich immunoassay of biomolecules, where the SERS signals do not come directly from the biological analyte, but from the tag. Therefore, the sensitivity can be greatly improved and a library of ERLs can be implemented for analytical multiplexing.[261] In some cases, this Raman tagging system suffers from weak stability and easy aggregation. Although the aggregation issue can be addressed by proper surface modification,[262] the competitive adsorption between the tag molecules and the antibody or DNA on the Au surfaces may pose limitations in certain applications.

To address this limitation, Natan and coworkers further developed Au@tag@SiO_2 nanoparticles, incorporating Raman tags within a silica shell,[253] adapting Liz-Marzán's method.[263] These particles featured a 35 nm Au core and a 40 nm thick silica shell.[253] The silica shell protected the Raman tags, significantly enhancing the system's stability. Additionally, antibodies or DNA used in sandwich immunoassays could be assembled on the silica shell, preventing competitive adsorption with the Raman tags. This approach enabled the preparation of a large library of unique Raman tags, facilitating the probing of multiple biological components in both *in vitro* and *in vivo* environment (Fig. 25e).[264]

Nie and coworkers further enhanced the detection sensitivity of the Au@tag@SiO_2 system by replacing the tag with dye molecules (Fig. 24d and 25d).[247] In their system, SERS enhancement was combined with the SERRS effect of the dyes, resulting in total EFs up to 10^{13}–10^{14}, thereby opening new possibilities for ultrahigh-sensitive bioanalysis. They also explored alternative shell materials, such as multiple ligands[265] and polymers,[266] to accommodate different detection scenarios. These tagged core–shell nanoparticles have been widely used

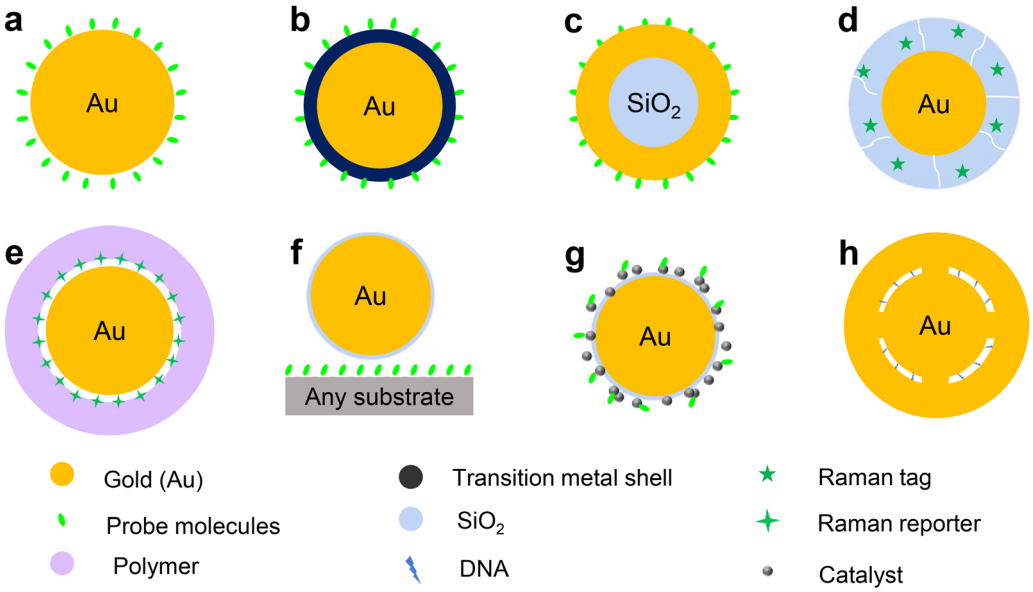

Fig. 25 Schematic of eight different strategies used for SERS measurements of probe molecules: (a) pure Au nanoparticles developed by Natan group.[187] (b) Au nanoparticle coated with an ultrathin transition metal shell by Weaver group.[252] (c) Au nanoshells by Halas group. (d) Au core coated with a porous and thick silica shell and Raman tags by Nie and Natan groups.[247,253] (e) Au core bonded with Raman reporters and coated with thiol-modified PEG and heterofunctional PEG (SH-PEG-COOH).[254] (f) Au core coated with a dense and ultra-thin silica shell by Tian group.[20] (g) Au core coated with a dense and ultra-thin silica shell and modified nano-catalysts by Li group.[255] (h) DNA-anchored nanobridged nanogap particles by Suh and Nam groups.[237]

in SERS bioanalysis, including *in vitro* diagnostics, *in vivo* spectroscopic detection, and image-guided cancer surgery.[28] For instance, they achieved the specific Raman detection of tumor cells *in vitro* and *in vivo* by conjugating these core–shell tag nanoparticles to tumor-targeting ligands.[254]

Building on the core–shell tag strategy, Ren and colleagues developed a quantitative SERS method in 2015, utilizing the tag as an internal standard (IS) (Fig. 24e).[248] Quantitative analysis in SERS is often challenging due to the low uniformity and reproducibility of SERS signals, which arise from the sensitivity of signal enhancement to the local structure of hot spots. In their systems, the IS molecules were embedded within the shell while the target molecules were adsorbed onto the outer surface. This configuration prevents competition for surface binding sites, ensuring that the IS signal remains unaffected by the surrounding detection environment. The IS signal effectively corrects for signal fluctuations caused by variations in the SERS substrate and detection conditions, enabling accurate quantitative SERS analysis across diverse environments (see Section 4.8 for details).

However, it should be noted that strong Raman enhancements have predominantly been obtained on Au, Ag, Cu nanoparticles or nanostructures, a limitation commonly referred to as the ''material limitation of SERS''. This limitation has significantly hindered the applications of SERS in the study of important surface and interface processes of a great diversity of materials. To address this long-standing issue, the ''borrowing SERS activity'' strategy was developed.[137–139,141,142,144] Early research primarily focused on depositing transition metal shells on rough Au or Ag electrode surfaces (see Section 3.1).

In 2002, Weaver group took the advantage of the advancement of nanoscience, introducing a synthesis nanoparticle overcoated electrode technique to replace the electrochemically roughened electrode using underpotential deposition (UPD) and redox replacement to coat Au nanoparticles with a transition metal layer, thereby creating more versatile nanoparticle-based SERS substrates.[252] This work, for the first time, transformed the SERS substrate from roughened electrodes to self-assembled nanoparticle structures, moving from ill-defined structures to well-defined ones. Initially, gold nanoparticles were assembled on an indium tin oxide (ITO) surface using a coupling agent that interacted with amine groups. A monolayer of Cu was then electrochemically deposited *via* the UPD method, then was chemically replaced by Pt or Pd. This process resulted in a pinhole-free, single-atomic-layer thick transition metal coating on the gold nanoparticles. As a result, the strong electromagnetic fields generated by the ordered nanostructure enhance the Raman signals adsorbed on the transition metal shells. Compared with traditional rough electrodes, such a nanoparticle-based substrate is more ordered, offer better control, and exhibit higher Raman enhancement capability. However, this process was highly complex, involving surface functionalization, electrochemical UPD, and redox replacement for the coating of each monolayer.

To address the issue of the cumbersome nature of the above method, Zhang and colleagues developed a more versatile and simplified wet-chemical synthesis technique to create Au@Pt core–shell nanoparticles and collaborated with Tian group to test the SERS performance.[267] By combining two approaches from Weaver group and Zhang group, Tian and colleagues have

systematically developed the ''borrowing SERS activity'' strategy based on the Au core-transition metal shell (Au@TM, TM = Pt, Pd, Rh, Ru, Co, Ni, *etc.*) nanoparticles, extending SERS applications to transition metal electrode surfaces. By precisely controlling the ratio of gold nanoparticles to transition metal precursors in the solution, accurate modulation of the transition metal shell can be achieved, thereby avoiding the cumbersome procedures associated with the above UPD method.[21,35] The transition metal shell comprised only a few atomic layers, with the inner Au nanoparticle serving as a plasmonic core to enhance Raman signals from molecules adsorbed on the shell.

This approach provided a strong enhancement (around 4–5 orders of magnitude), sufficient for molecular-level analysis.[35] A key advantage of this method was the ability to easily adjust the shell thickness by varying the ratio of Au nanoparticles to transition metal precursors, making the process both simple and flexible.[143,268] Additionally, the synthesized nanoparticles could be directly assembled on electrode surfaces without interference from coupling agents, thus facilitating their use in electrochemical studies.

It must be emphasized that although the ''borrowing SERS activity'' strategy has somewhat expanded material versatility, many metals, alloys, semiconductors, and polymers cannot be effectively utilized with such ultrathin coatings. Consequently, a fundamentally different approach is needed. Tian and colleagues identified this bottleneck:[21,35,269] all previous SERS-active substrates inherently functioned as both signal amplifiers and sites for molecular adsorption, creating a conflict between these two roles.[269] For example, it's nearly impossible to use one hand to cook while simultaneously using the other to write a paper! In other words, the traditional working mechanism of SERS is based on a contact mode, where the analyte must be directly adsorbed onto the surface of the Raman-enhancing material. However, for many studies, it is necessary to develop a non-contact mode, in which the analyte adsorbs onto the surface of the material of interest rather than directly contacting the SERS-active material, thereby avoiding signal interference.

The optimal solution is to separate these two functions: the SERS-active core should be coated by an inert layer that does not adsorb any probed molecules, allowing it to act solely as an electromagnetic field enhancer. This separation could overcome the limitations related to material and morphology, thereby improving the versatility and applicability of SERS studies. However, finding an effective method to coat a chemically and electrically inert ultrathin layer remains a significant challenge.

To address this issue, Tian group developed a new technique named shell-isolated nanoparticle-enhanced Raman spectroscopy or SHINERS by using Au nanoparticles coated with ultrathin, pinhole-free silica shells as Raman amplifiers (see Section 4.6.5).[20] The key technical challenge was synthesizing an ultrathin, pinhole-free dielectric shell. They devoted over two years optimizing the synthesis of ultra-thin and dense SiO_2 coated Au nanoparticles (Fig. 24f and 25f).[20] Characterization of such ultra-thin silica shells on the Au nanoparticles was also very challenging at that time. Collaborated with Wang on high-resolution TEM, they demonstrated the pinhole-free shells with a thickness of $\sim$2 nm have been homogeneously coated on the Au nanoparticles.[20]

The principle of SHINERS is fundamentally different from the Au@SiO_2 particles with thick and porous shells developed by Natan and Nie, as ultrathin but pinhole-free silica shells coated Au nanoparticles are employed as the Raman amplifiers. Meanwhile, the signals for the core–shell tag strategy are from the Raman markers, while the core–shell tag strategy produces signals from Raman markers, SHINERS detects signals directly from the target species, making it particularly promising for *in situ* monitoring of structural evolution and chemical reactions of target species (see Section 5.2.2).

However, widely used nanocatalysts are typically on a support (oxide, carbon, *etc.*) with a high specific surface area, and the concentration of active sites is relatively low. For oxide bulk materials, there is no strong plasmonic coupling effect between shell-isolated nanoparticles (SHINs) and supported nanocatalysts, leading to weaker enhancement (generally only 10^3–10^4). To address this issue, Li, Chen, Fu and colleagues developed a SHINERS-satellites strategy to achieve an *in situ* Raman study on practical catalysis,[255] by assembling nanocatalysts on the surface of SHINs, forming a nanostructure with Au as the core, silica as the shell, and nanocatalysts as satellites (Fig. 25g). Such a structure ensures that the nanocatalysts are within the enhancement range of Au, and the plasmonic coupling effect generated by hotspots of the SHINs particles leads to a Raman EF 2–3 orders of magnitude higher than that of dispersed SHINs. This configuration enables *in situ* study of the reaction processes on the surface of the nanocatalysts. Using this SHINERS-satellite strategy, the effects of catalyst composition, size, and support on the surface reaction processes and catalyst performance were studied at the molecular level.[270]

Another interesting class of core–shell nanoparticles comprises the coating of SERS-active by thermosensitive polymer shells (*e.g.* poly-*N*-isopropylacrylamide, pNIPAM).[271] Through changes in the hydrophilic/hydrophobic character of the polymer shell, Liz-Marzán and co-workers demonstrated the possibility of reversibly trapping and detecting molecules without affinity for the metal surface, such as 1-naphthol.[271]

As the SERS signals from coupled nanoparticles are highly sensitive to the interparticle distance and orientation, to achieve uniform and reproducible SERS signals essential for the quantitative analysis, precise control of particle configuration is crucial. Controlling the coupling between nanoparticles is an effective approach to generate SERS hotspots. Mirkin and colleagues fabricated controllable Au disk dimers, trimers, tetramers, and pentamers using an on-wire-lithography method (Fig. 24g).[197] Xia and co-workers controllably synthesized Ag nanosphere dimers with a diameter of around 30 nm and an interparticle gap size of approximately 1.8 nm (Fig. 24h).[191] Controlled assembly of nanoparticles for SERS have also been demonstrated using DNA origami,[272] polymeric self-driven arrangements[273] and supramolecular chemistry[274] among other approaches. Nam and coworkers synthesized DNA-tethered Au nanosphere dimers overgrown

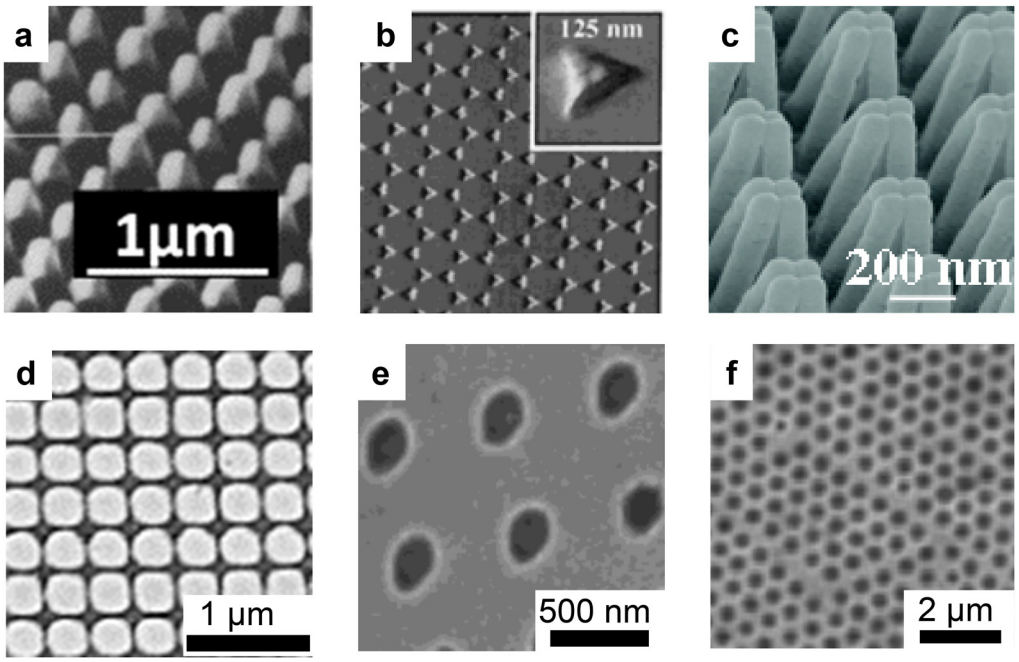

Fig. 26 Array substrate fabricated using top-down methods for SERS. (a) SEM image of a Ag particle array produced by evaporating Ag onto sides of SiO_2 posts. (b) AFM image of single-layer periodic particle arrays fabricated by NSL. (c) SEM image of closed Au nanofingers after molecule trapping. (d) SEM image of a periodic array of Ag particles, fabricated by electron beam lithography and reactive ion etching. (e) SEM image of a periodic arrays of sub-wavelength nanoholes in Au films, fabricated by focused ion beam milling. (f) SEM images of a sculpted substrate prepared using 600 nm diameter spheres. Reproduced from ref. 184, 192, 241 and 278–280 with permission. Copyright 1981 Elsevier. Copyright 2001&2010 American Chemical Society. Copyright 1998 Elsevier. Copyright 2004 American Chemical Society. Copyright 2005 Royal Society of Chemistry.

with a conformal Ag nanoshell (Fig. 24i).[236,249,275] These Au@Ag nanodumbbells with a ~1 nm nanogap exhibited high EFs capable of even single-molecule detection due to the ultra-narrow gap coupled with the Ag shell.

By uniformly synthesizing core–gap–shell nanoparticles with ~1 nm nanogaps at high yield, Nam group achieved significant SERS enhancement with a narrow EF distribution.[237] For the synthesis of the Au nanobridged-nanogap particles (AuNNPs), an Au core was grafted with dye-modified DNA followed by the budding and growth of an Au shell while leaving 1-nm gap inside the particle (Fig. 25h). The DNA strands acted as surface blocking ligands to generate the nanogap, with thickness equal to the width (~1 nm) of DNA.[276] The dual role of DNA – as both a morphology-determining agent and a carrier for incorporating Raman tags into the gap – became the basis for the design and synthesis of a series of nanoparticles with controlled interior and exterior nanogaps.

Solid SERS substrates require consistent SERS signals across a sufficiently large area. Therefore, achieving moderate reproducibility requires the nanoparticles on a solid support to be arranged in a close-packed manner. Yang and coworkers prepared a monolayer of Ag nanowire thin film using the Langmuir–Blodgett method (Fig. 24j),[250] while Liz-Marzán and coworkers synthesized a 3D superlattice of Au nanorods (Fig. 24k),[193] achieving uniform electric field enhancement as well as high reproducibility and sensitivity for SERS detection. Lee and coworkers prepared a high-density nanoparticle thin film (Fig. 24l) by self-assembling through the Langmuir–Blodgett (LB) technique on a water surface, serving as an excellent substrate for SERS.[251]

4.4.3 Development of SERS-active nanostructures by top-down fabrications. In addition to the previously mentioned methods, top-down approaches are employed to directly fabricate nanostructures on solid supports, avoiding contamination from the synthesis process. In 1981, Liao and colleagues from Bell Labs, along with Economou from MIT reported the preparation of SiO_2 array posts using UV lithography at 325 nm,[184] followed by Ag ellipsoidal arrays using vapor deposition. A Raman EF of up to 10^7 was observed on these structures (Fig. 26a).[184] Although photolithography methods can be used to fabricate large-area periodic structures, the high initial equipment costs limited early adoption in laboratories. Holographic (interference) lithography offers a more affordable approach for generating sub-wavelength features suitable for SERS using visible lasers,[277] though it is more complex than simple photolithography.

In 1995, Van Duyne and coworker developed nanosphere lithography (NSL), a cost-effective, easy-to-implement, inherently parallel, high-throughput, and versatile nanofabrication technique capable of producing a wide variety of nanoparticle structures and well-ordered 2D nanoparticle arrays (Fig. 26b).[278] Importantly, NSL allowed for systematic tuning of the localized surface plasmon resonance, enabling detailed studies on the relationship between nanoparticle optical properties and SERS EFs.[190]

Nanolithography techniques, such as electron beam lithography (EBL) and focused ion-beam (FIB) milling, provide

precise control over the size, morphology, and interparticle distance of nanostructures,[279–282] though achieving feature spacings below 10 nm remains challenging. Substrates produced by these methods are typically highly uniform and reproducible but offer moderate SERS enhancement. Li and colleagues employed imprint lithography to fabricate nanofinger arrays, allowing for the inexpensive duplication of identical structures over a large area (Fig. 26c).[192] Kahl and colleagues fabricated an array of Ag nanoparticles using EBL technique (Fig. 26d),[279] achieving a Raman EF one order of magnitude higher than that of island films. Brolo and colleagues utilized FIB technique to prepare periodic nanoholes in a Au film (Fig. 26e),[280] enabling SERS detection through extraordinary optical transmission.[282] Russell, Baumberg, Bartlett and coworkers fabricated sculpted SERS-active substrates by assembling a close packed monolayer of uniform polystyrene colloidal particles (ranging from 350 to 800 nm in diameter) on a Au-coated surface.[241] Subsequently, they electrodeposited Au through this template to create films with controlled thickness. Selecting suitable void diameters and film thicknesses allows for customization of the optical characteristics of SERS substrates, so as to achieve maximal enhancement (Fig. 26f).[241] Lipkowski and colleagues developed a Au nanowire array in which only transverse plasmons were exited, allowing for the measurement of temporal changes in the passive layer during Au dissolution in $Na_2S_2O_3$ solutions unaffected by the length of the nanowire.[283,284]

One major drawback of nanolithographic methods based on FIB and EBL is that they are not suitable for mass fabrication. However, they generate high quality nanostructures in silicon that can be used for a nanofabrication method based on template stripping.[285] In template stripping, a plasmonic metal (Au or Ag, for instance) is deposited in nanopatterned silicon substrates (prepared by methods such as EBL), and then an adhesive layer is applied to the deposited metal. Since the metal–silicon interaction is weak, the metal film can be simply separated from the silicon surface by pulling them apart. The resulting nanopatterned metal surface is ultra-smooth and mass fabrication with high reproducibility can be achieved using this method.[286]

4.4.4 Development of methods for guiding target objects into hotspots. In addition to creating hotspots in nanostructures, ensuring that molecules remain within these hotspots is also crucial for achieving highly sensitive and stable SERS. One approach is to increase the number of hotspots, enhancing the probability of molecules entering them, such as by aggregating nanoparticles into solid films. Alternatively, controlling the interaction between molecules and nanostructures can facilitate the adsorption of molecules onto the hotspots, for example, by employing capillary force to actively trap molecules into small gaps.

A common technique for generating high-density hotspots involves the formation of solid films from colloidal nanostructures. In 2001, Nie group pioneered the creation of nanostructured thin films by depositing monodisperse Ag nanoparticles onto polycarbonate membranes.[287] In 2005, Halas group fabricated highly ordered Au nanoparticle arrays with sub-10 nm spacing between adjacent nanoparticles, this is the beginning of the assembly of ordered nanostructures which exhibits high, stable, and reproducible SERS activity.[288] Fabrizio group demonstrated the super-hydrophobic surface to realize a concentration factor of at least 10^4 in comparison with conventional flat plasmonic substrate and break the diffusion limit with super-hydrophobic delivery of molecules to plasmonic SERS structures.[289] Notably, particle anisotropy and substrate coverage significantly impact the SERS enhancement of assembled solid films. Large-scale simulations by García de Abajo, Obelleiro and coworkers[290] showed that, for monolayer films composed of nanorods or nanospheres, the average SERS EF increases significantly with higher particle coverage due to stronger interparticle coupling (Fig. 27a and b). In contrast, for nanostars, the EF remains nearly constant.

These dry solid films can generate high-density hotspots, but they are often easily prone to damage from prolonged laser illumination, leading to challenges in spectral reproducibility and stability. To improve stability, Yang, Liu and coworkers proposed a dynamic SERS (D-SERS) method in 2014.[291] This technique relies on the transition of nanoparticles from a wet to a dry state, with measurements taken during the colloidal phase, including the solvent and evaporation processes. They discovered that during evaporation, a 3D hotspot matrix is formed with minimal particle size polydispersity and maximum uniformity in particle spacing-features distinct from the dry state (Fig. 27c). In addition to assembling films on solid substrates, methods have been developed to control the assembly of nanoparticles at liquid interfaces, which provides a self-healing and reproducible approach for the detection of multi-analytes in the aqueous. In 2012, Edel, Kornyshev and coworkers[293] successfully demonstrated the formation of densely packed nanoparticle arrays through a process of self-assembly at liquid–liquid or liquid–air interfaces. They were able to modulate the density of the nanoparticle arrays by altering the functional groups present on the nanoparticles, the pH level of the surrounding solution, and the concentration of salts within the medium. Subsequently, Kang and coworkers[292] demonstrated a versatile liquid–liquid interface capable of functioning as a substrate for the orientation of colloidal Au nanorods (GNRs), as shown in Fig. 27d and e.

An alternative approach to enhancing SERS detection is to guide molecules into hotspots. Conventional methods often fail to position analytes in these regions due to contamination by impurities or ligands during the preparation process. Additionally, spatial constraints can prevent molecules from entering the tiny gaps between nanoparticles. Fang, Ren and coworkers introduced the buoyant plasmonic-particulate-based few-to-single particle-nano-sensors method, leveraging force analysis at three-phase interfaces and the Young–Laplace equation.[294] This approach not only mitigates the coffee-ring effect but also enhances analyte enrichment in plasmonic sensitive sites. Inspired by transpiration in plants, where capillary action and osmotic pressure facilitate water transport, Yang and coworkers

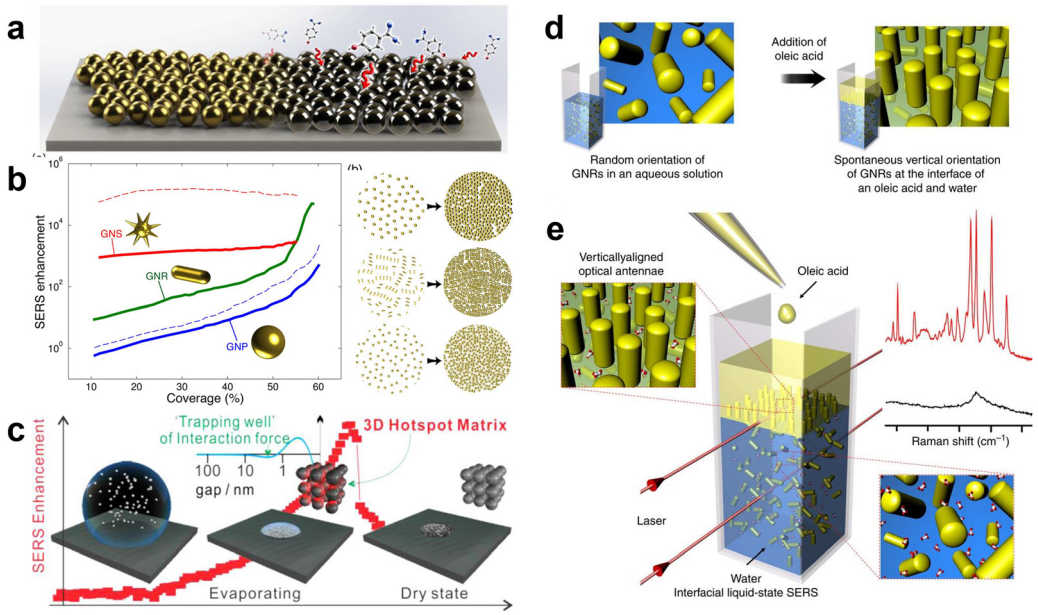

Fig. 27 (a) Simulation model of molecular coverages on a randomly arranged monolayer of Au nanospheres (GNPs) deposited on glass. (b) Density dependence of SERS performance in planar monolayers of nanoparticles with varying morphologies. Particle coverage is defined as the fraction of the area occupied by the projection of the metal along the plane normal. Figures a and b are reproduced from ref. 290 with permission. Copyright 2016 American Chemical Society. (c) 3D hotspot matrix of Ag sols generated during the water evaporation process. The sketches representing (I) a droplet of Ag sols on a hydrophobic surface, (II) the adhesive-force-constructed closely packed particles in 3D space formed in the water-evaporation process, and (III) the aggregation and deposition of particles on the dried substrate, which quenches the 3D hotspot matrix. Figure c is adapted from ref. 291 with permission. Copyright 2014 American Chemical Society. (d) Spontaneous and collective vertical alignment of GNRs (GNRs) at the oleic acid–water interface. (e) Interfacial liquid-state label-free detection method consists of three steps including mixing GNRs and targets, molecules, adding oleic acid, and conducting Raman measurements at the clearly visible interface. Figures d and e are reproduced from ref. 292 with permission. Copyright 2013 Springer Nature.

proposed the nanocapillary pumping model, which exploits capillary action and solvent evaporation to promote rapid and sensitive SERS detection.[295] This method ensures the ubiquity of hotspots and the inevitability of molecular entry, resulting in comprehensive hotspot activation. The nanocapillary pumping effect demonstrates versatility in detecting various analytes with high sensitivity and maintains stable signals for 1–2 minutes during dynamic detection processes.

The rapid advancement of nanotechnology has significantly propelled the development of SERS. However, SERS has also inherited some inherent limitations of nanotechnology, particularly the instability of nanostructures, leading to unstable SERS spectra. To address these challenges, a Faraday Discussions meeting was convened in London in 2005, focusing on several critical scientific issues: (1) what is the magnitude of the chemical enhancement mechanism, if it indeed exists? (2) Are SERS hotspots present, and if so, what are their origins and compositions? (3) How should SERS EFs be defined and quantitatively assessed? (4) Can nanotechnology facilitate the fabrication of substrates? The detailed topics are listed in Table 2.

In the concluding remarks of the conference, Natan posited a SERS version of the "uncertainty principle":[296] the greater the enhancement, the less we can know about the atomic-level details of the substructures involved. It's primarily due to the mobility of atoms on noble metal surfaces and the mobility of analyte molecules on such surfaces, which contributes to the phenomenon of SERS "blinking'. This principle underscores the complex relationship between enhancement and structural stability in SERS.

4.4.5 Active control of the nanogap. Previous methods used chemical synthesis and micro-fabrication to create nanostructures, however, the nanogaps between the nanostructures were normally fixed and unable to be adjusted. In 2006, Tian, Tao and coworkers developed an approach that combines SERS with a mechanically controllable break junction (MCBJ) technique to enable fine-tuning of the gap width.[297] A metal nanowire (such as Au) fixed onto a flexible substrate is stretched and broken into two nanotip-electrodes which serve as a model for a Au tip dimer when the substrate is bent. The well-defined nanogap can be modulated with a resolution up to sub-angström level, which enables the enhanced Raman signal to be characterized inside the nanogap (Fig. 28a–c).

In 2013, Murakoshi, Kiguchi and colleagues used the MCBJ technique to simultaneously measure the conductivity and the SERS of a single 4,4′-bipyridine molecular junction in solution at room temperature (Fig. 28d and e).[298] The significant changes in SERS intensity and Raman vibrational band selectivity are related to the current fluctuations during the fracture and formation of single-molecule junctions. Through the mode

Table 2 The timetable and program of the Faraday discussions on SERS in 2005

Monday 19 September

	Session 1 Physical Models W. Ewen Smith, *University of Strathclyde, UK*
14:00	**Introductory Lecture:** Richard P. Van Duyne, *Northwestern University, USA*
15:00	**SERS Signals at the Anti Stokes Side of the Excitation Laser in Extremely High Local Optical Fields of Silver and Gold Nanoclusters** Katrin Kneipp, *Harvard Medical School, USA*
15:30	**On the Importance of Optical Forces in Surface-Enhanced Raman Scattering (SERS)** Mikael Käll, *Chalmers University of Technology, Sweden*
16:30	**Single Molecule Sensitivity in SERS: Importance of Junction of Adjacent Ag Nanoparticles** Masayuki Futamata, *National Institute of Advanced Industrial Science and Technology, Japan*
17:00	**Vibrational Pumping and Heating under SERS Conditions: Fact or Myth?** Eric C. Le Ru*, *Victoria University of Wellington, New Zealand*
17:30	**A Study of Local Heating of Molecules under Surface Enhanced Raman Scattering (SERS) Conditions using the Anti-Stokes/Stokes Ratio** Robert C. Maher*, *Imperial College London, UK*

Tuesday 20 September

	Session 2 Novel Chemistries / Chemistry of SERS Richard Brown, National Physical Laboratory, UK
09: 30	***In Situ* Surface-Enhanced Raman Scattering Spectroelectrochemistry of Oxygen Species** Takashi Itoh, *Tohoku University, Japan*
10: 00	**Long Distance Electron Transfer in Cytochrome C Oxidase Immobilised on Electrodes. A Surface Enhanced Resonance Raman Spectroscopic Study** Peter Hildebrandt, *Technische Universität Berlin, Germany*
10: 30	**Surface-Enhanced Raman Scattering Investigations of 4-Nitro(Pyridine *N*-Oxide) and 4,4'-Azobis (Pyridine *N*-Oxide) Adsorbed on Silver Colloidal Nanoparticles** Barbara Pergolese, *University of Trieste, Italy*
11: 30	**Probing Strong Optical Fields in Compact Aggregates of Silver Nanoparticles by SERRS of Protoporphyrin IX** Blanka Vlčkovà, *Charles University in Prague, Czech Republic*
12: 00	**Practical Control of SERRS Enhancement** Dale Cunningham, *University of Strathclyde, UK*
	Session 3 Surfaces / Substrates Alan Creighton, University of Kent, UK
14: 00	**Surface-Enhanced Raman Scattering from Transition Metals with Special Surface Morphology and Nanoparticle Shape** Zhong-Qun Tian, *Xiamen University, China*
14: 30	**A TEM and Electron Energy Loss Spectroscopy (EELS) Investigation of Active and Inactive Silver Particles for Surface Enhanced Resonance Raman Spectroscopy (SERRS)** Imran Khan, *Imperial College London, UK*
15: 00	**Control of Near-Infrared Optical Response of Metal Nano-Structured Film on Glass Substrate for Intense Raman Scattering** Kei Murakoshi, *Hokkaido University, Japan*
16: 00	**Sculpted Substrates for SERS** Andrea E. Russell, *University of Southampton, UK*
16: 30	**Electromagnetic Modelling of Raman Enhancement from Nanoscale Substrates: A Route to Estimation of the Magnitude of the Chemical Enhancement Mechanism in SERS** Richard J.C. Brown, *National Physical Laboratory, UK*
17: 00	**Nanoscale Imaging of Carbon Nanotubes using Tip Enhanced Raman Spectroscopy in Reflection Mode** Debdulal Roy, *University of Cambridge, UK*

Wednesday 21 September

	Session 4 Applications Lesley Cohen, Imperial College London, UK
09:00	**Re-examining the Origins of Spectral Blinking in Single-Molecule and Single-Nanoparticle SERS** Shuming Nie, *Emory University, USA*
09:30	**A New Approach for DNA Detection by SERRS** Duncan Graham, *University of Strathclyde, UK*
10:00	**SERS Platforms for High Density DNA Arrays** Mino Green, *Imperial College London, UK*
11:00	**Surface-Enhanced Raman Scattering for the Rapid Discrimination of Bacteria** Royston Goodacre, *University of Manchester, UK*
11:30	**Synthesis and Characterization of SERS Gene Probe for BRCA-1 (Breast Cancer)** Anjali Pal, *Indian Institute of Technology, India*
12:00	**SERRS Labelled Beads for Multiplex Detection** Ailie F. McCabe, *University of Strathclyde, UK*
12:30	**Concluding Remarks** Michael Natan, *Nanoplex Technologies Inc., USA*

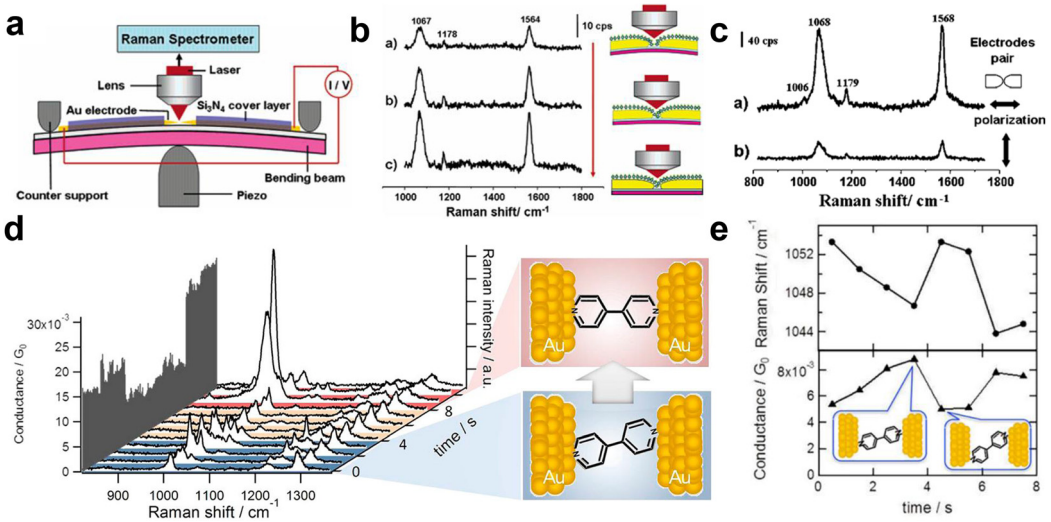

Fig. 28 Combined mechanically controllable break junction (MCBJ) and SERS. (a) Schematic of the setup. The gap distance between two Au electrodes can be precisely controlled by the bottom piezoelectric transducer. With laser illumination, the gap also hosts as the hotspots for SERS measurement. (b) SERS of 1,4-benzenedithiol in the nanogap with the process of bending the metallic electrodes pair. The gap width 8 Å, 6 Å, 4 Å, respectively (from top to bottom panel). (c) The distinct different SERS signals when the Au electrodes pair has its axis parallel and perpendicular to the incident polarization. (d) Three types of SERS spectra of a single 4,4′-bipyridine molecule junction and possible geometrical structures. (e) The SERS signal fluctuation along with the conductance changes resulting from the junction configuration changes. Figures are reproduced from ref. 297 and 298 with permission. Copyright 2006 & 2012 American Chemical Society.

switching between b_1 and b_2 in SERS, the authors observed the movement of 4,4′-bipyridine between vertical and tilted configurations in the nanogap inside the Au electrode pair. This study indicates that individual molecules at metal gaps generate Raman spectra, which contain detailed information on molecular electronic and geometric structure.[298]

The MCBJ technique allows for precise and stable adjustment of the separation between the electrodes on a chip by using a piezoelectric transducer, ranging from a few angströms to several nanometers with a resolution of one angström. Therefore, this method also makes it possible to monitor chemical reactions at the single-molecule level inside the nanogap. In 2018, Hong, Yang and colleagues investigated the charge transport through a BDT molecular junction with a combined MCBJ and SERS approach.[299] They observed Raman characteristic peaks of S–S bonds in different conductance states of the BDT molecule, revealing that the BDT molecules had undergone dimerization. This finding demonstrated that the low conductance state originated from dimerized-BDT, thereby resolving a long-standing controversy regarding the relationship between BDT molecular junction configurations and their multiple conductance states.[299]

In 2016, the first work on selective adsorption sites on the single-molecule scale was carried out using this technique by Kiguchi group.[300] The SERS signals distinguished three substates of 1,4-benzenedithiol generated by different adsorption sites, corresponding to the bridge, hollow, and atop sites, respectively. This study reveals that the SERS intensity depends on the strength of the molecule–metal interaction, showing the interdependence between the optical and electronic properties of single-molecule junctions.[300] On this basis, they reported in 2019 that the modulation and monitoring of aminobenzenethiol and benzenedithiol single-molecule adsorption sites was achieved by means of regulating the applied bias voltage, which provides new perspectives for studying and controlling single-molecule circuits.[301]

4.4.6 Breakdown of selection rules in the extremely strong hotspots. With the continuous advancement of nanotechnology, significant progress has been made in the fabrication and characterization of nanostructures. This has enabled the construction of much smaller SERS/TERS hotspots, reaching even the atomic scale. The small mode volume results in strong electric fields with fine structures of both vacuum fluctuation and light confined inside the hotspots. In such diminutive hotspots, the interaction between molecules and confined electromagnetic fields is substantially enhanced, rendering the approximations in the standard spectroscopic analysis, commonly based on weak coupling and homogeneous illumination, potentially invalid.[302] Moreover, as the hotspots' volume becomes comparable to that of the molecules, the dipole excitation approximation is no longer adequate, possibly leading to significant changes in molecular transition selection rules. These effects contribute to the emergence of new SERS/TERS phenomena and mechanisms within the hotspots. We here introduce that the breakdowns of Kasha's rule and long wavelength approximation result in an ultrafast fluorescence and the modifications of the excitation selection rule. These phenomena open new research fields in SERS and TERS.

The radiative de-excitation rate of surface-enhanced fluorescence (SEF) has been assumed to be smaller than the vibrational decay rate of the electronic excited state as shown in

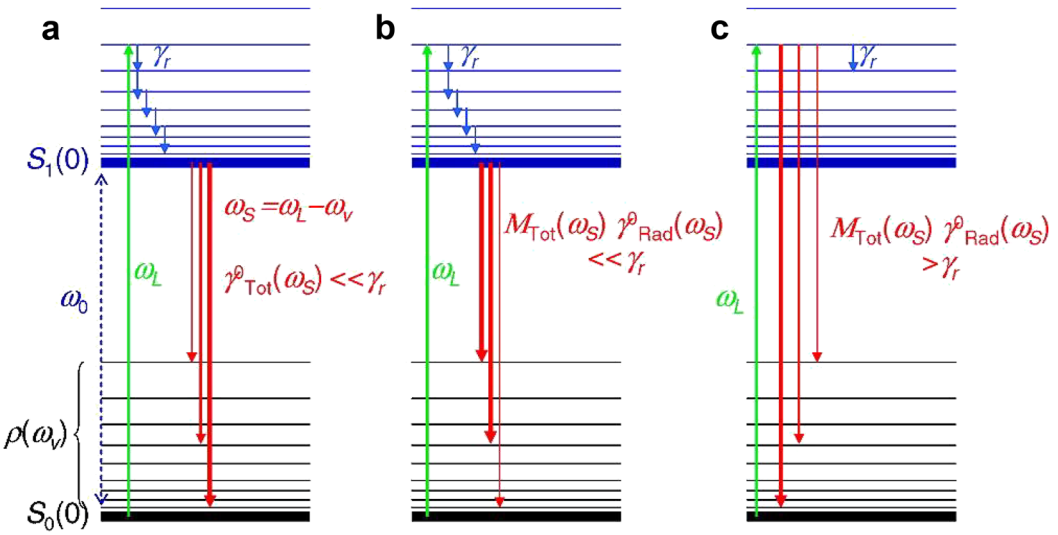

Fig. 29 Simplified Jablonski diagrams depicting the fluorescence processes in the three possible situations: (a) Standard fluorescence; (b) SEF in which the vibrational decay rate is faster than the SEF rate; and (c) SEF in which the vibrational decay rate is slower than the SEF rate. Reprinted with permission from ref. 303 Copyright 2007 American Chemical Society.

Fig. 29a and b. However, the radiative de-excitation rate for a molecule inside the hotspots is largely enhanced by plasmon resonance and can become greater than the vibrational decay rate.[303] Thus, in this situation SEF light can be emitted from a vibrational excited state as shown in Fig. 29c, resulting in broadband light emitted in SEF which appears as a background in SERS and TERS spectra. This type of SEF process means the breakdown of Kasha's rule, in which an excited molecule is supposed to emit fluorescence from the vibrational ground state.[304] This type of SEF is useful for investigating ultrafast electronic dynamics in the electronic excited state of molecules inside the hotspots.

In free space, the length of oscillation of the electromagnetic fields in an optical cycle is much larger than that of a molecule (and thus the extension of the electronic transitions). This assumption is referred to as the long wavelength approximation, in which the excitation selection rule does not depend on the spatial extension and structure of light. However, the volume of the electromagnetic field mode can be compressed to nanometer-size within hotspots. Within the hotspots, the gradient of the electric field escalates to dimensions commensurate with the electronic transition scale of a molecule. This escalation precipitates the failure of the long-wavelength approximation.[305] Hence, the excitation of multi-poles, such as a quadrupole, becomes non-negligible as shown in Fig. 30.[306] In such a situation, the excitation selection rule needs to be modified. This modification was investigated through the observation of forbidden transition modes, such as the activation of certain IR modes in SERS and TERS spectra. For example, Murakoshi and colleagues reported the observation of the dipole forbidden electronic transition through the SERRS of a carbon nanotube located in a plasmonic nanogap. They presented evidence suggesting the field-gradient effect would affect SERS.[305]

In Section 4.5.3, we will address the achievement of sub-nanometric resolution in TERS thanks to the use of atomic-scale localization of electromagnetic fields. Such localization also affects Raman selection rules, by activating forbidden vibrational modes for homogeneous illumination. An example of such activation of Raman lines by atomic-scale hot spots is shown in Fig. 38d.

4.4.7 Development of Raman instrument for high sensitivity. In addition to the nanostructure optimizations and fabrications, the development of Raman instrumentation also plays essential roles in improving sensitivity. The discovery of the Raman effect nearly a century ago originated from a seemingly simple yet rationally and systematically designed experimental apparatus. The core of the SERS field is the continuous enhancement of detection sensitivity, from the origins of the SERS field 50 years ago to the latest advancements. We have witnessed various examples of introducing and designing special or completely new instruments to meet the needs of innovative experiments and to verify new theoretical models. This includes performance improvements and inventions in the entire instrumental system, from optical excitation and collection macroscopic devices to microscopic plasmon-enhanced nanostructure designs, as well as instrument-driven and data processing software. For example, in the linear response regime, the surface enhancement Raman intensity (I_{SERS}) can be expressed as:[165]

$$I_{SERS} = \frac{2^7}{3^2}\frac{\pi^5}{c^4} I_0 (\nu_0 - \nu_{mn})^4 \sum_{\rho\sigma} \left| \left(\alpha_{\rho\sigma}\right)_{mn} \right|^2 NA\Omega Q T_m T_0 G_{SERS} \quad (4)$$

where c denotes the speed of light; I_0 represents the intensity of the incident light; the frequencies of the incident light and the vibrational normal mode are indicated by ν_0 and ν_{mn},

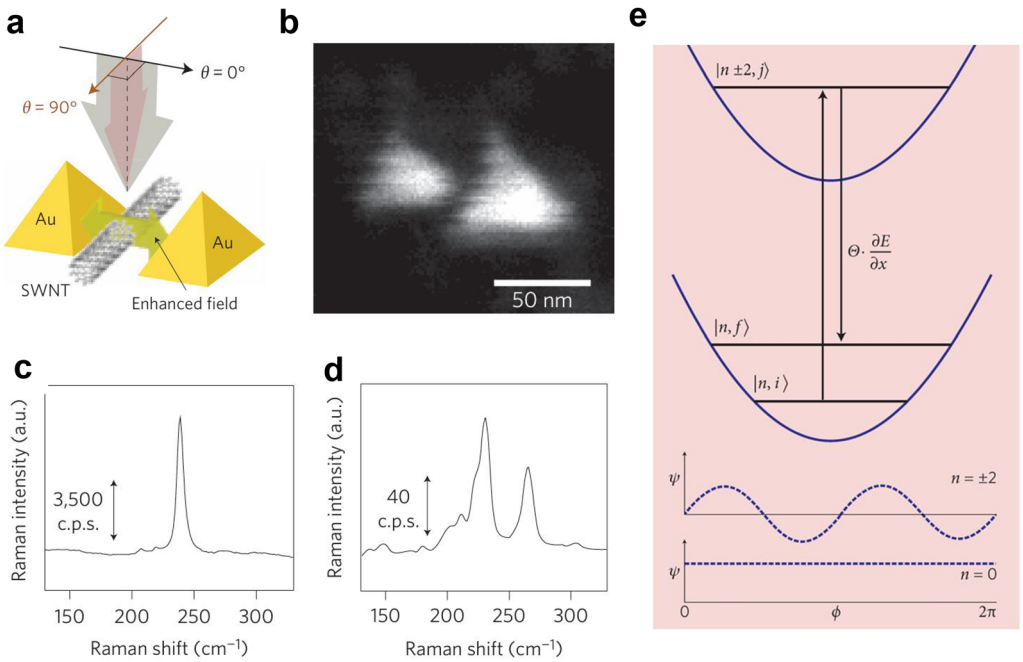

Fig. 30 Selection-rule breakdown in plasmon-induced electronic excitation of an isolated single-walled carbon nanotube (SWNT). (a) Illustration of an SWNT lying in the nanogap of a dimer and the enhanced field polarization. (b) SEM images of a well-defined Au nanodimers. (c) SERS spectra showing the radial-breathing (RBM) mode of an isolated SWNT in the nanogap. The applied-field polarization is parallel to the long axis of the nanodimer. (d) Typical resonance Raman scattering spectrum of bundled SWNTs dispersed on flat glass. (e) The forbidden electronic transitions for resonance SERS spectroscopy. The $\Delta n = \pm 2$ transition has a nonzero quadrupole transition moment Θ, which couples to the field gradient to give resonance SERS. Figures are reproduced from ref. 305 and 306 with permission. Copyright 2013 Springer Nature.

respectively; $(\alpha_{\rho\sigma})_{mn}$ refers to the $\rho\sigma$ component of derivative of the molecular polarizability associated with the normal mode; N is the number density of the adsorbate on the surface (molecule cm^{-2}); A indicates the surface area that is illuminated by the laser beam (cm^2); Ω is the solid angle of the collection optics (sr); QT_mT_0 is the product of the detector efficiency, the throughput of the dispersion system, and the transmittance of the collection optics; and G_{SERS} is the SERS EF discussed in Section 4.4.1.

The G_{SERS} and $(\alpha_{\rho\sigma})_{mn}$ terms represent the contributions from electromagnetic fields and from adsorbed molecules, respectively, while QT_mT_0 represent instrumental contributions. Accordingly, SERS sensitivity can be improved from different aspects including increasing the SERS activity of the substrates (electromagnetic fields, the G_{SERS} term), utilizing molecules with large Raman cross-sections including those with resonance Raman effects (the $(\alpha_{\rho\sigma})_{mn}$ term), as well as continuously improving the collection and detection efficiency of instruments, *etc.* Therefore, integrating experiments, theory, and instrumentation into a cohesive trinity is essential and even decisive for making breakthroughs. A comprehensive and systematic consideration of the entire SERS process is necessary. This holistic approach extends beyond merely selecting appropriate nanostructures, molecules, and excitation wavelengths. It necessitates the rational optimization of efficiency at each stage of the instrumental system, encompassing excitation, collection, grating dispersion and detector detection.

For example, in the STM-Raman setup as we explain in the following section, optical fibers were arranged in a circular shape to better collect scattered light and improve sensitivity. In early confocal Raman systems as well as the first EC-TERS systems, instrument improvements were crucial for achieving high sensitivities.

4.4.8 Development of chemical enhancement mechanism. In fact, the scientific significance of the SERS effect could be broader than commonly perceived. It encompasses any molecule/surface system where there is an enhancement of the Raman scattering cross-section of adsorbed molecules compared to the same molecules in the liquid or gas phase (referred to as free molecules). The interaction between adsorbed molecules and the material surface generally alters the spectroscopic signals from molecules, either enhancing or diminishing them, which is a common and studied phenomenon.[21,165] The relevant surface selection rules are within the realm of surface science, particularly surface spectroscopy.

It is important to clarify that physical enhancement based on surface plasmons can increase the Raman scattering cross-section by a factor of 10^6 to 10^8 (the G_{SERS}) term in eqn (4) playing a dominant role.[35,307,308] In contrast, chemical enhancement typically results in an increase of 1–3 orders of magnitude (the $(\alpha_{\rho\sigma})_{mn}$) term in eqn (4), even higher SERS EF were predicted.[309–311] Physical enhancement is primarily responsible for the enhancement of the SERS effect; without the plasmonic enhancement mechanism, the establishment and advancement of the SERS field would not have occurred.

However, chemical enhancement should not be overlooked. A comprehensive understanding and effective utilization of the SERS effect necessitates consideration of both physical and chemical enhancement mechanisms. Moreover, the study of chemical enhancement mechanisms has practical applications. From a surface chemistry perspective, comprehending the interaction between molecules and surfaces *via* SERS requires knowledge of chemical enhancement mechanisms. Crucially, for applying SERS in diverse analytical fields, particularly in quantitative or semi-quantitative analysis systems aimed at commercialization, a clear grasp of chemical enhancement mechanisms is indispensable. Hence, researchers continue to make sustained efforts and contributions in exploring these chemical mechanisms, including unified mechanisms that incorporate both physical and chemical enhancement.[312–314]

The utilization of the chemical enhancement is intrinsically linked to a profound understanding of the CE mechanism in SERS. During this period, significant theoretical advancements were also made on the basis of the first-principle *ab initio* quantum chemical calculations. It is summarized that the CE mechanism mainly involves three scenarios contributing to the total polarizability part of $\sum_{\rho\sigma}\left|\left(\alpha_{\rho\sigma}\right)_{mn}\right|^2$ in eqn (4):[166,310,315] (1) enhancement arising from chemical bonding interactions in the ground state between the molecule and the nanoparticle, which occur independently of any excitations within the nanoparticle-molecule system. (2) Resonance Raman enhancement, where the excitation wavelength aligns with an internal transition of the molecule. (3) CT resonance Raman enhancement, characterized by the excitation wavelength being resonant with charge-transfer transitions between the metal and the molecule.

The non-resonant chemical mechanism is challenging to detect experimentally due to its contribution to the overall SERS EF being strongly dependent on physical or chemical adsorption of probe molecules, despite ongoing experimental endeavors to quantify it. Theoretical investigations are expected to play a crucial role in clarifying this mechanism, as it is likely shaped by the local molecular environment.[310] This environment can be effectively modeled using small metal clusters, which allow for the representation of the localization of chemical bonds as determined through density functional theory calculations. Consequently, numerous electronic structure investigations have been conducted on the impact of small metal clusters on the Raman characteristics of small molecules.[315–317] Experimentally, a significant chemical EF was observed in the specific wagging vibrational mode of benzyl radical and aniline adsorbed on Ag electrodes and Ag colloids.[311,318]

The resonance Raman effect is observed when the wavelength of the incident laser light corresponds to the electronic absorption energy of the sample being analyzed, significantly boosting the likelihood of Raman scattering by several orders of magnitude. When a molecule is adsorbed onto the surface of a plasmonic-active nanostructure, SERRS can be utilized for detection.[14,24,319,320] The added signal amplification stemming from this molecular electronic resonance renders SERRS an exceptionally sensitive vibrational spectroscopic method. Although SERRS can achieve higher sensitivity, resonance Raman imposes limitations on the universality of molecules as well as laser excitation wavelengths and may introduce significant fluorescence background.

4.4.9 Development of charge transfer mechanism. The CT mechanism can be considered to be the direct CT process and the indirect CT process for adsorbed molecules on roughed metal surfaces.[321] The Raman intensities of active vibrational modes were theoretically based on the surface resonance-like Raman theory, which describes the Franck–Condon term related to two electronic states and the Herzberg–Teller vibronic term related to three electronic states. First-principles *ab initio*/density functional theory (DFT) calculations can directly be used to predict the electronic and vibrational properties close to some real systems.

It should be noticed that two distinct types of electric fields, the optical electromagnetic field and the electrochemical electrostatic field, co-exist in electrochemical interfaces systems with various nanostructures (Fig. 31).[166] Both chemical and physical enhancements can be influenced to some extent by applying an electrode potential, making EC-SERS one of the most complex systems in SERS. Significant efforts have been made to thoroughly understand SERS and analyze EC-SERS spectra based on chemical and physical enhancement mechanisms, providing valuable insights into the mechanisms of electrochemical adsorption and reactions.

The intensity of SERS observed in various EC-SERS systems is notably influenced by both the applied potential and the nature of the metal substrate. This observation provides compelling evidence for a synergistic relationship between CT and EM enhancement. As depicted in Fig. 31a, HOMO and LUMO refer to the highest occupied molecular orbital and the lowest unoccupied molecular orbital of the adsorbed species, respectively.[166] Additionally, $\Psi_g(V_i)$ represents the molecular adsorption ground state, while $\Psi_{CT}(V_i)$ denotes the photon-induced CT excited state, which is generated by the transition from a filled metallic level to the LUMO of the adsorbed molecule at an applied potential, V_i. The right part of Fig. 31a presents a conceptual picture relevant to not only the energy level but also the vibronic energy states along the vibrational coordinates.[166] It displays much more clearly the change of the surface electronic ground state and corresponding vibrational levels of the adsorbate with electrode potential. Please note that each energy level represents the total energy of the combined system of the adsorbed molecule and interacting metal electrode (molecule/metal) in the excited or ground electronic state that can be influenced by applied potentials.

It is assumed that the energy position of the photon-driven CT state remains constant regardless of the applied potential. The observed SERS signal initially increases and then decreases as the electrode potential is adjusted to more negative values. This variation in SERS intensity can be attributed to the photon-driven CT from the metal to the molecule, as explained by the energy levels or states associated with interfacial energy

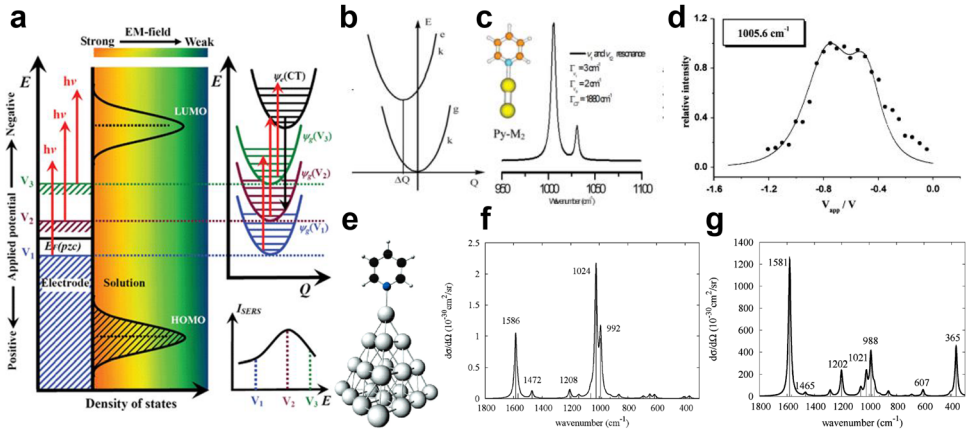

Fig. 31 (a) Schematic diagrams of the photon-driven CT from a metal electrode to an adsorbed molecule in the EC-SERS system. Left: The conceptual model of the energy levels changed with the electrode potential in the CT process. Right: The relevant energy states involved in the electronic levels and the vibrational levels in the CT process. Right bottom: The corresponding SERS intensity-potential profile and V_i denotes the applied potential. Reproduced from ref. 166 with permission. Copyright 2008 Royal Society of Chemistry. (b) Displaced harmonic potential energy curves of both electronic ground state and CT state. (c) The relative Raman intensities of the ring breathing mode and triangle deformation mode of pyridine binding to Ag dimer (Ag_2). Figure c is reproduced from ref. 322 with permission. Copyright 2004 Elsevier. (d) The potential-intensity profile of the ring breath mode for pyridine adsorbed on Ag electrodes reproduced from DFT calculations and Raman scattering theory. Reproduced from ref. 323 with permission. Copyright 2005 AIP publishing. (e) Pyridine–Ag_{20} complex model. (f) Simulated Raman spectrum and (g) CT resonant-like Raman spectrum from pyridine–Ag_{20} complex. Figures (e)–(g) are reproduced from ref. 324 with permission. Copyright 2006 American Chemical Society.

level alignment. As illustrated on the left side of the figure (energy level concept), at the applied potential V_1, the conditions are inadequate to generate photon-driven CT states on the surface with an excitation energy of $h\nu$. Consequently, the observed changes in relative SERS intensity are primarily governed by bonding effects. When the potential is adjusted to V_2, the increase in the Fermi level of the metal electrode aligns the excitation photon energy with the required energy for photon-driven CT, resulting in resonance-like Raman scattering and a pronounced enhancement in the SERS intensity of the associated vibrational modes. However, if the potential is further shifted to V_3 in the negative direction, the excitation energy no longer falls within the optimal resonance conditions, leading to a reduction in the contribution of the CT states to the overall SERS signal.

These early studies were based mainly on phenomenological theoretical models to consider the mechanism of CT enhancement. In the early 2000s, the theoretical models were investigated on the basis of DFT calculations combining with the molecule–metallic cluster model or the first-principles periodic slab model.[315] By combining the DFT calculations and Raman scattering theory, the CT enhancement mechanism was found to be closely associated with the displacement of the minima of the excited state with respect to the ground states along a given normal coordinate with the totally symmetric representation (Fig. 31b).[310] When the effect of applied potentials was considered to be equivalent to tuning the Fermi level of metal electrodes, the resonance-like CT enhancement mechanism was realized to match the energy levels from excitation laser wavelength through applied potentials at electrochemical interfaces (Fig. 31c).[322] In this case, the ring breathing mode of pyridine interacting with a silver cluster displayed a stronger Raman signal than that of the triangle deformation mode when the photon-driven CT mechanism occurs.

For pyridine adsorbed on Ag electrodes, the CT mechanism combining with the chemical adsorption interaction describes the potential-dependent Raman intensity profile of the ring breathing mode (Fig. 31d) well even using a small metallic cluster.[323,325] Such a simple model is reasonable to describe the interfacial chemisorption bond from the basic bonding principles, *i.e.*, energy similarity, symmetry matching, and maximum overlap of the interacting orbitals. Furthermore, the potential energy surfaces of the photon-driven CT excited state should be predicted well based on the TD-DFT approach for pyridine adsorbed on silver surfaces.

The resonant-like Raman effect needs to accurately consider the interfacial energy state alignment. Schatz and coworkers made significant contribution to understand the chemical enhancement mechanism.[326,327] Their TD-DFT approach can predict the significant enhancement of several CT excited states contributing to the SERS intensities of pyridine–Ag_{20} to mimicking the pyridine adsorbed on Ag colloids. The use of large metallic clusters can improve the utility of the calculations in describing the characters of interfacial chemical bonds at different surface sites. Jensen and colleagues found that the simulated SERS spectra still strongly depend on the specific chemisorption bond for pyridine adsorbed on surface active sites (Fig. 31e and f).[324] The interfacial energy level alignment also directly influences the relative Raman intensities of pyridine–Ag_{20} (Fig. 31g).[324]

The idea further was extended by Jensen and colleagues to investigate the molecule–surface chemical coupling SERS effect from electronic structures of *meta*- and *para*-substituted pyridines interacting with a Ag_{20} cluster.[316] They found that the magnitude of chemical enhancement is governed to a large

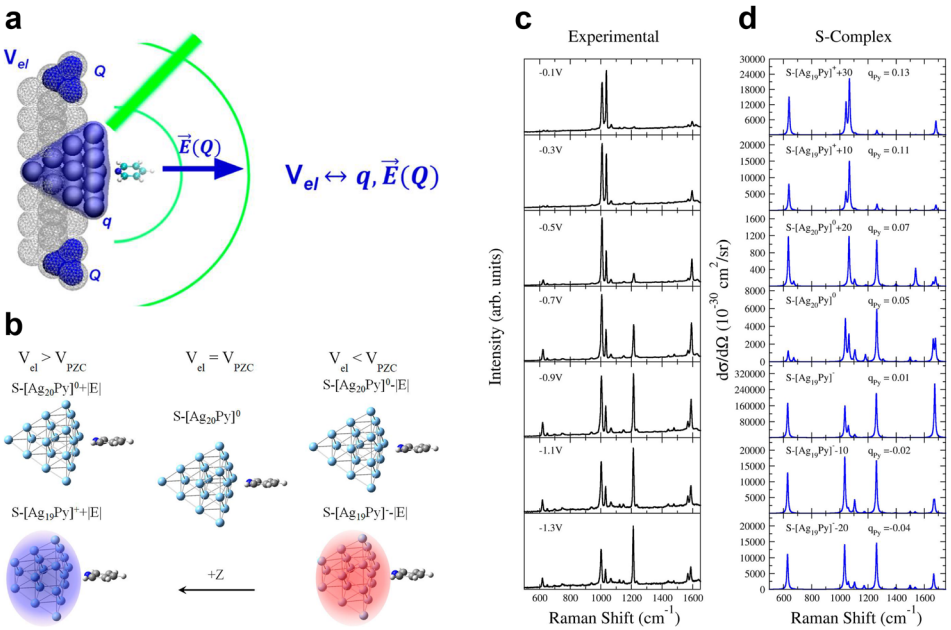

Fig. 32 Electrochemical SERS enhancement mechanism of pyridine on silver electrodes. (a) Molecular model for SERS of pyridine that is adsorbed on Ag electrodes in surface S-complexes. (b) The charges on the adsorption site are included explicitly in the metal cluster when considered, while an external electric field applied along the Z-direction reproduces the effect of the nearby surface charges. (c) Experimental SERS and (d) calculated resonance Raman spectra for the bright states for matched values of V_{el} and q_{Py}. Notice that each panel has a different Y-axis scale. Stick lines were convoluted with a Lorentzian of HWHM = 5 cm^{-1}. All E in 10^{-4} a.u. CAM-B3LYP-D3/6-31+G(2d,2p)/LANL2DZ level of theory. Figures are adapted from ref. 328 with permission. Copyright 2022 American Chemical Society.

extent by the energy difference between the highest occupied energy level (HOMO) of the metal and the lowest unoccupied energy level (LUMO) of the molecule. The trend was verified by considering substituted benzenethiols, small molecules, and silver clusters of varying sizes. The findings provide the framework for designing new molecules which exhibit high chemical enhancements.

The experimental and theoretical research by Aranda, Otero, Santoro and colleagues[328,329] have led to the development of a computational model for electrochemical surface-enhanced Raman scattering (EC-SERS). In this model, the surface excess charge induced by the electrode potential (V_{el}) was introduced by applying an external electric field to a series of clusters $[Ag_n]q$, specifically with (n = 20, q) values of (19, ±1) or (n = 20, 0), onto which a pyridine molecule is adsorbed (Fig. 32a). They estimated the EFs involved in SERS mechanisms, including chemical or non-resonant, and resonance Raman with bright states of the adsorbate, charge-transfer (CT) states, and plasmon-like excitations on the metal cluster (Fig. 32b). Employing DFT and TD-DFT calculations, the metal–molecule complexes were categorized based on the partial charge of the adsorbate. The primary properties influenced by V_{el} were analyzed concurrently, facilitated by vibronic resonance Raman calculations that identified shifts in vibrational wavenumbers and relative intensities.

By inspecting detailed experimental EC-SERS data (Fig. 32c), they tested the mentioned above model for pyridine adsorbed on Ag electrode. They noted that the electrode potential V_{el} has a remarkable effect on the simulated Raman spectra. The findings successfully replicated the majority of experimental observations, while also offering a critical evaluation of the approach's limitations (Fig. 32d). The explicit consideration of surface charges is essential for EC-SERS modeling, and the highest calculated EFs, ranging from 10^7 to 10^8, were attributed to the coupling between bright local excitations of the metal cluster and CT states. These results indicated that the importance of nonadiabatic effects in SERS and the capabilities of EC-SERS as the theoretical approach to study the coupling between the CT excited-state and plasmon-like states by tuning applied potentials.

To investigate the CT mechanism has opened the question of whether the possibility to induce chemical transformations by plasmonic hot carriers (hot electrons and hot holes). This can be rationalized as the reactive analogue of the well-established concept of optical hot spots to the chemical hot spots, which have drawn a great deal of attention to plasmonic nanostructures for their ability to tune the photochemical reaction efficiency and selectivity.[330–335] Thus it should be careful sometimes the observed SERS signals were products of photochemical reactions rather than the initially added probe molecules, such as *p*-aminothiophenol,[310,336] adenine,[337] and 8-bromoadenine.[338]

The photon-driven CT process was discovered that it can lead to profound changes in Raman spectra, in addition to changes of vibrational wavenumbers and relative intensities. In the initial stage of SERS study, these changes were often considered as negative examples of the photodecomposition or thermal decomposition caused by the focused lasers.

Recently, it was found that these changes in spectra resulted from the selective chemical reactions mediated by the photon-driven CT process, namely plasmon-mediated chemical reactions (PMCRs).[332,339] In such process, reactions happen on the charged state to form targeted chemicals under mild conditions, but during which usually a longer lifetime of the charged state is needed. More detailed discussions are shown in relevant reviews.[332,340,341]

Now the chemical reactivity of plasmonic systems is deeply influenced by the dynamics of photons, plasmon-polaritons, carriers, phonons, and molecular states. These degrees of freedom can affect the reaction rates, the product selectivity, or the spatial localization of a chemical reaction in nanostructures.[330] It is important to tailor the generation of non-thermal carriers and phonons in metallic nanostructures and their dissipation relaxation is shown as a promise to understand and exploit thermal photocatalysis at the nanoscale. This is useful to control these processes for the rational design of solar nanometric photocatalysts.

4.4.10 Development of hybridization theory for understanding plasmonic resonances. The plasmon hybridization theory, developed by Nordlander, Halas, and their colleagues in 2003,[258] is based on a compelling analogy between the plasmon resonances of metallic nanoparticles and the wave functions of simple atoms and molecules. This theory provides a framework for understanding the relationship between the geometry of metallic nanostructures and their optical properties. It was originally developed to understand the tunability of nanoshell plasmon resonances and has been extended to a multitude of various structures and geometries including nano-particles, multiple-nanoparticle assemblies and nanoparticles on films.[198,342]

For nanoshells, the theory provided an intuitive understanding of both the tunability and their large field enhancements. In Fig. 33a–c, it showed that the hybridized plasmon modes arise due to a coupling between the plasmon modes on the inner and outer surfaces of the shell.[198] For a thin shell, the interaction between the plasmons is very large, leading to a strong tunable redshifted ''bonding'' plasmon. The wave function of this plasmon has the charge density associated with the cavity and the inner and outer surfaces aligned, resulting in a larger charge density than for a solid sphere, corresponding to large field enhancements. More efficient SERS substrates can be constructed using nanoshells as building blocks for composite structures. The prime example is the nanoshell dimer,[343] providing larger field enhancements and SERS sensitivities in orders of magnitude. The large field enhancements explicitly showed in Fig. 33d and e. The nanoshell dimer exhibits large field enhancements in the junction, and also illustrates that the field enhancements can be made even larger by texturing the surface of the nanoshells, resulting in a much larger hot spot volume.

Based on the hybridization theory, it's possible to design nanostructures with continuously tunable plasmon resonance from the visible to the mid-infrared. Another highly useful example is the hexagonally close-packed (HCP) nanoshell array.[344] As illustrated in Fig. 33f and g, which shows the optical properties of this structure, the difference in hybridization between the dipolar and the quadrupolar nanoshell resonances is shown. Here the quadrupolar plasmon modes in the visible/near IR interact only weakly, resulting in a nondispersive plasmon mode similar to the d band in a solid. In contrast, the dipolar plasmons interact very strongly, resulting in a broad, strongly redshifted mode in the mid infrared. Both of those modes provide large field enhancements: the quadrupolar modes, at 700 nm, and the dipolar modes, at 3.0 microns. What is remarkable about these field enhancements is that they appear at the same spatial region of the arrays, enabling the possibility of doing both surface-enhanced Raman and IR absorption spectroscopy (SEIRA) on the same molecules on the substrate. Combined SERS and SEIRA provides a much more comprehensive chemical fingerprint of an analyte molecule for accurate chemical identification and this dual functionality has been used extensively for chemical fingerprinting applications.[345]

4.5 Key methods for high spatial and temporal resolution

4.5.1 Combined STM and SERS instrument. During the same period when high-sensitivity single-molecule SERS was being achieved, another challenge was how to achieve high spatial resolution. This led to attempts to integrate vibrational spectroscopy techniques with scanning probe microscopy (SPM). In 1994, Tian group developed a combined STM-Raman setup by introducing optical fibers into an STM setup, demonstrating the first simultaneous STM and SERS measurements at electrochemical interfaces (Fig. 34).[346–348] Their goal was to use STM to characterize the SERS-active surface at the nanoscale before and after electrochemical deposition of Ag islands on a smooth highly oriented pyrolytic graphite (HOPG) surface, then correlate it with the observed SERS intensity. However, at that time, the critical role of the gap-mode coupling between the tip and the substrate was not recognized. Consequently, the tip and electrode surfaces were not optimized, resulting in limited spatial resolution and sensitivity of the STM-SERS measurement.

4.5.2 Invention of TERS. Six years later, Zenobi, Deckert and coworkers of ETH Zurich, Anderson of the California Institute of Technology, Kawata and coworkers of Osaka University, and Pettinger *et al.* of the Fritz Haber Institute almost simultaneously reported the invention of TERS based on AFM/STM techniques in 2000.[16–19] By utilizing the localized enhancement effect at the very tip apex, a spatial resolution of 50 nm was conservatively claimed based on step size and tip radius (Fig. 35). The popular name of tip-enhanced Raman spectroscopy, *i.e.* TERS, was coined by Zenobi, Deckert and coworkers.[16] Anderson named it as ''locally enhanced Raman spectroscopy''.[17] In Kawata's paper it was ''Metallized tip amplification''[18] and in Pettinger's paper there wasn't really any name.[19] A good name turned out to be quite important in solidifying scientific discovery and communicating it to a wider scientific community.

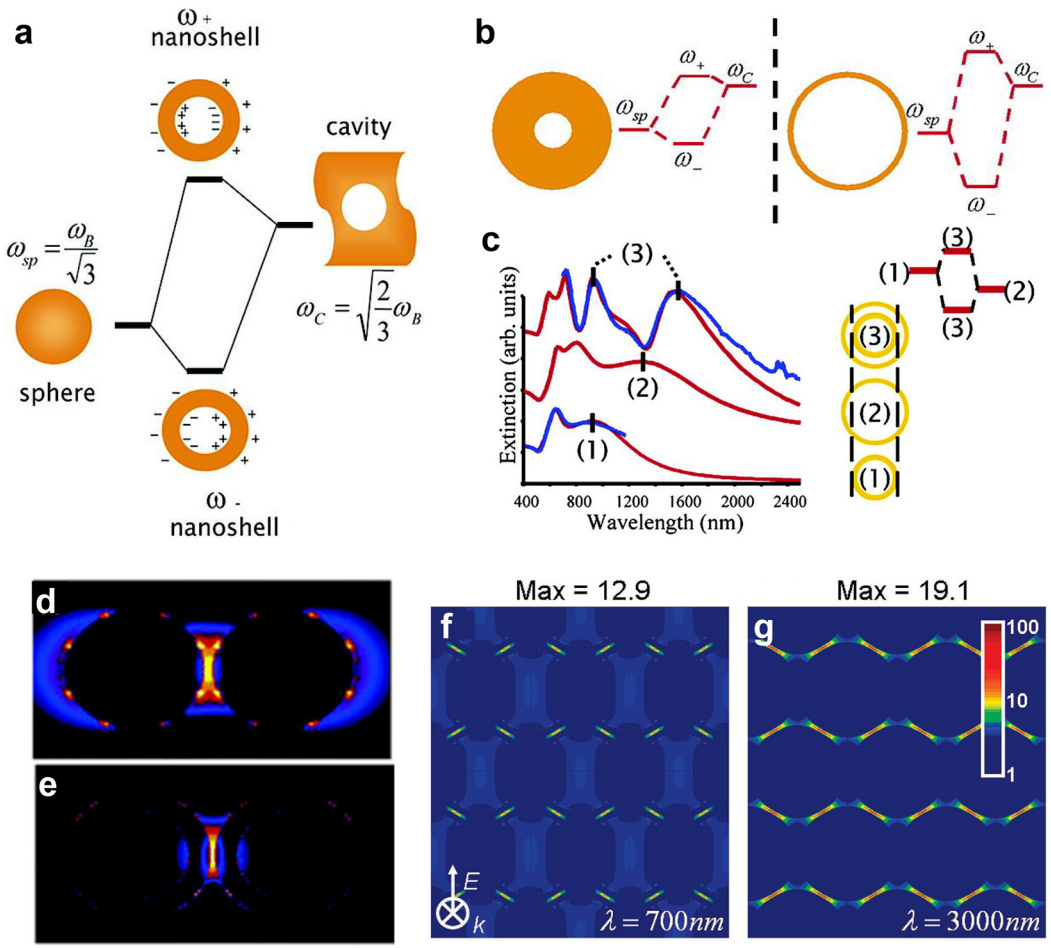

Fig. 33 (a) Energy level diagrams depicting plasmon hybridization in metal nanoshells resulting from interacting sphere and cavity plasmons with the two hybridized plasmon modes being an anti-symmetric or "antibonding" plasmon resonance (ω_+) and a symmetric or "bonding" plasmon resonance (ω_-). (b) Illustrating the dependence of nanoshell plasmon energies on the strength of the interaction between the sphere and cavity plasmons, determined by the thickness of the metallic shell. (c) Experimental (blue) and theoretical (red) extinction spectra for concentric nanoshells (3) compared to the inner (1) and outer (2) nanoshell plasmon resonances. (d) Electromagnetic near field enhancement at the excitation laser's wavelength (633 nm) for an adjacent nanosphere pair with interparticle axis parallel to the incident polarization, and (e) a nanoshell dimer with interparticle axis parallel to the incident polarization. (f) FDTD simulation results of the local electric field enhancement for a hexagonally close-packed (HCP) Au nanoshell array, at wavelength of 700 nm and (g) 3000 nm, respectively. Figures are reproduced from ref. 198, 258, 343 and 344 with permissions. Copyright 2003 AAAS. Copyright 2005 & 2007 & 2008 American Chemical Society.

Later on, by optimizing the tip structure, excitation and collection conditions, and controlling the tip–substrate coupling distance, researchers could confirm the extremely high spatial resolution of TERS,[349–351] reaching a level of approximately 10 nm. At that time, whether the spatial resolution limit of TERS could break the 1 nm barrier to achieve single-molecule resolution was an intriguing but unresolved question. Theoretical predictions suggested that due to quantum tunneling and non-local effects of electrons,[352,353] the confinement of light cannot be reduced to 1 nm at least not in the preferred gap-mode configuration. Additionally, the mobility of molecules on the surface and the thermal drift of the instrument also hindered further improvements in TERS spatial resolution.

4.5.3 TERS with sub-nanometer resolution. However, in 2013, Dong, Hou and coworkers reported landmark work in which they achieved TERS imaging of a single porphyrin derivative on a Ag(111) surface under low-temperature, ultra-high vacuum (LT-UHV) conditions, with a surprising spatial resolution of 0.5 nm, as shown in Fig. 36.[354] By using STM induced luminescence techniques, they could monitor and tune the nanocavity plasmon mode *in situ* so as to generate an efficient double-resonance enhancement scheme for both Raman excitation and emission, particularly the downward transition for the emission of Raman photons. While they believe the highly confined and broadband nature of the nanocavity plasmon field is crucial for ultrahigh-resolution Raman imaging, they viewed their spectral-matching TERS as an analogue to the femtosecond stimulated Raman process in terms of the similarity in spectral profiles and the nonlinear effect observed in experiments, and speculated this might be the reasons for both enhanced signals and improved spatial resolution. Later, Luo and coworkers successfully established a

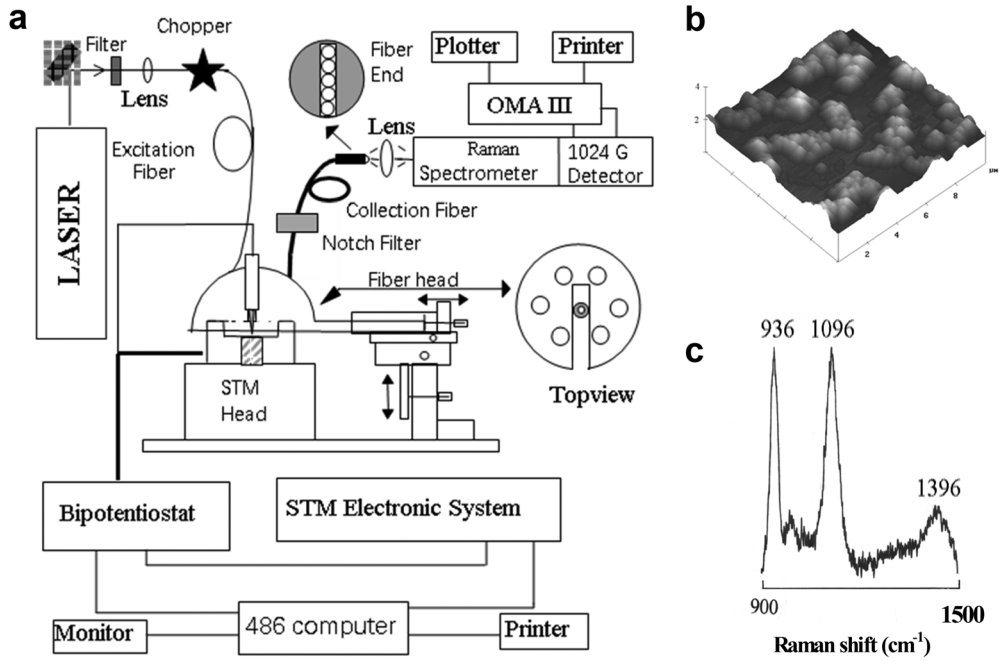

Fig. 34 The combined STM and SERS experiments. (a) Schematics of the combined STM with Raman instrument based on the remote operation of optical fiber, which enables the simultaneous measurements of STM and SERS of an electrochemical cell. (b) STM images of a HOPG surface after the stripping of Ag. (c) A SERS spectrum of thiourea adsorbed on the surface of (b). Figures are adapted from ref. 347 and 348 Copyright 2007 Wiley. Copyright 1996 Elsevier.

quantum mechanical model, which quantitatively reproduces all the experimental measurements and thus reveals the essential factor responsible for the super-high resolution as the quantum interaction between the transition density and the inhomogeneous plasmonic field.[355]

This experiment also triggered the reconsideration of plasmonic optical processes at atomic scales. Subsequently, Aizpurua, Sánchez-Portal and coworkers reported detailed time-dependent density functional theory calculations of the optical response of metal nanoparticles with atomic-scale features, and they showed that several atomistic protrusions could confine the optical field to sub-nanometer or even atomic scales[356,357] as shown in Fig. 37a–c. This was spurred by their collaboration with Baumberg and coworkers, who demonstrated experimentally that a picocavity can be formed by a few adatoms in a nanoparticle-on-mirror (NPoM) configuration,[358] boosting new Raman lines, as shown in Fig. 38.

Since then, the importance of atomic-scale structures on nanostructure surfaces has gained increasing attention in the SERS and plasmonic community. At the same time, a different approach was proposed based on the assumption that even without any external fields the energy levels and consequently the vibrations must change with respect to the positioning of the tip. Theoretical modelling of Raman spectra of a silver atom scanning over an adenine molecule at different heights clearly showed this chemical effect.[360] Deckert and colleagues showed in classical electromagnetic models that atomic scale protrusions on TERS tips exist and can act as the previously mentioned enhancing sites, which are further responsible for the chemically induced band shifts and leading to a higher resolution.[361]

This atomistic-scale lightning rod effect leads to highly intense and localized hot spots, which differs from the general understanding of localization of plasmonic fields. Although the calculation model was simplified as a Na_{380} dimer with a size of 2 nm, which is much smaller than commonly used nanostructures, those results solidly indicate that the presence of atomic-scale structures at plasmonic interfaces,[356] additionally enhancing the underlying plasmonic field, appears as a new arena of research in extreme filed localization and attracts tremendous attention to investigations of plasmon–matter interactions at the atomic scale. More recently, another transient phenomenon observed in all SERS measurements was also understood by the Aizpurua and Baumberg teams, from an entire patch of the surface atomic monolayer lifting, which generates intense broadband light modulated by plasmonic resonances, and known as flares.[362,363]

Shortly after, Galland, Kippenberg and colleagues[364] and Aizpurua, Schmidt and colleagues[359] independently developed an optomechanical model of SERS and provided a quantum electrodynamics (QED) description of the coherent interaction of plasmons and molecular vibrations (Fig. 37d). They showed that the optomechanical interaction between the molecules and extremely trapped optical fields can explain the high spatial resolution in TERS as well as the nonlinear behavior of the Raman signal with laser intensity. Other important effects from these optomechanical interactions are also seen such as SERS peak shifts.[365] The dynamics of the formation and

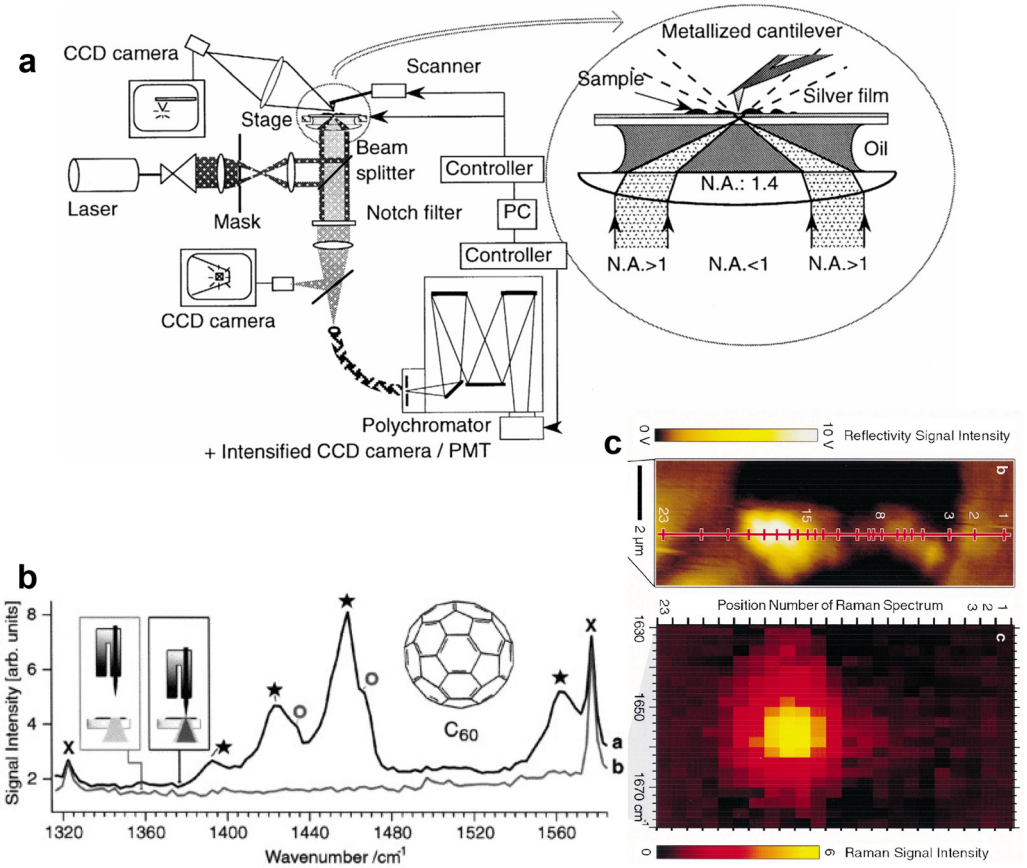

Fig. 35 The first demonstration of TERS. (a) The configuration of the TERS setup developed based on a near-field Raman microscope. (b) The demonstration of TERS based on a combined Raman and AFM instrument using a metallic AFM tip in shear-force mode. The Raman spectra of C_{60} is shown with an Ag tip in contact with the sample (trace a), and tip retracted (trace b). Circles mark C_{60} normal modes, stars mark C_{60} modes due to CT with an Au tip. The crosses mark Raman bands of the immersion oil. (c) Demonstration of the spatially resolved Raman measurement by TERS, with a standard silver island coated AFM cantilever tip. The Raman spectra of an ultra-flat homogeneous brilliant cresyl blue (BCB) sample were measured along the line in top panel at the marked positions, and the position dependent Raman spectra are displayed in the bottom panel. No additional cavity/gap-mode effect was required. Note that the silver film was not present in the examples in (b) and (c). And a tuning-force setup was used in (b). Figures are adapted from ref. 16 and 18 with permissions. Copyright 2000 Elsevier.

destruction of these adatoms under laser illumination leads to fluctuations in SERS intensities that can be observed when using high-speed acquisition rates.[366,367] Based on these achievements, recently the spatial resolution of TERS have been successfully pushed to single-bond[368,369] and single-atom limits.[370] We will discuss the details of these recent advances in atomistic TERS in Section 5.1.

It's noted that in the first SM-SERS experiments[14] in 1997 and the first sub-nanometer TERS experiments in 2013, the resonance Raman effect was employed to achieve the best sensitivity. This is because the intensity of the Raman signal is collectively determined by the structural EF, the intrinsic cross-section of the molecule, and the optimization of the instrumentation, as discussed in eqn (4). Therefore, for establishing new methods, or exploring/optimizing new nanostructures/systems, it is beneficial to test with resonance Raman molecules for high detection sensitivity. When pursuing further improvement on the landmark work, however, testing non-resonance Raman molecules and expanding molecular generality in more applications and systems are inevitable. From a methodological point of view, resonance Raman and non-resonance Raman are two different aspects in the same development line approaching the high sensitivity of SERS.

In recognition of this relationship, attention should be paid to the related consideration of EFs (see Section 4.7). There is no need to emphasize how high the EF is when resonance Raman molecules are used, as it is not the practical goal of the research method. It cannot be compared with the EF of non-resonance Raman systems, because the purpose of the two is different, moreover in the end non-resonant molecules are more relevant to general SERS applications.

4.5.4 Electrochemical TERS. Since the invention of TERS[16–19] in 2000, there is a growing interest in expanding the application of this nano-resolved spectroscopy in liquid conditions, especially electrochemical conditions to study some important chemical and biological processes occurred at the solid–liquid interface. Compared with ambient TERS or UHV-TERS, electrochemical TERS (EC-TERS) provides a convenient

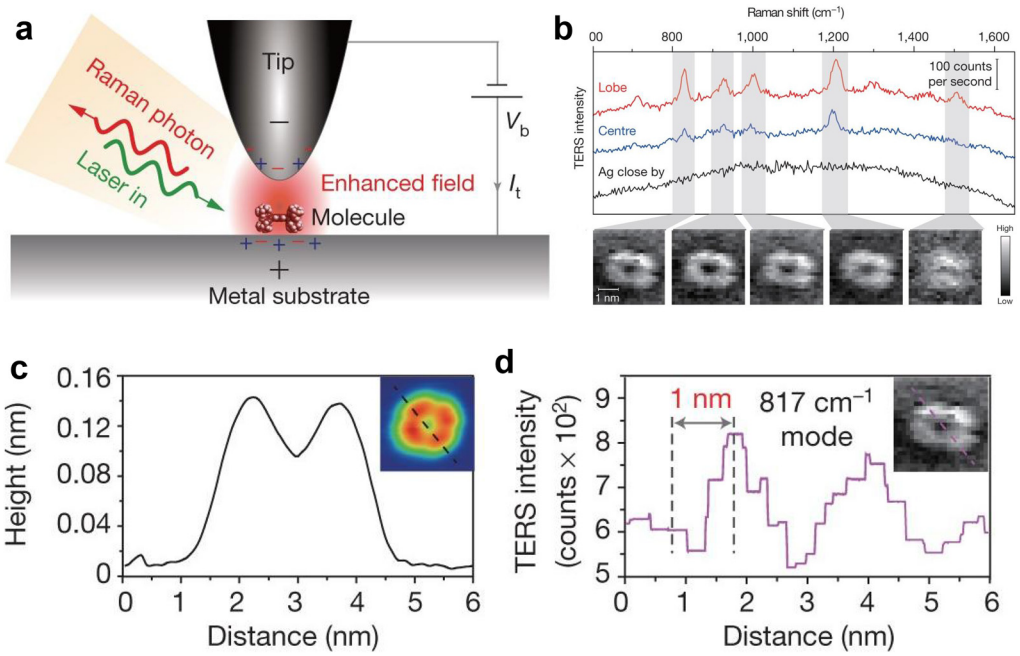

Fig. 36 (a) Schematic of single-molecule TERS at LT-UHV condition. (b) The typical Raman spectrum taken from different positions of molecules. (c) Height profile of a line trace in the inset STM topograph. (d) TERS intensity profile of the same line trace for the inset Raman map associated with the 817 cm^{-1} Raman peak. Figures are reproduced from ref. 354 with permission. Copyright 2013 Springer Nature.

way to control the surface state and the interfacial process by modulating the applied electrode potential. In addition, the EC-TERS technique is able to reveal the molecular structure at the electrochemical interface and obtain the correlated morphological and chemical information at a nanoscale spatial resolution under the reaction condition, thus shedding light on the establishment of an accurate structure–activity relationship. However, EC-TERS requires an efficient integration of SPM, electrochemistry and SERS technique, which is quite challenging. The main challenge lies in how to maintain a high excitation and collection efficiency with the existence of liquid in the optical path that leads to severe optical distortion.

In 2015, Ren and coworkers developed an EC-TERS approach based on STM by directing light horizontally into an EC-TERS cell to minimize optical distortion (Fig. 39a).[371] They reported potential-dependent behaviors of an aromatic molecule adsorbed on a well-defined Au(111) surface (Fig. 39b), highlighting significant alterations in the molecular configuration due to protonation and deprotonation phenomena. Simultaneously, Van Duyne and coworkers developed the AFM-based EC-TERS with a bottom-illumination configuration and investigated the nanoscale redox behavior of Nile Blue (NB) on a transparent ITO substrate.[372] The disappearance of the 591 cm^{-1} peak of NB upon reduction and its reversible reappearance during oxidation was monitored and used to form the TERS voltammetry (TERS-CV) (Fig. 39c and d). They observed a shift in the redox potential between the TERS-CV and the conventional CV, which was attributed to the perturbation of the electric double layer by the TERS tip. Thereafter, EC-TERS images over a Au plate on ITO electrode was performed. Following the fitting of EC-TERS spectra obtained at various potentials for each position, the site-dependent formal potentials corresponding to the Au and ITO electrodes were derived. Notably, a more negative formal potential was observed at the Au electrode, along with a heterogeneous distribution of formal potentials across the ITO electrode.[373]

In recent years, the introduction of water-immersion objectives by Ren and coworkers,[374,375] and Maisonhaute, Lucas and coworkers[376] fully avoided the optical distortion, significantly improving the sensitivity of EC-TERS. As a result, EC-TERS can be used to study more electrochemical processes, such as electrocatalysis. In 2019, Domke and colleagues investigated the site-dependent variations over the Au(111) surface during the oxygen evolution reaction by EC-TERS.[377] They observed the formation of AuO_x over the defect sites before the oxidation of the terrace sites, indicating varying activities over the Au(111) surface. In 2024, Ren, Tan, Wang and colleagues utilized EC-TERS to study the active sites of MoS_2 during the hydrogen evolution reaction (HER).[378] They observed that the edge induced electron transition region and lattice reconstruction region kept changing during the HER process until the highest activity was obtained, revealing the generation and dynamic variation of active sites during electrocatalytical reactions.

4.5.5 Depth-penetrated SERS. Another aspect of spatially resolved SERS is the penetration depth. To break the limitation of micrometer level penetration depth inherent in traditional Raman spectroscopy, Matousek and colleagues introduced spatially offset Raman spectroscopy (SORS)[379] and transmission Raman spectroscopy (TRS)[380] to SERS.

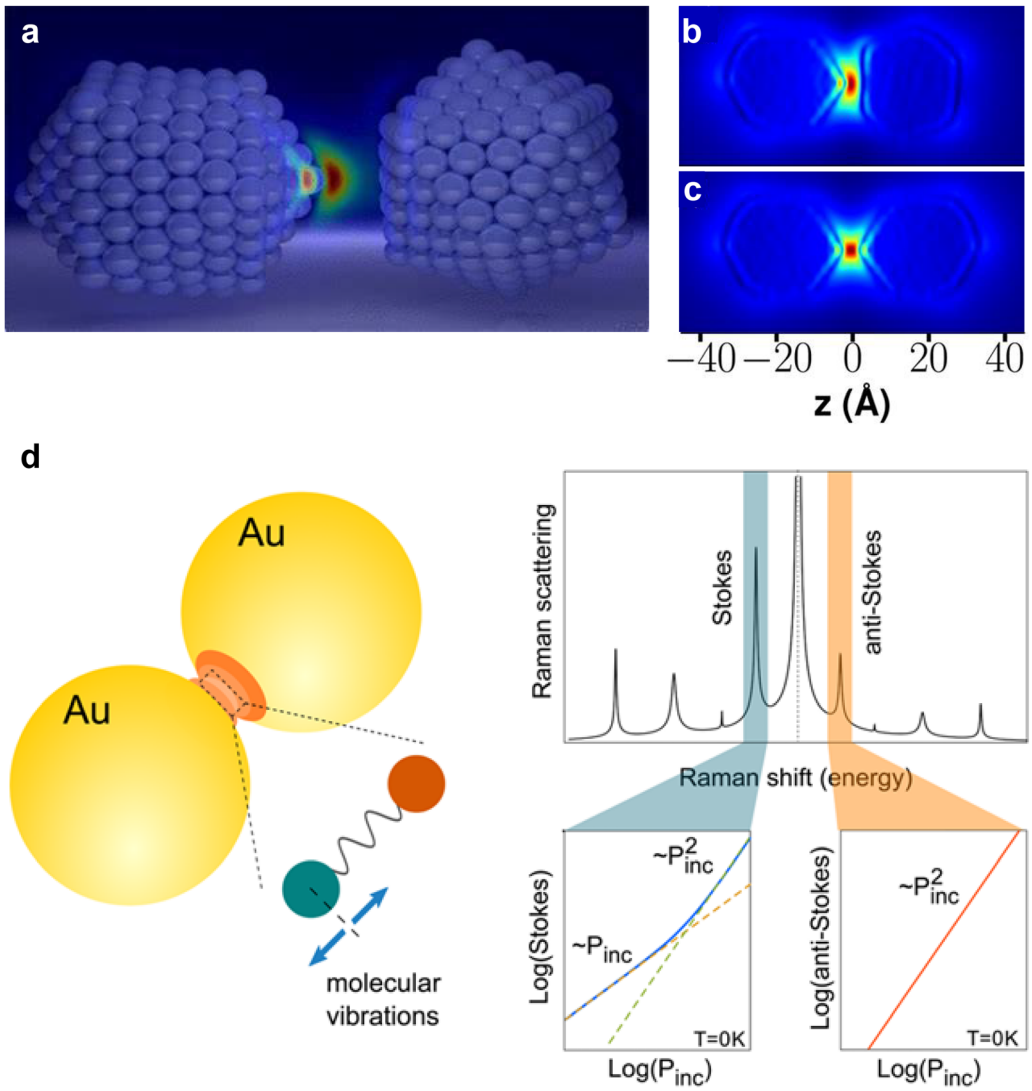

Fig. 37 (a) Schematics of atomistic near field generated by the atomistic protrusions at metallic interfaces in clusters. (b) Calculated electromagnetic field enhancement of a Na dimer with a gap distance of 0.6 nm, with tip-to-facet configuration and (c) tip-to-tip configuration. Maximum enhancement value of ~40 is colored in red. (d) Schematics of the molecular optomechanical description of SERS process. Figures are adapted from ref. 356 and 359 with permissions. Copyright 2015 & 2016 American Chemical Society.

SORS capitalizes on the principle that Raman photons emitted from deeper regions of a sample experience increased lateral diffusion owing to multiple scattering events, which differentiate them from those originating in superficial layers. In practice, SORS collects Raman spectra at a spatial offset relative to the laser incidence point. This method, augmented by sophisticated multivariate data analysis and processing techniques, enables the differentiation and deconvolution of signals arising from various depths. The deconvoluted Raman spectra unveils layer-specific information, thereby facilitating the analysis of subsurface layers within complex samples.

Different from the backscattering collection mode commonly utilized in Raman measurements, TRS features a configuration where the laser is incident on one side of the sample, and the Raman scattered light is collected from the opposing side, allowing TRS to probe deeper regions within the sample, effectively extending the penetration depth beyond conventional capabilities.

Stone and colleagues further combined SORS and TRS with SERS and developed surface-enhanced spatially offset Raman spectroscopy (SESORS)[381] and surface-enhanced transmission Raman spectroscopy (SETRS).[382] The two techniques have significantly extended the penetration depth of SERS up to the millimeter and even centimeter level. This breakthrough has paved the way for *in vivo* diagnostic applications, allowing for the non-invasive examination of biological tissues at greater depths than ever before.

4.5.6 Nonlinear and ultrafast SERS and TERS. The enhancement of non-linear Raman processes by SERS has been discussed since the early days of SERS.[383,384] Specifically the spontaneous, two-photon excited process of hyper Raman

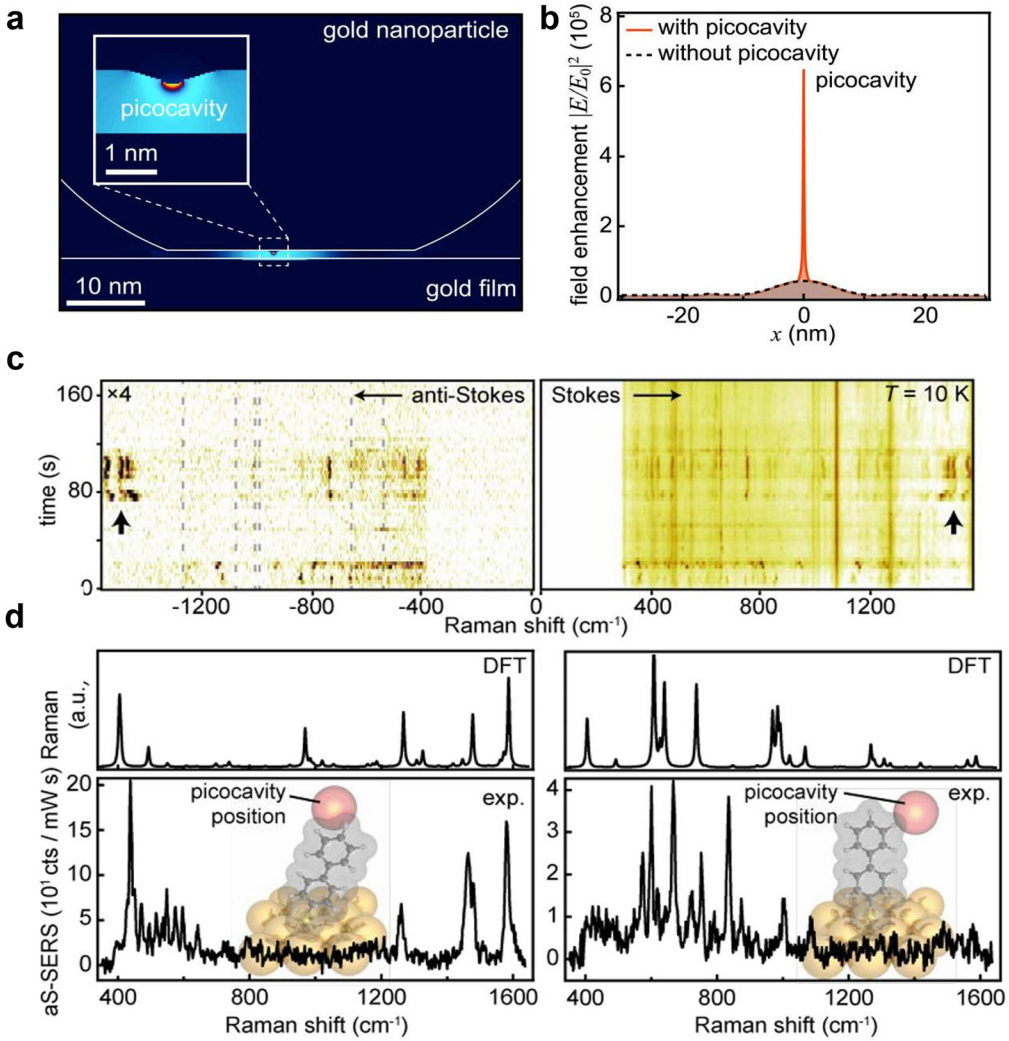

Fig. 38 (a) The schematics of picocavity formed by adatoms on Au nanoparticles. (b) Near field enhancement in the cavity. (c) Time-series anti-Stokes and Stokes SERS in the picocavity. (d) Comparison of two experimental spectra (bottom) with DFT simulated spectra (top) under the assumption of atomic-scale field confinement (inset shows geometries, red sphere shows field ocalization for simulations). Figures are reproduced from ref. 358 with permission. Copyright 2016 AAAS.

scattering (HRS) benefits from high electromagnetic enhancement, as well as from chemical effects. With HRS relying on different selection rules, SEHRS can provide new and additional structural information of molecules and materials. As shown by Kneipp *et al.* in non-resonant experiments, both SERS and SEHRS spectra can be acquired simultaneously, enabling an estimate of the contribution of electromagnetic enhancement to both processes.[385] In 2006, the group of Van Duyne demonstrated the extremely high sensitivity of SEHRS towards local adsorbate geometry and surface environment.[386] As shown by Kneipp *et al.* in the same year, the extremely high enhancement in SEHRS yield effective cross-sections for the non-resonant process that are better than typical cross sections of typical two-photon fluorescence.[387] They also reported the first SEHRS spectra from intact cells that revealed complementary vibrational information on biomolecule nanostructure interaction.[387] Meanwhile a large number of studies were conducted on different types of biomolecules, including proteins, nucleic acids, and chromophores.[388] In resonance with molecular electronic transitions, SEHRS spectra can evidence that electronic "dark" states that are not allowed in one-photon absorption can be probed, as demonstrated by Camden, Jensen and coworkers.[389]

Temporal resolution is also a crucial aspect of SERS.[217] Ultrafast Raman spectroscopy often employs modulation techniques, such as Kerr gating, to provide background-free Raman spectra with high signal-to-noise ratios and rapid acquisition times. In 1999, Matousek *et al.* demonstrated the efficacy of picosecond Kerr gating in rejecting fluorescence background interference by obtaining time-resolved spectra of *p*-quaterphenyl from solutions that were contaminated with a fluorescent dye.[390] Subsequently, researchers developed other ultrafast SERS techniques, including time-resolved coherent anti-Stokes Raman spectroscopy (tr-CARS)[391,392] and time-

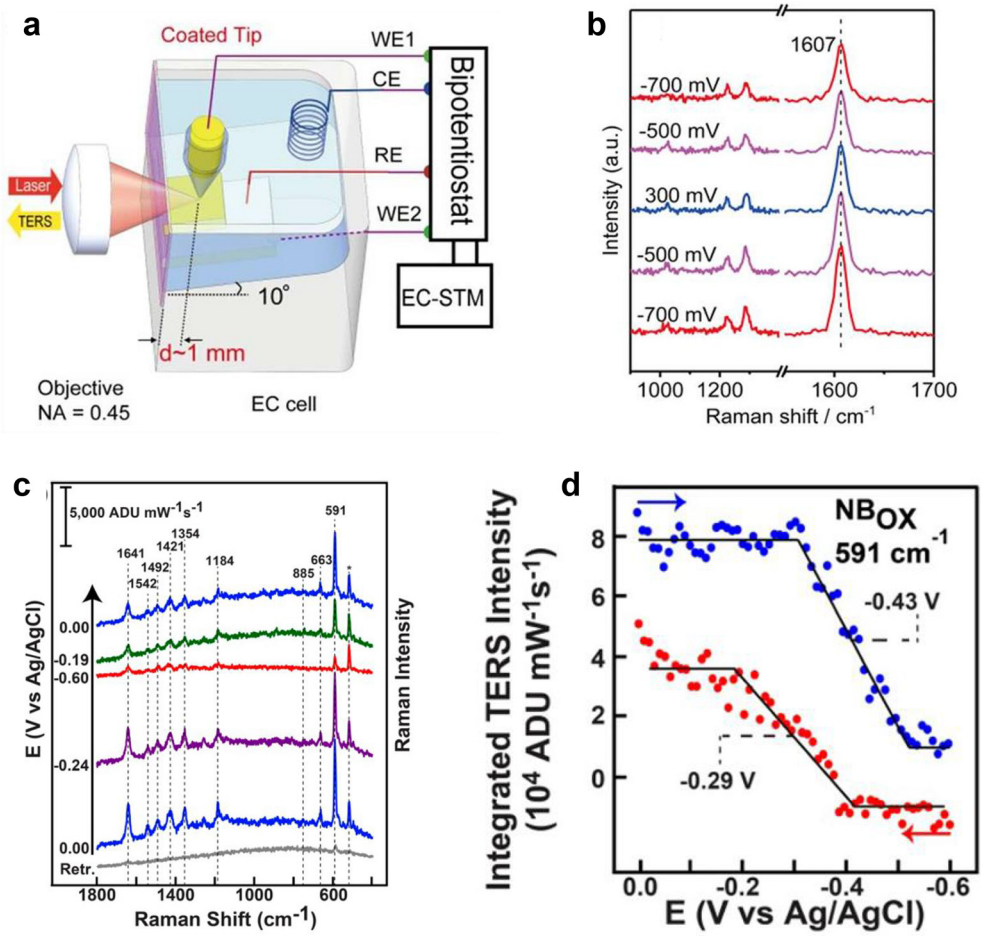

Fig. 39 The electrochemical TERS (EC-TERS). (a) The schematics of EC-TERS setup. (b) The potential dependent EC-TERS spectra of 4-PBT adsorbed on Au(111) surface. Tip potential was −200 mV, and the tunneling current was 500 pA. (c) EC-TER spectra of NB acquired at different potentials during cyclic voltammetry showing reversible reduction and oxidation of NB. P = 110 μW, t = 1 s, λ = 633 nm, scan rate = 10 mV s^{-1}. The asterisk denotes the Si Raman band from the AFM tip. (d) Potential dependence of the integrated TERS intensity of the 591 cm^{-1} band of NB_{OX}. Figures are reproduced from ref. 371 and 372 with permissions. Copyright 2015 American Chemical Society.

resolved stimulated Raman spectroscopy (tr-SRS).[393,394] A significant milestone was achieved in 2011 by Van Duyne group, who pioneered the integration of SERS with femtosecond stimulated Raman spectroscopy (FSRS).[394] They presented the first demonstration of surface-enhanced femtosecond stimulated Raman spectroscopy (SE-FSRS), using an experimental setup featuring picosecond pulses for the Raman pump, femtosecond pulses for the broadband Raman probe, and Au nanoantennae for signal enhancement (Fig. 40). This configuration achieved an EF estimated to be between 10^4 and 10^6. They further found that the signal-to-noise ratio can be significantly improved by choosing approximate repetition rates of the fs-laser.[395] Latter work used picosecond time-resolved SERS to probe processes like plasmon-driven electron transfer and plasmonic heating of adsorbates.[396,397] These results open new avenues for exploring the ultrafast dynamics of plasmonic materials and small homogeneous molecular subsets.

The integration of ultrafast spectroscopy with TERS offers a powerful approach for investigating the nanoscale molecular dynamics with both spatial and temporal resolution. One of the earliest and most advanced applications in this field is tip-enhanced coherent anti-Stokes Raman spectroscopy (TECARS), which was firstly demonstrated by Inouye and colleagues in 2004.[398] They successfully coupled 5 ps pulses with a plasmonic tip and operated at an 800 kHz repetition rate. This technique allowed them to acquire high-resolution TECAR images of adenine molecules within DNA clusters, capitalizing on the localized electric field enhancement beneath the metallic nanoprobe (Fig. 41a–d).

In 2014, Van Duyne group reported the integration of picosecond-pulsed irradiation from an optical parametric oscillator (OPO) with a UHV-TERS system (Fig. 41e and f).[399] They demonstrated that picosecond UHV-TERS of resonant adsorbates can be observed without permanent signal loss, which typically affects picosecond TERS in ambient conditions. This suggests that a UHV environment is a valuable asset for temporally resolved TERS experiments. Recently, Garg group demonstrated ultrafast LT-UHV TERS excited by ultrashort laser pulses (500 fs),[400] laying the foundation for future experiments involving time-resolved femtosecond TERS.

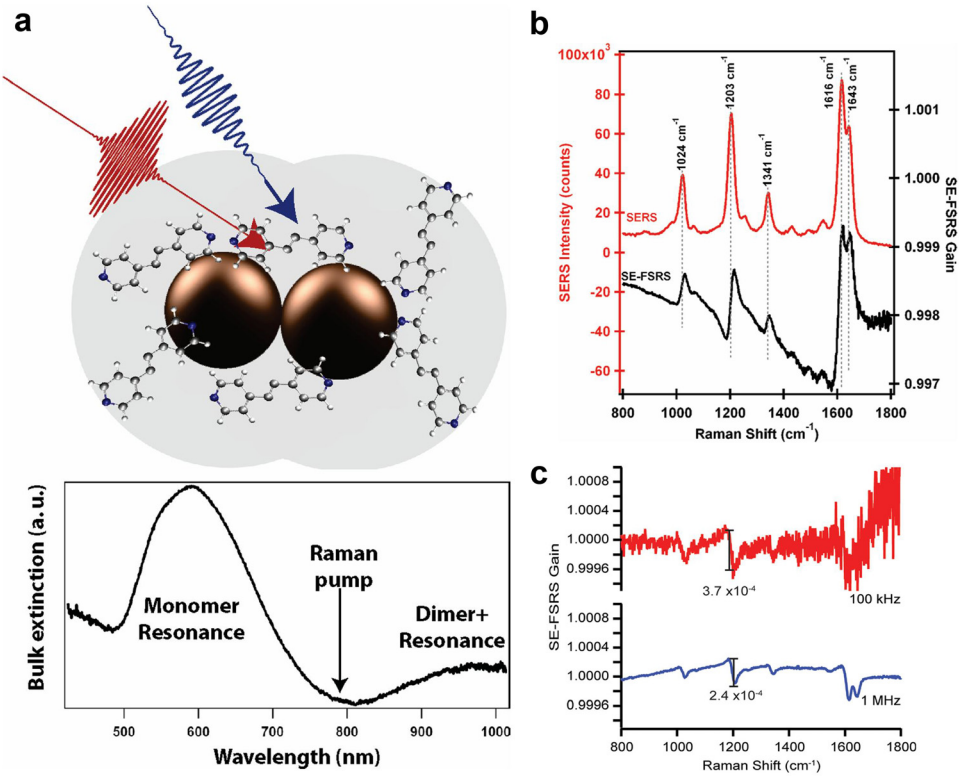

Fig. 40 The demonstration of surface-enhanced femtosecond stimulated Raman spectroscopy (SE-FSRS). (a) Schematic depiction of the nanoantennas used in the SE-FSRS experiments. Bottom panel show the extinction spectrum of the *trans*-1,2-bis(4-pyridyl) ethylene (BPE)-functionalized nanoantennas. (b) SERS spectrum (red curves) and SE-FSRS spectrum (black curves) of BPE-functionalized nanoantennas. The SE-FSRS spectrum shows dispersive peaks due to resonance effects from the plasmon. (c) SE-FSRS spectra obtained from BPE-nanoparticle assemblies with 100 kHz (red) and 1 MHz (blue) repetition rates of pulse. The pump pulse energy and average pump power are equal in both experiments. The spectra obtained at 100 kHz exhibit noise in the spectral region of 1000–1200 cm^{-1} that is approximately 10× greater than that obtained at 1 MHz. Figures are adapted from ref. 394 and 395 with permission. Copyright 2011 & 2016 American Chemical Society.

4.6 Key methods for expanding the generalities of SERS substrate materials and morphologies

4.6.1 SERS on non-traditional transition metals. In parallel to the demonstration of SM-SERS, Tian group demonstrated that SERS can be directly generated on electrode surfaces made from surface-roughed transition metals in 1996.[181,401] This was achieved by the joint improvement of Raman instrumentation as well as the nanostructure fabrication methods. First, the confocal Raman microscope (Fig. 42a) was used for signal collection,[165,402] which provides higher detection sensitivity. Second, various methods for fabricating nanostructured surfaces (Fig. 42b and c) were developed.[165] For instance, the electrodes were treated with an electrochemical ORC process to achieve surface roughening (Fig. 42d and f).[165] They reported the first results of enhanced Raman spectra of hydrogen adsorption (Fig. 42e),[181] CO adsorption (Fig. 42g)[403] and pyridine adsorption (Fig. 42h)[165] on the roughened surfaces of various transition metal electrodes, including Pt, Fe, Ru, Rh, Co, Ni, and Pd.[165]

While there was experimental progress in transition metal SERS, how to understand the enhancement mechanism behind it remained an important issue in the SERS field. SERS is significantly influenced by the electromagnetic enhancement mechanism, which is predominantly attributed to the LSPR exhibited by nanoparticles composed of coinage metals. When exposed to visible light, the conduction electrons within these nanoparticles can be induced to oscillate collectively, thereby producing a robust electromagnetic field in proximity to the nanoparticle's surface. A high-quality SPR effect should meet two conditions: first, the real part of the dielectric constant of the nanoparticle must be negative; second, the imaginary part of the dielectric constant should be as close to 0 as possible.[404] In contrast to noble and alkali metals, transition metals exhibit distinct electronic structures characterized by the positioning of the Fermi level within the d band. This configuration results in a high probability of interband excitations occurring within the visible light spectrum. The interaction between conduction electrons and interband electronic transitions significantly diminishes the quality of the SPR in transition metals.[269] This considerably reduces the SERS effect, as observed in many experiments.

Based on the two-dimensional particle array model, Tian group carefully studied the correlation between the SERS EF and the morphology of the ellipsoidal particles, especially the aspect ratio of the particles and the frequency of the excitation light.[405] The maximum electromagnetic EF for SERS on Ni is

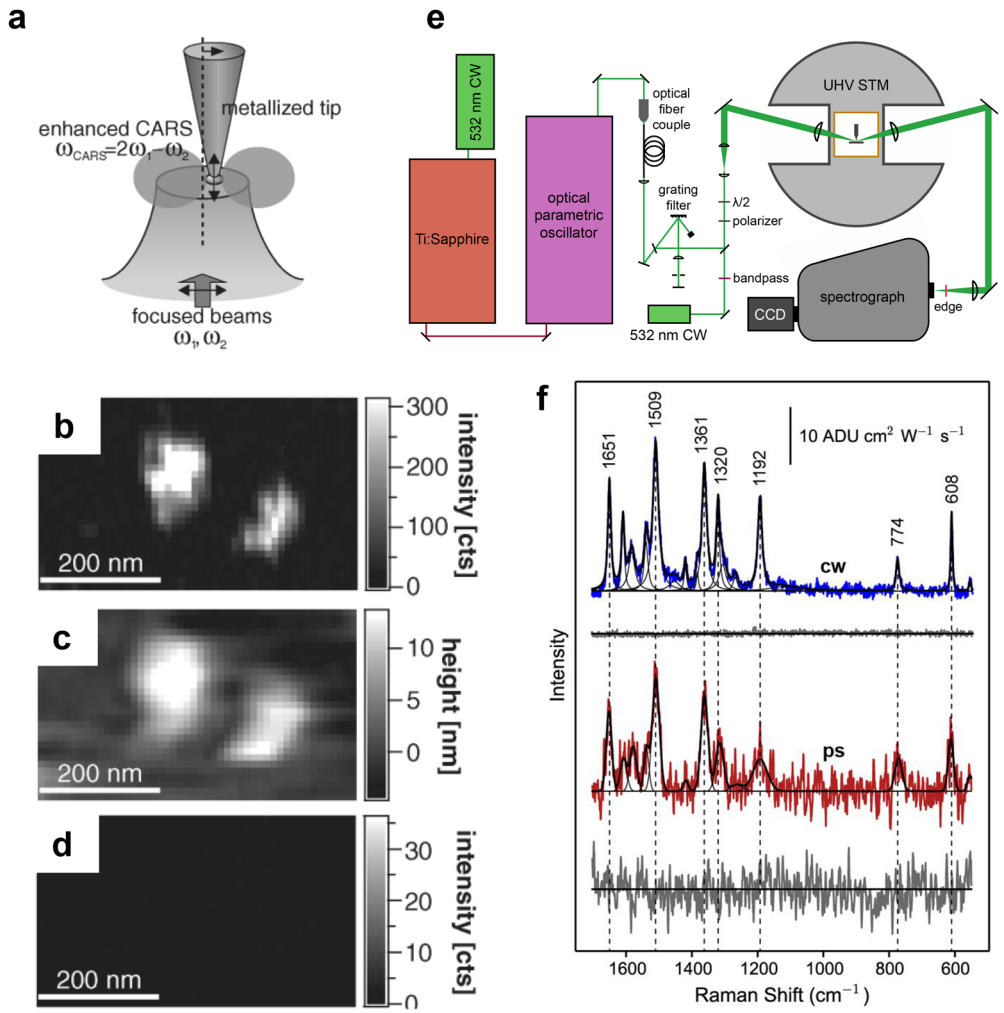

Fig. 41 Nonlinear and ultrafast TERS. (a) Schematics of the first tip-enhanced CARS (TE-CARS) of molecules near the metallic tips. (b) TE-CARS imaging of the DNA clusters at resonant frequency. (c) The topographic image of DNA clusters. (d) Far-field CARS image of the corresponding area obtained without the Ag tip. (e) Schematics of a picosecond pulse excited TERS (in a UHV environment). (f) Comparison of the TERS spectra of R6G molecules, under continuous wave (cw) and picosecond pulse (ps) excitation, respectively. Figures are adapted from ref. 398 and 399 with permissions. Copyright 2004 American Physical Society. Copyright 2014 American Chemical Society.

observed to range between two to four orders of magnitude, with a marked increase corresponding to higher aspect ratios. This phenomenon can be elucidated through the lightning rod effect, which typically leads to significant electric field enhancement in regions with pronounced curvature on the surface. Furthermore, the data indicates a pronounced increase in the SERS EF for Ag when the frequency of the incident light approaches the frequency of surface plasmon resonance. In contrast, the EF for the Ni electrode remains relatively across the same orders of magnitude, provided the aspect ratio of the particles is maintained. This observation suggests that the SERS response of Ni does not exhibit the distinctive characteristics associated with SPR, with the EF demonstrating only minor fluctuations in response to variations in incident photon energy. Experimental findings corroborate this, revealing that the SERS enhancement for the Ni substrate remains nearly unchanged when the excitation laser wavelength is adjusted from 632.8 nm (1.96 eV) to 514.5 nm (2.41 eV), assuming all other experimental conditions are held constant. The critical role of morphology was also emphasized by Moskovits and coworkers in 2017, they showed that any metal can produce intense SERS when properly structured.[406]

Everything that has been learned regarding single molecule SERS since 1997 has led scientists to believe that the SERS-active system is also strongly dependent on the particle–particle, particle–substrate or tip–substrate near-field coupling effect. Therefore, the quantitative evaluation of SERS EFs in actual transition metal systems inevitably involves non-spherically symmetric particles and complex near field coupling between particles. Thus, it was important that the research model for the EM enhancement mechanism of SERS for transition metals changed its focus from highly symmetric particles to particle aggregates of arbitrary size and shape.

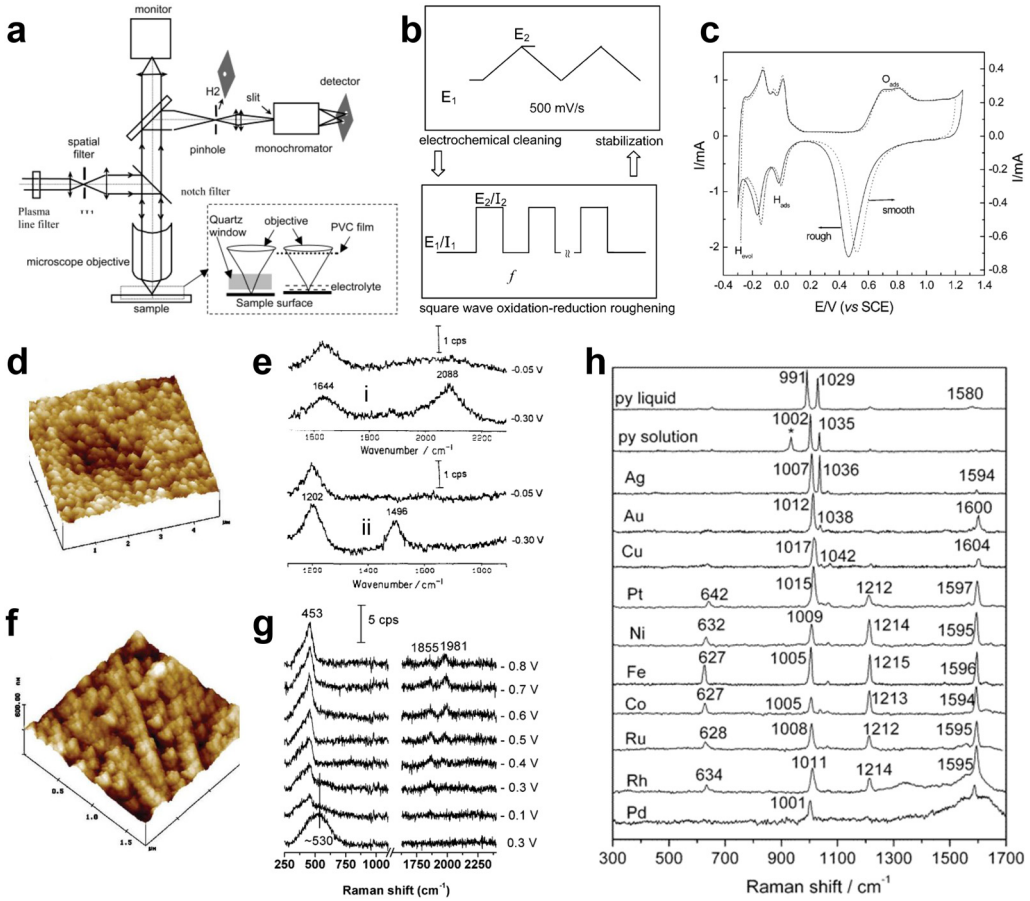

Fig. 42 (a) Schematic diagram of a confocal microprobe Raman system. Insertion: two possible configurations of the experimental setup between the collection microscope objective and the electrode surface. (b) Illustration of the roughening procedure for Pt and Rh surfaces by using square-wave potential (by controlling the E_1/E_2) or current (by controlling the I_1/I_2) oxidation–reduction method. The solution used is 0.5 M H_2SO_4 (c) a comparison of the cyclic voltammograms of roughened (solid line) and smooth (dotted line) Pt electrodes in 0.5 M H_2SO_4 solution. Scan rate: 50 mV s^{-1}. (d) The STM image of a Pt electrode after electrochemical ORC roughening treatment. (e) Potential dependent surface Raman spectra of (i) hydrogen adsorption in 0.5 M H_2SO_4 + H_2O and (ii) deuterium adsorption in 0.5 M H_2SO_4 + D_2O at roughened Pt surfaces. (f) The AFM image of an Rh electrode after electrochemical ORC roughening treatment. (g) Surface-enhanced Raman spectra of a roughened Rh surface in 0.1 M CH_3OH + 0.1 M Na_2SO_4. 0.2 M methanol was added into a Raman cell containing 0.2 M Na_2SO_4 solution with the electrode controlled at −0.6 V to form the final measuring solution. (h) Raman spectra of pure pyridine, pyridine solution, and pyridine that is adsorbed on noble metal and transition metal surfaces at open circuit potentials. Figures are adapted from ref. 165, 181 and 403 with permission. Copyright 1996 Elsevier. Copyright 2002 & 2003 American Chemical Society.

In order to conduct electrodynamic calculations of light scattering from complex SERS-active systems, the application of numerical methods is essential. Various techniques, such as the finite difference time domain (FDTD), finite element method (FEM), boundary element method (BEM), and discrete dipole approximation (DDA), have been developed to analyze the electromagnetic fields surrounding individual non-spherical metallic nanoparticles as well as nanoparticle arrays in the context of surface-enhanced spectroscopy. Among these approaches, the FDTD method stands out as a comprehensive, systematic, and versatile tool for evaluating the optical response of nanostructures with arbitrary geometries and symmetries to incident light waves. It has been effectively employed in SERS research involving transition metals. A typical simulated SERS enhancement for transition metal systems with a cauliflower-like morphology is shown in Fig. 43a and b.[407] Two distinct models were employed to simulate the cauliflower-like nanoparticles: one model consisted of a Rh sphere with a diameter of 120 nm, which was coated with 20-nm semispherical particles, while the other model featured a flat Rh surface adorned with 20-nm nanohemispheres, as illustrated in Fig. 43a. The computed electric field distribution across the surface is depicted using color visualization. The greatest enhancement of the electric field is typically observed at the apex of the smaller hemispheres within the ''cauliflower'' structure, which contrasts with the maximum field enhancement typically found at the junctions of two nanoparticles. However, when the cauliflower structure is separated and arranged into a planar grating-like configuration, the location of the field maximum shifts the crevices, as demonstrated in Fig. 43b. These findings suggest that the electromagnetic enhancement is highly sensitive not only to the polarization

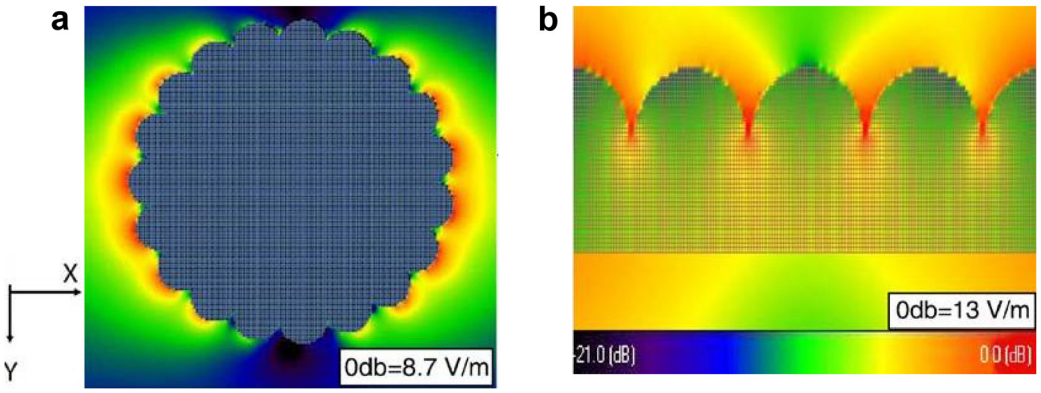

Fig. 43 (a) FDTD simulated electric-field distribution for a cauliflower-like Rh nanoparticle and (b) a flat Rh surface decorated with small nanohemispheres. The laser beam illuminates along the *y*-direction with *x* polarization. The scale bar is given at the bottom of (b). Figures are adapted from ref. 405 and 407 with permission. Copyright 2006 Springer Nature. Copyright 2006 Royal Society of Chemistry.

of the incident light, the electronic characteristics of the metal, and the surface morphology, but also to the symmetrical properties of the SERS nanostructures.

4.6.2 SERS on semiconductors. After the demonstration of transition metal-based SERS, other non-traditional SERS materials including graphene,[408] metal–organic framework (MOF) and related materials have also been demonstrated.[165,409,410] An interesting example is the dielectric and semiconductor material-based SERS-active substrates, such as TiO_2, ZnO, and SiO_2.[243] These materials can function as either complementary or alternative options to traditional metal-based SERS substrates, providing considerable advantages in terms of reproducibility, versatility, and recyclability.

Enhanced Raman scattering based on semiconductors stretched back to 1980s. In 1982 Yamada *et al.* reported enhanced Raman signal of pyridine adsorbed on the surface of single-crystal NiO(110).[411] They also made similar observation for the surface of Ti and single-crystal TiO_2(001).[135] Although the mechanism of enhancement was attributed to the CT mechanism at that time, it was actually difficult to distinguish between CT and resonance Raman effects in the experiments.[69] In 1988, Hayashi *et al.* found the enhanced Raman scattering derived from electromagnetic mechanism for copper phthalocyanine molecules with strong resonance Raman effect on GaP NPs.[412] The development of semiconductor enhanced Raman scattering stagnated in the 1990s probably due to very low EF. Semiconductor-enhanced Raman scattering was looked at again after 2000. For example, Zhao, Lombardi and colleagues reported semiconductor-enhanced Raman scattering for metal oxides, metal tellurides, metal sulfides, and so on.[413–415] Based on these studies they proposed a clear CT model to explain the enhanced Raman on semiconductor materials.

There are several kinds of semiconductor materials for enhanced Raman scattering. Metal oxides such as TiO_2 and ZnO are representative of these. Metal chalcogenides such as CdS, CdSe, PbS, and ZnSe are also popular materials for semiconductor-enhanced Raman scattering. Other semiconductor materials for enhanced Raman scattering are doped semiconductors like doped TiO_2, graphene, Si, and Si and Ge nanowires. The representative enhanced Raman active semiconductor materials are summarized in ref. 34, 243, 416 and 417. The EF of semiconductor-enhanced Raman scattering is, in general, 10^3–10^8.

The advantages of semiconductor enhanced Raman scattering are summarized as follows:[34,243,416,417]

(1) Semiconductor materials have excellent high chemical and thermal stability. Thus, they can avoid the problem of signal reproducibility caused by substrate oxidation. Moreover, they have broadened the applicable media of enhanced Raman technique, such as strong oxidation medium, strong acid medium, high-pressure medium and so on.

(2) Semiconductor materials have superb surface modifiability. In contrast to metal materials, most of common functional groups can be directly adsorbed on semiconductor materials surfaces. In other words, the surface of semiconductor materials is modified more flexibly than that of metal materials.

(3) Semiconductor materials have good biocompatibility. They have several hydroxyl groups on their surface, allowing them to combine with proteins through amino groups and carboxyl groups. Such binding ability solves the problem of biocompatibility of metal-based SERS technique.

(4) Semiconductor materials encompass a diverse range of species that are characterized by their low cost and established preparation methods. The energy levels and structural properties of these semiconductors can be finely tuned through various techniques, including adjustments to size, shape, material composition, and doping. This versatility facilitates the selection of appropriate semiconductor substrates tailored to meet specific detection requirements.

(5) Semiconductor materials have been used extensively as active components in a variety of practical devices. The wide applicability of semiconductor materials provides more possibilities for the application of enhanced Raman scattering.

The SERS enhancement mechanisms for dielectrics, particularly semiconductors, also encompass both electromagnetic

and chemical enhancement.[21] Unlike metals, which exhibit LSPR due to high-density of free electrons, the dielectric materials primarily achieve electromagnetic enhancement through light-trapping and subwavelength-focusing capabilities, as well as morphology-dependent resonances such as Mie resonance. These enhancement effects are closely related to the morphology of the dielectric material. For highly doped semiconductors, plasmonic resonances can be induced in the low-frequency range (generally in the near-infrared to mid-infrared regime).

Additionally, CT process between semiconductors and molecules constitutes an important chemical enhancement mechanism in semiconductor SERS substrates. In fact, most of the current CT mechanism models in semiconductor SERS originate from Lombardi's pioneering work in 1979.[115] The CT process is influenced by the vibronic coupling between the conduction band (CB) and the valence band (VB), as well as between the excited and ground states of the molecules involved.[415] CT models applicable to semiconductor-enhanced Raman scattering can be categorized into three distinct types: ground-state CT, electronic resonant transitions, and excited-state CT. The first two categories align with the CT models established for metal-based surface-enhanced Raman scattering (SERS), whereas the excited-state CT model for semiconductor SERS exhibits greater complexity. For example, a CT complex (similar as a new molecule) formed by the strong chemical bonding between the molecule and semiconductor generally possesses new energy levels, providing additional CT pathways.[418] This is even more important when the excitation light does not have enough energy to excite CT transitions between two original energy levels in a semiconductor–molecule system. Fig. 44 shows various mechanisms of a photo-induced CT process (blue line) and coupling scheme (purple line) in semiconductor–molecule systems.

From a methodological perspective, it is important to note that highly efficient CT transitions typically occur in semiconductor-molecule systems at the nanometer scale due to the size-dependent behavior of electronic properties in semiconductor nanomaterials. Therefore, theoretical modeling should account for the size effect. Although various CT pathways have been proposed based on DFT calculations, experimental investigations into semiconductor CT mechanisms remain relatively limited.[243] To elucidate the specific enhancement mechanisms, more systematic and correlated experiments, such as ultrafast dynamics studies, are essential.

Another challenge lies in the size mismatch issue. While CT transitions typically occur in nanoscale semiconductors, effective regulation of the visible and near-infrared electromagnetic fields requires semiconductor materials with feature sizes ranging from sub-micrometers to micrometers. To address this size mismatch issue, a rational approach is to design semiconductor superstructures, which allows for the integration and further optimization of the synergistic effect between electromagnetic and chemical enhancement.[419,420] In such a superstructure, the engineering of size and morphology can induce light-trapping effects, subwavelength focusing capabilities, and morphology-dependent resonances. These modifications contribute to a substantial electromagnetic enhancement of SERS. Additionally, a highly efficient CT contribution arising from the structure of the superstructure further amplifies the SERS signals.

Note that SPR in semiconducting materials could be contributable to SERS on semiconductors.[421] In such case, plasmons may lower the material stability. The carrier density of semiconductors can span several orders of magnitude based on doping techniques, increasing opportunities for SERS-based applications.[422] In addition, noble metal SPR is found to be capable of promoting CT in semiconductor–molecule systems, and their synergistic contribution enables giant Raman signal enhancement on metal–semiconductor heterostructures.[423,424]

Semiconductor-enhanced Raman scattering has opened a variety of new research fields in photoelectrochemistry, catalysis research, bioscience, and sensing technology. The high chemical stability of semiconductor materials enhances the sensing performance including spectral reproducibility increasing the reliability of enhanced Raman scattering analytical experiments. The superior biocompatibility has opened a variety of new applications in life sciences.

For example, Hildebrandt, Weidinger and colleagues reported the redox process of heme proteins on nanostructured TiO_2 electrodes.[425] It has also become possible to explore the photoelectrical properties of adsorbents on the semiconductor surfaces such as dye-sensitized solar cells, lithium–ion batteries, and semiconductor-supported photocatalytic process. A number of new applications have emerged; for example, submicron-sized ZnO superstructures have demonstrated excellent SERS performances with the synergistic effect of Mie resonance-induced electric field with CT.[419] Furthermore, ZIF-8 coated ZnO superstructures could further concentrate the electric field around particle surface, permitting signal enhancement for the detection of non-adsorbing volatile organic compounds.[426] Besides, Ji, Ozaki, Xie and colleagues, demonstrated the feasibility of large-area fabricating SERS-active semiconductor substrates for the assessment of heavy metal ion toxicity based on screen-printing of micron-sized TiO_2 inks synthesized through a simple flame thermal-assisted method.[427] The resultant TiO_2 microspherical arrays (MSAs) exhibit extraordinary SERS sensitivity with an EF of 3.28×10^7, which represents one of the highest sensitivity and are the easiest strategy among the reported SERS-active semiconductor substrates.

Note that caution must be exercised when quantifying EFs in these systems, particularly when using widely employed fluorescent molecules, as resonance Raman effects and fluorescence quenching may lead to a significant overestimation of the SERS EF (see Section 4.7.1 for detailed discussions). For a comprehensive discussion on this topic, we recommend the reviews by Lombardi and Alessandri,[243] and Ozaki, Itoh, Procházka, Dong and colleagues.[34]

4.6.3 Graphene-enhanced Raman scattering. In 2010, Zhang, Liu and coauthors found that monolayer graphene

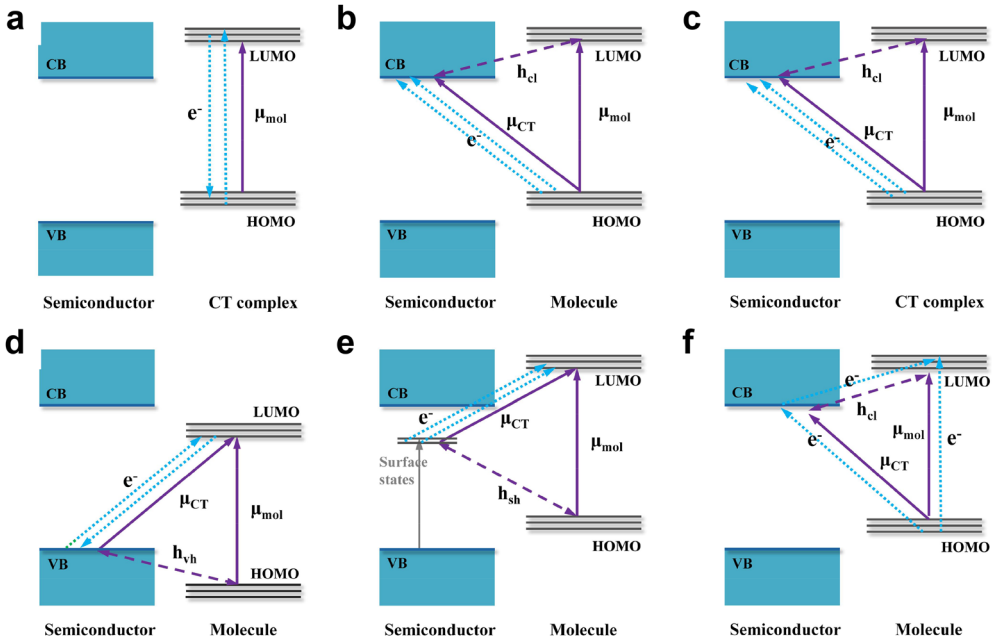

Fig. 44 Various mechanisms of a photo-induced CT process (blue line) and coupling scheme (purple line) in semiconductor–molecule systems. (a) Resonant excitation of the CT complex, (b) molecular HOMO-to-CB, (c) CT complex-to-CB, (d) VB-to-molecular LUMO, (e) surface state to molecular LUMO, and (f) molecular excited state-to-CB transitions. Figures are adapted from ref. 417 with permission. Copyright 2018 World Scientific Publishing Europe Ltd.

can quench the fluorescence of R6G molecules, while simultaneously enhancing their Raman scattering by tens of times, termed as graphene-enhanced Raman scattering (GERS).[408] Due to the lack of surface plasmon in the visible optical region in graphene, GERS was attributed to a pure chemical mechanism.[428] The EF is accordingly dependent on the LUMO/HOMO positions and the steric configuration of molecules as discussed in Section 2.6.6. Later on, the combination of graphene and metal nanoparticles was developed for sensitive detection of molecules. Zhang and coauthors further reported a type of flat SERS substrate, that is, graphene-mediated SERS, where a monolayer of graphene is on the surface of metal nano islands supported by a transparent polymer film,[429] which makes graphene possible for practical SERS detection. This concept is similar to SHINERS with the ultrathin core replaced by monolayer graphene. The fact that graphene can enhance the Raman signal expands SERS substrates to the family of two-dimensional layered materials, which can be either metallic or semiconducting.[430,431] The reported limits of detection of a few two-dimensional materials and van Hove heterostructures can be surprisingly down to 10^{-13} M *via* resonance design.[432] Nevertheless, Raman enhancement on two-dimensional materials provides a platform to study material properties, and more efforts are necessary to move to practical SERS detection.

The position of the Fermi level in graphene plays a crucial role in determining the EF of GERS.[433] Consequently, modulating the Fermi level in graphene provides a valuable strategy for controlling the EF of GERS. In recent years, dynamic modulation approaches have emerged as an effective means to address the limitations posed by the fixed optical properties of conventional SERS substrates post-preparation. Notably, photo modulation has been employed to dynamically control SERS signals by manipulating the Fermi level of graphene or other materials through UV-induced adsorption and desorption of gas molecules, as evidenced in studies utilizing reduced graphene oxide (rGO) and polystyrene (PS) nanoarrays.[434] Additionally, electrical modulation techniques, including piezoelectric,[435] thermoelectric,[436] and pyroelectric methods,[437] have garnered significant attention. For example, piezoelectric substrates convert mechanical pressure into electrical energy, thereby enhancing SERS signals through charge injection into plasmonic nanostructures.[435] Likewise, thermoelectric substrates, such as those incorporating GaN with Ag nanoparticles, capitalize on temperature gradients to regulate CT, significantly improving SERS signal intensity.[436] Furthermore, ferroelectric materials have been utilized to modulate the energy band structure of graphene oxide, facilitating flexible tuning of CT processes and enhancing SERS responses across various analytes.[438] Collectively, these advancements underscore the potential of active modulation techniques to enable real-time adjustments in SERS performance, thereby expanding the applicability of this sensitive analytical tool in diverse fields, including environmental monitoring and biomedical diagnostics.

4.6.4 Non-traditional excitation wavelength SERS: the UV and NIR-SERS. Besides the materials generality, extending the excitation laser wavelength of SERS beyond the visible regime is another viable way for expanding the generality and versatility of SERS as a powerful analytical technique. Extending towards NIR was achieved much earlier than the opposite UV direction, as the SPR of Ag and Au usually extends to NIR, while due to

their electronic structure limit the frequency of SPR to visible range (also related to the dielectric constant of metals), it is difficult to generate SPR in the ultraviolet region. Extension to the UV direction was on the other hand, somehow done in parallel to the exploration of new substrate materials beyond the coinage metals.

Near-infrared Fourier transform surface-enhanced Raman spectroscopy (NIR-FT-SERS) microprobe spectroscopy offers distinct advantages over visible SERS due to the reduced likelihood of surface photochemical changes induced by near-infrared radiation, potential avoidance of sample fluorescence, and an EF that is approximately an order of magnitude greater than that achieved with visible excitation. In NIR-FT-SERS, the excitation of Raman scattering is facilitated by a Nd:YAG laser operating at wavelength of 1064 nm, with spectrum acquisition conducted using a Fourier Transform Infrared (IR) spectrometer that operates within the near-infrared spectral range. Owing to these advantages, significant interest has emerged in utilizing NIR-SERS spectroscopy as a novel analytical technique for acquiring structural insights regarding adsorption and reactivity within the initial adsorption layer. Fig. 45a and b depicts the NIR-SERS microprobe spectra of pyridine adsorbed on a roughened Au or electrode in a 0.5 M LiCl aqueous solution under 1064 nm excitation at various characteristic potentials in 1988.[439]

However, this strategy cannot be applied to the UV region. This is because the SPR of SERS-active materials such as Ag and Au is difficult to extend to the UV range, where the interband transition from d band to sp band is dominated. The development of new substrate materials is necessary for such an extension. Tian and colleagues were the first to observe SERS excited by UV light on transition-metal electrodes (Fig. 45c and d).[441] The adsorption of pyridine and SCN^- on roughened Rh and Ru electrodes, respectively, was investigated with 325 nm laser excitation. The experimental UV-SERS findings in 2003 align with initial theoretical calculations grounded in the electromagnetic enhancement mechanism, indicating an EF of approximately two orders of magnitude for Rh and Ru electrodes under 325 nm excitation.

Popp group found later that Al acts as a SERS-active substrate for deep-UV excitation wavelengths in 2008. They reported a UV-SERS spectrum of a 1×10^{-4} M crystal violet solution on a 50 nm thick Al surface, excited with a 244 nm laser (Fig. 45e).[440] Al with different nanostructures, such as nanovoids and Al film-over-nanosphere substrates, was then gradually developed into a main deep-UV SERS-active substrate. In 2014, Halas group reported the fabrication of Al nanodisks using electron beam lithography, demonstrating tunable plasmon resonance from UV to visible region, as shown in Fig. 46a.[442] However, individual nanodisks struggled to generate sufficiently strong hot spots for SERS detection. In 2016, Van Duyne group reported the first fabrication of Al film-over nanosphere (AlFON) substrates for UV SERRS at the deepest UV wavelength (λ_{ext} = 229 nm).[443]

Subsequently, in 2017, Halas group achieved SERS measurements using Al nanocrystals (NCs), which involved a chemical synthesis with uniform shape and controllable size, as shown in Fig. 46b.[445] Interest in Al nanocrystal plasmonics for SERS is due to the sustainable and earth-abundant nature of Al (20 000 times less expensive than Au). Most importantly, the development of bottom-up chemical syntheses resulted in highly pure Al with far fewer impurities than top-down fabrication methods. For SERS, this results in substrates with significantly larger field enhancements than obtainable with Al SERS substrates fabricated using film deposition methods. Other advantage of Al is the remarkable size-tunability, ranging from the UV into the mid-infrared and the thin oxide surface of Al, which facilitates far more binding chemistries than Au-based SERS substrates.[446] In contrast to Ag nanoparticles, the self-terminating surface oxide passivates the Al nanocrystal surface, making the metal nanoparticle more stable. Fig. 46c shows how Al nanocrystals of different sizes can be synthesized by a straightforward change in their growth conditions (solvent used during synthesis).[444] Fig. 46d and e compares the SERS spectrum obtained with both Al and Au substrates and with the normal Raman spectrum of the molecules under study.[445] It is worth pointing out that in the case of Al SERS substrates, the analyte spectrum is more similar to that of the unenhanced Raman spectrum than for Au substrates.

4.6.5 Shell-isolated nanoparticle-enhanced Raman spectroscopy. As discussed in previous sections, researchers have made significant strides in expanding the applicability of SERS to various materials through the ''borrowing SERS activity'' strategies (see Section 3.1). While these methods have broadened the general applicability of SERS materials, they encounter difficulties when applied to the detection on smooth surfaces and well-defined crystalline surfaces. In terms of surface morphology, it is essential to explore alternative methods for generating SERS activity on atomically flat single-crystal surfaces.

One potential approach involves the excitation of SPPs on the flat metallic surface through the implementation of a specialized optical configuration. Although the ATR-SERS had been developed since the 1980s to study the smooth single-crystal surfaces, the EF is limited to around one to two orders of magnitude. The invention of TERS in 2000 provided a solution to the limited surface generality of SERS. In TERS, the LSPR effect is harnessed to amplify the electromagnetic field at the apex of a plasmonic probe. When the probe is irradiated with a laser source of appropriate wavelength, the resultant enhanced electromagnetic field can interact with a sample positioned in close proximity to the probe's apex. In principle, TERS is promising for solving the issue of substrate and surface generalities as the Raman signals from any substrate regardless of material and surface smoothness can be increased by borrowing from the tip apex enhancement, as shown in Table 3. However, TERS is strongly dependent on sophisticated instrumentation, and its total Raman signals are very low as only a singular nanotip works as the Raman amplifier. These issues make TERS impractical for many applications.

In 2010, SHINERS[20] was invented to tackle the above-mentioned limitations of SERS in study of single-crystal

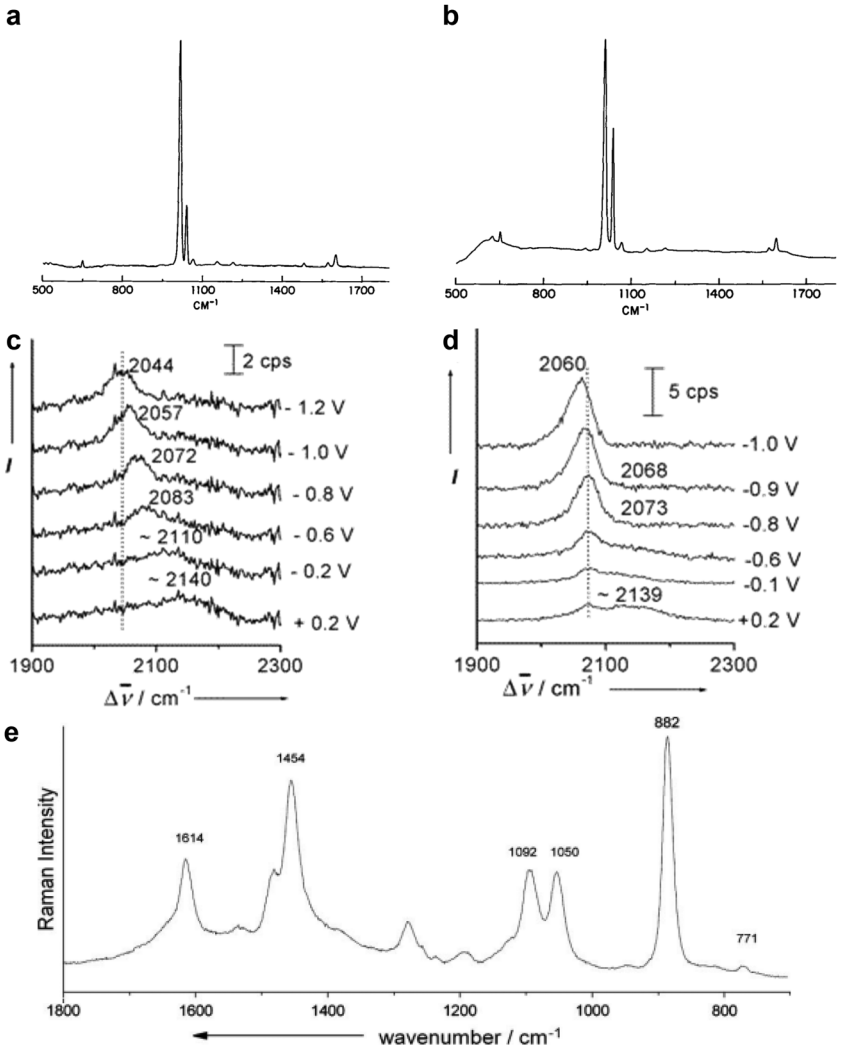

Fig. 45 (a) and (b) NIR-SERS spectrum of (a) a pyridine/Au electrode and (b) a pyridine/Ag electrode at −0.6 V *versus* Ag/AgCl 0.05 M pyridine, 0.5 M LiCl after roughening. UV-SERS spectra of SCN^- on Rh (c) and Ru (d) electrodes as a function of the applied potential. (e) Deep-UV SERS spectrum of a 1×10^{-4} M crystal violet solution on a 50 nm thick aluminum surface, the wavelength of the incident laser was 244 nm. Reproduced from ref. 439–441 with permissions. Copyright 1988 Society for Applied Spectroscopy, Copyright 2003 American Chemical Society. Copyright 2007 Wiley.

surfaces and SERS-inactive materials (Fig. 47). SHINERS is the latest version of the ''borrowing SERS activity'' strategy and utilizes shell-isolated nanoparticles that feature plasmonic cores made of Au or Ag and are encased in ultrathin (1–5 nm) shells that are chemically and electrically inert, such as SiO_2 or Al_2O_3. In SHINERS, the Au cores can generate strong electromagnetic fields to enhance the Raman signals of molecules nearby, while the chemically and electrically inert silica shells can prevent direct contact between the Au/Ag core and probe materials, thus avoiding interference from the metal cores and improving the universality of probed materials and surface morphology (Fig. 24f and 25f). In principle, SHINERS can achieve trace analysis on any surfaces by simply spreading many Au@SiO_2 core–shell nanoparticles – typically around a thousand within the light spot – on the surface to be probed, thus solving, at least to some extent, the long-standing materials and morphology limitations of traditional SERS.

The benefits of SHINERS are multifaceted. Firstly, the ultrathin, pinhole-free shells effectively isolate the core particles from the surrounding material surface and environment, thereby reducing interference from the Au and Ag cores. Secondly, the chemically inert nature of the shell inhibits fusion of both interparticle and particles with the metal substrate, thus significantly improving the stability of the nanoparticles and probe configurations. Thirdly, the thickness of the shell can be manipulated to regulate the nanogap between the Au or Ag core particles and the substrate, which in turn influences the electromagnetic coupling between the particles and the substrate. Finally, the Au and Ag cores enhance the local electromagnetic field, thereby amplifying Raman signals from the probe substrate while maintaining its structural integrity.

SHINERS is distinguished from contact-mode SERS and TERS by the presence of an inert, ultrathin shell, which acts

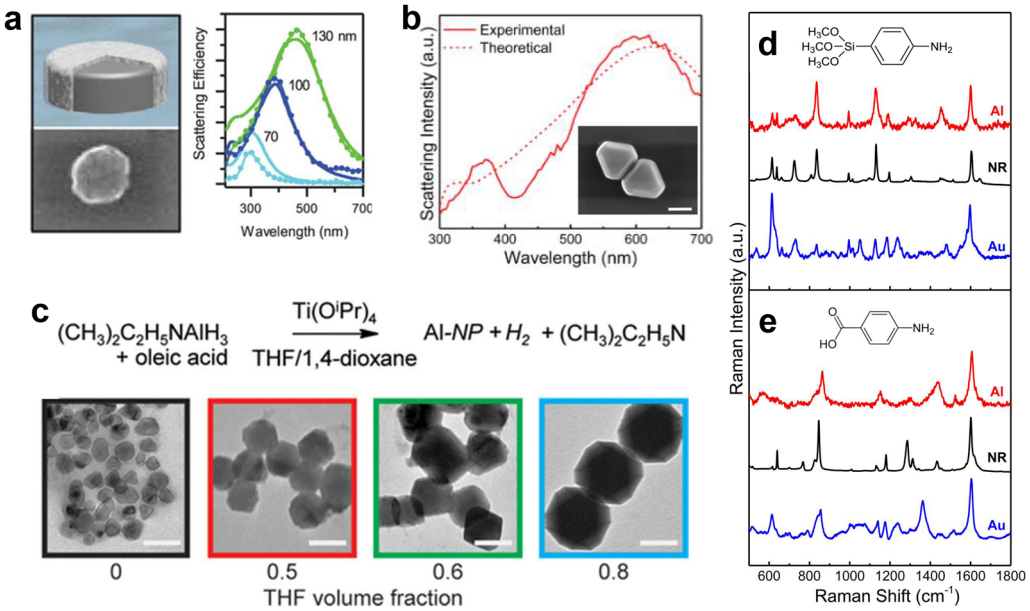

Fig. 46 (a) Aluminum plasmon generated by aluminum nano disk. (b) Experimental and theoretical extinction spectra of monodisperse Al nanocrystals in isopropanol, the inset shows the SEM image of an Al dimer (scale bar = 200 nm). (c) Size control of aluminum nanocrystals. Increasing the fraction of tetrahydrafuran (THF) in a 1,4-dioxane/THF solution yields larger nanocrystals. The top panel shows the reaction scheme for synthesis of aluminum nanocrystals. The bottom panel shows the representative TEM images from synthesis with 0, 0.5, 0.6, and 0.8 THF volume fractions in a THF/1,4-dioxane solution (from left to right) (scale bar = 100 nm). (d) SERS spectra of APhS and (e) PABA on Al (red) and Au (blue) substrates with normal Raman spectra (black) as reference. Figures are adapted from ref. 442, 444 and 445 with permissions. Copyright 2014, 2015 & 2017 American Chemical Society.

Table 3 The comparison between localized surface plasmon, Raman spectroscopy, SERS, TERS, and SHINERS

	Localized surface plasmon, LSP	Raman spectroscopy	SERS (LSP + Raman)	TERS (LSP + Raman + tip)	SHINERS (LSP + Raman + shell)
Sensitivity	Excellent Single molecules	Poor Many molecules	Excellent Single molecules	Excellent Single bond	Excellent Single molecules
Energetic resolution	Poor $\sim 10^{-2}$ eV	Excellent $\sim 10^{-4}$ eV (1 cm^{-1})	Excellent $\sim 10^{-4}$ eV (1 cm^{-1})	Excellent $\sim 10^{-4}$ eV (1 cm^{-1})	Excellent $\sim 10^{-4}$ eV (1 cm^{-1})
Spatial resolution	Good-excellent $\sim$200 nm (far field) $\sim$3 nm (near field)	Good $\sim$200 nm	Good $\sim$200 nm	Excellent $\sim$3 nm (Ambient) Sub-Å (UHV, LT)	Good $\sim$200 nm
Materials generality	Poor Au, Ag, Cu, Li, ...	Excellent	Poor Au, Ag, Cu, Li, ...	Poor Au, Ag, Cu, Li, ...	Poor Au, Ag, Cu, Li, ...
Morphology generality	Nanostructure	Any morphologies	Nanostructure	Flat surface	Any morphologies
Molecule generality	Adsorbed molecules	Any molecules	Adsorbed molecules	Adsorbed molecules	Adsorbed molecules
Nanostructure Stability	Poor Atomic migration	—	Poor Atomic migration	Poor Atomic migration	Good Shell protected

as an insulating barrier, preventing direct interaction between the probe materials and the noble-metal cores composed of Au and Ag (shell-isolated mode). SERS implicitly involves direct contact between the SPR-active nanostructure surface and the probe target (molecules or materials) (contact mode), as shown in Fig. 47a and b. Therefore, SHINERS cannot be classified as a SERS technique. This distinction also applies to TERS. However, since SERS, TERS, and SHINERS all involve local field enhancement primarily from SPR enhancement, each can be considered as a unique PERS (plasmon-enhanced raman spectroscopy) technique. The detailed comparison of the LSP, Raman and those PERS techniques are shown in Table 3. Based on SHINERS, Tian group successfully acquired Raman signals of molecules adsorbed on Au and Pt single-crystals. The average EFs for Au(110) and Pt(110) reach 10^6 and 10^5, respectively, which are found to be equivalent to, or in some instances surpass, the EFs achieved with bare Au nanoparticles.[447] Moreover, this approach enables *in situ* Raman measurements of weakly adsorbed species like water molecules on single-crystal transition metal surfaces, a feat previously unattainable (see Section 5.2.1).

It should be noted that, although SHINERS addresses several limitations associated with contact-mode SERS for surface analysis, it is accompanied by a reduction in Raman enhancement.[21,269] Specifically, the interparticle plasmonic coupling and the coupling between the nanoparticles and the

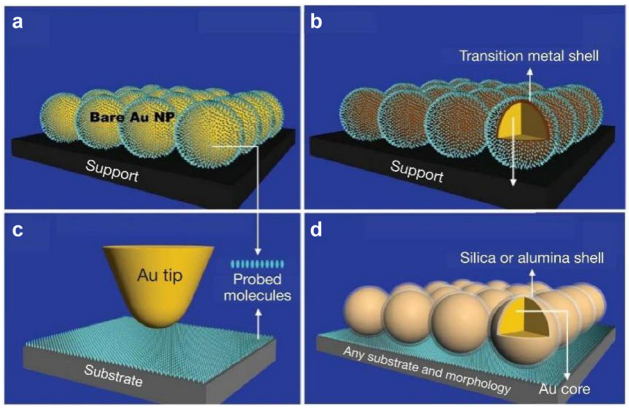

Fig. 47 Schematic of the mode of SERS, TERS, and SHINERS. (a) Bare Au nanoparticles: contact mode. (b) Au core–transition metal shell nanoparticles adsorbed by probed molecules: contact mode. (c) TERS: non-contact mode. (d) SHINERS: shell-isolated mode. Figures are reproduced from ref. 20 with permission. Copyright 2010 Springer Nature.

substrate in shell-isolated nanoparticle-on-substrate configurations are relatively moderate when compared with bare nanoparticle-on-substrate systems. Consequently, dependent on the thickness and dielectric constant of the shells, the average enhancement factor achieved through SHINERS may be lower than that obtained from a bare gold nanoparticle dimer situated on silicon and platinum substrates, respectively. However, theoretical studies have shown that by optimizing the thickness and refractive index of the SHIN shell, the sensitivity of SHINERS can even surpass that of traditional bare Au nanoparticles. Nevertheless, achieving this goal remains experimentally challenging due to the need to fabricate ultrathin yet dense shells.

Another important development of SHINERS is that the ultrathin inert shell-isolated strategy is also applied to TERS by Li and Zenobi group and named as shell-isolated tip-enhanced Raman spectroscopy (SITERS).[448] In traditional TERS, although its working principle is based on the non-contact mode (someone called as the gap mode), the exposed tip may still lead to direct adsorption of the analyte molecules onto the tip surface, causing signal interference, especially in studying different facets of single crystal surfaces. This issue is particularly evident in solution systems. Therefore, coating the tip with an inert shell to shift from the traditional non-contact mode to a shell-isolated mode can prevent the adsorption of analyte molecules on the tip, thereby expanding the application range of TERS. In addition, the shell of SHINs can be functionalized by modifying its composition to meet specific detection requirements, such as acid and alkali resistance or anti-sintering properties.

4.7 Key methods for evaluation of enhancement factors

To ensure the precision and reliability of SERS, it is essential to develop quantitative analysis techniques for SERS. The emergence of the SERS field can be traced back to Van Duyne's quantitative analysis of spectral EFs.[2] In 1983, Moskovits and colleagues observed an enhancement exceeding 4×10^6 for colloidal Ag nanoparticles (Ag NPs) by comparing the Raman intensity of the SERS signal with that of normal Raman spectroscopy under the same experimental conditions.[449] From the current definition, this article was the first to calculate the average Raman EF.

Notably, the EF encompasses not only electromagnetic enhancement from nanostructures but also chemical enhancement mechanisms, including resonant Raman effects and charge transfer processes (see eqn (4) and Fig. 49). Consequently, EF can be defined and quantified differently depending on the specific aspects under consideration, leading to varying values across different analytical frameworks. In 1984, Stockburger and colleagues introduced the concept of EF to assess the SERS performance of colloidal substrates.[450] They defined EF as

$$\mathrm{EF} = \frac{I_{\mathrm{SERS}}}{c_{\mathrm{surf}} \cdot f_{\mathrm{sh}}} \Big/ \frac{I_{\mathrm{Raman}}}{c_{\mathrm{bulk}}} \tag{5}$$

where c_{surf} and c_{bulk} represent the concentrations of molecules at the surface and in solution, respectively, and f_{sh} signifies the shielding effect of colloidal particles on incident and scattered light. The researchers recommended determining I_{SERS} within the linear adsorption isotherm range but did not provide guidance on how to establish c_{surf}.

In 1997, two groups[14,15] reported the observation of SERS spectra from single dye molecules on Ag nanoparticle colloids independently. The single-molecule EF, which is the SERS enhancement of a given molecule at a specific point, is influenced by various factors, such as the Raman tensor of the molecule, its orientation on the SERS substrate, and the local electric field at the specific point. Additionally, the orientation of the SERS substrate in relation to the incident laser polarization and direction also plays a significant role in determining EF. Therefore, a precise definition of the SERS substrate geometry and the accurate positioning and orientation of the molecule on the substrate are essential in calculating EF. The single molecule EF is defined as

$$\mathrm{EF} = I^{\mathrm{SM}}_{\mathrm{SERS}} / I^{\mathrm{SM}}_{\mathrm{Raman}} \tag{6}$$

where $I^{\mathrm{SM}}_{\mathrm{SERS}}$ denotes the SERS intensity associated with the specific single molecule being analyzed and $I^{\mathrm{SM}}_{\mathrm{Raman}}$ represents the average Raman intensity per molecule for the same probe.[203]

It should be noted that in the original SM-SERS report, EFs of the order of 10^{14} $I^{\mathrm{SM}}_{\mathrm{SERS}}$ were taken for a resonant molecule.[14] Even in the absence of plasmonic nanostructures, the Raman EFs of resonant molecules induced by resonance Raman effects can achieve 10^4–10^6. Therefore, more realistic EFs of SM-SERS in terms of EM enhancement are of the order of 10^8–10^{10}, which is sufficient for SM-SERS detection in the best conditions with dye molecules such as R6G with resonance Raman enhancement of 10^6. It is crucial to distinguish whether the study concerns SERS (non-resonant molecules) or SERRS (resonant molecules) when quantifying the Raman EF. If the process under investigation is SERRS, it is essential to exclude the

Raman enhancement resulting from the resonance Raman effect in the resonant molecules to obtain an accurate Raman EF from nanostructures.

In 1998, Tian and coworkers[402] proposed a similar EF for evaluating solid SERS substrates as

$$\mathrm{EF} = \frac{I_{\mathrm{SERS}}}{N_{\mathrm{SERS}}} \Big/ \frac{I_{\mathrm{Raman}}}{N_{\mathrm{Raman}}} \tag{7}$$

where I_{SERS} and I_{Raman} denote SERS and normal Raman intensities, while N_{SERS} and N_{Raman} indicate the number of molecules contributing to the respective signals. This formulation elucidates the essence of SERS enhancement and found widespread use in assessing the SERS activity of different substrates. Nevertheless, accurately determining N_{SERS} and N_{Raman} experimentally, particularly for molecules with poorly characterized adsorption behaviors, poses challenges and may lead to significant variations in EF, even within the same type of SERS substrates.

The confocal microscope possesses excellent depth discrimination, ensuring that only a minuscule effective volume of the solution is probed. This capability significantly reduces the interference from robust Raman signals that may arise from the bulk phase of the solution. Furthermore, the integration of the confocal microscope system facilitates a considerable enhancement in the numerical aperture (N.A.) of the objective lens, which in turn greatly increases the solid angle available for the collection of scattered photons. The direct determination of the term N_{Raman} should be derived by considering the confocal properties of the microscope. Fig. 48 illustrates the spatial intensity distribution, specifically the waist contour, of a laser beam that has been focused within an aqueous medium. Conventionally, it is assumed that all molecules within the irradiated volume of the solution contribute to the quantity denoted as N_{Raman}. However, the efficiency of photon collection from molecules dispersed throughout the solution exhibits variation in accordance with the confocal depth, which influences the efficiency of scattered photon detection across different planes within the illuminated volume. Molecules located at the ideally focused plane (where z equals zero) contribute the most to the overall intensity. Thus the N_{Raman} should be written as $N_{\mathrm{Raman}} = AhcN_{\mathrm{A}}$, where A is the area of the focal spot of laser. h is the height of the effective layer, depending on the pinhole size and the objective lens. c is the concentration of the molecules and N_{A} is the Avogadro constant.

In 2007, Etchegoin, Le Ru and coworkers introduced the analytical EF (AEF) as

$$\mathrm{AEF} = \frac{I_{\mathrm{SERS}}}{C_{\mathrm{SERS}}} \Big/ \frac{I_{\mathrm{Raman}}}{C_{\mathrm{Raman}}} \tag{8}$$

where C_{SERS} and C_{Raman} represent the solution concentrations used for SERS and normal Raman spectroscopy, respectively.[203] AEF offers a practical alternative for evaluating substrates' sensitivity to analytes initially in solution or gas phase. However, Le Ru and colleagues noted that AEF, being more experimentally oriented, overlooks the transfer of analytes from bulk to the surface and provides averaged results. This characteristic renders AEF susceptible to changes with varying experimental conditions, including alterations in C_{SERS} and C_{Raman}, making theoretical modeling challenging. The issues related to the determination of the number of species being probed (N_{Raman} or N_{SERS}) led Brolo group to suggest a new procedure for the evaluation of SERS substrates that utilizes single-molecule statistics in SERS.[451] The method does not require the determination of N_{Raman} as single molecules are involved in the SERS experiments. The method allows substrates to be evaluated using three different metrics related to the maximum average EF, the density of hot spots within the probed area and the average hot spot localization.

TERS significantly enhances signals due to the intensified electromagnetic field at the tip apex, a result of the LSP and the lightning rod effect. The technique detects a rapidly diminishing near-field signal from a minuscule scattering volume, which is scattered by the tip in the presence of a far-field background emanating from the entire illuminated region. The expression of the EF in TERS is defined as[452]

$$\mathrm{EF}_{\mathrm{TERS}} = \left(\frac{I_{\mathrm{Tip}} - I_0}{I_0}\right)\frac{{R_{\mathrm{FF}}}^2}{{R_{\mathrm{NF}}}^2} \tag{9}$$

where I_{Tip} and I_0 are the Raman signal intensities with the tip in contact and retracted from the sample, respectively. R_{FF} is the radii of the focus laser beam spot, and R_{NF} is the radii of sample areas probed in the near-field. There are two methods to calculate R_{NF}: one is based on the tip apex curvature radius,[453] and the other is derived from the spatial resolution of the TERS imaging.[452]

From a fundamental research perspective, there remains a considerable discrepancy between theoretical predictions and experimental measurements of SERS/TERS EFs. For instance, experimentally calculated EFs are often significantly lower than those predicted theoretically. Accurate quantification necessitates accounting for not only the electromagnetic mechanism in nanostructures, which can be strongly orientation-dependent, but also the chemical enhancement mechanism. This includes considering both resonant and non-resonant effects, as well as the average effect of single and multiple hot spots, which remains a substantial challenge in the field.

This challenge also partly arises from an inherent contradiction between the ultra-sensitivity of SERS substrates and their capability for quantitative detection. The ultra-sensitive SERS "hotspots" required for high sensitivity detection can dramatically amplify molecular signals, making it exceedingly difficult to accurately estimate the number of molecules. Furthermore, metal colloids and solid substrates are prone to aggregation, contamination, surface reconstruction, and degradation when exposed to ambient environments. These factors, along with variations of laser and optical alignment, lead to instability in SERS signals, thereby affecting the accuracy and reproducibility of quantitative analysis.

Overcoming the primary challenge in achieving quantitative analysis with SERS involves addressing the uniformity and reliability of the SERS substrates, which requires the standardized production of uniform SERS substrates, such as

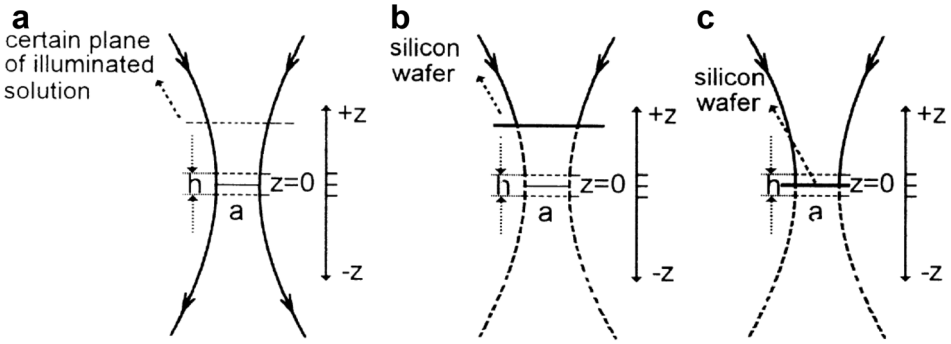

Fig. 48 (a) Illustration of the contribution to I_{Raman} from a certain plane of illuminated solution. (b) and (c) Illustration of vertical movement of a flat Si waver for obtaining the confocal depth dependence of the Raman signal. Reproduced from ref. 402 with permission. Copyright 1998 Elsevier.

nanoarrays with specific arrangements.[454] Bell, Xu, and coworkers showcased emulsion-templated self-assembly as a method capable of producing consistently spherical colloidal aggregates that are free of surface modifications and maintain stability for extended periods.[455] The robust stability and potent plasmonic enhancement of these aggregates enable precise and quantitative detection of weakly adsorbing analytes in protein-rich biomedia through SERS.

Therefore, when analyzing the total SERS EF (Fig. 49), it is crucial to consider the contributions of SERS enhancement from different aspects quantitively and distinguish between average EF and maximal EF. The former is typically associated with large-area SERS substrates, while the latter is commonly estimated in single-molecule or single-particle experiments. For instance, the widely accepted SERS EF for colloidal Au and Ag nanoparticles is often cited as 10^6,[456] which generally refers to the average EF. In contrast, single-molecule SERS experiments frequently report factors of up to 10^{15},[14,457] which are typically defined as the maximal EF. It is important to note that such maximal EF usually encompass the combined contributions of multiple enhancement mechanisms, including electromagnetic field enhancement, resonance effects, and chemical enhancement, as shown in Fig. 49.

In the context of EM mechanism, the quality factor (or the loss of the plasmonic mode) and the mode volume of the plasmonic mode are the key factors to determine the EM enhancement. For individual Ag, Au nanoparticles, average SERS EF typically range from 10 to 10^3, with maximal EF from 10^2 to 10^4.[21,456] Notably, plasmonic coupling between nanostructures can significantly reduce the mode volume, thereby generating intense hotspots. In such coupled systems, maximal SERS EF can reach 10^8–10^{10}, with average EFs exceeding 10^6.[21,456] In extreme cases involving atomic-scale protrusions within the hotspots, such as the picocavity, maximal EF can surpass 10^{12}.[34,358,457]

Conversely, for non-traditional metals other than Ag and Au, increased plasmonic losses lead to decreased plasmonic resonance quality, resulting in reduced SERS EFs. For instance, typical average EFs for these materials generally fall within the range of 10 to 10^4.[165] In addition to metallic materials, the SERS EF of dielectric substrates, utilizing Mie scattering and the lightning rod effect, can reach up to 10^3.[458] Further, materials such as graphene achieve an SERS EF by a factor of approximately 10 *via* CE mechanism while the SERS EF on semiconductors can reach up to 10^7 or even 10^8.[408]

Another significant yet often overlooked effect in SERS is the resonance effect, which is associated with molecular electronic state transitions and excitation wavelength. This effect can provide additional signal enhancement beyond the electromagnetic (EM) mechanism. For instance, in the case of common R6G dye molecules, resonant excitation can contribute a resonance EF of up to 10^6.[456,457] This resonance effect plays a crucial role in compensating for signal enhancement in SM-SERS experiments. However, as previously discussed, the resonance effect is not general in SERS analytes. Besides, it should be noted that the resonance EFs for most fluorescent molecules beyond R6G are typically limited from 10^2 to 10^4. Moreover, upon surface adsorption, the anticipated resonance enhancement is usually attenuated due to chemisorption induced quenching, leading to less pronounced enhancement than expected. Consequently, an excessive focus on the substantial EFs or absolute signal intensities resulting from resonance Raman effects often has limited significance in broader SERS applications.

The CT mechanism in SERS is influenced by various factors, including the adsorption state, molecular orientation, and CT processes. While the contribution of chemical enhancement to the overall SERS enhancement is typically modest, ranging from 10 to 1000,[19,456,457] its significance should not be underestimated. From a surface chemistry perspective, understanding the CE mechanism is crucial for elucidating molecule–surface interactions *via* SERS. Moreover, for the application of SERS across diverse analytical fields, particularly in the development of quantitative or semi-quantitative analysis systems aimed at commercialization, a comprehensive grasp of chemical enhancement mechanisms is indispensable.

Moreover, for specific materials and systems under investigation, it is crucial to comprehensively evaluate the interplay between EM and CE mechanisms on enhancement factors. Notably, this interaction cannot be simplified as a mere

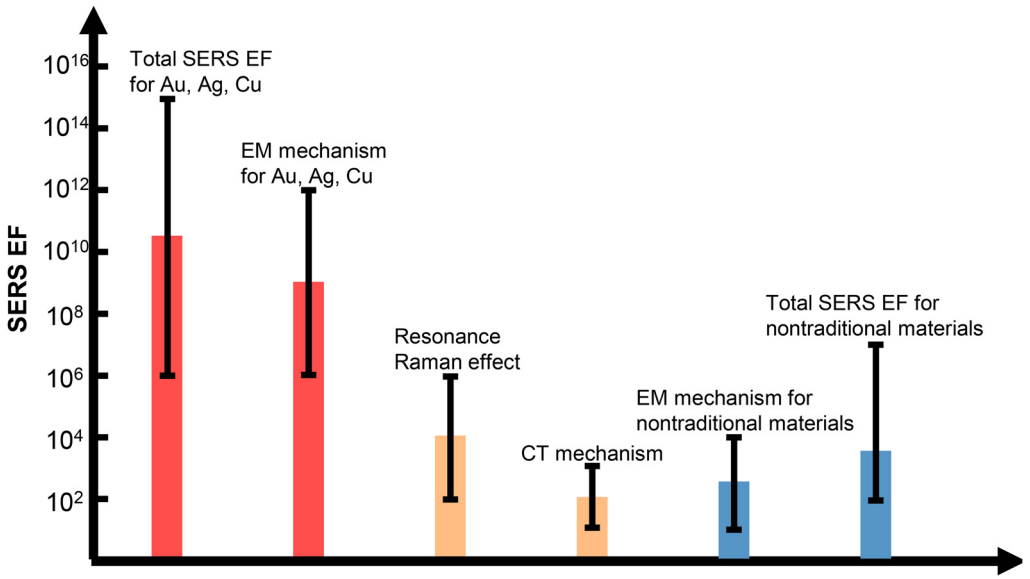

Fig. 49 Typical ranges of EM and CE contributions to the total SERS EF. The total SERS EF of Au, Ag, Cu and nontraditional materials have several contributions, including EM mechanism, resonance Raman effect and CT mechanism. The error bars represent the typical range of each contribution. For Au, Ag and Cu, the typical contribution of EM mechanism is 6 to 12 orders of magnitude, while that for nontraditional SERS materials is 1 to 4 orders of magnitude. The typical SERS EF resulted from the resonance Raman effect is approximately 2 to 6 orders of magnitude, while the that contributed by CT mechanism is about 1 to 3 orders of magnitude.

product of EM and CE contributions; rather, it demands comprehensive analysis of their complex interdependence. A prime example is the phenomenon of molecular adsorption at interfaces, which can simultaneously modify the interfacial refractive index,[459] thereby affecting both the optical response of nanostructures and the EM EF at hotspots. Consequently, the development of a self-consistent theoretical framework that integrates both physical and chemical enhancement effects[355,460,461] remains crucial for accurate SERS enhancement factor evaluation, although significant challenges persist in this endeavor.

4.8 Key methods for quantitative analysis

Quantitative analysis of molecular concentration and number is crucial for both fundamental research and practical applications of SERS. For example, in the development of SM-SERS, following its initial observation, SM-SERS faced considerable controversy within the scientific community. It wasn't until a decade after its first reported detection that SM-SERS was unequivocally validated. This confirmation came through rigorous quantitative analysis based on bi-analyte SERS experiments utilizing isotopically edited molecules.[212–214,462,463]

Quantitative analysis can be traced back to 1981, as shown in Fig. 22d, in which the first attempt was tried by Pemberton and Buck.[464] As they stated that "*To this time, little emphasis has been placed on development of analytical implications of this technique…. However, no systematic investigation of SERS + RRS behavior for adsorption from varying starting solution concentrations of a colored adsorbate at an enhancing metal electrode has been made. The work presented here was undertaken in an attempt to demonstrate the analytical utility of SERS + RRS in detecting surface species adsorbed at an enhancing metal electrode from solutions initially of low concentration in adsorbate.*". Normally, according to the surface adsorption isothermal, a linear relation is possible between SERS intensity of a certain Raman peak and the concentration of the analyte, and a much wider linearity range could be realized *via* a log/log plot. Note that the univariate evaluation relying solely on the peak intensity of a single Raman peak may introduce potential qualitative deviations.

The surface coverage plays a crucial role in the quantitative analysis of SERS. In 1981, Shen and coworkers investigated the adsorption of pyridine adsorbed on a Ag electrode–electrolytic solution by using SERS[465] and surface second harmonic generation (SHG).[466] The observed adsorption isotherms can be approximated by the Langmuir isotherm, while the transient adsorption following a simple Langmuir kinetic model was difficult to descript surface adsorption of pyridine on Ag electrode.

Similar to fluorescence, SERS exhibits a linear relationship with surface concentration at low to moderate coverage levels. However, deviations from this linearity occur at higher surface coverages. It is important to note that it only applies to surface coverages not to bulk concentrations. When the adsorption is less than 2/3 of a monolayer for various analytes, a linear correlation between SERS intensity and analyte concentration in the bulk solution may be observed, suggesting that solutions should be diluted, akin to conditions in molecular fluorescence.

This conclusion also helps in understanding the early observations of potential-dependent SERS, as discussed in Fig. 12. At that time, this phenomenon was considered direct

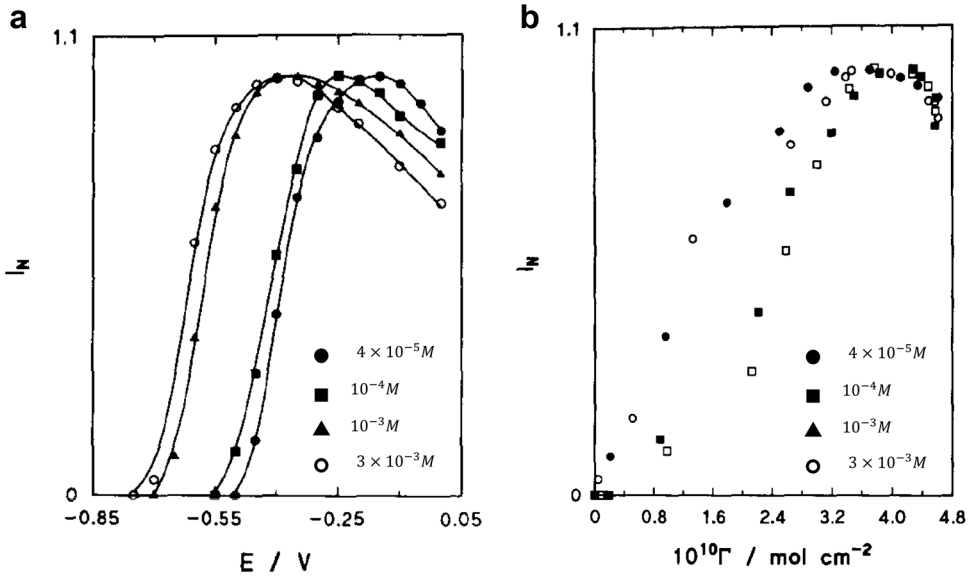

Fig. 50 (a) Plots of the intensity of the 1010 cm^{-1} band on the electrode potential (*E vs.* SCE) for the varied bulk pyridine concentrations. (b) Data from panel a plotted *versus* surface concentration of pyridine Γ. Figures are adapted from ref. 119 with permission. Copyright 1991 Elsevier.

evidence of the CT mechanism. This phenomenon was considered direct evidence of the CT mechanism. However, in 1991, Stolberg *et al.* correlated SERS intensity with the independently measured surface concentration for various bulk pyridine concentrations and variable electrode potentials.[119]

Fig. 50a presents the 1010 cm^{-1} band intensity as a function of electrode potential for four different bulk pyridine concentrations. These plots display characteristic maxima similar to those observed in Fig. 12a. However, when the same data are plotted against the surface coverage of pyridine, as seen in Fig. 50b, the dependence on bulk concentration is eliminated. This data aligns with a single relationship, featuring a maximum at a surface concentration of 4×10^{-10} mol cm^{-2}, which corresponds to 2/3 of a monolayer coverage. It indicates that observed SERS intensity depends on coverage.

Later in 1999 and 2001, a more solid quantitative analysis was achieved by considering more information from the peak or the whole Raman spectrum with the introduction of multivariate calibration with partial least squares (PLS), one of the mostly commonly used machine learning techniques. The experimental variations (such as reproducibility and uniformity of SERS substrate, the modified interaction between analyte and SERS substrate, and the instrument conditions) make the accurate quantitative analysis challenging, however by careful consideration of the surface adsorption chemistry and control of the reproducibility of the surface used for enhancement, accurate and reliable quantitation can be achieved using SERS. Initially the focus of quantitative SERS analysis using Ag nanoparticles resulted in a series of studies to improve the synthesis of the nanoparticles[467] and to understand the surface chemistry of adsorption,[468] before extending to the measurement of therapeutic drugs,[469] illicit substances[470] and biomolecules.[471] These select studies showed this approach with many more studies reported covering multiple targets with the focus being on control of the surface adsorption and aggregation of nanoparticles. Many comprehensive reviews are dedicated to this topic and have more information on this key area of performance for utilization of SERS.[472–474]

An alternative approach is to rely on a calibration strategy *via* an internal standard. A trusted internal standard should be able compensate for the above variations with a SERS signal free of interference with that of the analyte. The isotopic internal standard method was proposed independently by Bell *et al.*[475] and Zhang *et al.*[476]

In 2004, Bell and colleagues used isotopic pyridine as an internal standard to realize quantitative analysis of nicotine over a wide concentration range (0.1–10 ppm) with a R^2 of 0.998.[475] Independently, in 2005, Zhang *et al.* used the isotopic rhodamine 6G as internal standard for rhodamine 6G, by which a better than 3% batch-to-batch reproducibility over a concentration range of 200 pM–2 μM was accomplished.[476] Instead of using the expensive isotopic reagents, Bell *et al.* introduced CNS^- as the internal standard for the SERS detection of dipicolinic acid, a marker for bacterial spores, and achieved a linear range of 0–50 ppm with a R^2 of 0.986.[477]

An alternative quantitative analysis is to use frequency shift, which originated from the change in relative intensity of probe molecules before and after interaction with analyte. In 2012, Olivo group demonstrated the frequency shift-based quantification of antigen triggered by biomarker-ligand recognition.[478]

Despite being well demonstrated, it is difficult to avoid the dynamic exchange and competitive adsorption between analyte and the internal standard molecule when their concentrations are significantly different. Thanks to the development of SERS-active core–molecule–shell nanoparticles (CMS NPs),[237,247] in which a molecular layer is interposed between the core and shell, the SERS signal of the embedding molecular layer is not influenced by the external environment, and can be used as a

novel internal standard for quantitative analysis. The CMS based internal standard strategy was independently developed by Zhang group[479] and Ren group in 2015.[248] They convincingly demonstrated the capability of these nanoparticles to quantitatively analyze target molecules across a wide concentration range, exhibiting a linear relationship between the relative SERS intensity and the surface coverage. Additionally, enhancing the specificity of substrates towards analytes through surface modification and functionalization also promises to improve the accuracy and save time in quantitative analysis.

It seems the CMS based internal standard strategy for quantitative analysis is the most promising one among the above ones. Nevertheless, realizing a reliable quantitative analysis in real samples remains an unresolved challenge. This endeavor encompasses several key areas, such as the controllable large-scale production of CMS NPs, which serve as the foundation for SERS assays. Additionally, efficient sample pretreatment is a critical preliminary step for SERS analysis of most real samples, as it can significantly influence the qualitative and quantitative analysis. Moreover, the working curve for quantitative analysis may be subject to potential deviations due to the competitive adsorption of residual impurities on the SERS substrate. Addressing these concerns is crucial for advancing the field of SERS-based quantitative analysis.

To apply comparable and reproducible measuring conditions in SERS, microfluidic devices were developed and combined with a Raman microscope for readout, which could help to average SERS signal over either time or space to reduce the signal fluctuation and improve the reliability of quantitative analysis. The first study on quantitative analysis utilizing SERS in microfluidic environments date back to 2002,[480] where a model derivative of TNT was developed within the lab-on-a-chip paradigm, employing solely the analyte and readily accessible reagents. In 2006, the quantitative detection of nicotine within the range of 0.1 ppm and 10 ppm[481] as well as the quantification of the pesticide methyl parathion between 0.1 ppm and 1 ppm[482] was achieved. In 2007, by applying a liquid/liquid segmented flow within a microfluidic device, individual droplets of 180 nL were investigated illustrating the high potential of SERS to quantify substances in sub-μL volumes without the agglomeration of colloidal nanoparticles at the channel walls avoiding the memory effect.[483] Later, droplet-based microfluidic SERS approaches prove their potential in drug monitoring by quantification of levofloxacin[484] or nitroxoline[485] in spiked human urine samples.

It should be noted that the complexity of the multiple interactions among the laser, molecules, and nanostructures that generate the SERS signal may exceed our imagination, often leading to significant differences in the SERS spectra obtained by different experimental groups due to variations in experimental details. For example, since Fleischmann and coworkers reported the first SERS spectra of pyridine on a Ag electrode 50 years ago, over 2000 studies on the SERS of pyridine have been published, some of which reported different spectral features. In Fleischmann *et al.*'s spectra, a new and strong peak at 1025 cm^{-1} appeared (Fig. 3g–h), as we mentioned in Section 2.5, which differed from those reported by others later. This discrepancy arose because they electrochemically roughened the Ag electrode under high-power laser irradiation in a solution containing pyridine and KCl, performing nearly 200 oxidation–reduction cycles. Upon further investigation, it was found that the 1025 cm^{-1} peak most likely originates from a surface complex of pyridine with Ag clusters and chloride ions formed through a laser-induced surface chemical process, rather than from free pyridine molecules adsorbed on the electrode surface.

Kudelski and coworkers also found that for Ag nanoparticle structures, this peak is either very weak or difficult to observe when spherical Ag nanoparticles are used as the SERS substrate, but it is more easily detected on irregular flattened Ag nanoparticles.[486] Muniz-Miranda attributed this peak to a complex formed between pyridine and the positively charged Ag_3^{2+} cluster, which is related to the chloride ions present in the electrolyte solution.[487] Therefore, to accurately analyze the Raman peaks in SERS spectra for nanoparticles or substrates prepared by different experimental methods, it is necessary to precisely correlate all the relationships of interface species formed and all experimental parameters. This is crucial for methodology and establishing detailed benchmark experiments to study the SERS mechanism and facilitate commercialization successfully.

5. Advances in recent years (mid-2010s–mid-2020s)

The rapid advancement of nanoscience and the urgent needs of analytical science, surface science, electrochemistry, biology and other disciplines initiated the second upsurge of SERS. As summarized in Fig. 17, it shows that the number of SERS related publications increased rapidly from 1995–2015. It should be noted that the exponential growth in the number of publications since 2000 was largely due to lower technological threshold for nano synthesis and the increased accessibility of SERS research. However, the key foundations of the outbreak were laid in 1974–2000.[14–19,187]

There have been many excellent reviews about the theories,[21,32,34,242,243,269,404,452,488,489] experimental methods,[21,25,30–34,166,242,243,269,404,452,489–500] and practical applications[21,25,28,30–32,34,242,269,452,490–493,497,501] of SERS, which can be referred to for more detailed progress in the field for this period. We emphasize that the methodological foundations underpinning these advancements were largely established within the first two decades of SERS research. These early contributions laid the groundwork for subsequent developments and applications. Comprehensive discussions of these methodologies and their applications can be found in several seminal books in the field.[12,62,502–510]

Although the annual output of SERS-related articles remains high, with around four thousand papers published each year, a closer examination reveals a diminishing growth rate since 2015, leading to a recent plateau (see Fig. 17). This trend is

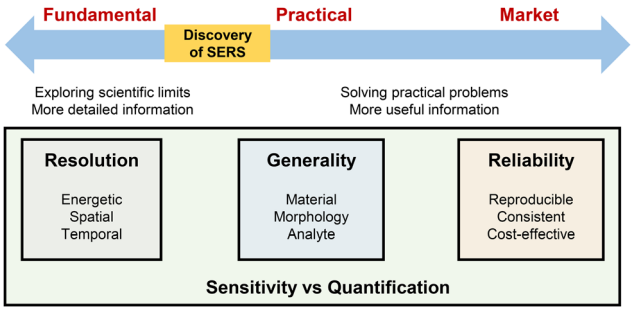

Fig. 51 The different development directions and focus of SERS since its discovery.

explained by the fact that most published papers employ SERS merely as a readily accessible characterization technique or analytical method, rather than generating innovative contributions or breakthroughs in SERS methodology and commercialization. The stagnation in the growth of SERS-related publications may signal the need to reinvigorate scientific momentum and advance SERS research. To achieve this, it is crucial to proactively embrace emerging science, develop novel methodologies, and push the boundaries of current practices.

To achieve a new vibrant state in SERS, it is essential to delineate the three distinct paths that have emerged since its discovery. Each path presents unique development challenges and leads to significant milestones: deep fundamental research, broad application techniques, and extensive instrument commercialization, as illustrated in Fig. 51.

In the realm of fundamental research, the focus is on advancing new theories, instruments, and experimental methods to overcome detection sensitivity and resolution limits, thereby expanding the boundaries of what was previously deemed impossible. Researchers in this area often utilize highly idealized model systems and environments, such as LT-UHV settings and resonant molecules, to approach detection limits as closely as possible. For instance, in Section 5.1, we will explore recent breakthroughs in spatial resolution within fundamental research. The implementation of TERS at liquid helium temperatures has enabled unprecedented advancements in spatial resolution, achieving angström-scale and even atomic-level resolution. This remarkable progress marks a significant leap forward in our capacity to probe and characterize materials at the most fundamental scales.

In the context of general applications, the emphasis shifts to the expansion of SERS versatility, including substrate materials, morphologies, and molecular generality beyond the scope of traditional Raman spectroscopy. This approach facilitates the integration of SERS into diverse research fields such as physics, chemistry, biology, and materials science, thereby supporting fundamental research in these areas. Consequently, the priority in this direction is not solely on achieving the highest signal strength with resonant molecules, as their practical and scientific value may be limited except when used as labels. Instead, the focus should be on more realistic scenarios, such as detecting non-resonant molecules in complex environments, to enhance the practical utility of SERS. In Section 5.2, we will discuss recent efforts to extend SERS applications to weakly adsorbed molecules, diverse surface-interface systems, and complex environments like biological research. These advancements have significantly broadened the general applicability of SERS. Notably, in general applications, the quantitative analytical capabilities of SERS may be more critical than its sensitivity, as elaborated in Section 5.3.

The third path poses the greatest challenges, as SERS must be recognized as a significant analytical technique for its relevant instruments to be realized and widely adopted. In the context of commercial and market applications, consistency and stability of spectral signals, as well as cost efficiency, become paramount. Developing reliable, reproducible, and affordable SERS techniques is crucial for their successful integration into the market and everyday use.

During this period, the themes and directions of exploration in SERS Frontiers and applications were highlighted at the Faraday discussions meeting held in Glasgow, UK, in 2017, chaired by Duncan Graham (see Fig. 52 and Table 4). On the first day of the conference, there was an in-depth discussion on the theory of SERS, with a particular focus on the quantum electrodynamics description theory of SERS, especially following the recent demonstration of picocavity SERS.[358] The second

Fig. 52 Group photo of the Faraday discussions meeting on SERS, 30 August–1 September 2017, Glasgow, UK.

Table 4 The timetable and program of the Faraday Discussions meeting on SERS 2017

Wednesday 30th August

12:45	**Welcome and Introductions** Duncan Graham, *Chair of Scientific Committee*
12:55	**Outline of Discussion Format** *Royal Society of Chemistry Publishing Editors*
13:00	**Introductory Lecture** (Session Chair:) Richard Van Duyne, *Northwestern University*
	Session 1 - Theory of SERS enhancement Jeremy Baumberg, *University of Cambridge*
14:00	**Linking classical and molecular optomechanics descriptions of SERS** Javier Aizpurua, *University of the Basque Country*
14:05	**Monitoring plasmon coupling and SERS enhancement through in situ nanoparticle spacing modulation** Leonora Velleman, *Imperial College London*
14:10	**Plasmonic enhancement of SERS measured on molecules in carbon nanotubes** Stephanie Reich, *Freie Universität Berlin*
16:00	**The Theory of Surface-Enhanced Raman Scattering on Semiconductor Nanoparticles; Toward Optimization of SERS Sensors** John Lombardi, *City College of New York*
16:05	**Novel Routes to Electromagnetic Enhancement and its Characterisation in Surface- and Tip-enhanced Raman Scattering** Paul Dawson, *Queens University Belfast*
16:10	**Theoretical Modeling of Voltage Effects and the Chemical Mechanism in Surface-Enhanced Raman Scattering** George Schatz, *Northwestern University*

Thursday 31st August

	Session 2 - Ultrasensitive and towards single molecule SERS Joshua Edel, *Imperial College London*
09:00	**Plasmon induced polymerization using a TERS approach: a platform for nanostructured 2D/1D material production** Volker Deckert, *Friedrich Schiller University Jena*
09:05	**First demonstration of Surface Enhanced - Stimulated Raman Spectroscopy (SE-SRS) using low-power CW sources** Kevin Hewitt, *Dalhousie University*
09:10	**The effect of STM parameters on tip-enhanced Raman spectra** Natalia Martin Sabanes, *Max Planck Institute for Polymer Research*
11:00	**Imaging out-of-plane polarized emission patterns on gap mode SERS substrates: from high molecular coverage to the single molecule regime** Kallie Willets, *Temple University*
11:05	**Electrochemical Control of Strong Coupling States Between Localized Surface Plasmons and Molecule Excitons for Raman Enhancement** Kei Murakoshi, *Hokkaido University*
11:10	**SERS-active metal-dielectric nanostructures integrated in microfluidic devices for label-free quantitative detection of miRNA** Fabrizio Giorgis, *Politecnico di Torino*
	Session 3 - SERS in biology/biomedical SERS Karen Faulds, *University of Strathclyde*
13:30	**Quantitative detection of isotopically enriched *E. coli* cells by SERS** Roy Goodacre, *University of Manchester*
13:35	**Gold Nanodome SERS platform for label-free detection of protease activity** Pieter Wuytens, *Universiteit Gent-imec*
15:00	**Monitoring plasmon coupling and SERS enhancement through in situ nanoparticle spacing modulation** Luis Liz-Marzan, *CIC biomaGUNE*
15:05	**Fast and Reproducible iSERS Microscopy of Single HER2-positive Breast Cancer Cells using Gold Nanostars as SERS Nanotags** Sebastian Schlücker *Universität Duisburg-Essen*
15:10	**Dynamic SERS nanosensor for neurotransmitters sensing near neurons** Jean Francois Masson *Universite de Montreal*
15:15	**What do we actually see in intracellular SERS? Investigating nanosensor-induced variation** Sumeet Mahajan, *University of Southampton*

Friday 1st September

	Session 4 – Analytical SERS (Jürgen Popp)
09:00	**Further expanding versatility of surface-enhanced Raman spectroscopy: from non-traditional SERS-active to SERS-inactive substrates and single shell-isolated nanoparticle** Zhong-Qun Tian, *Xiamen University*
09:05	**Shell Isolated Nanoparticles for Enhanced Raman Spectroscopy Studies in Lithium-Oxygen Cells** Laurence Hardwick, *University of Liverpool*
09:10	**Quantitative SERS by Hot Spot Normalization – Surface Enhanced Rayleigh Band Intensity as an Alternative Evaluation Parameter for SERS Substrate Performance** Peter Vikesland, Virginia Tech
09:15	**Smart Supramolecular Sensing with Cucurbit[n]urils** Oren Scherman, *University of Cambridge*
11:30	**Quantitative Surface-enhanced Raman Spectroscopy of Single Bases in Oligodeoxynucleotides** Steven Bell, *Queens University Belfast*
11:35	**Plasmonic response and SERS modulation in electrochemical applied potentials** Giuliana Di Martino, *University of Cambridge*
11:40	**Reassessing SERS Enhancement Factors: Using Thermodynamics to Drive Substrate Design** Jason Guicheteau, *USA RDECOM EDGEWOOD CHEMICAL BIOLOGICAL CENTER*
13:00	**Concluding Remarks Lecture** (Duncan Graham) Marc Porter, *University of Utah*

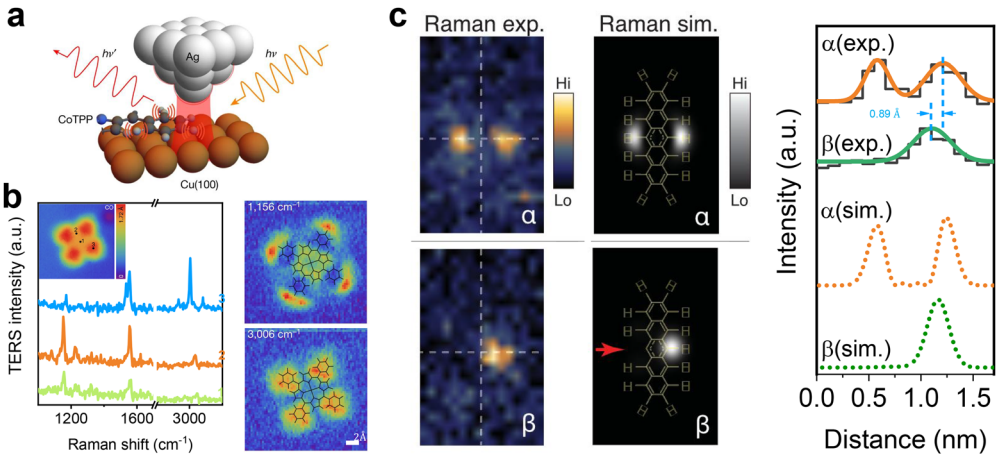

Fig. 53 Representative research work on TERS to achieve ultimate sensitivity and spatial resolution. (a) Schematic of TERS of the Co(II)–tetraphenyl porphyrin (CoTPP) molecule immobilized on Cu(100) in the LT-UHV TERS (6 K) system. (b) Spectra recorded on cobalt (1), pyrrole (2) and a phenyl group (3) are shown. The inset is the corresponding topography (left panel). The TERS mapping of Raman modes at 1156 cm^{-1} and 3006 cm^{-1} are shown (right panel). Scale bars are 2 Å. Reproduced from ref. 368 with permission. Copyright 2019 Springer Nature. (c) Measured and simulated maps for the C–H stretching mode of the pentacene species α and β on the Ag(110) surface. Vertical and horizontal lines indicate the long and short molecular axes, respectively (left panel). Line profiles obtained along the short molecular axis. The orange and green curves are the Gaussian fitting of the peaks. Reproduced from ref. 370 with permission. Copyright 2021 AAAS.

day commenced with discussions on ultra-sensitive SERS, examining how the technique's sensitivity could be maximized. This was followed by examples of biological SERS. Throughout the day, a clear theme emerged: the SERS community was perhaps underselling itself regarding the reproducibility and quantitative nature of the technique when used in appropriate applications—a strong view that was emphasized in the discussions. On the final day, the focus was on the analytical uses of SERS, discussing real-life examples and the impact of SERS in various fields.

Notably, Richard Van Duyne, one of the two major pioneers in the SERS field and a leading scientist with over four decades of significant contributions, was honored with the Spiers Medal, presented by Eleanor Campbell, President of the Faraday Division, just before his outstanding opening lecture.

5.1 TERS in the atomistic near field (ATERS)

Currently, both SERS and TERS have achieved remarkable milestones in fundamental studies. In terms of spatial resolution, in the ambient condition, TERS has achieved spatial resolution of 3 nm.[511] Furthermore, in LT-UHV condition, individual chemical bonds can be resolved by TERS[368,369,511] and even sub-angström (Å) level spatial resolution is achieved.[370] This fascinating advance originates from a deep understanding of light–matter interactions in optical cavities.

The Å-scale in optical microscopy was reported in 2017 by Apkarian, Jensen and coworkers through TERS carried out in the atomistic near-field (ANF), ATERS for short.[512,513] They used a CO terminated tip to map out the electrostatic potential surfaces inside individual metalloporphyrin molecules, along with providing fully resolved images of vicinal CH bonds separated by 2.5 Å.[514] The full power of ATERS was illustrated by them in 2019 by visualizing the vibrational normal modes within a single molecule (Fig. 53a and b)[368] and by recording atom resolved images of a 2D insulating Cu_2N film.[515] ATERS image of vibrational normal modes within a single Mg–porphine was also reported in the same year by Dong, Hou, Luo and coworkers.[369] In a notable subsequent illustration, they combined STM and noncontact AFM with TERS to image the three pentacene-derivatives obtained by sequentially breaking its individual carbon–hydrogen bonds (Fig. 53c).[370] Highlighted in Fig. 53c is the resolved 0.89 Å displacement in peak location of the imaged CH-stretch, which is in excellent agreement with their theoretical simulation. The ATERS image resolution, as defined by the full width at half maximum of observable features, is limited by the Wigner Seitz radius of the terminal atom at the tip apex, demonstrably 1.6 Å for atomically terminated Ag tips.[368–370,515]

The attained resolution verifies atomic confinement of the apex mode on atomically terminated plasmonic tips, as anticipated by two seminal works: Takahara had pointed out that there is no cut-off for TM_0 plasmons on nanowires of negative dielectric,[516] and Nerkararyan and coworkers[517,518] pointed that lateral confinement of plasmons, d, on a conical tip of negative dielectric scales as $1/\rho^2$, where ρ is the height-dependent cone radius. Therefore, classically, there is no limit to confinement of the photon since $d \rightarrow 0$ as $\rho \rightarrow 0$; however, quantization of matter sets the limit to the minimum attainable value of ρ to the atomic radius, as realized experimentally.[368–370,515] Beyond the confinement of optical field, Luo and colleagues also showed that in non-resonance Raman conditions, Raman images can visualize vibrational modes owing to the accessibility of the Herzberg–Teller contributions.[519]

Operationally, optical microscopy in the ANF is reached using atomically terminated plasmonic tips, scanned with sub-Å precision afforded by ultrahigh vacuum cryogenic STMs. The paradigm shift in ATERS arises in that the measurements

are carried out at junction gaps where tip and substrate wavefunctions overlap, as attested by the dc tunneling current used for tip placement. This is most directly manifested under resonance Raman conditions, where the local optical density of states images molecular orbitals,[520,521] also as shown in Fig. 36. Notably, the TERS signal intensity peaks at contact,[512,515] which by virtue of its lateral confinement forms a quantum pointed contact (QPC),[522] as recognized by Kumagai and coworkers,[523–525] and realized in implementations where approach curves are extended to contact,[526] in space-time resolved THz microscopy,[527] in CARS on graphene nanoribons.[528] This is in stark contrast with standard TERS, or more generally, near-field scanning optical microscopy (NSOM), which is formulated and carried out in the electrostatic near-field.[529] In the ANF, the external radiation field is excluded from the junction, the scattering is driven by the optical current of tunneling or conductive plasmons, reducing ATERS to the alternating current analog of scanning tunneling electron microscopy.[530]

It should be emphasized that the novel observable in ATERS is the intramolecular polarization current, which, at contact, extends into the tip. In visualizing vibrational normal modes involving unresolvable atomic displacements of order 0.1–0.01 Å, what is imaged is the nonlocal time-harmonic vibronic polarization current associated with a given mode, which is nicely formulated in the recently introduced Raman bond model (RBM) by Jensen and coworkers.[531–533] Indeed, a variety of theoretical adaptations have been implemented to model and interpret the advances cited in this section and to revise the fundamental understanding of the science underlying SERS and TERS on that basis. We should stress that with the extreme confinement, other components in the plasmonic field, including magnetic field[534] as well as momentum distribution,[535] which are negligible in conventional optical fields, would come into play, opening an entirely new territory for not only SERS and TERS but also nano-optics. We refer the reader to a recent comprehensive review for theoretical predictions in such highly inhomogeneous optical fields.[536]

5.2 SERS on weakly adsorbed molecules and interfacial structures

5.2.1 Probing weakly adsorbed molecules. Currently, most SERS analytes are strong adsorbates with large Raman scattering cross-sections. Expanding detection to include weakly adsorbed molecules is crucial for a comprehensive surface analysis. For example, the solvent and electrolyte ions, which play key roles in the interfacial processes, usually exhibit weak SERS signals. Further pushing the sensitivity limits to enable the SERS detection of those low surface coverage, dynamic, weakly interacted molecules could significantly expand the molecular generality of SERS in detecting various species. Moreover, it provides new information to understand their roles in related electro/bio-chemical processes and complete the jigsaw puzzle of studied surfaces/interfaces.

To ensure reliable analysis of weakly adsorbed molecules by SERS, it's essential to exclude the effect of surfactants and contaminants, which is distinctly different from the strongly adsorbed systems. Three critical aspects warrant careful consideration during measurement protocols. First, preliminary surface cleaning through either chemical[537–539] or physical[540,541] methods is essential to eliminate competitive adsorption from surfactants (such as citrate, ascorbic, CTAB and PVP), thereby ensuring measurement accuracy. Chemical cleaning procedures may involve various protocols including acid treatment or plasma cleaning, while physical methods typically encompass thermal or mechanical approaches. Second, comprehensive concentration titration across a broad range is imperative to identify potential interference from ultra-trace strongly adsorbed contaminants, which may originate from reagents used[542] or plastic lab containers.[543] Third, SERS performance must demonstrate independence from laser power to exclude the possibility of laser-induced photochemical reactions during measurement, which could otherwise compromise data integrity. These methodological considerations are fundamental to achieving reproducible and reliable SERS measurements for weakly adsorbed molecular species.[544,545]

Lipkowski and colleagues developed an ordered array of ~50 nm Au nanoparticles by dissolving the shell from an assembly of silica coated SHINs and applied it to measure SERS of sugars (weak adsorbers and weak Raman scatterers) at Au. In this way, they avoided coalescence of Au nanoparticles produced by the citrate method into random clusters.[546] Up to now, various strategies have been applied to improve the sensitivity by strengthening interfacial interactions,[547] such as electrostatic interactions,[539] molecular steric effect,[548–551] host–guest recognition,[552,553] and introducing probe molecules *via* biological recognition, chemical derivatization, hydrogen bonding, ion–dipole interactions, and so on.[554–558]

Water molecules, as special weakly adsorbed species with hydrogen bond network interacting with electrolyte ions extending to several water layers. It exhibits complicated interfacial structures that are intrinsically linked to electrochemical reactions, electrical double layer formation, and water dissociation processes. SHINERS serves as an ideal tool for investigating interfacial water adsorption on single-crystal surfaces. By depositing SHINs onto metal single-crystals, NPoM configurations with significant Raman enhancement can be constructed. The NPoM structure can also be excited through the Kretschmann or Otto configuration, leveraging the coupling between SPP and LSP.[489] At the critical angle where SPP excitation at the film/air interface occurs, the SERS intensity at the film surface reaches its peak either with or without the coupled nanoparticles.[559–561] This configuration has been termed as the SPR-SERS configuration.

To further enhance the sensitivity of SHINERS, precise control over the coupling of SHINs particles is crucial. Recently, Li and coworkers demonstrated that assembling multiple $Ag@SiO_2$ SHINs particles on an Ag film surface can effectively amplify the Raman signal intensity, enabling simultaneous measurements of single-molecule fluorescence and single-molecule Raman spectra of individual rhodamine B isothiocyanate (RITC) molecules.[562]

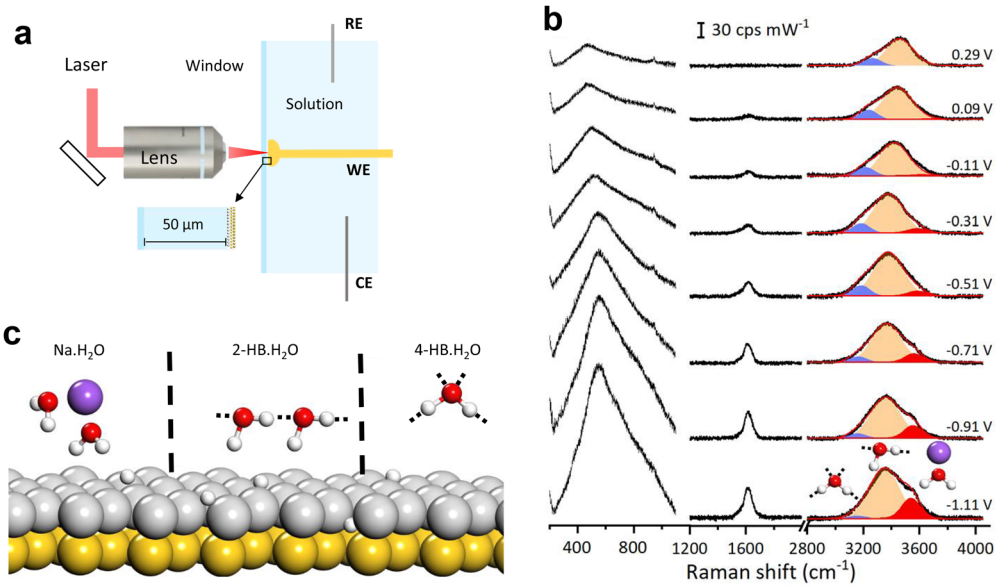

Fig. 54 (a) *In situ* SHINERS of interfacial water on Pd(*hkl*) single-crystal surface and reveal that interfacial water consists of hydrogen-bonded and Na^+ hydrated water. CE, counter electrode; RE, reference electrode; WE, working electrode. (b) The *in situ* Raman spectra of interfacial water on a Pd(111) electrode in a 0.1 M $NaClO_4$ solution (pH 11) were shown. Gaussian fits of three O–H stretching modes are shown in blue, orange, and red, respectively. (c) Schematic of the three types of interfacial water on the Pd/Au surface. Reproduced from ref. 565 with permission. Copyright 2021 Springer Nature.

Therefore, leveraging the high sensitivity of the gap mode, SHINERS can be utilized to investigate interfacial dynamic processes across various single-crystal surfaces and reveal the mechanism of important interfacial processes, especially *in situ* probes of interfacial water by Raman spectroscopy. For instance, the advent of SHINERS has revitalized Raman spectroscopy research on interfacial water, an area that had seen little progress for over a decade. Cheng, Li and coworkers utilized SHINERS to study the interfacial water on Au(111) and Au(100) single-crystals under hydrogen evolution reaction (HER) conditions.[563] They observed three types of interfacial water molecules undergoing configurational changes with varying potentials: with the negative shift of the potential, the interfacial water changed from a ''parallel'' configuration to ''one-H-down'', and then to ''two-H-down''.

Compared to Au, platinum-group metal surfaces have garnered more attention due to their extensive applications in catalysis and energy. However, the plasmonic coupling effect between SHINs particles and platinum group metal surfaces is weak, leading to a reduction in the EF of SHINERS by 2–3 orders of magnitude.[564] This limits the detection of trace species on their surfaces. For example, Pd is one of the most active HER catalytic materials, but the weak plasmonic coupling between Pd and SHINs makes it extremely challenging to study the structure of interfacial water using SHINERS. To address this issue, Li, Pan, and coworkers deposited different atomic layers of Pd on a Au single-crystal surface by alternately using Cu UPD and spontaneous displacement methods. Thus, based on the ''borrowing SERS activity'' strategy, strong plasmonic coupling effect between the underlying Au single-crystal and SHINs could achieve a Raman EF as high as 10^7–10^8. With such a strategy, they further employed SHINERS to *in situ* investigate the structure and dissociation of interfacial water on a Pd single-crystal surface(Fig. 54),[565] and obtained spectral evolutions of hydrogen-bonded and Na^+ hydrated water during the hydrogen evolution reactions (HER). At HER potentials, interfacial water undergoes dynamic structural changes, transitioning from random to ordered arrangements facilitated by the bias potential and Na^+ ion cooperation. This ordered water structure enhances electron transfer and HER rates. Electrolytes and electrode surface properties influence interfacial water structure, suggesting potential for improved electrocatalytic reaction rates through local cation tuning strategies.[565]

5.2.2 *In situ* monitoring of reaction processes and intermediates. SERS can provide the fingerprint structural information of the reaction intermediates with ultrahigh surface sensitivity; thus, it is a promising tool for the *in situ* study of the reaction mechanism and structure–activity relationship of catalysis. However, due to the long-standing material and morphology limitations, its application in the study o f reaction processes on catalytically active transition metal surfaces is highly restricted. To overcome this limitation, the ''borrowing SERS activity strategy'' was developed by coating ultrathin transition metal shells on plasmonic Au cores.[35]Therefore, the Au can generate strong electromagnetic field to enhance the Raman signals of species adsorbed on the transition metal shells, thus allowing the *in situ* monitoring of the reaction processes occurring on them.

Using this strategy, Li, Dong, Wang and coworkers have *in situ* studied the evolution of the intermediates and the structure of catalysts during hydrogen oxidation reaction (HOR) on PtRu surfaces, which is the main composition of commercial HOR catalysts (Fig. 55a).[566] As shown in Fig. 55b–e, Pt shells were first coated on Au cores, and Ru was then

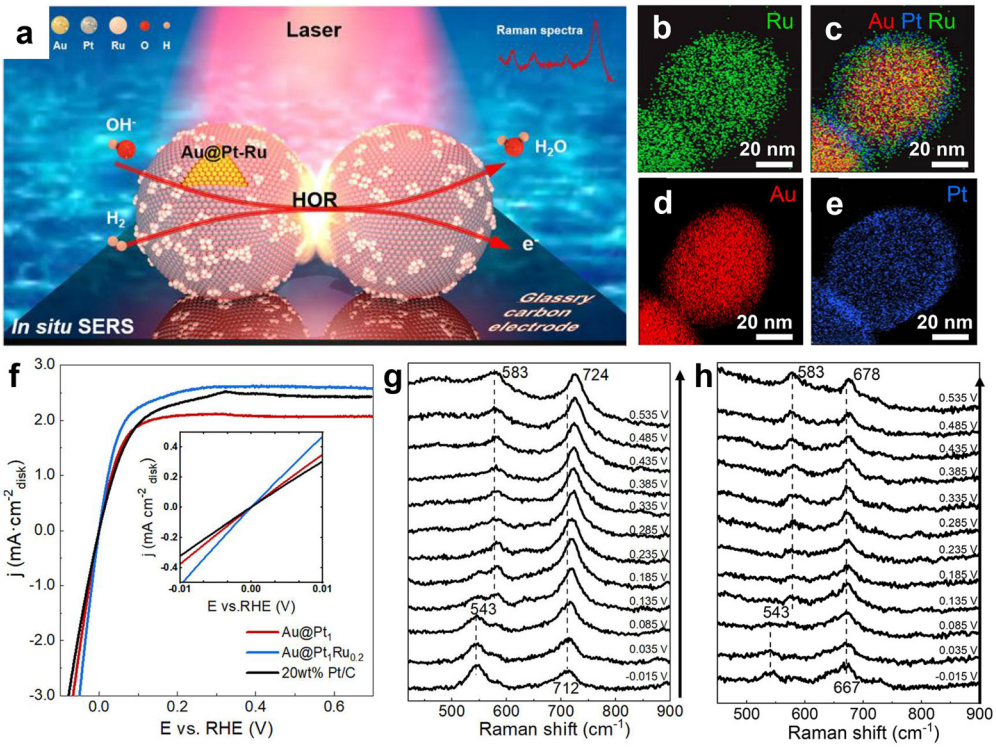

Fig. 55 (a) Schematic illustration of *in situ* SERS study of HOR on Au@PtRu. (b)–(e) Elemental mapping images of the Au@PtRu nanoparticles. (f) HOR polarization curves of commercial 20 wt% Pt/C, Au@Pt, and Au@PtRu. Sweep rate: 10 mV s^{-1}. Rotation rate: 1600 rpm. (g) *In situ* SERS spectra of HOR on Au@PtRu and (h) the deuterium isotope experimental results. Reproduced from ref. 566 with permission. Copyright 2022 American Chemical Society.

deposited on the outer surface of the Pt shell. The resulting Au@PtRu display superior HOR performance compared to Au@Pt and commercial Pt/C (Fig. 55f). *In situ* SERS reveals Ru(+4)O_x (583 cm^{-1}) surface oxides, and OH_{ad} (712 cm^{-1}) species appeared during the HOR process, based on the isotope experimental results (Fig. 55g and h). Meanwhile, H_{ad} species were also observed at lower potentials on the catalysts. The observation of OH_{ad} species indicates HOR on PtRu follows the bifunctional mechanism. By comparing the *in situ* spectroscopic results for PtRu with those for pure Pt surfaces, they found that the introduction of RuO_x on the Pt surface can optimize the adsorption energy of OH_{ad}, thus improving HOR performance. Using the similar "borrowing SERS activity" strategy based on Au core transition shell nanoparticles, Li and coworkers have also investigated the reaction mechanisms of various important catalytic reactions including HOR, oxygen reduction reaction, CO oxidation, *etc.*[420,567–569]

5.2.3 From interface to interphase detection. With the rapid advancement of electrochemical energy science and technology over the last decade, research on electrochemical interfaces is experiencing a significant shift from traditional two-dimensional interfaces to intricate three-dimensional interfaces (interphases), For example, the lithium battery industry urgently needs to characterize and gain a deep understanding of such a three-dimensional solid electrolyte interphase (SEI), as depicted in Fig. 56. To really solve the real industrial problems, it is important to fully understand the interphase representing a distinct solid phase generated from the interaction between the electrode and the solution.[570] This additional phase adds a layer of complexity to the traditional electrode–solution interface, transforming it into a multifaceted composition comprised of one phase and two interfaces: solid–solid and solid–liquid. Despite offering new avenues for exploration, the complexity of interfacial structures within three-dimensional interfaces (interphases) poses a significant challenge in accurately discerning the vertical orientation of interfacial species with high spatial resolution, ranging from angströms to nanometers, especially under practical electrochemical operating conditions. This transition presents fundamental and practical challenges for traditional SERS or SHINERS, which grapple with limited detection sensitivity along the vertical axis in the face of these complexities.

One illustrative example is the spectroscopic analysis of SEI formation on lithium-based battery anodes, which is a prime representation of a complex three-dimensional interphase. The SEI, formed through (electro) chemical reactions between anodes and electrolytes, functions as both an electronic insulator and Li-ionic conductor,[571] significantly impacting battery performance.[572] However, characterizing SEIs presents significant challenges due to their thin, nonuniform nature, complex composition, and dynamic evolution during cycling. Additionally, analyzing these reactive surfaces within organic electrolytes requires precise spectroscopic measurement techniques.

To tackle this complexity, direct *in situ* and real-time methods with structure-specific and depth-sensitive features are essential. These methods are crucial for tracking the dynamic

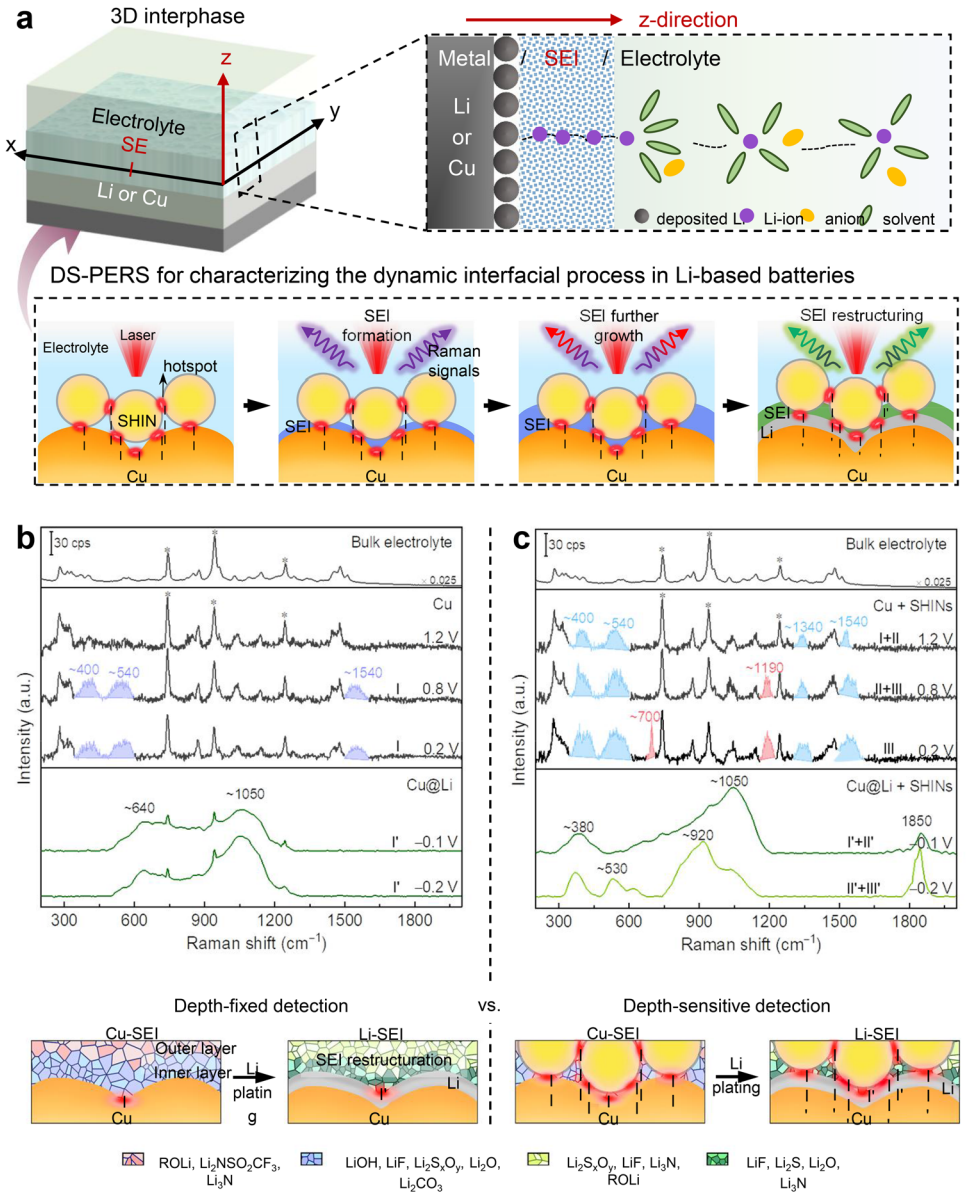

Fig. 56 DS-PERS vertical direction sensing of the complex 3D interfacial process. (a) Schematics of DS-PERS for depth-resolved detection of SEI in Li-based batteries. (b) and (c) Comparison of the depth-fixed strategy based on LSPs of nanostructured Cu alone and the depth-sensitive strategy based on synergetic LSPs of integrated Cu-SHINs for *in situ* characterizing the formation and reconstruction of SEI. *In situ* Raman spectra showing the formation and evolution of SEIs on the nanostructured Cu substrate (b) and the Cu-SHINs substrates (c) in normal ether-based electrolyte. Reproduced from ref. 568 with permission. Copyright 2023 Springer Nature.

interfacial processes of the anode, guiding the rational enhancement of SEIs in lithium-based batteries. Recently, Mao, Cui, Tian and coworkers devised and developed a unique *in situ* depth-sensitive plasmon-enhanced Raman spectroscopy (DS-PERS) method, integrating SERS and SHINERS for real-time characterization of SEIs of Li metal anodes.[568,573] This method integrated two techniques based on the "borrowing SERS activity" strategy and utilized the combined LSP effects of nanostructured Cu, Li deposits and SHINs, as shown in Fig. 56.

The synergistic plasmonic enhancement enables depth-sensitive detection of signals from an SEI of tens of nanometers and from the Cu/SEI and Li/SEI interfaces during SEI formation at different stages. The application of the DS-PERS method revealed that for Li metal anodes initiating from bare Cu as the current collector, SEIs are formed sequentially on Cu prior to Li deposition and then on freshly deposited Li during normal galvanostatic polarization. Notably, the primary SEI formed on Cu contains less stable higher-oxidation-state components and undergoes restructuring to finally form the SEI on Li. They also proposed that reducing the duration time in bare Cu state facilitates the rapid and direct formation of thinner SEI on Li enriched with more desirable lower-oxidation-state components.

This advancement in understanding the formation mechanisms of SEIs and the significant impact of metallic Li offers insights for optimizing operational procedures for Li anodes. Furthermore, the DS-PERS offers a valuable approach for the nondestructive characterization of intricate nanoscale interphases and interfaces, delivering high spatial information. This capability addresses significant challenges encountered across various disciplines, including materials science and energy science and technology. It is crucial to recognize that complex three-dimensional interfacial phases like the SEI are constantly evolving with different battery systems. The spectral information obtained can be highly intricate, and the development of AI-assisted SERS/SHINERS techniques have the potential to illuminate the complexities of interfaces/interphases further.

5.3 Quantitative analysis

5.3.1 Aspects for consideration on reliable and quantitative SERS. Achieving reliable and quantitative SERS is needed for making the transition from a technique, which is dominantly used in academic institutions for fundamental and applied research, to a robust analytical technique. However, experimental SERS results obtained by researchers in different laboratories world-wide can differ significantly. This illustrates the need for joint efforts to increase the comparability of inter-laboratory comparability of SERS and potentially even to standardize it. At present, this seems to be anything but a trivial task. Why is this so? Under the assumption that the identity of the sample and its corresponding Raman scattering cross section is known, any SERS measurement is essentially determined by three factors such as, (i) the number of molecules present in the enhanced region, which is being probed, (ii) the amplification provided by the substrate, and (iii) instrument settings and performance. Albeit simple at first sight, these three factors are the convolution of many confounding variables, some of which are difficult to measure. For example, the number of molecules in the enhanced region in (ii) depends on both the surface area within the probed volume and the surface coverage. The latter is usually not determined by independent methods.

A key parameter that is often overlooked is the analyte's surface affinity. In colloidal SERS, the analyte molecules are frequently required to displace a surfactant or traverse a stabilizing/capping layer that is present on the surface of the nanoparticles. As a result, the SERS signal is highly dependent upon the interaction affinity of the analyte with the nanoparticle's surface. Weakly adsorbing molecules will give lower SERS intensities compared to stronger adsorbing ones. This may be interpreted wrongly by a lower SERS EF of the plasmonic substrate. Selecting a 'neutral' analyte that exhibits a potentially high binding affinity, along with the capacity to displace existing surface species or to co-adsorb, may present a viable solution. The Table 1 in ref. 473 contains a list of potential SERS reporter/probe molecules that are considered to be useful, together with a short description of their respective strengths and limitations. Briefly, 4-mercaptobenzoic acid (4-MBA), which is deprotonated at pH 10, along with adenine, are recommended as standard Raman reporters due to their strong adsorption characteristics and non-resonant behavior. Dyes such as R6G and CV are not recommended. In the future, the SERS community will have to decide on less-strongly adsorbing compounds that complement this initial suggestion.

The SERS EF is a key figure of merit in factor (ii) above. Variations in the EF can be alleviated through the incorporation of a standard whose response is affected in a manner consistent with that of the target analyte in response to experimental fluctuations. By using such a standard, the target SERS signal can then be normalized to that of the internal standard. Isotopologues are the most obvious internal standards. Alternatively, chemically similar compounds or standard addition may be employed. Importantly, by such an appropriate internal intensity standard, quantitative SERS analysis can be achieved even without very highly reproducible substrates. With respect to good analytical practice, separate calibration and validation steps are essential. SERS-based detection scheme without a validation step should be questioned regarding its relevance to an analytical application. A significant issue with quantitative SERS measurements is reproducibility. Generally, repeated measurements are necessary for confirming reproducibility. Suggestions for both colloidal and solid SERS substrates are available.[473]

Overall, three aspects may be recommended:[473] (a) to characterize the solid or colloidal SERS substrate through the integration of correlative electron microscopy, optical microscopy, and spectroscopy techniques; (b) to evaluate the SERS EF, incorporating appropriate Raman reporter or probe molecules; and (c) to implement stringent analytical practices throughout the research process. Nevertheless, we are just at the beginning and a substantial collaborative effort towards SERS metrology is needed until, in the hopefully not-too-distant future, we may call SERS a truly robust and quantitative tool for molecular sciences.

5.3.2 Quenched enhancement factor by charge transfer. Beyond the electromagnetic enhancement arising from hot spots, the chemical enhancement processes are also indispensable for quantitative evaluation of EF and molecular concentration in SERS. In fact, the SERS process involves intricately a trinity of interactions among nanostructures, molecules, and light, in which molecular polarizability plays a pivotal role that bridges the electromagnetic enhancement and chemical enhancement *via* the reaction field mechanism.[574] Neglecting the chemical enhancement effects induced by the molecule–surface interactions, such as CT and resonance enhancement, which alter the spectral features of molecules, would render accurate quantification unattainable.

In 2023, Dong and coworkers utilized the LT-UHV-TERS system to investigate such chemical effects through TERS of a single planar ZnPc molecule with varying but controlled contact environments.[575] The TERS signals obtained from zinc phthalocyanine (ZnPc) that was chemisorbed in a flat orientation onto the metal substrates exhibited significant quenching. This phenomenon can be attributed to the screening effect of Raman polarizability, which arises from dynamic CT at the

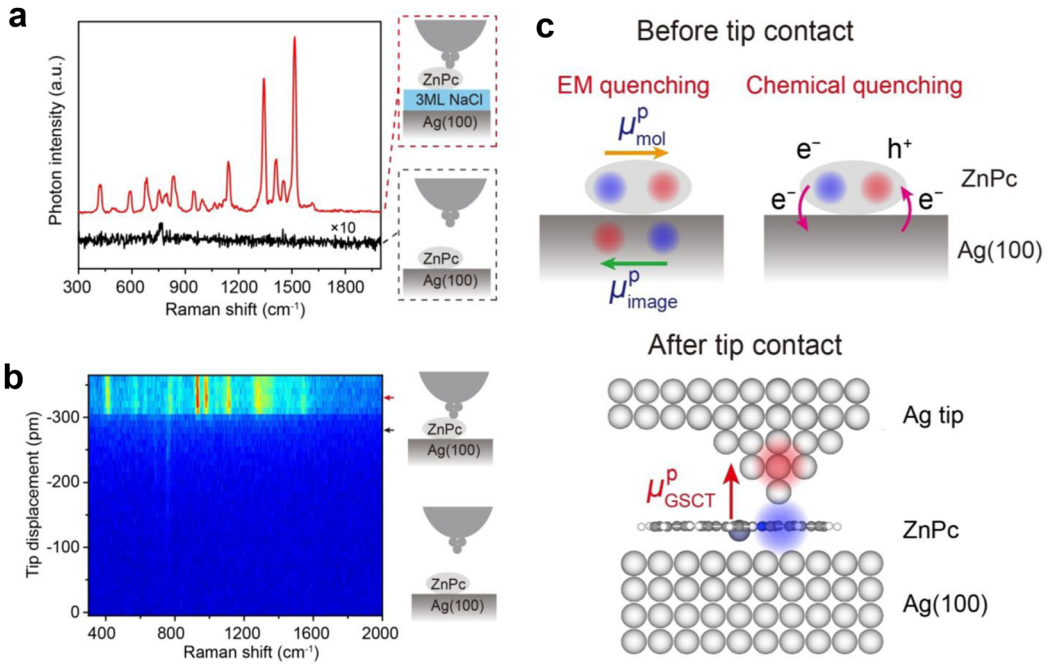

Fig. 57 Quenching of TERS signals induced by the face contact with a metal substrate. (a) Quenched TERS signals acquired from ZnPc adsorbed on Ag(100) without tip–molecule contact (black curve), in sharp contrast to the dramatically enhanced TERS spectrum measured on a NaCl-decoupled ZnPc with tip–molecule contact (red curve). (b) Waterfall plot for TERS spectra from ZnPc/Ag(100) as a function of tip displacements showing dramatic spectral changes upon the tip–molecule contact. (c) Upper panel: Schematic illustrating the electromagnetic (left) and chemical (right) quenching mechanisms for ZnPc flatly lying on Ag(100). Lower panel: Schematic illustrating the mechanism of TERS enhancement caused by the tip–molecule point contact. Figures are reproduced from ref. 575 with permission. Copyright 2023 Wiley.

interface, as illustrated in Fig. 57. However, the quenched Raman signals can be "rescued" and enhanced in the tip-molecule point contact configuration. These results suggest that the so-called chemically enhanced Raman signals, typically attributed to CT effects, in fact, is the result of a combination of chemical (CT) and physical (electromagnetic field) effects, rather than solely chemical in origin. Additionally, the commonly considered resonance CT enhancement mechanism may be challenging to achieve in many systems, and the enhancement effect may still arise from the influence of ground-state chemical interactions on the Raman polarizability and its orientation. Thus, a comprehensive understanding and consideration of both electromagnetic and chemical enhancement mechanisms are crucial for realizing precise quantitative analysis in SERS.

5.3.3 Digital-SERS for quantitative analysis of molecular concentrations. Digital-SERS is an alternative strategy towards quantitative analysis, which derives from the well-established digital analysis in biomedical research.[576] Both the temporal and spatial variations in SERS intensities increase as the concentration of analytes decreases, posing challenges for trace quantification by SERS. Below a certain concentration threshold, those variations become even more pronounced with several events (either time or spatial measurement), failing to produce detectable SERS signals, while other events exhibiting SERS intensities far exceeding the average. Digital counting offers a potential solution to overcome these limits, as long as "positive" signal events are generated by a small number of entities (*e.g.*, single molecule or single particle). The key to digital analysis is the binary readout: "1" for positive and "0" for negative, respectively. By constraining the number of targets in the measured space to either zero ("0") or a single molecule (or particle) ("1"), the target concentration can be quantified by calculating the ratio of number of positive to the overall number of positive and negative readouts. For digital SERS, the rational ratio of targets to SERS substrates (whether in solid or colloid states)[577] is critical to ensure accurate detection of single molecules, considering that both low and high ratio can affect the quantification distribution according to the Poisson distribution law.

In 2018, Brolo and coworkers demonstrated the concept of digital analysis in SERS measurements by combing SM-SERS and a bi-analyte strategy, as shown in Fig. 58, realizing a LOQ at pM level for enrofloxacin and ciprofloxacin.[578] Later, Trau, Wuethrich, Lobb and coworkers extended digital SERS to biomedical research and achieved the attomolar level sensitivity by utilizing a pillar array SERS substrate to hold the single cytokine and single-particle active SERS nanotags for cytokine identification and counting.[579]

Recently, Ye and coworkers further advanced digital SERS to femtomolar-level sensitivity with improved reproducibility for various molecules by using colloidal SERS substrate and leveraging advanced data analysis.[577] Shortly, Li, Xu and their colleagues reported a statistical route to SM-SERS quantitation

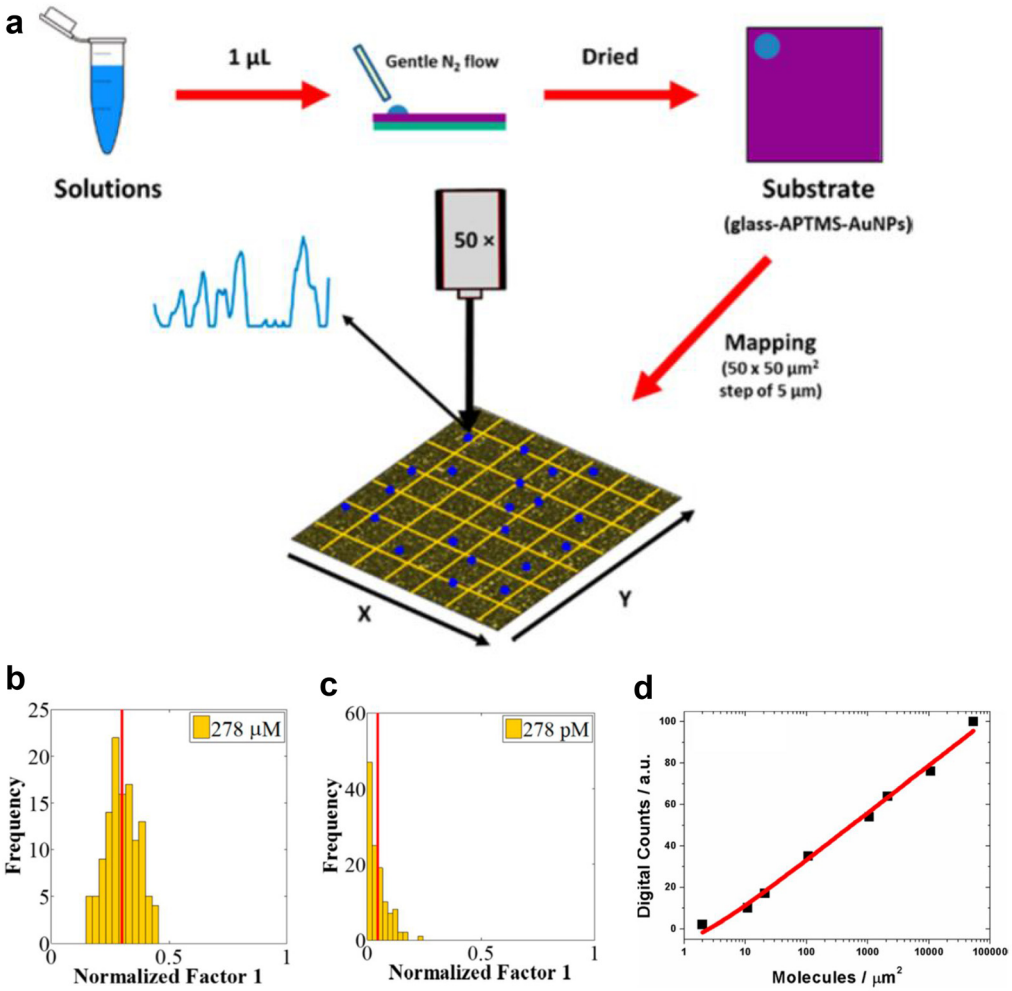

Fig. 58 The digital analysis in SERS measurement. (a) Schematics of the experimental procedure. (b) Histogram showing the frequency of normalized scores from ''factor 1'', which corresponds to the spectral signature of the analyte. The data is obtained from high concentration regime and (c) ultralow concentration regime. (d) Digital calibration curve at ultralow concentration. Figures are adapted from ref. 578 with permission. Copyright 2018 American Chemical Society.

by gauging SERS probability.[580] The rise of statistical quantitative spectroscopy by digital counting, that is, gauging SERS probability rather than traditional intensity, would bring a new quantitation tool for ultra-sensitive SERS detection and analysis.

The digital SERS approach can also be applied in immunoassays based on SERS probes.[581] Moreover, instead of using only the peak intensity from a single peak in the spectrum to count ''0'' and ''1'', Schultz and coworkers considered the overall contribution of the whole spectral information by introducing multivariate curve resolution with an established score threshold.[582] Note that in digital-SERS, the deviation of quantitative analysis is quite large when expanding the lower limit of the SERS linear range to its lowest physical limit, although this error can be minimized by increasing the number of counts.[582]

5.4 Development of SERS methods in bio research

The high sensitivity and unique fingerprint information provided by SERS justify its lively applications in bioanalysis.[31,492,501,583–586] SERS in bio research can be tracked back as early as 1980, when Cotton *et al.* reported the SERRS from cytochrome *c* and myoglobin adsorbed on a silver electrode.[169] Following the nano-driven SERS starting in mid-1990s, an upsurge of bio-related SERS researches started in about mid-2000s, and the number of related publications is *ca.* a quarter of total SERS publications in recent five years. The bio-related applications of SERS primarily focus on hierarchical levels of samples, including biomolecules, biofluids, living cells, and living organisms.[501,587]

It is noteworthy that in the adaptation process to bio-related targets/environments, SERS has been evolving in both SERS substrates and combining various contemporary techniques such as microdevices and microfluidics,[586] 3D printing,[501] machine learning[587] to strengthen its power in bio-related detections. In particular, the increasing integration of SERS into point-of-care testing (POCT) allows for real-time analysis of on-site samples by SERS.[588–590] This progress has been facilitated by advancement in portable Raman spectrometers and microdevices such as lateral flow assay (LFA) strips and

microfluidic channels.[586] All these advancements have significantly contributed to the steady progress of SERS toward precise clinical diagnostics and high-throughput omics research.

5.4.1 Direct bioanalytical SERS detection. Direct (label-free) detection presents the most unique advantage of bio-SERS with the spectral information reflecting the conformation of investigated biological systems directly.[591–593] However, diverse biochemical properties of different biomolecules, such as metabolites, proteins, and DNA, pose different challenges for the direct SERS detection in the early time. For instance, glucose, features small cross sections and low affinity to metal surface.[594] Van Duyne and his colleagues developed a series of self-assemble Ag layer on nanoparticle for partitioning glucose.[595–597] In 2011, they demonstrated *in vivo* glucose sensing with the aid of surface enhanced spatially offset Raman spectroscopy, which is feasible to continuous monitoring up to 17 days.[598]

Unlike carbohydrates, proteins bare relatively large cross section; however, they suffer from complex composition and adsorption configuration, leading to broad and irreproducible spectra. Moreover, except proteins with cofactors, most proteins still require higher concentration to achieve detectable signal, necessitating purification from biological fluids to avoid dominance by concentrated and strongly adsorbing species. To address these issues, Ozaki, Zhao and colleagues conducted systematic tests,[599,600] and proposed a technique called ''Western SERS,'' which replaces the standard silver staining step with silver colloid staining.[601] This approach allows colloids to adsorb to the protein blots and enables subsequent SERS analysis of the separated proteins. To improve reproducibility, Ren group reported a method by utilizing Ag NPs with iodide monolayers to eliminate protein denaturation for more reproducible label-free SERS detection.[602] It is found that iodide's strong adsorption interactions with metal surfaces improved SERS signal reproducibility by preventing structural changes in proteins upon adsorption. Based on this substrate, Yang and colleagues further proposed dynamic SERS to form controllable hotspot taking advantage of solvent evaporation and nanocapillary pumping,[295] which has shown promise for dynamic detection of native proteins.[603]

Regarding nucleic acids detection, Bell group obtained the SERS spectra for all the DNA/RNA mononucleotides with Ag NPs.[592] However, DNA detection faces similar problems as that of proteins, which leads to bad spectral reproducibility. In this context, Halas group developed a series of methods to achieve stable conformations and improve reproducibility.[591,604] Additionally, surface modification plays a crucial role; for instance, Abell and colleagues utilized mercaptohexanol molecules as spacers to protect the substrate and enhance hybridization,[605] while Graham and colleagues introduced spermine to facilitate DNA adhesion and trigger aggregation in colloidal solutions.[606] Thereafter, the strategies have been substantially expanded as summarized by a comprehensive review by Guerrini, Alvarez-Puebla and colleagues.[607]

The constitution of living organisms, particularly living cells, can be directly analyzed as well. By detecting SERS spectra of pathogens or intracellular species, identifying, classifying cells, and monitoring molecular evolution can be achieved. For instance, Popp and colleagues applied SERS-based microfluidic techniques into bacterial strain identification, enabling high spectral acquisition throughput and high reproducibility.[608] Moreover, Ziegler group introduced statistical methods and optimized the procedures for monitoring evolution of different cells.[609–611] Additionally, SERS-active solid substrates such as nanopipette, have been recently developed for precisely detecting and monitoring of cellular responses in real time.[612]

To date, these methods have expanded the application of SERS in bioanalysis from the quantitative and qualitative detection of biomolecules to the analysis of cells, paving the way for new applications in structural biology and metabolomics of living cells and organisms.[501,613–616] Moreover, recent advancements have demonstrated its application to the discovery of novel communication mechanisms between cancer cells[617] and the immune system.[618] Nevertheless, the application of direct detection is limited, owing to both the intrinsically low sensitivity of some biomolecules and the complex spectral information involving the entire biological system. This challenge is further compounded when attempting to measure local pH and the temperature inside a cell. Recent developments in this direction have shown that 3D cell models can be constructed by means of 3D printing, allowing not only to replicate the cellular environment but also to incorporate plasmonic nanoparticles as SERS substrates.[501] In a representative example, Liz-Marzán and colleagues have developed a microfluidic chip that allows evaluation of drug efficacy by monitoring drug diffusion by SERS in correlation with cell death (see Fig. 59).[619]

To acquire better analyte SERS signals requires well-designed substrates, in this regard, Nam and coworkers synthesized an Au-Ag bimetallic nanosnowman structure with a nanocrevice at the junction between Au and Ag.[620,621] Anisotropic growth of Ag bodies on an Au core was achieved by tuning salt concentration to hinder Ag nucleation. Another method for selective nucleation was based on the intrinsic morphological characteristics of core particles. Because ligand packing density is lower at regions of higher curvature, deposition is facilitated at, for example, nanorod tips and nanocube corners. On nanorods, this principle was used to synthesize Au dual-gap nanodumbbells (AuDGNs), with dumbbell-like head structures grown on both tips (Fig. 60a and b).[622] Open nanogaps were present between the core and dumbbell shell, as well as between the dumbbells. Similarly, corner-specific growth on Au nanocubes generated open cross-gap (OXNCs) with eight nanocubes grown onto the central cube (Fig. 60d and e).[623] The AuDGN was capable of label-free discrimination of DNA bases (Fig. 60c), while the OXNC could detect the molecular fingerprint Raman spectra of various proteins (Fig. 60f).

5.4.2 Indirect bioanalytical SERS detection using labels. The primary challenge of direct SERS detection lies in the complexity of the resulting spectra to be analyzed and the intrinsically weak signals of certain target molecules (no inherent molecules for physical properties), which can be easily

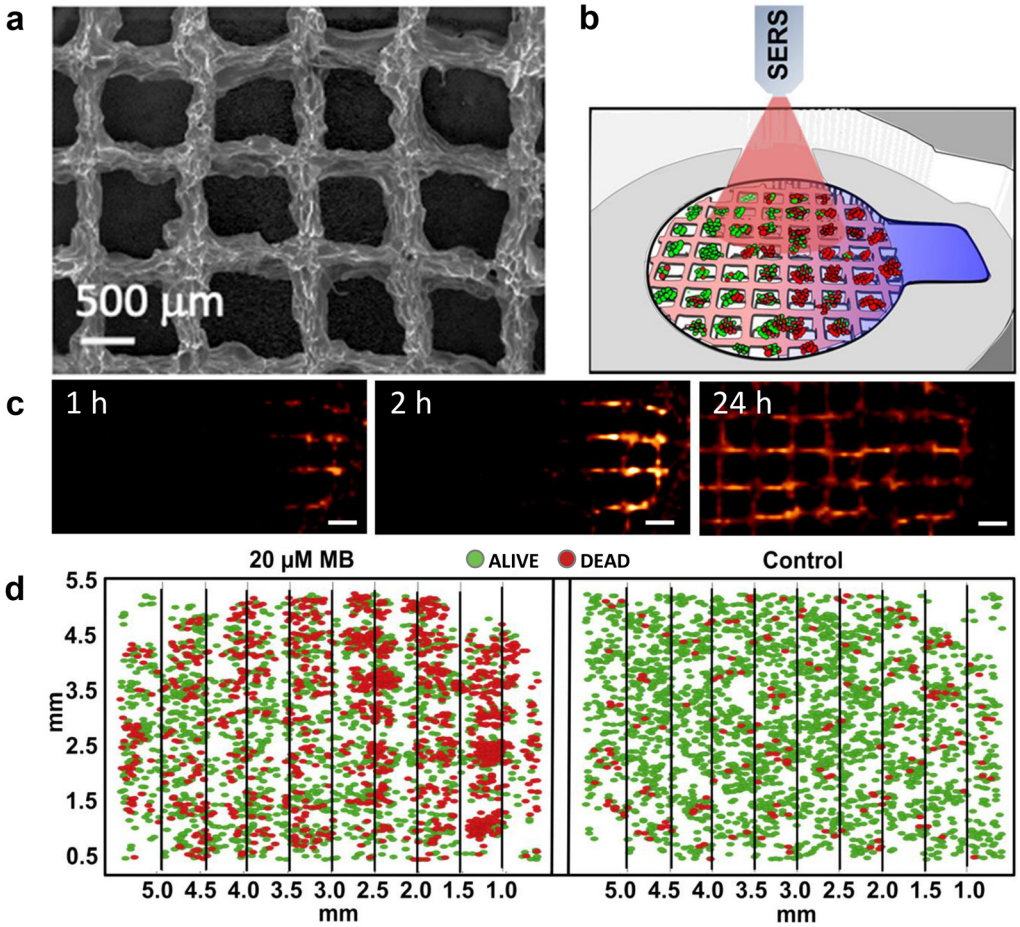

Fig. 59 (a) SEM image of a 3D printed hydrogel-AuNR nanocomposite scaffold. (b) A set-up integrating a nanocomposite scaffold with a tumor cell environment (Matrigel) and a reservoir for drug delivery (right). (c) Methylene blue diffusion patterns along the scaffold containing Matrigel and cancer cells. (d) Confocal fluorescence microscopy evaluation of cell death before (right) and 2 hours after (left) methylene blue injection. Adapted with permission from ref. 619. Copyright 2021 American Chemical Society.

overwhelmed by irrelevant substances. In this regard, indirect (labeled) detection strategies provide an alternative but powerful way for qualitatively and quantitatively monitor physicochemical change in the biological systems investigated. Typically, SERS active nanoparticles can be labeled by molecules with large Raman cross section, *i.e.* SERS reporter, and targeting ligands. Although indirect detection loses the fingerprint information from molecules of interest, the multifunctional SERS reporters possess high sensitivity, specificity, and selectivity. For instance, when the SERS reporter is sensitive to environmental pH, this strategy can be applied to monitor pH changes between the inner and outer parts of living cells.[624]

Immunoassay is of special interest in biomedical diagnostics due to its superior specificity. Great efforts have been devoted to combine immunoassay with indirect SERS detection. In 1989, the binding between biomolecules with mutual affinity, including antigen–antibody interactions, was measured by SERRS on a roughened silver film.[625] With advances in nanoscience, SERS-based immunoassays on Au NPs were reported by Porter and colleagues in 1999.[259] They immobilized antibodies onto Au substrates to capture target antigens, forming sandwich immunocomplexes, and then introduced SERS nanotags labeled with detection antibodies and SERS reporter. The further introduction of immunogold labeling demonstrated ultrasensitive SERS detection for prostate-specific antigen, achieving detection limits down to the femtomolar level.[492,626] Subsequently, SERS-based immunoassays have rapidly developed, driven by diverse newly prepared substrate materials and SERS reporters, thus enabling multiplex detection. Its platform encompasses a range of options, including microfluidic chips, paper devices, and optical fibers with various combinations of solid substrates and liquid phases, enabling the analysis of various biological species as well as cells.[627]

On the other hand, the growing demand for high-throughput, multiplex SERS-based bioassays underscores the importance of integrating various microdevices. In 2005, Choo and colleagues developed a SERS-based microfluidic channel capable of detecting two types of dye-labeled DNA nucleotides.[628] They effectively mixed two types of dye-labeled sex-determining Y genes with Ag nanoparticles within a microfluidic channel shape similar to an alligator tooth, adsorbed the target genes onto particle surfaces, and then measured the SERS signals. The result, showed that these genes could be

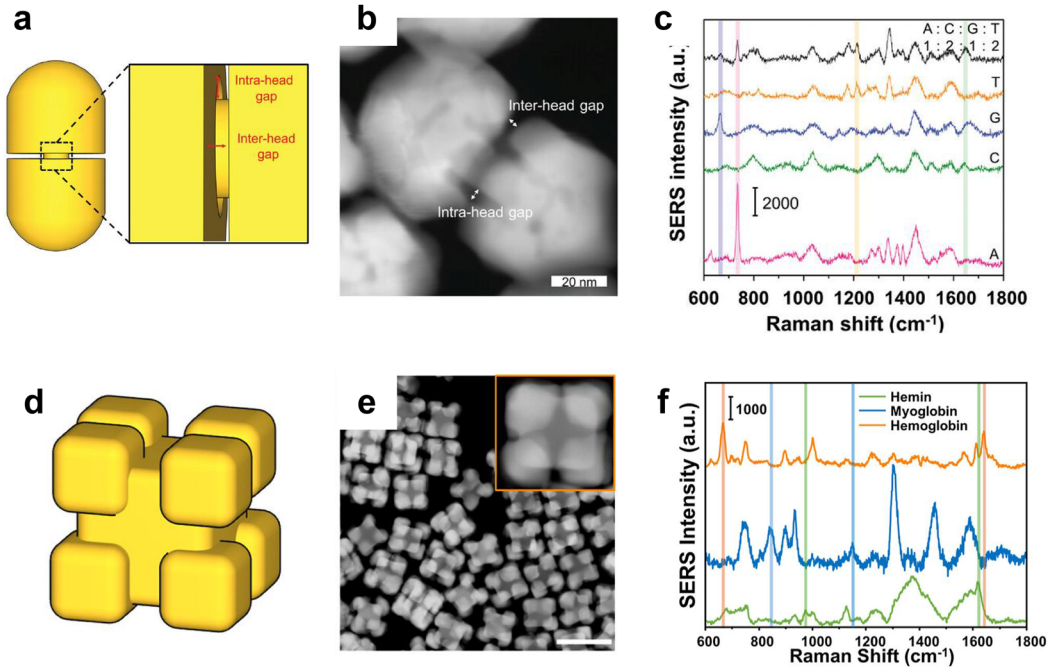

Fig. 60 (a) Schematic of AuDGNs with controllable gap sizes. (b) HAADF-STEM image of AuDGN showing both inter and intra-head gaps. (c) SERS spectra of the four nucleobases. Pink, green, blue, and orange lines indicate fingerprint SERS peaks of adenine (A), cytosine (C), guanine (G), and thymine (T), respectively. The concentrations of A, C, G, and T are 0.01, 0.01, 0.01, and 0.1 mM, respectively. The black line indicates the SERS spectrum of the mixture containing four nucleobases with a 1 : 2:1 : 2 (A : C : G : T) ratio. Reproduced from ref. 622 with permission. Copyright 2023 Wiley. (d) Schematic of OXNCs. (e) HAADF-STEM image of OXNCs with a gap size of 5.6 nm approximately. The inset shows a magnified image of the structure. The scale bars indicate 100 nm. (f) SERS spectra of hemin mixed with the OXNC with 2.6 nm gaps, myoglobin with the OXNC with 5.6 nm gaps, and hemoglobin mixed with the OXNC with 5.6 nm gaps. Panel (d)–(f) are reproduced from ref. 623 with permission, copyright 2024 American Chemical Society.

detected with high sensitivity at concentrations as low as 10^{-11} M. In 2007, Freeman and colleagues introduced a concept of SERS based LFA strip.[629] They used three glass-coated SERS nanotags on an LFA strip to form sandwich immunocomplexes

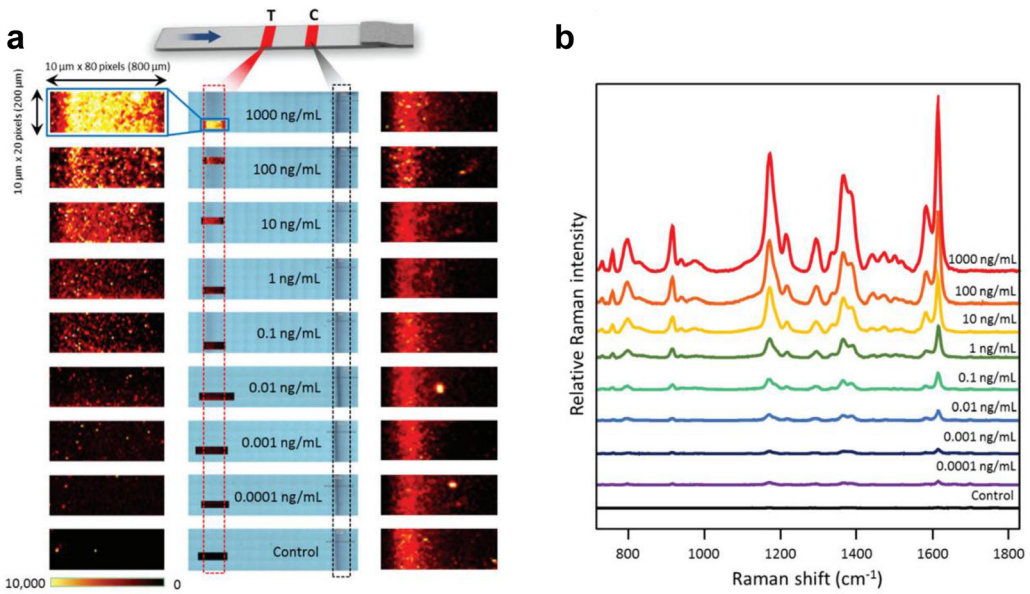

Fig. 61 SERS-based immunoassays using SERS-LFA: (a) schematic illustration of the structure of SERS-LFA strip. SERS mapping images were acquired using a peak intensity at 1615 cm^{-1} for nine different target concentrations ranging from 0.1 pg mL^{-1} to 1000 ng mL^{-1}. For each concentration, images were taken with a resolution of 80 × 20 pixels (1 pixel = 10 μm × 10 μm). The color bar at the bottom indicates changes in Raman peak intensity. (b) Average Raman spectra of 1600-pixel points from the SERS mapping zones. Figures are adapted from ref. 632 with permission. Copyright 2016 Royal Society of Chemistry.

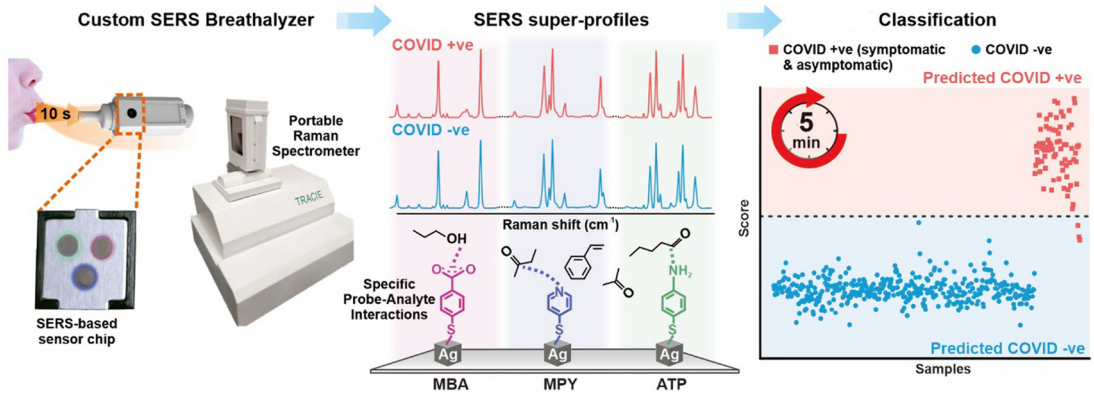

Fig. 62 Using multiple molecular receptor-functionalized SERS substrate to capture and detect breath volatile organic compounds related to COVID-19, then using partial least squares discriminant analysis (PLS-DA) to classify SERS spectra based on their COVID-19 infection status. Figures are adapted from ref. 633 with permission. Copyright 2022 American Chemical Society.

and measured their Raman signal intensities, demonstrating the ability to distinguish three different viruses simultaneously. Since the publication of this paper, various SERS-based LFA strips capable of diagnosing different diseases on-site have been developed. In 2008, Sha and colleagues introduced the idea of labeling circulating tumor cells in whole blood with SERS nanotags on their surface biomarker proteins, then fixing and separating these cells using magnetic beads to quantitatively analyze their SERS signal.[630] After years of development, numerous strategies have been proposed based on the properties of the analytes, enabling high-throughput separation and SERS detection.[586]

Despite these advancements, challenges remain in ensuring the reproducibility of SERS enhancement levels for accurate quantitative analysis of target biomarkers. Variations primarily stem from difficulties in controlling particle aggregation and achieving uniform distribution of analytes on the substrate surface.[631] To address these reproducibility issues, methods such as Raman mapping for LFA strips and average ensemble measurements for microfluidic sensors have been introduced in SERS-based POCT microdevices.[586] Choo and colleagues proposed a method to enhance reproducibility by using Raman mapping for accurate quantitative analysis of target antigens at the test and control lines of the LFA strip.[632] Fig. 61 presents a schematic illustration of the LFA strip's structure. As the sample containing target antigens and SERS nanotags flowed toward the absorption pad and reached the test line, the antigens were captured by antibodies immobilized on the test

Table 5 A summary of application fields of SERS in recent years

	Field	Content	Method & strategy	Materials	Reviews
Surface & interface	Electrochemistry Catalysis Energy Materials	Adsorption, reaction process and interfacial structure	Electrochemical roughening, chemical & physical bottom-up or top-down synthesis & assembly	Noble (Au, Ag, Cu) & transition metals (Pt, Pd, Ru, Rh *etc.*), semiconductors (quantum dots, graphene and MOF *etc.*)	Ref. 26,32,216,217,269, 496,634,635
Life science & medicine	Life science & clinic	Biomarker, DNA, protein, cell, microorganism, drug delivery, therapeutic drug monitoring, enzyme catalysis...	Chemical & physical bottom-up or top-down synthesis & assembly, flexible support (paper, membrane, tap, cotton); label-free & labeled method (electrostatic modification, host–guest recognition molecular steric effect, biological recognition, chemical derivatization, stable isotope probing, *etc.*); lab-on-chip (mill-/micro-/nano-fluidic control)	Metals (Au, Ag, Cu, Pt, Rh, Pd, Ru, Fe, Zn, Al, Li, *etc.*), semiconductors (0D) (quantum dots), 2D (graphene, MXene, hexagonal boron nitride, graphitic carbon nitride, transition metal dichalcogenide, black phosphorus *etc.*) and 3D (MOF, COF, *etc.*), multi-component (mixture, alloy, core–shell, heterojunction, *etc.*)	Ref. 31,501,586,589,590, 607,627,636–638
Trace analysis	Environmental monitoring	Pollutants in ecosystem (air, water and soil)			Ref. 639–643
	Food safety	Illegal additive, pesticide, heavy metal ions, bacteria, micro-/nano-plastics			
	Forensics	Natural and synthesized poisons, bacteria			
	Public security	Abused/illicit drugs, explosive, bacterial			
Others	Art and archaeology	Natural and artificial dyes			Ref. 644,645
	Aerospace	Biosignatures (*e.g.*, carotenoids, chlorophyll, oxalates), astronaut health monitoring, hazardous contaminants in airborne			

line, forming sandwich immunocomplexes. To minimize errors caused by spot-to-spot fluctuations brought by the non-uniform distribution of SERS nanotags on the test line, SERS mapping was applied to different target concentrations. The average Raman spectra of the 1600-pixel points enabled precise quantitative analysis of the target antigen in the SERS-LFA system to improve the reproducibility of SERS-LFA strips.

Recently, the integration of machine learning (ML) with SERS has become a game-changer in solving complex real life sample problems. ML algorithms overcome the limitations of manual spectra analysis, enabling quick and accurate interpretation of the data. Critically, ML tools can elucidate subtle signal variances and establish prediction models to rapidly classify and quantify target analytes accurately, especially for multiplexed analytes in complex matrices. For example, Ling and coworkers used PLS-DA to differentiate breath samples of COVID-19 patients from healthy individuals in a case-control study.[633] An array of SERS platforms, each functionalized with different molecular receptors, was used to capture and detect different volatile organic compounds in breath samples (Fig. 62). The PLS-DA model achieved a classification sensitivity of 96.2% and specificity of 99.9% for both asymptomatic and symptomatic COVID-19 patients.

To date, practical and reliable bioanalytical SERS have been achievable. However, caution is still warranted regarding SERS biodetection, owing to the complicated nano-bio-interactions, *i.e.* chemical and physical interactions between nanomaterials and biological systems, especially in the presence of laser illuminations. These factors also pose significant challenges for spectral analysis and interpretation. As advancements in nanotechnology and machine learning continue to evolve, the future of SERS holds immense potential for even more sophisticated and accessible biosensing solutions, paving the way for next-generation diagnostic tools and comprehensive omics analysis.

Due to space constraints, we are unable to provide an exhaustive review of SERS applications across various fields. Instead, we have compiled a selection of recently published review articles in Table 5 to offer a comprehensive overview of diverse applications of SERS, including surface and interfacial detection, life sciences and medicine, trace analysis and beyond. Readers seeking in-depth discussions on specific SERS applications are encouraged to consult these references for detailed insights into the current state of research and emerging trends in the respective areas.

6. Summary and inspirations from the SERS history

The corresponding author of this review was extremely fortunate to enter this field as a PhD student of Fleischmann and to have the opportunity to get to know all the pioneers well starting from 1983. This privileged perspective allowed a deep understanding of how the 'genetic makeup' of SERS was shaped by Fleischmann and Van Duyne. These major pioneers together formed the foundation of SERS, turning what seemed impossible into reality and establishing the methodological roots and richness of the field.

We meticulously present the history of the discovery of SERS and its foundational era from a methodological standpoint, weaving together the memorial notes of the pioneers themselves, like stringing sparkling pearls into a necklace infused with their scientific spirit and creative methods. We aim to provide a more precise and comprehensive picture, particularly highlighting those who made significant contributions in the first two decades but might be less known to younger generations.

Although there have been over 800 review articles on SERS, our main goal of recounting this long and intricate scientific journey from different perspectives is to raise a fundamental question: What can we learn from the discovery and advancement of SERS for future scientific explorations? We aim to extract the invaluable spirit behind the serendipitous discovery and arduous journey of SERS and distill deep insights and creativity from the pioneers into ten key inspirations, which could serve as treasures for younger generations.

6.1 Collective contribution in opening a new scientific field

Opening a new scientific field, such as the full discovery of the SERS effect, is contributed collectively by several pioneering groups during the intricate early stages of SERS. It constitutes four elementary pieces: The first experimental observation of abnormally intense Raman signals from pyridine adsorbed on a roughened Ag electrode. The first recognition of the huge 10^5–10^6 surface enhancement factor. The initial proposal of the surface plasmon mechanism. The naming of SERS. These contributions laid the groundwork for the field and exemplify how collaborative efforts and multiple discoveries can synergistically establish a new area of scientific research.

6.2 Challenge to conventional wisdom and transforming the impossible into reality

The story of discovering SERS as the first phase of its 50-year history has been incredibly inspiring and encouraging for younger generations. In the mid-1970s, it was widely believed, based on established textbooks, that Raman spectroscopy could not be a tool for surface analysis. The pioneers, filled with strong curiosity, courageous challenges to impossibilities or authority, expert cross-border cooperation, and perseverance in seeking truth despite negative feedback, proved otherwise. This spirit extended to making other milestones, such as single-molecule SERS, TERS beyond the diffraction limitation, SHINERS for non-SERS active substrates. It demonstrates the power of challenging conventional wisdom and transforming what was once considered impossible into reality.

6.3 Learning from the premature and discovery of SERS

It is especially interesting to reflect on the entire journey of SERS, which prematurely emerged about two decades ahead of its time. Without the bold challenges to conventional wisdom posed by its pioneers, the serendipitous discovery of this phenomenon might not have occurred in the mid-1970s.

This research would have been much easier to initiate in the mid-1990s, during the boom of nanoscience, as SERS is fundamentally a branch of nanoscience, with its sensitivity and spectral characteristics critically dependent on nanostructures.

Accordingly, it becomes much clearer why SERS faced significant challenges and underwent a difficult and complex journey before the mid-1990s. However, this also underscores SERS as one of the oldest branches of plasmon-enhanced spectroscopy, plasmonics, and even the broader field of nanoscience. The first chapter of the SERS story is thus unique and inspiring compared to many other scientific fields. Therefore, all the pioneers and trailblazers who collectively established the foundation of SERS in those early decades deserve our utmost respect and should serve as a source of learning.

6.4 Entering a new field as early as possible

Most of the fundamental concepts and strategies for developing SERS and its relevant subbranches were established between 1974 and 1985. These include the first SERS in roughened electrodes and colloid sols, the first ''borrowing SERS activity'' strategy, the first dimer as the 'hot spot' concept, and the initial concept of TERS. These pioneering works and far-reaching ideas were recognized and validated only after several decades. In fact, based on the keywords 'SERS' and 'surface-enhanced Raman' in the Web of Science database, only about 860 papers were published during those ten years, while approximately 80 000 papers have been published up to now (September 2024). This clearly indicates the significant role played by the pioneers and trailblazers who laid the foundation of SERS. This scenario is common in different fields of science and demonstrates the essence of creativity and pioneering work. It is therefore crucial for anyone to be sensitive to opportunities and enter newly emerging fields as early as possible.

6.5 Significant discoveries are often accompanied by initial incorrect explanations

The phenomenon of great discoveries accompanied by incorrect theories occurs quite often in the history of science because groundbreaking discoveries push the boundaries of what is considered possible, often relying on new mechanisms that extend beyond existing knowledge. As a result, initial explanations based on prior understanding frequently fall short, leading to controversies, and some experimental results may not be reproducible by other groups. However, the scientific community should be more tolerant and open to unconventional views, focusing on scientific discussion and arguments rather than negative or harsh criticism. This openness is essential for healthfully opening a new field, laying groundwork, and making advancements smoothly.

6.6 Perseverant searching in times of low tide may lead to triumph

In the second phase (mid-1980s to mid-1990s) of SERS, the wave of excitement was tempered by the realization that the enhancement heavily relied on fine structures (the term ''nano'' was not yet in use at that time) consisting of specific free-electron metals like Au, Ag, Cu, and Li with poorly characterized and uncontrollable morphologies. The mainstream considered the Achilles' heel of SERS to be its lack of versatility and applicability, which significantly impeded enthusiasm for SERS. Many groups had to leave this field mainly due to a shortage of funding support, while some groups continued to make efforts to break through the seemingly impossible barriers. It is therefore important for anyone not to easily give up in a new and promising field (such as one with extremely high detection sensitivity) even when there are many negative views and uncertainties. Perseverant searching can eventually lead to breakthroughs and significant advancements, although nobody can predict when they will occur. The story of SERS is a testament to the importance of persistence and dedication in scientific research because luck is what happens when preparation meets opportunity.

6.7 Proactively embracing and adopting new science and technology

The huge upsurge of SERS from the mid-1990s was accompanied by and driven by the newly established and rapidly developing fields of nanoscience and nanotechnology. This provided an unprecedented opportunity and marked a new era of nano-driven SERS because the SERS effect is one of the phenomena that can truly be described as nanoscience. The SERS activity depends critically on the size, shape, inter-particle space, and optical properties of material nanostructures with tunable extinction, local field enhancement, and excited carriers. With the broad advancement of synthesis, fabrication, and characterization methods for nanomaterials, structural features of SERS-active substrates evolved from discrete size distributions (electrochemically roughened surfaces) to monodisperse nanostructures (nanoparticle-based SERS) and singular nanotips (TERS), from irregular agglomeration (colloid-based SERS) to controlled dimers or multimers (SM-SERS), and from naked surfaces to core–shell nanoparticles (SHINERS). Recent progress in TERS introduced the highest spatial resolution to the angström level, while SHINERS enabled the characterization on various single-crystal surfaces of materials. These advancements allowed for structurally well-defined and rationally designed nanostructures, fostering a deeper understanding of the SERS mechanism.

In fact, throughout the entire trajectory of SERS, proactively embracing newly emerging science and technology has been the key to opening new fields and setting milestones. For instance, Raman spectroscopy embraced laser technology in the 1960s, and SERS leveraged nanoscience for rapid and significant enhancements in various aspects in the 1990s. It now appears to be the right time for nano-driven SERS to fully embrace AI science and technology in the 2020s.

6.8 High level and high-quality interdisciplinary collaboration

Given that transformative scientific revolutions may occur about once every half-century, a small number of people can encounter them during the height of their research careers.

However, throughout several decades of research, there are still opportunities for breakthroughs in their fields. These require pushing beyond current knowledge boundaries and engaging in interdisciplinary collaboration. Only high-level expert cross-disciplinary collaborations with brainstorming and rational designing can make these breakthroughs successful. Examples include combining electrochemistry with Raman spectroscopy, plasmonics with surface spectroscopy, SERS with scanning probe microscopy, and AI with analytical techniques.

It may be necessary to note that nowadays the entry threshold to the SERS field is quite low compared to the very high thresholds for TERS and SHINERS. The synthesis of metal nanoparticles has become so easy and routine that many researchers from different fields widely use SERS-active particles for measurements and publications. Consequently, the high quantity of publications shown in Fig. 17 may not always signify high-quality collaboration or the prosperity of the field. Accordingly, for anyone looking to break developmental bottlenecks in their chosen direction, carefully building their own capabilities and seeking expert collaborators across different disciplines is crucial.

6.9 Comprehensive methodology is the key driver for major advancements

The methodology is always essential for discovery and advancing milestones, a theme prevalent throughout this review. The integration of experimental, theoretical, and instrumental methods is vital for addressing complex challenges and achieving breakthroughs. Nearly a century ago, the discovery of the Raman effect stemmed from what appeared to be a simple, yet meticulously and systematically designed experimental apparatus. Similarly, at the heart of the SERS field is the continuous push to enhance detection sensitivity, evolving from its origins 50 years ago to the latest cutting-edge advancements. This evolution includes the development and design of specialized or entirely new instruments tailored to meet the needs of innovative experiments and to validate emerging theoretical models. These innovations span the full spectrum of instrumental optimization—from macroscopic devices for optical excitation and collection to the microscopic design of plasmon-enhanced nanostructures, as well as instrument-driven data processing software. A prime example is the invention of TERS, where the design and custom construction of scientific instruments played a pivotal role. Thus, the comprehensive and seamless integration of experiment, theory, and instrumentation into a unified methodological approach is not only essential but often decisive for achieving breakthroughs.

6.10 Boldly venture out of the comfort zone of your familiar research to tackle more complex challenges

From the broadest perspective, spanning from basic upstream research to market downstream for everyday use by the public, it is regrettable to observe that the transition of SERS into a widely commercially viable technique has been surprisingly sluggish in comparison with the fundamental breakthroughs over the past decades. The reasons for this unexpectedly slow progress may encompass both surface-level issues and deeper underlying factors. Because SERS offers numerous advantages over other optical spectroscopies, researchers often achieve results easily, publish and cite them, and thus remain within their comfort zones without tackling more complex and challenging issues. The deeper-level challenge is the intrinsic instability of nanostructured hot-spots at the 1 to 3 nanometer scale because SERS is scientifically characterized by a tripartite interaction involving nanostructures, photons, and molecules, making the hot-spots even more unstable. Therefore, the high and mixed demands of long-term durability, measurement reproducibility, product batch consistency, and wide viability of commercial SERS technique remain largely unresolved.

In fact, this is a grand challenge not only for SERS but also for other nanotechnologies in expediting their transition to commercially viable technologies. However, imagine what pioneers in the SERS field could achieve. They would seize the upcoming AI era as a grand opportunity to spark another revolution. AI-assisted nanostructure guidance and pre-trained AI models can quantitatively establish complex high-dimensional correlations between SERS substrate manufacturing parameters, morphology, and spectral responses. This approach offers the prospect of designing novel SERS nanostructures and devices that have not been explored, addressing the trade-off between sensitivity and stability. Moreover, the consistency of SERS nanostructures can also be dramatically improved by utilizing AI-guided automated manufacturing and measurement systematically. Due to the length limitations of this review, the future AI-Nano-Driven SERS will be presented in detail elsewhere.[646]

Overall, we hope that all these inspirations encapsulate the essence of the SERS journey and its pioneers, serving as guiding principles for future scientific endeavors as each generation faces grand challenges and emerging opportunities. Looking forward, we foresee that the ongoing emergence of new technologies, such as advancements in nanotechnology over the past 30 years and recent breakthroughs in AI technology, will drive serendipitous discoveries and new applications. These innovations are likely to provide fresh and powerful momentum for the pivotal new phase of SERS development, ensuring its continued prosperity in the coming half-century.

Author contributions

This historical perspective serves as the inaugural paper in the themed collection for Chemical Society Reviews, celebrating the 50th anniversary of SERS, co-edited by Duncan Graham and Zhong-Qun Tian. The writing process occurred in two phases: the structure and main content were first compiled by members of Tian group and collaborators at Xiamen University, while significant enrichment, particularly in Sec. 4 and 5, was collectively contributed by authors from various active

groups. The detailed contributions by each author are listed in the ESI.†

Data availability

The data of the number of publications in Fig. 17 was searched through publicly available data from the core database of Web of Science. The keywords used for SERS include ''Surface-enhanced Raman'', ''SERS'', ''Surface-enhanced Resonant Raman'' and ''SERRS''. The keyword used for nano is ''Nano''.

Conflicts of interest

There are no conflicts to declare.

Acknowledgements

We would like to dedicate this commemorative review article specifically to M. Fleischmann and R. P. Van Duyne, the key pioneers and figures of the SERS field. Their groundbreaking work laid the foundation for countless advancements in this area. We also extend our deepest gratitude to other pioneers, P. J. Hendra, J. A. Creighton, M. Moskovits and A. J. McQuillan for their invaluable comments and suggestions regarding the discovery of SERS, and for generously providing their photographs for this review. We also express our heartfelt gratitude to some trailblazers, A. Otto, E. Burstein, J. Lombardi, B. Pettinger, K. Kerker, H. Metiu, A. Nitzan, R. K. Chang, T. M. Cotton, J. E. Pemberton, W. E. Smith, M. J. Natan, M. J. Weaver, S. Kawata, D. Irish, P. G. Etchegoin, V. Shalaev, M. Käll and F. Javier García de Abajo *et al.* for their important contributions to the SERS field, which have inspired and helped the authors in the past four decades. Whenever work from the authors' groups is mentioned, we express our deep gratitude to the self-motivated and hard-working students, as well as all other group members, for their invaluable contributions over the past four decades. We sincerely thank L. Tay and R. N. Zare for their valuable contributions and helpful suggestions to the article. The work mentioned has been made possible by continuous financial support on (NSFC 91427304, 21533006, 21321062, 21522508, 20021002, 21473140, 22272140, 22202162, 22272139, 22032004, and 22372072), (MOST 2015CB932300), (CAS 2023-ZW03-A-014). J. Aizpurua acknowledge support from project PID2022-139579NB-I00 funded by Spanish Ministry of Science and Innovation, IT 1526-22 from the Basque Government, and Elkartek project u4Smart of the Department of Economy of the Basque Country. J. Choo acknowledges support from National Research Foundation of Korea (grant numbers 2020R1A5A1018052 and RS-2024-00352256). Z. C. Dong, Yang Zhang, Yao Zhang acknowledge support from Innovation Program for Quantum Science and Technology (2021ZD0303301). N. Halas and P. Nordlander acknowledge support from the Robert A. Welch Foundation under grants C-1220 and C-1222. J.-M. Nam acknowledges the support by the National Research Foundation of Korea (NRF) grants funded by the Korea Government (MSIT) (NRF-2021R1A2C3010083 and No. RS-2024-00397807). V. Deckert acknowledges support from the German Science Foundation *via* the CRC 1375 NOA and the CRC 234 CataLight.

Notes and references

1 M. Fleischmann, P. J. Hendra and A. J. McQuillan, *Chem. Phys. Lett.*, 1974, **26**, 163–166.
2 D. L. Jeanmaire and R. P. Van Duyne, *J. Electroanal. Chem.*, 1977, **84**, 1–20.
3 M. G. Albrecht and J. A. Creighton, *J. Am. Chem. Soc.*, 1977, **99**, 5215–5217.
4 M. Moskovits, *J. Chem. Phys.*, 1978, **69**, 4159–4161.
5 R. P. Van Duyne, in *Chemical and Biochemical Applications of Lasers*, ed. C. B. Moore, Academic Press, 1979, pp. 101–185, DOI: **10.1016/B978-0-12-505404-1.50009-X**.
6 A. Smekal, *Naturwissenschaften*, 1923, **11**, 873–875.
7 C. V. Raman and K. S. Krishnan, *Nature*, 1928, **121**, 501–502.
8 C. V. Raman, *Indian J. Phys.*, 1928, **2**, 387–398.
9 G. S. Landsberg and L. I. Mandelstam, *Naturwissenschaften*, 1928, **16**, 557–558.
10 G. Landesberg and L. Mandelstam, *Compted Rendus*, 1928, **187**, 109–110.
11 R. Singh and F. Riess, *Notes Records R. Soc. London*, 2001, **55**, 267–283.
12 E. C. Le Ru and P. G. Etchegoin, *Principles of Surface-Enhanced Raman Spectroscopy and Related Plasmonic Effects*, Elsevier, Amsterdam, 2009.
13 L. Guerrini and D. Graham, *Chem. Soc. Rev.*, 2012, **41**, 7085–7107.
14 S. Nie and S. R. Emory, *Science*, 1997, **275**, 1102–1106.
15 K. Kneipp, Y. Wang, H. Kneipp, L. T. Perelman, I. Itzkan, R. R. Dasari and M. S. Feld, *Phys. Rev. Lett.*, 1997, **78**, 1667–1670.
16 R. M. Stöckle, Y. D. Suh, V. Deckert and R. Zenobi, *Chem. Phys. Lett.*, 2000, **318**, 131–136.
17 M. S. Anderson, *Appl. Phys. Lett.*, 2000, **76**, 3130–3132.
18 N. Hayazawa, Y. Inouye, Z. Sekkat and S. Kawata, *Opt. Commun.*, 2000, **183**, 333–336.
19 B. Pettinger, G. Picardi, R. Schuster and G. Ertl, *Electrochemistry*, 2000, **68**, 942–949.
20 J.-F. Li, Y. F. Huang, Y. Ding, Z.-L. Yang, S. B. Li, X.-S. Zhou, F.-R. Fan, W. Zhang, Z.-Y. Zhou, D.-Y. Wu, B. Ren, Z. L. Wang and Z.-Q. Tian, *Nature*, 2010, **464**, 392–395.
21 S.-Y. Ding, J. Yi, J.-F. Li, B. Ren, D.-Y. Wu, R. Panneerselvam and Z.-Q. Tian, *Nat. Rev. Mater.*, 2016, **1**, 16021.
22 D. Graham and K. Faulds, *Chem. Soc. Rev.*, 2008, **37**, 1042–1051.
23 I. A. Larmour and D. Graham, *Analyst*, 2011, **136**, 3831–3853.
24 G. McNay, D. Eustace, W. E. Smith, K. Faulds and D. Graham, *Appl. Spectrosc.*, 2011, **65**, 825–837.

25 B. Sharma, R. R. Frontiera, A.-I. Henry, E. Ringe and R. P. Van Duyne, *Mater. Today*, 2012, **15**, 16–25.
26 S. Schlücker, *Angew. Chem., Int. Ed.*, 2014, **53**, 4756–4795.
27 S. McAughtrie, K. Faulds and D. Graham, *J. Photochem. Photobiol., C*, 2014, **21**, 40–53.
28 L. A. Lane, X. Qian and S. Nie, *Chem. Rev.*, 2015, **115**, 10489–10529.
29 S. Laing, L. E. Jamieson, K. Faulds and D. Graham, *Nat. Rev. Chem.*, 2017, **1**, 0060.
30 R. Panneerselvam, G.-K. Liu, Y.-H. Wang, J.-Y. Liu, S.-Y. Ding, J.-F. Li, D.-Y. Wu and Z.-Q. Tian, *Chem. Commun.*, 2018, **54**, 10–25.
31 C. Zong, M. Xu, L.-J. Xu, T. Wei, X. Ma, X.-S. Zheng, R. Hu and B. Ren, *Chem. Rev.*, 2018, **118**, 4946–4980.
32 J. Langer, D. Jimenez de Aberasturi, J. Aizpurua, R. A. Alvarez-Puebla, B. Auguié, J. J. Baumberg, G. C. Bazan, S. E. J. Bell, A. Boisen, A. G. Brolo, J. Choo, D. Cialla-May, V. Deckert, L. Fabris, K. Faulds, F. J. García de Abajo, R. Goodacre, D. Graham, A. J. Haes, C. L. Haynes, C. Huck, T. Itoh, M. Käll, J. Kneipp, N. A. Kotov, H. Kuang, E. C. Le Ru, H. K. Lee, J.-F. Li, X. Y. Ling, S. A. Maier, T. Mayerhöfer, M. Moskovits, K. Murakoshi, J.-M. Nam, S. Nie, Y. Ozaki, I. Pastoriza-Santos, J. Perez-Juste, J. Popp, A. Pucci, S. Reich, B. Ren, G. C. Schatz, T. Shegai, S. Schlücker, L.-L. Tay, K. G. Thomas, Z.-Q. Tian, R. P. Van Duyne, T. Vo-Dinh, Y. Wang, K. A. Willets, C. Xu, H. Xu, Y. Xu, Y. S. Yamamoto, B. Zhao and L. M. Liz-Marzán, *ACS Nano*, 2020, **14**, 28–117.
33 X. X. Han, R. S. Rodriguez, C. L. Haynes, Y. Ozaki and B. Zhao, *Nat. Rev. Methods Primers*, 2022, **1**, 87.
34 T. Itoh, M. Procházka, Z.-C. Dong, W. Ji, Y. S. Yamamoto, Y. Zhang and Y. Ozaki, *Chem. Rev.*, 2023, **123**, 1552–1634.
35 Z.-Q. Tian, B. Ren, J.-F. Li and Z.-L. Yang, *Chem. Commun.*, 2007, 3514–3534, DOI: **10.1039/B616986D**.
36 R. Singh and F. Riess, *Curr. Sci.*, 1998, **74**, 1112–1115.
37 M. H. Harper, *Appl. Opt.*, 1962, **1**, 139–146.
38 G. J. Thomas, *Annu. Rev. Biophys. Biomol. Struct.*, 1999, **28**, 1–27.
39 R. L. McCreery, *Raman Spectroscopy for Chemical Analysis*, 2000, pp. 373–413, DOI: **10.1002/0471721646.ch13**.
40 L. P. Choo-Smith, H. G. M. Edwards, H. P. Endtz, J. M. Kros, F. Heule, H. Barr, J. S. Robinson Jr, H. A. Bruining and G. J. Puppels, *Biopolymers*, 2002, **67**, 1–9.
41 A. E. Grow, L. L. Wood, J. L. Claycomb and P. A. Thompson, *J. Microbiol. Methods*, 2003, **53**, 221–233.
42 R. Hochleitner, N. Tarcea, G. Simon, W. Kiefer and J. Popp, *J. Raman Spectrosc.*, 2004, **35**, 515–518.
43 H. G. M. Edwards, P. Vandenabeele and P. Colomban, *Raman Spectroscopy in Cultural Heritage Preservation*, 2023.
44 P. J. Hendra, J. R. Horder and E. J. Loader, *J. Chem. Soc. A*, 1971, 1766–1770, DOI: **10.1039/J19710001766**.
45 P. J. Hendra, I. D. M. Turner, E. J. Loader and M. Stacey, *J. Phys. Chem.*, 1974, **78**, 300–304.
46 T. A. Egerton and A. H. Hardin, *Catal. Rev.*, 1975, **11**, 71–116.
47 H. Gerischer, R. F. Broman, W. R. Heineman, T. Kuwana, W. J. Albery, M. D. Archer, N. J. Field, A. D. Turner, G. C. Barker, D. McKeown, M. J. Williams, G. Bottura, V. Concialini, Yu. V. Pleskov, Z. A. Rotenberg, V. V. Eletsky, V. I. Lakomov, R. Parsons, A. A. Vlček, G. Porter, A. Bewick, B. Kastening, B. R. Eggins, R. M. Reeves, Frank R. Smith, J. W. Schultze, I. E. Epelboin, D. J. Schiffrin, A. W. B. Aylmer-Kelly, P. R. Cantrill, A. M. Tuxford, O. R. Brown, B. E. Conway, J. D. E. McIntyre, W. F. Peck, D. M. Kolb, I. Bergman, C. L. Gardner, E. J. Casey, M. A. Barrett, H. Angerstein-Kozlowska, M. Keddam, A. J. McQuillan, J. S. Clarke, A. T. Kuhn, W. J. Orville-Thomas, W. Davison, J. A. Harrison, J. Thompson, P. Bindra, M. Fleischmann, J. W. Oldfield, D. Singleton, A. R. Despić, M. Vuković, V. Pravdić, H. R. Thirsk, F. C. Ho, J. Klinger, B. MacDougall, S. Gottesfeld, E. Gileadi, A. Capon, K. J. Vetter, H. P. Dhar, R. D. Armstrong, R. E. Firman, J. C. Lestrade, S. Bruckenstein, J. Comeau, L. Pospíšil, J. Volke, O. Manoušek, A. Rusina, J. Heitbaum, D. J. Brown, L. N. Nekrasov, A. H. Davis, A. J. Mason, J. K. Dohrmann, F. Gallusser, H. Wittchen, B. Gostiša-Mihelcić, J. Divišek, A. J. Bard, V. J. Puglisi, J. V. Kenkel, A. Lomax, R. E. W. Jansson, R. D. Rieke and J. E. B. Randles, *Faraday Discuss. Chem. Soc.*, 1973, **56**, 1–383.
48 R. E. White, J. O. M. Bockris, B. E. Conway and E. Yeager, *Comprehensive Treatise of Electrochemistry*, Springer US, Boston, MA, 1984.
49 H. D. Abruña, *Electrochemical Interfaces: Modern Techniques for In-Situ Interface Characterization*, VCH Publishers Inc., New York, Weinheim, Cambridge, 1991.
50 J. Lipkowski and P. N. Ross, *Adsorption of Molecules at Metal Electrodes*, VCH, Weinheim, New York, 1992.
51 D. Pletcher, Z.-Q. Tian and D. E. Williams, *Developments in Electrochemistry*, Wiley, online, 2014.
52 C.-Y. Li and Z.-Q. Tian, *Chem. Soc. Rev.*, 2024, **53**, 3579–3605.
53 A. J. McQuillan, *Notes Records R. Soc.*, 2009, **63**, 105–109.
54 P. Hendra, *Internet J. Vib. Spectrosc.*, 1999, **4**(2), 1, **https://www.irdg.org/ijvs/volume-4-edition-2/editorial**.
55 M. Fleischmann, P. J. Hendra and A. J. McQuillan, *J. Chem. Soc., Chem. Commun.*, 1973, 80–81, DOI: **10.1039/C39730000080**.
56 P. Hendra, *Analyst*, 2016, **141**, 4996–4999.
57 I. Bergman, B. E. Conway, A. Bewick, T. Kuwana, J. D. E. McIntyre, C. L. Gardner, E. J. Casey, M. A. Barrett, H. Angerstein-Kozlowska, D. M. Kolb, M. Keddam, A. J. McQuillan, J. S. Clarke, A. T. Kuhn and W. J. Orville-Thomas, *Faraday Discuss. Chem. Soc.*, 1973, **56**, 152–170.
58 G. C. Schatz, *J. Raman Spectrosc.*, 2021, **52**, 268–278.
59 C. L. Haynes, C. R. Yonzon, X. Zhang and R. P. Van Duyne, *J. Raman Spectrosc.*, 2005, **36**, 471–484.
60 D. L. Jeanmaire, M. R. Suchanski and R. P. Van Duyne, *J. Am. Chem. Soc.*, 1975, **97**, 1699–1707.
61 T. E. Furtak and J. Reyes, *Surf. Sci.*, 1980, **93**, 351–382.
62 in, *Surface Enhanced Raman Scattering*, ed. R. K. Chang and T. E. Furtak, Plenum Press, New York and London, 1982.

63 T. E. Furtak, *J. Electroanal. Chem.*, 1983, **150**, 375–388.
64 M. Kerker, *Acc. Chem. Res.*, 1984, **17**, 271–277.
65 H. Metiu and P. Das, *Annu. Rev. Phys. Chem.*, 1984, **35**, 507–536.
66 A. Otto, in *Light Scattering in Solids IV: Electronics Scattering, Spin Effects, SERS, and Morphic Effects*, ed. M. Cardona and G. Güntherodt, Springer Berlin Heidelberg, Berlin, Heidelberg, 1984, pp. 289–418, DOI: 10.1007/3-540-11942-6_24.
67 G. C. Schatz, *Acc. Chem. Res.*, 1984, **17**, 370–376.
68 A. Campion, *Annu. Rev. Phys. Chem.*, 1985, **36**, 549–572.
69 M. Moskovits, *Rev. Mod. Phys.*, 1985, **57**, 783.
70 J. A. Creighton, C. G. Blatchford and M. G. Albrecht, *J. Chem. Soc., Faraday Trans. 2*, 1979, **75**, 790–798.
71 M. J. Dignam and M. Moskovits, *J. Chem. Soc., Faraday Trans. 2*, 1973, **69**, 65–78.
72 J. A. Creighton, M. G. Albrecht, R. E. Hester and J. A. D. Matthew, *Chem. Phys. Lett.*, 1978, **55**, 55–58.
73 M. Moskovits, *Notes Records R. Soc.*, 2012, **66**, 195–203.
74 J. A. Creighton, *Notes Records R. Soc.*, 2009, **64**, 175–183.
75 U. Laor and G. C. Schatz, *Chem. Phys. Lett.*, 1981, **82**, 566–570.
76 U. Laor and G. C. Schatz, *J. Chem. Phys.*, 1982, **76**, 2888–2899.
77 P. K. Aravind, A. Nitzan and H. Metiu, *Surf. Sci.*, 1981, **110**, 189–204.
78 P. K. Aravind and H. Metiu, *Surf. Sci.*, 1983, **124**, 506–528.
79 M. Kerker, *Appl. Opt.*, 1979, **18**, 1180–1189.
80 M. Kerker, D.-S. Wang and H. Chew, *Appl. Opt.*, 1980, **19**, 4159–4174.
81 J. Gersten and A. Nitzan, *J. Chem. Phys.*, 1980, **73**, 3023–3037.
82 W. H. Weber and G. W. Ford, *Phys. Rev. Lett.*, 1980, **44**, 1774–1777.
83 S. L. McCall and P. M. Platzman, *Phys. Rev. B: Condens. Matter Mater. Phys.*, 1980, **22**, 1660–1662.
84 S. L. McCall, P. M. Platzman and P. A. Wolff, *Phys. Lett. A*, 1980, **77**, 381–383.
85 F. W. King, R. P. Van Duyne and G. C. Schatz, *J. Chem. Phys.*, 1978, **69**, 4472–4481.
86 S. Efrima and H. Metiu, *J. Chem. Phys.*, 1979, **70**, 1602–1613.
87 S. Efrima and H. Metiu, *J. Chem. Phys.*, 1979, **70**, 1939–1947.
88 S. Efrima and H. Metiu, *J. Chem. Phys.*, 1979, **70**, 2297–2309.
89 M. Moskovits, *J. Chem. Phys.*, 1982, **77**, 4408–4416.
90 M. Kerker, D. S. Wang and H. Chew, *Appl. Opt.*, 1980, **19**, 3373–3388.
91 E. Kretschmann and H. Raether, *Z. Naturf. A*, 1968, **23**, 2135–2136.
92 A. Otto, *Z. Phys. A Hadrons Nuclei*, 1968, **216**, 398–410.
93 H. Raether, in *Surface Plasmons on Smooth and Rough Surfaces and on Gratings*, ed. H. Raether, Springer Berlin Heidelberg, Berlin, Heidelberg, 1988, pp. 4–39, DOI: 10.1007/BFb0048319.
94 B. Pettinger, A. Tadjeddine and D. M. Kolb, *Chem. Phys. Lett.*, 1979, **66**, 544–548.
95 Y. J. Chen, W. P. Chen and E. Burstein, *Phys. Rev. Lett.*, 1976, **36**, 1207–1210.
96 B. Pettinger, U. Wenning and H. Wetzel, *Surf. Sci.*, 1980, **101**, 409–416.
97 R. Dornhaus, R. E. Benner, R. K. Chang and I. Chabay, *Surf. Sci.*, 1980, **101**, 367–373.
98 H. W. K. Tom, C. K. Chen, A. R. B. de Castro and Y. R. Shen, *Solid State Commun.*, 1982, **41**, 259–262.
99 M. R. Philpott, *J. Chem. Phys.*, 1975, **62**, 1812–1817.
100 J. C. Tsang, J. R. Kirtley and J. A. Bradley, *Phys. Rev. Lett.*, 1979, **43**, 772–775.
101 A. Girlando, M. R. Philpott, D. Heitmann, J. D. Swalen and R. Santo, *J. Chem. Phys.*, 1980, **72**, 5187–5191.
102 J. R. Kirtley, S. S. Jha and J. C. Tsang, *Solid State Commun.*, 1980, **35**, 509–512.
103 J. Wessel, *J. Opt. Soc. Am. B*, 1985, **2**, 1538–1541.
104 X. Wang, S.-C. Huang, T.-X. Huang, H.-S. Su, J.-H. Zhong, Z.-C. Zeng, M.-H. Li and B. Ren, *Chem. Soc. Rev.*, 2017, **46**, 4020–4041.
105 J. Billmann and A. Otto, *Solid State Commun.*, 1982, **44**, 105–107.
106 I. Pockrand, J. Billmann and A. Otto, *J. Chem. Phys.*, 1983, **78**, 6384–6390.
107 A. Otto, J. Billmann, J. Eickmans, U. Ertürk and C. Pettenkofer, *Surf. Sci.*, 1984, **138**, 319–338.
108 H. Ueba and S. Ichimura, *J. Chem. Phys.*, 1981, **74**, 3070–3075.
109 H. Ueba, S. Ichimura and H. Yamada, *Surf. Sci.*, 1982, **119**, 433–448.
110 T. E. Furtak and S. H. Macomber, *Chem. Phys. Lett.*, 1983, **95**, 328–332.
111 T. E. Furtak and D. Roy, *Phys. Rev. Lett.*, 1983, **50**, 1301–1304.
112 J. R. Lombardi, R. L. Birke, L. A. Sanchez, I. Bernard and S. C. Sun, *Chem. Phys. Lett.*, 1984, **104**, 240–247.
113 M. J. Weaver, S. Farquharson and M. A. Tadayyoni, *J. Chem. Phys.*, 1985, **82**, 4867–4874.
114 E. Burstein, Y. J. Chen, C. Y. Chen, S. Lundquist and E. Tosatti, *Solid State Commun.*, 1979, **29**, 567–570.
115 J. I. Gersten, R. L. Birke and J. R. Lombardi, *Phys. Rev. Lett.*, 1979, **43**, 147–150.
116 J. E. Demuth and P. N. Sanda, *Phys. Rev. Lett.*, 1981, **47**, 57–60.
117 B. N. J. Persson, *Chem. Phys. Lett.*, 1981, **82**, 561–565.
118 J. R. Lombardi, R. L. Birke, T. Lu and J. Xu, *J. Chem. Phys.*, 1986, **84**, 4174–4180.
119 L. Stolberg, J. Lipkowski and D. E. Irish, *J. Electroanal. Chem. Interfacial Electrochem.*, 1991, **300**, 563–584.
120 F. J. Adrian, *J. Chem. Phys.*, 1982, **77**, 5302–5314.
121 J. Tang and A. C. Albrecht, in *Raman Spectroscopy: Theory and Practice*, ed. H. A. Szymanski, Springer US, Boston, MA, 1970, pp. 33–68, DOI: 10.1007/978-1-4684-3027-1_2.
122 B. Pettinger, *J. Chem. Phys.*, 1986, **85**, 7442–7451.
123 I. Pockrand, *Chem. Phys. Lett.*, 1982, **92**, 514–518.

124 P. Gao, M. L. Patterson, M. A. Tadayyoni and M. J. Weaver, *Langmuir*, 1985, **1**, 173–176.
125 B. Pettinger, M. R. Philpott and J. G. Gordon, II, *J. Phys. Chem.*, 1981, **85**, 2746–2751.
126 H. Wetzel, H. Gerischer and B. Pettinger, *Chem. Phys. Lett.*, 1981, **78**, 392–397.
127 M. Fleischmann, I. R. Hill and M. E. Pemble, *J. Electroanal. Chem. Interfacial Electrochem.*, 1982, **136**, 361–370.
128 L. Moerl and B. Pettinger, *Solid State Commun.*, 1982, **43**, 315–320.
129 R. P. Cooney, M. Fleischmann and P. J. Hendra, *J. Chem. Soc., Chem. Commun.*, 1977, 235–237, DOI: **10.1039/C39770000235**.
130 B. Pettinger and U. Tiedemann, *J. Electroanal. Chem. Interfacial Electrochem.*, 1987, **228**, 219–228.
131 M. A. Bryant, S. L. Joa and J. E. Pemberton, *Langmuir*, 1992, **8**, 753–756.
132 T. Maeda, Y. Sasaki, C. Horie and M. Osawa, *J. Electron Spectrosc. Relat. Phenom.*, 1993, **64–65**, 381–389.
133 S. A. Bilmes, J. C. Rubim, A. Otto and A. J. Arvia, *Chem. Phys. Lett.*, 1989, **159**, 89–96.
134 C. Shannon and A. Campion, *J. Phys. Chem.*, 1988, **92**, 1385–1387.
135 H. Yamada and Y. Yamamoto, *Surf. Sci.*, 1983, **134**, 71–90.
136 R. K. Chang and B. L. Laube, *Crit. Rev. Solid State Mater. Sci.*, 1984, **12**, 1–73.
137 R. P. Van Duyne and J. P. Haushalter, *J. Phys. Chem.*, 1983, **87**, 2999–3003.
138 M. Fleischmann, Z. Q. Tian and L. J. Li, *J. Electroanal. Chem. Interfacial Electrochem.*, 1987, **217**, 397–410.
139 L. W. H. Leung and M. J. Weaver, *J. Am. Chem. Soc.*, 1987, **109**, 5113–5119.
140 R. P. Van Duyne, J. P. Haushalter, M. Janik-Czachor and N. Levinger, *J. Phys. Chem.*, 1985, **89**, 4055–4061.
141 G. Mengoli, M. M. Musiani, M. Fleischmann, B. Mao and Z. Q. Tian, *Electrochim. Acta*, 1987, **32**, 1239–1245.
142 L. W. H. Leung and M. J. Weaver, *J. Electroanal. Chem.*, 1987, **217**, 367–384.
143 J. F. Li, Z. L. Yang, B. Ren, G. K. Liu, P. P. Fang, Y. X. Jiang, D. Y. Wu and Z. Q. Tian, *Langmuir*, 2006, **22**, 10372–10379.
144 L. W. H. Leung and M. J. Weaver, *Langmuir*, 1988, **4**, 1076–1083.
145 R. E. Holt and T. M. Cotton, *J. Am. Chem. Soc.*, 1987, **109**, 1841–1845.
146 H. Feilchenfeld and M. J. Weaver, *J. Phys. Chem.*, 1991, **95**, 7771–7777.
147 J. Hu, R. S. Sheng, Z. S. Xu and Y. E. Zeng, *Spectrochim. Acta, Part A*, 1995, **51**, 1087–1096.
148 A. Helmenstine, M. Uziel and T. Vo-Dinh, *J. Toxicol. Environ. Health*, 1993, **40**, 195–202.
149 M. Osawa, N. Matsuda, K. Yoshii and I. Uchida, *J. Phys. Chem.*, 1994, **98**, 12702–12707.
150 Y. Yamamoto, H. Nishihara and K. Aramaki, *J. Electrochem. Soc.*, 1993, **140**, 436.
151 M. Fleischmann and Z. Q. Tian, *J. Electroanal. Chem. Interfacial Electrochem.*, 1987, **217**, 385–395.
152 B. Pettinger, *Surf. Sci.*, 1985, **158**, 409–410.
153 N. A. Cross and J. E. Pemberton, *J. Electroanal. Chem. Interfacial Electrochem.*, 1987, **217**, 93–100.
154 J. C. Rubim, J.-H. Kim, E. Henderson and T. M. Cotton, *Appl. Spectrosc.*, 1993, **47**, 80–84.
155 M. E. Kordesch, W. Stenzel and H. Conrad, *Surf. Sci.*, 1987, **186**, 601–623.
156 K. T. Carron, G. Xue and M. L. Lewis, *Langmuir*, 1991, **7**, 2–4.
157 G. Xue, J. Ding, P. Lu and J. Dong, *J. Phys. Chem.*, 1991, **95**, 7380–7384.
158 A. Hamelin, L. Stoicoviciu, S.-C. Chang and M. J. Weaver, *J. Electroanal. Chem. Interfacial Electrochem.*, 1991, **307**, 183–194.
159 I. Mrozek and A. Otto, *J. Electron Spectrosc. Relat. Phenom.*, 1990, **54–55**, 895–911.
160 M. Fleischmann, G. Sundholm and Z. Q. Tian, *Electrochim. Acta*, 1986, **31**, 907–916.
161 A. Henglein, P. Mulvaney and T. Linnert, *Electrochim. Acta*, 1991, **36**, 1743–1745.
162 J. Neddersen, G. Chumanov and T. M. Cotton, *Appl. Spectrosc.*, 1993, **47**, 1959–1964.
163 M. Fan, G. F. S. Andrade and A. G. Brolo, *Anal. Chim. Acta*, 2011, **693**, 7–25.
164 P. Gao, D. Gosztola, L.-W. H. Leung and M. J. Weaver, *J. Electroanal. Chem. Interfacial Electrochem.*, 1987, **233**, 211–222.
165 Z.-Q. Tian, B. Ren and D.-Y. Wu, *J. Phys. Chem. B*, 2002, **106**, 9463–9483.
166 D.-Y. Wu, J.-F. Li, B. Ren and Z.-Q. Tian, *Chem. Soc. Rev.*, 2008, **37**, 1025–1041.
167 M. Fleischmann and I. R. Hill, in *Comprehensive Treatise of Electrochemistry: Experimental Methods in Electrochemistry*, ed. R. E. White, J. O. M. Bockris, B. E. Conway and E. Yeager, Springer US, Boston, MA, 1984, vol. 8, pp. 373–432, DOI: **10.1007/978-1-4613-2679-3_6**.
168 T. M. Cotton, J.-H. Kim and G. D. Chumanov, *J. Raman Spectrosc.*, 1991, **22**, 729–742.
169 T. M. Cotton, S. G. Schultz and R. P. Van Duyne, *J. Am. Chem. Soc.*, 1980, **102**, 7960–7962.
170 E. Koglin and J.-M. Séquaris, Surface enhanced raman scattering of biomolecules, in *Analytical Problems. Topics in Current Chemistry*, Springer, Berlin, Heidelberg, 1986, vol. 134.
171 I. R. Nabiev, R. G. Efremov and G. D. Chumanov, *Phys.-Usp.*, 1988, **31**, 241.
172 T. Watanabe, O. Kawanami, H. Katoh, K. Honda, Y. Nishimura and M. Tsuboi, *Surf. Sci.*, 1985, **158**, 341–351.
173 K. Kneipp and J. Flemming, *J. Mol. Struct.*, 1986, **145**, 173–179.
174 T. Vo-Dinh, K. Houck and D. L. Stokes, *Anal. Chem.*, 1994, **66**, 3379–3383.
175 T. Vo-Dinh, M. Uziel and A. L. Morrison, *Appl. Spectrosc.*, 1987, **41**, 605–610.

176 M. Fleischmann, P. J. Hendra, I. R. Hill and M. E. Pemble, *J. Electroanal. Chem. Interfacial Electrochem.*, 1981, **117**, 243–255.
177 B. Pettinger, M. R. Philpott and J. G. Gordon, II, *J. Chem. Phys.*, 1981, **74**, 934–940.
178 T. E. Furtak and D. Roy, *Surf. Sci.*, 1985, **158**, 126–146.
179 A. M. Funtikov, S. K. Sigalaev and V. E. Kazarinov, *J. Electroanal. Chem. Interfacial Electrochem.*, 1987, **228**, 197–218.
180 Z. Q. Tian, S. K. Sigalaev, S. Z. Zou, B. W. Mao, A. M. Funtikov and V. E. Kazarinov, *Electrochim. Acta*, 1994, **39**, 2195–2196.
181 B. Ren, Q. J. Huang, W. B. Cai, B. W. Mao, F. M. Liu and Z. Q. Tian, *J. Electroanal. Chem.*, 1996, **415**, 175–178.
182 R. Feynmann, presented in part at the American Physical Society annual meeting, CalTech, 1959.
183 M. Moskovits and D. P. DiLella, *J. Chem. Phys.*, 1980, **73**, 6068–6075.
184 P. F. Liao, J. G. Bergman, D. S. Chemla, A. Wokaun, J. Melngailis, A. M. Hawryluk and N. P. Economou, *Chem. Phys. Lett.*, 1981, **82**, 355–359.
185 H. Wang, F. Tam, N. K. Grady and N. J. Halas, *J. Phys. Chem. B*, 2005, **109**, 18218–18222.
186 G. H. Chan, J. Zhao, E. M. Hicks, G. C. Schatz and R. P. Van Duyne, *Nano Lett.*, 2007, **7**, 1947–1952.
187 R. G. Freeman, K. C. Grabar, K. J. Allison, R. M. Bright, J. A. Davis, A. P. Guthrie, M. B. Hommer, M. A. Jackson, P. C. Smith, D. G. Walter and M. J. Natan, *Science*, 1995, **267**, 1629–1632.
188 S. J. Oldenburg, S. L. Westcott, R. D. Averitt and N. J. Halas, *J. Chem. Phys.*, 1999, **111**, 4729–4735.
189 L. A. Dick, A. D. McFarland, C. L. Haynes and R. P. Van Duyne, *J. Phys. Chem. B*, 2002, **106**, 853–860.
190 C. L. Haynes and R. P. Van Duyne, *J. Phys. Chem. B*, 2003, **107**, 7426–7433.
191 W. Li, P. H. C. Camargo, X. Lu and Y. Xia, *Nano Lett.*, 2009, **9**, 485–490.
192 M. Hu, F. S. Ou, W. Wu, I. Naumov, X. Li, A. M. Bratkovsky, R. S. Williams and Z. Li, *J. Am. Chem. Soc.*, 2010, **132**, 12820–12822.
193 R. A. Alvarez-Puebla, A. Agarwal, P. Manna, B. P. Khanal, P. Aldeanueva-Potel, E. Carbo-Argibay, N. Pazos-Perez, L. Vigderman, E. R. Zubarev, N. A. Kotov and L. M. Liz-Marzan, *Proc. Natl. Acad. Sci. U. S. A.*, 2011, **108**, 8157–8161.
194 N. G. Greeneltch, M. G. Blaber, A.-I. Henry, G. C. Schatz and R. P. Van Duyne, *Anal. Chem.*, 2013, **85**, 2297–2303.
195 X. Zhang, Y. Zheng, X. Liu, W. Lu, J. Dai, D. Y. Lei and D. R. MacFarlane, *Adv. Mater.*, 2015, **27**, 1090–1096.
196 M. J. Mulvihill, X. Y. Ling, J. Henzie and P. Yang, *J. Am. Chem. Soc.*, 2010, **132**, 268–274.
197 L. Qin, S. Zou, C. Xue, A. Atkinson, G. C. Schatz and C. A. Mirkin, *Proc. Natl. Acad. Sci. U. S. A.*, 2006, **103**, 13300–13303.
198 H. Wang, D. W. Brandl, P. Nordlander and N. J. Halas, *Acc. Chem. Res.*, 2007, **40**, 53–62.
199 C. G. Blatchford, J. R. Campbell and J. A. Creighton, *Surf. Sci.*, 1982, **120**, 435–455.
200 S. G. Schultz, M. Janik-Czachor and R. P. Van Duyne, *Surf. Sci.*, 1981, **104**, 419–434.
201 H. Xu, E. J. Bjerneld, M. Käll and L. Börjesson, *Phys. Rev. Lett.*, 1999, **83**, 4357–4360.
202 S. P. S. Porto and D. L. Wood, *J. Opt. Soc. Am.*, 1962, **52**, 251–252.
203 E. C. Le Ru, E. Blackie, M. Meyer and P. G. Etchegoin, *J. Phys. Chem. C*, 2007, **111**, 13794–13803.
204 K. Kneipp, H. Kneipp, V. B. Kartha, R. Manoharan, G. Deinum, I. Itzkan, R. R. Dasari and M. S. Feld, *Phys. Rev. E:Stat. Phys., Plasmas, Fluids, Relat. Interdiscip. Top.*, 1998, **57**, R6281–R6284.
205 K. Kneipp, Y. Wang, H. Kneipp, I. Itzkan, R. R. Dasari and M. S. Feld, *Phys. Rev. Lett.*, 1996, **76**, 2444–2447.
206 M. I. Stockman, V. M. Shalaev, M. Moskovits, R. Botet and T. F. George, *Phys. Rev. B: Condens. Matter Mater. Phys.*, 1992, **46**, 2821–2830.
207 H. Xu, J. Aizpurua, M. Käll and P. Apell, *Phys. Rev. E:Stat., Nonlinear, Soft Matter Phys.*, 2000, **62**, 4318–4324.
208 A. M. Michaels, M. Nirmal and L. E. Brus, *J. Am. Chem. Soc.*, 1999, **121**, 9932–9939.
209 J. Jiang, K. Bosnick, M. Maillard and L. Brus, *J. Phys. Chem. B*, 2003, **107**, 9964–9972.
210 V. M. Shalaev and A. K. Sarychev, *Phys. Rev. B: Condens. Matter Mater. Phys.*, 1998, **57**, 13265–13288.
211 H. Xu and M. Käll, *Phys. Rev. Lett.*, 2002, **89**, 246802.
212 E. C. Le Ru, M. Meyer and P. G. Etchegoin, *J. Phys. Chem. B*, 2006, **110**, 1944–1948.
213 J. A. Dieringer, R. B. Lettan, K. A. Scheidt and R. P. Van Duyne, *J. Am. Chem. Soc.*, 2007, **129**, 16249–16256.
214 P. G. Etchegoin, M. Meyer, E. Blackie and E. C. Le Ru, *Anal. Chem.*, 2007, **79**, 8411–8415.
215 E. C. Le Ru and P. G. Etchegoin, *Annu. Rev. Phys. Chem.*, 2012, **63**, 65–87.
216 A. B. Zrimsek, N. Chiang, M. Mattei, S. Zaleski, M. O. McAnally, C. T. Chapman, A.-I. Henry, G. C. Schatz and R. P. Van Duyne, *Chem. Rev.*, 2017, **117**, 7583–7613.
217 N. L. Gruenke, M. F. Cardinal, M. O. McAnally, R. R. Frontiera, G. C. Schatz and R. P. Van Duyne, *Chem. Soc. Rev.*, 2016, **45**, 2263–2290.
218 F. Neubrech, C. Huck, K. Weber, A. Pucci and H. Giessen, *Chem. Rev.*, 2017, **117**, 5110–5145.
219 J.-F. Li, C.-Y. Li and R. F. Aroca, *Chem. Soc. Rev.*, 2017, **46**, 3962–3979.
220 S. Shen, L. Meng, Y. Zhang, J. Han, Z. Ma, S. Hu, Y. He, J. Li, B. Ren, T.-M. Shih, Z. Wang, Z. Yang and Z. Tian, *Nano Lett.*, 2015, **15**, 6716–6721.
221 W.-T. Liu and Y. R. Shen, *Proc. Natl. Acad. Sci. U. S. A.*, 2014, **111**, 1293–1297.
222 G. Hajisalem, M. S. Nezami and R. Gordon, *Nano Lett.*, 2014, **14**, 6651–6654.

223 M. Danckwerts and L. Novotny, *Phys. Rev. Lett.*, 2007, **98**, 026104.
224 X. Hua, D. V. Voronine, C. W. Ballmann, A. M. Sinyukov, A. V. Sokolov and M. O. Scully, *Phys. Rev. A: At., Mol., Opt. Phys.*, 2014, **89**, 043841.
225 J. A. Dieringer, A. D. McFarland, N. C. Shah, D. A. Stuart, A. V. Whitney, C. R. Yonzon, M. A. Young, X. Zhang, R. Van Duyne, K. Kneipp, H. Kneipp, F. Svedburg, M. Käll, M. Futamata, E. Le Ru, P. G. Etchegoin, R. Maher, L. F. Cohen, B. Vlćková, G. Lucassen, Z.-Q. Tian, B. Pettinger, B. Ren, A. E. Russell, M. J. Natan, J. J. Baumberg, G. McNay, K. Murakoshi, S. Nie, R. Aggarwal, T. A. Kelf, T. Itoh, T. Maeda, A. Kasuya, B. Pergolese, M. Muniz-Miranda, G. Sbrana, A. Bigotto, M. Sládková, P. Mojzeš, M. Šlouf, C. Naudin, G. Le Bourdon, D. G. Cunningham, R. E. Littleford, W. E. Smith, P. J. Lundahl, I. Khan, D. W. McComb, D. Graham, N. Laforest, K. F. Domke, B. D. Alexander, E. Blanch, C. Eliasson, A. Pal, M. J. T. Milton, R. Goodacre, E. M. Kosower, O. Glembocki, Z.-L. Yang, J.-F. Li, Y. Zhang, X.-F. Lin, J.-W. Hu, D.-Y. Wu, S. Lazar, Y. Sawai, B. Takimoto, H. Nabika, K. Ajito, S. H. Cintra, M. E. Abdelsalam, P. N. Bartlett, Y. Sugawara, R. J. C. Brown, J. Wang, R. Tantra, R. E. Yardley, D. Roy, M. E. Welland, W. I. Barnes, J. A. Creighton, M. Green, V. Poponin, N. Stone, D. Richards, R. M. Jarvis, M. Whitby, S. R. Emory, R. A. Jensen, T. Wenda, M. Han, K. J. Faulds, L. Fruk, D. C. Robson, D. G. Thompson, A. Enright, P. Köllensperger, T. Cass, A. Brooker, N. R. Isola, J. P. Alarie, D. L. Stokes, T. Vo-Dinh, A. F. McCabe, R. A. Prasath, A. Hernandez-Santana, L. Stevenson, I. Apple, P. A. G. Cormack, P. Corish, S. J. Lipscomb, E. R. Holland, P. D. Prince, B. Foulger, M. Zoorob, B. Pearson, P. Donaldson, N. E. Cant and T. Pal, *Faraday Discuss.*, 2006, **132**, 1–340.
226 A.-I. Henry, T. W. Ueltschi, M. O. McAnally, R. P. Van Duyne, M. K. Schmidt, R. Esteban, F. Benz, J. J. Baumberg, J. Aizpurua, L. Velleman, L. Scarabelli, D. Sikdar, A. A. Kornyshev, L. M. Liz-Marzán, J. B. Edel, N. S. Mueller, S. Heeg, P. Kusch, E. Gaufrès, N. Y.-W. Tang, U. Hübner, R. Martel, A. Vijayaraghavan, S. Reich, J. R. Lombardi, P. Dawson, D. Frey, V. Kalathingal, R. Mehfuz, J. Mitra, R. L. Gieseking, M. A. Ratner, G. C. Schatz, D. Graham, R. Goodacre, H. Arnolds, J.-F. Masson, D.-H. Kim, W. Lum, A. Silvestri, B. de Nijs, Y. Xu, G. D. Martino, M. Natan, S. Schlücker, P. Wuytens, I. Bruzas, C. Kuttner, M. Hardy, R. Chikkaraddy, N. M. Sabanés, I. Delfino, S. Gawinkowski, N. Bontempi, S. Mahajan, B. Hourahine, S. Bell, A. Królikowska, M. Porter, A. Keeler, M. Kamp, A. Fountain, C. Fasolato, F. Giorgis, J. C. Otero, C. Matricardi, V. Deckert, Z. Zhang, M. Richard-Lacroix, C. L. D. Lee, K. C. Hewitt, A. Elizabeth, J. H. K. Pfisterer, K. F. Domke, P. B. Joshi, T. P. Anthony, A. J. Wilson, K. A. Willets, H. Minamimoto, F. Kato, F. Nagasawa, M. Takase, K. Murakoshi, C. Novara, A. Chiadò, N. Paccotti, S. Catuogno, C. L. Esposito, G. Condorelli, V. De Franciscis, F. Geobaldo, P. Rivolo, M. Chisanga, H. Fleming, C. Heck, L. Jamieson, N. Lidgi-Guigui, C. Lightner, H. Muhamadali, J. Popp, Z.-Q. Tian, A. Tripathi, X. Wang, A. Wark, K. (Kallie) Willets, M. Willner, R. Kimber, H. Demol, N. Turk, K. Gevaert, A. G. Skirtach, M. Lamkanfi, R. Baets, J. Langer, I. García, B. Walkenfort, M. König, L. König, S. Kasimir-Bauer, F. Lussier, T. Brulé, M.-J. Bourque, C. Ducrot, L.-É. Trudeau, J. Taylor, J. Milton, M. Willett, J. Wingfield, A. Bonifacio, S. Corsetti, O. Eremina, K. Faulds, T. Keyes, F. Nicolson, E. Nikelshparg, K. Plakas, D. Prezgot, N. Pytlik, N. Stone, S.-Y. Ding, E.-M. You, J. Yi, J.-F. Li, T. A. Galloway, L. Cabo-Fernandez, I. M. Aldous, F. Braga, L. J. Hardwick, H. Wei, A. McCarthy, J. Song, W. Zhou, P. J. Vikesland, I. Szabó, S. J. Barrow, G. Wu, C. Carnegie, W. Wang, W. M. Deacon, E. Rosta, O. A. Scherman, S. Dick, V. A. Turek, C. Tserkezis, A. Lombardi, A. Kuhn, J. A. Guicheteau, E. D. Emmons, S. D. Christesen, H. Aitchison, M. G. Castano, J. Gracie, J. Guicheteau and J. H. Granger, *Faraday Discuss.*, 2017, **205**, 1–626.
227 G. Di Martino, H. Fleming, M. Kamp and F. Lussier, *Chem. Commun.*, 2017, **53**, 12726–12733.
228 E. C. Le Ru, P. G. Etchegoin and M. Meyer, *J. Chem. Phys.*, 2006, **125**, 204701.
229 J. M. McMahon, S. Li, L. K. Ausman and G. C. Schatz, *J. Phys. Chem. C*, 2012, **116**, 1627–1637.
230 A. Moreau, C. Ciracì, J. J. Mock, R. T. Hill, Q. Wang, B. J. Wiley, A. Chilkoti and D. R. Smith, *Nature*, 2012, **492**, 86–89.
231 B. Pettinger, P. Schambach, C. J. Villagómez and N. Scott, *Annu. Rev. Phys. Chem.*, 2012, **63**, 379–399.
232 S. L. Kleinman, R. R. Frontiera, A.-I. Henry, J. A. Dieringer and R. P. Van Duyne, *Phys. Chem. Chem. Phys.*, 2013, **15**, 21–36.
233 H. Wei and H. Xu, *Nanoscale*, 2013, **5**, 10794–10805.
234 A. Shiohara, Y. Wang and L. M. Liz-Marzán, *J. Photochem. Photobiol., C*, 2014, **21**, 2–25.
235 J. J. Baumberg, J. Aizpurua, M. H. Mikkelsen and D. R. Smith, *Nat. Mater.*, 2019, **18**, 668–678.
236 D.-K. Lim, K.-S. Jeon, H. M. Kim, J.-M. Nam and Y. D. Suh, *Nat. Mater.*, 2010, **9**, 60–67.
237 D.-K. Lim, K.-S. Jeon, J.-H. Hwang, H. Kim, S. Kwon, Y. D. Suh and J.-M. Nam, *Nat. Nanotechnol.*, 2011, **6**, 452–460.
238 P. G. Etchegoin and E. C. Le Ru, *Phys. Chem. Chem. Phys.*, 2008, **10**, 6079–6089.
239 J. A. Dieringer, K. L. Wustholz, D. J. Masiello, J. P. Camden, S. L. Kleinman, G. C. Schatz and R. P. Van Duyne, *J. Am. Chem. Soc.*, 2009, **131**, 849–854.
240 S. L. Kleinman, E. Ringe, N. Valley, K. L. Wustholz, E. Phillips, K. A. Scheidt, G. C. Schatz and R. P. Van Duyne, *J. Am. Chem. Soc.*, 2011, **133**, 4115–4122.
241 S. Cintra, M. E. Abdelsalam, P. N. Bartlett, J. J. Baumberg, T. A. Kelf, Y. Sugawara and A. E. Russell, *Faraday Discuss.*, 2006, **132**, 191–199.
242 P. L. Stiles, J. A. Dieringer, N. C. Shah and R. P. Van Duyne, *Annu. Rev. Anal. Chem.*, 2008, **1**, 601–626.

243 I. Alessandri and J. R. Lombardi, *Chem. Rev.*, 2016, **116**, 14921–14981.
244 J. M. McLellan, A. Siekkinen, J. Chen and Y. Xia, *Chem. Phys. Lett.*, 2006, **427**, 122–126.
245 J. M. McLellan, Z.-Y. Li, A. R. Siekkinen and Y. Xia, *Nano Lett.*, 2007, **7**, 1013–1017.
246 L. Rodríguez-Lorenzo, R. A. Álvarez-Puebla, I. Pastoriza-Santos, S. Mazzucco, O. Stéphan, M. Kociak, L. M. Liz-Marzán and F. J. García de Abajo, *J. Am. Chem. Soc.*, 2009, **131**, 4616–4618.
247 W. E. Doering and S. Nie, *Anal. Chem.*, 2003, **75**, 6171–6176.
248 W. Shen, X. Lin, C. Jiang, C. Li, H. Lin, J. Huang, S. Wang, G. Liu, X. Yan, Q. Zhong and B. Ren, *Angew. Chem., Int. Ed.*, 2015, **54**, 7308–7312.
249 H. Lee, J.-H. Lee, S. M. Jin, Y. D. Suh and J.-M. Nam, *Nano Lett.*, 2013, **13**, 6113–6121.
250 A. Tao, F. Kim, C. Hess, J. Goldberger, R. He, Y. Sun, Y. Xia and P. Yang, *Nano Lett.*, 2003, **3**, 1229–1233.
251 Y. Lu, G. L. Liu and L. P. Lee, *Nano Lett.*, 2005, **5**, 5–9.
252 S. Park, P. Yang, P. Corredor and M. J. Weaver, *J. Am. Chem. Soc.*, 2002, **124**, 2428–2429.
253 S. P. Mulvaney, M. D. Musick, C. D. Keating and M. J. Natan, *Langmuir*, 2003, **19**, 4784–4790.
254 X. Qian, X.-H. Peng, D. O. Ansari, Q. Yin-Goen, G. Z. Chen, D. M. Shin, L. Yang, A. N. Young, M. D. Wang and S. Nie, *Nat. Biotechnol.*, 2008, **26**, 83–90.
255 H. Zhang, C. Wang, H.-L. Sun, G. Fu, S. Chen, Y.-J. Zhang, B.-H. Chen, J. R. Anema, Z.-L. Yang, J.-F. Li and Z.-Q. Tian, *Nat. Commun.*, 2017, **8**, 15447.
256 R. D. Averitt, D. Sarkar and N. J. Halas, *Phys. Rev. Lett.*, 1997, **78**, 4217–4220.
257 S. J. Oldenburg, R. D. Averitt, S. L. Westcott and N. J. Halas, *Chem. Phys. Lett.*, 1998, **288**, 243–247.
258 E. Prodan, C. Radloff, N. J. Halas and P. Nordlander, *Science*, 2003, **302**, 419–422.
259 J. Ni, R. J. Lipert, G. B. Dawson and M. D. Porter, *Anal. Chem.*, 1999, **71**, 4903–4908.
260 Y. C. Cao, R. Jin and C. A. Mirkin, *Science*, 2002, **297**, 1536–1540.
261 G. Wang, H.-Y. Park, R. J. Lipert and M. D. Porter, *Anal. Chem.*, 2009, **81**, 9643–9650.
262 F. Burgio, D. Piffaretti, F. Schmidt, U. Pieles, M. Reinert, M.-F. Ritz and S. Saxer, *ACS Appl. Nano Mater.*, 2020, **3**, 2447–2454.
263 L. M. Liz-Marzán, M. Giersig and P. Mulvaney, *Langmuir*, 1996, **12**, 4329–4335.
264 O. E. Eremina, A. T. Czaja, A. Fernando, A. Aron, D. B. Eremin and C. Zavaleta, *ACS Nano*, 2022, **16**, 10341–10353.
265 B. A. Kairdolf and S. Nie, *J. Am. Chem. Soc.*, 2011, **133**, 7268–7271.
266 I. Srivastava, R. Xue, J. Jones, H. Rhee, K. Flatt, V. Gruev and S. Nie, *ACS Nano*, 2022, **16**, 8051–8063.
267 L. Lu, G. Sun, H. Zhang, H. Wang, S. Xi, J. Hu, Z. Tian and R. Chen, *J. Mater. Chem.*, 2004, **14**, 1005–1009.
268 J.-W. Hu, Y. Zhang, J.-F. Li, Z. Liu, B. Ren, S.-G. Sun, Z.-Q. Tian and T. Lian, *Chem. Phys. Lett.*, 2005, **408**, 354–359.
269 J.-F. Li, Y.-J. Zhang, S.-Y. Ding, R. Panneerselvam and Z.-Q. Tian, *Chem. Rev.*, 2017, **117**, 5002–5069.
270 H. Zhang, S. Duan, P. M. Radjenovic, Z.-Q. Tian and J.-F. Li, *Acc. Chem. Res.*, 2020, **53**, 729–739.
271 R. A. Álvarez-Puebla, R. Contreras-Cáceres, I. Pastoriza-Santos, J. Pérez-Juste and L. M. Liz-Marzán, *Angew. Chem., Int. Ed.*, 2009, **48**, 138–143.
272 V. V. Thacker, L. O. Herrmann, D. O. Sigle, T. Zhang, T. Liedl, J. J. Baumberg and U. F. Keyser, *Nat. Commun.*, 2014, **5**, 3448.
273 A. Lee, G. F. S. Andrade, A. Ahmed, M. L. Souza, N. Coombs, E. Tumarkin, K. Liu, R. Gordon, A. G. Brolo and E. Kumacheva, *J. Am. Chem. Soc.*, 2011, **133**, 7563–7570.
274 J. C. Fraire, V. N. Sueldo Ocello, L. G. Allende, A. V. Veglia and E. A. Coronado, *J. Phys. Chem. C*, 2015, **119**, 8876–8888.
275 J.-H. Lee, J.-M. Nam, K.-S. Jeon, D.-K. Lim, H. Kim, S. Kwon, H. Lee and Y. D. Suh, *ACS Nano*, 2012, **6**, 9574–9584.
276 J.-W. Oh, D.-K. Lim, G.-H. Kim, Y. D. Suh and J.-M. Nam, *J. Am. Chem. Soc.*, 2014, **136**, 14052–14059.
277 K. Y. Hong and A. G. Brolo, *Anal. Chim. Acta*, 2017, **972**, 73–80.
278 C. L. Haynes and R. P. Van Duyne, *J. Phys. Chem. B*, 2001, **105**, 5599–5611.
279 M. Kahl, E. Voges, S. Kostrewa, C. Viets and W. Hill, *Sens. Actuators, B*, 1998, **51**, 285–291.
280 A. G. Brolo, R. Gordon, B. Leathem and K. L. Kavanagh, *Langmuir*, 2004, **20**, 4813–4815.
281 A. Gopinath, S. V. Boriskina, B. M. Reinhard and L. D. Negro, *Opt. Express*, 2009, **17**, 3741–3753.
282 A. G. Brolo, E. Arctander, R. Gordon, B. Leathem and K. L. Kavanagh, *Nano Lett.*, 2004, **4**, 2015–2018.
283 S. R. Smith, C. Zhou, J. Y. Baron, Y. Choi and J. Lipkowski, *Electrochim. Acta*, 2016, **210**, 925–934.
284 S. R. Smith, J. J. Leitch, C. Zhou, J. Mirza, S.-B. Li, X.-D. Tian, Y.-F. Huang, Z.-Q. Tian, J. Y. Baron, Y. Choi and J. Lipkowski, *Anal. Chem.*, 2015, **87**, 3791–3799.
285 P. Nagpal, N. C. Lindquist, S.-H. Oh and D. J. Norris, *Science*, 2009, **325**, 594–597.
286 T. W. Johnson, Z. J. Lapin, R. Beams, N. C. Lindquist, S. G. Rodrigo, L. Novotny and S.-H. Oh, *ACS Nano*, 2012, **6**, 9168–9174.
287 D. J. Maxwell, S. R. Emory and S. Nie, *Chem. Mater.*, 2001, **13**, 1082–1088.
288 H. Wang, C. S. Levin and N. J. Halas, *J. Am. Chem. Soc.*, 2005, **127**, 14992–14993.
289 F. De Angelis, F. Gentile, F. Mecarini, G. Das, M. Moretti, P. Candeloro, M. L. Coluccio, G. Cojoc, A. Accardo, C. Liberale, R. P. Zaccaria, G. Perozziello, L. Tirinato, A. Toma, G. Cuda, R. Cingolani and E. Di Fabrizio, *Nat. Photonics*, 2011, **5**, 682–687.
290 D. M. Solís, J. M. Taboada, F. Obelleiro, L. M. Liz-Marzán and F. J. García de Abajo, *ACS Photonics*, 2017, **4**, 329–337.

291 H. Liu, Z. Yang, L. Meng, Y. Sun, J. Wang, L. Yang, J. Liu and Z. Tian, *J. Am. Chem. Soc.*, 2014, **136**, 5332–5341.
292 K. Kim, H. S. Han, I. Choi, C. Lee, S. Hong, S.-H. Suh, L. P. Lee and T. Kang, *Nat. Commun.*, 2013, **4**, 2182.
293 M. P. Cecchini, V. A. Turek, J. Paget, A. A. Kornyshev and J. B. Edel, *Nat. Mater.*, 2013, **12**, 165–171.
294 D. Zhang, L. Peng, X. Shang, W. Zheng, H. You, T. Xu, B. Ma, B. Ren and J. Fang, *Nat. Commun.*, 2020, **11**, 2603.
295 M. Ge, P. Li, G. Zhou, S. Chen, W. Han, F. Qin, Y. Nie, Y. Wang, M. Qin, G. Huang, S. Li, Y. Wang, L. Yang and Z. Tian, *J. Am. Chem. Soc.*, 2021, **143**, 7769–7776.
296 M. J. Natan, *Faraday Discuss.*, 2006, **132**, 321–328.
297 J.-H. Tian, B. Liu, X. Li, Z.-L. Yang, B. Ren, S.-T. Wu, N. Tao and Z.-Q. Tian, *J. Am. Chem. Soc.*, 2006, **128**, 14748–14749.
298 T. Konishi, M. Kiguchi, M. Takase, F. Nagasawa, H. Nabika, K. Ikeda, K. Uosaki, K. Ueno, H. Misawa and K. Murakoshi, *J. Am. Chem. Soc.*, 2013, **135**, 1009–1014.
299 J. Zheng, J. Liu, Y. Zhuo, R. Li, X. Jin, Y. Yang, Z.-B. Chen, J. Shi, Z. Xiao, W. Hong and Z.-Q. Tian, *Chem. Sci.*, 2018, **9**, 5033–5038.
300 S. Kaneko, D. Murai, S. Marqués-González, H. Nakamura, Y. Komoto, S. Fujii, T. Nishino, K. Ikeda, K. Tsukagoshi and M. Kiguchi, *J. Am. Chem. Soc.*, 2016, **138**, 1294–1300.
301 S. Kaneko, E. Montes, S. Suzuki, S. Fujii, T. Nishino, K. Tsukagoshi, K. Ikeda, H. Kano, H. Nakamura, H. Vázquez and M. Kiguchi, *Chem. Sci.*, 2019, **10**, 6261–6269.
302 T. Itoh, Y. S. Yamamoto, H. Tamaru, V. Biju, S.-I. Wakida and Y. Ozaki, *Phys. Rev. B: Condens. Matter Mater. Phys.*, 2014, **89**, 195436.
303 E. C. Le Ru, P. G. Etchegoin, J. Grand, N. Félidj, J. Aubard and G. Lévi, *J. Phys. Chem. C*, 2007, **111**, 16076–16079.
304 T. Itoh, Y. S. Yamamoto, H. Tamaru, V. Biju, N. Murase and Y. Ozaki, *Phys. Rev. B: Condens. Matter Mater. Phys.*, 2013, **87**, 235408.
305 M. Takase, H. Ajiki, Y. Mizumoto, K. Komeda, M. Nara, H. Nabika, S. Yasuda, H. Ishihara and K. Murakoshi, *Nat. Photonics*, 2013, **7**, 550–554.
306 C. M. Aikens, L. R. Madison and G. C. Schatz, *Nat. Photonics*, 2013, **7**, 508–510.
307 K. L. Kelly, E. Coronado, L. L. Zhao and G. C. Schatz, *J. Phys. Chem. B*, 2003, **107**, 668–677.
308 E. Hao and G. C. Schatz, *J. Chem. Phys.*, 2004, **120**, 357–366.
309 L. L. Zhao, L. Jensen and G. C. Schatz, *Nano Lett.*, 2006, **6**, 1229–1234.
310 D.-Y. Wu, X.-M. Liu, S. Duan, X. Xu, B. Ren, S.-H. Lin and Z.-Q. Tian, *J. Phys. Chem. C*, 2008, **112**, 4195–4204.
311 S. Tao, L.-J. Yu, R. Pang, Y.-F. Huang, D.-Y. Wu and Z.-Q. Tian, *J. Phys. Chem. C*, 2013, **117**, 18891–18903.
312 A. J. Haes and R. P. Van Duyne, *Anal. Bioanal. Chem.*, 2004, **379**, 920–930.
313 J. R. Lombardi and R. L. Birke, *J. Phys. Chem. C*, 2008, **112**, 5605–5617.
314 J. R. Lombardi and R. L. Birke, *Acc. Chem. Res.*, 2009, **42**, 734–742.
315 L. Jensen, C. M. Aikens and G. C. Schatz, *Chem. Soc. Rev.*, 2008, **37**, 1061–1073.
316 S. M. Morton and L. Jensen, *J. Am. Chem. Soc.*, 2009, **131**, 4090–4098.
317 D. J. Trivedi, B. Barrow and G. C. Schatz, *J. Chem. Phys.*, 2020, **153**, 124706.
318 A. Wang, Y.-F. Huang, U. K. Sur, D.-Y. Wu, B. Ren, S. Rondinini, C. Amatore and Z.-Q. Tian, *J. Am. Chem. Soc.*, 2010, **132**, 9534–9536.
319 H. M. Dykstra, S. B. Hall and M. R. Waterland, *J. Raman Spectrosc.*, 2017, **48**, 405–412.
320 D. H. Murgida and P. Hildebrandt, *Acc. Chem. Res.*, 2004, **37**, 854–861.
321 C. D. Lindstrom and X. Y. Zhu, *Chem. Rev.*, 2006, **106**, 4281–4300.
322 D. Y. Wu, M. Hayashi, S. H. Lin and Z. Q. Tian, *Spectrochim. Acta, Part A*, 2004, **60**, 137–146.
323 M. T. Lee, D. Y. Wu, Z. Q. Tian and S. H. Lin, *J. Chem. Phys.*, 2005, **122**, 094719.
324 L. L. Zhao, L. Jensen and G. C. Schatz, *J. Am. Chem. Soc.*, 2006, **128**, 2911–2919.
325 J. C. Rubim, P. Corio, M. C. C. Ribeiro and M. Matz, *J. Phys. Chem.*, 1995, **99**, 15765–15774.
326 L. Jensen and G. C. Schatz, *J. Phys. Chem. A*, 2006, **110**, 5973–5977.
327 N. Valley, N. Greeneltch, R. P. Van Duyne and G. C. Schatz, *J. Phys. Chem. Lett.*, 2013, **4**, 2599–2604.
328 D. Aranda, F. García-González, F. J. Avila Ferrer, I. López-Tocón, J. Soto and J. C. Otero, *J. Chem. Theory Comput.*, 2022, **18**, 6802–6815.
329 F. García-González, J. C. Otero, F. J. Ávila Ferrer, F. Santoro and D. Aranda, *J. Chem. Theory Comput.*, 2024, **20**, 3850–3863.
330 J. Gargiulo, R. Berté, Y. Li, S. A. Maier and E. Cortés, *Acc. Chem. Res.*, 2019, **52**, 2525–2535.
331 A. Nitzan and L. E. Brus, *J. Chem. Phys.*, 1981, **75**, 2205–2214.
332 C. Zhan, X.-J. Chen, J. Yi, J.-F. Li, D.-Y. Wu and Z.-Q. Tian, *Nat. Rev. Chem.*, 2018, **2**, 216–230.
333 L. Brus, *Acc. Chem. Res.*, 2008, **41**, 1742–1749.
334 E. S. Thrall, A. Preska Steinberg, X. Wu and L. E. Brus, *J. Phys. Chem. C*, 2013, **117**, 26238–26247.
335 S. Mukherjee, F. Libisch, N. Large, O. Neumann, L. V. Brown, J. Cheng, J. B. Lassiter, E. A. Carter, P. Nordlander and N. J. Halas, *Nano Lett.*, 2013, **13**, 240–247.
336 Y.-F. Huang, H.-P. Zhu, G.-K. Liu, D.-Y. Wu, B. Ren and Z.-Q. Tian, *J. Am. Chem. Soc.*, 2010, **132**, 9244–9246.
337 Y.-Q. Su, J. Liu, R. Huang, H.-T. Yang, M.-X. Li, R. Pang, M. Zhang, M.-H. Yang, H.-F. Su, R. Devasenathipathy, Y.-F. Wu, J.-Z. Zhou, D.-Y. Wu, S.-Y. Xie, B.-W. Mao and Z.-Q. Tian, *J. Phys. Chem. Lett.*, 2023, **14**, 5163–5171.
338 J. Liu, Z.-Y. Cai, W.-X. Sun, J.-Z. Wang, X.-R. Shen, C. Zhan, R. Devasenathipathy, J.-Z. Zhou, D.-Y. Wu, B.-W. Mao and Z.-Q. Tian, *J. Am. Chem. Soc.*, 2020, **142**, 17489–17498.
339 C. Zhan, J. Yi, S. Hu, X.-G. Zhang, D.-Y. Wu and Z.-Q. Tian, *Nat. Rev. Methods Primers*, 2023, **3**, 12.
340 S. Linic, S. Chavez and R. Elias, *Nat. Mater.*, 2021, **20**, 916–924.

341 A. Stefancu, N. J. Halas, P. Nordlander and E. Cortes, *Nat. Phys.*, 2024, **20**, 1065–1077.
342 N. J. Halas, S. Lal, S. Link, W.-S. Chang, D. Natelson, J. H. Hafner and P. Nordlander, *Adv. Mater.*, 2012, **24**, 4842–4877.
343 C. E. Talley, J. B. Jackson, C. Oubre, N. K. Grady, C. W. Hollars, S. M. Lane, T. R. Huser, P. Nordlander and N. J. Halas, *Nano Lett.*, 2005, **5**, 1569–1574.
344 F. Le, D. W. Brandl, Y. A. Urzhumov, H. Wang, J. Kundu, N. J. Halas, J. Aizpurua and P. Nordlander, *ACS Nano*, 2008, **2**, 707–718.
345 A. B. Sánchez-Alvarado, J. Zhou, P. Jin, O. Neumann, T. P. Senftle, P. Nordlander and N. J. Halas, *ACS Nano*, 2023, **17**, 25697–25706.
346 L. W.-H. Tian Zhong-Qun, M. Ji-Qian, M. Bing-Wei, C. Jie-Guang, Z. Xiang-Dong, Z. Wei, W. Duo and Y. En-Rou, *Acta Phys.-Chim. Sin.*, 1994, **10**, 1062–1065.
347 Z. Q. Tian, W. H. Li, B. Ren, B. W. Mao, J. G. Chen, J. Q. Mu, X. D. Zhuo and D. Wang, *J. Electroanal. Chem.*, 1996, **401**, 247–251.
348 Z.-Q. Tian and B. Ren, Raman Spectroscopy of Electrode Surfaces, in *Encyclopedia of Electrochemistry*, ed. A. J. Bard, Wiley-VCH, 2007, DOI: 10.1002/9783527610426.bard030306.
349 J. Stadler, T. Schmid and R. Zenobi, *Nano Lett.*, 2010, **10**, 4514–4520.
350 T. Ichimura, S. Fujii, P. Verma, T. Yano, Y. Inouye and S. Kawata, *Phys. Rev. Lett.*, 2009, **102**, 186101.
351 T.-a Yano, P. Verma, Y. Saito, T. Ichimura and S. Kawata, *Nat. Photonics*, 2009, **3**, 473–477.
352 R. Esteban, A. G. Borisov, P. Nordlander and J. Aizpurua, *Nat. Commun.*, 2012, **3**, 825.
353 C. Ciracì, R. T. Hill, J. J. Mock, Y. Urzhumov, A. I. Fernández-Domínguez, S. A. Maier, J. B. Pendry, A. Chilkoti and D. R. Smith, *Science*, 2012, **337**, 1072–1074.
354 R. Zhang, Y. Zhang, Z. C. Dong, S. Jiang, C. Zhang, L. G. Chen, L. Zhang, Y. Liao, J. Aizpurua, Y. Luo, J. L. Yang and J. G. Hou, *Nature*, 2013, **498**, 82–86.
355 S. Duan, G. Tian, Y. Ji, J. Shao, Z. Dong and Y. Luo, *J. Am. Chem. Soc.*, 2015, **137**, 9515–9518.
356 M. Barbry, P. Koval, F. Marchesin, R. Esteban, A. G. Borisov, J. Aizpurua and D. Sánchez-Portal, *Nano Lett.*, 2015, **15**, 3410–3419.
357 T. Neuman, R. Esteban, D. Casanova, F. J. García-Vidal and J. Aizpurua, *Nano Lett.*, 2018, **18**, 2358–2364.
358 F. Benz, M. K. Schmidt, A. Dreismann, R. Chikkaraddy, Y. Zhang, A. Demetriadou, C. Carnegie, H. Ohadi, B. de Nijs, R. Esteban, J. Aizpurua and J. J. Baumberg, *Science*, 2016, **354**, 726–729.
359 M. K. Schmidt, R. Esteban, A. González-Tudela, G. Giedke and J. Aizpurua, *ACS Nano*, 2016, **10**, 6291–6298.
360 F. Latorre, S. Kupfer, T. Bocklitz, D. Kinzel, S. Trautmann, S. Gräfe and V. Deckert, *Nanoscale*, 2016, **8**, 10229–10239.
361 S. Trautmann, J. Aizpurua, I. Götz, A. Undisz, J. Dellith, H. Schneidewind, M. Rettenmayr and V. Deckert, *Nanoscale*, 2017, **9**, 391–401.
362 C. Carnegie, M. Urbieta, R. Chikkaraddy, B. de Nijs, J. Griffiths, W. M. Deacon, M. Kamp, N. Zabala, J. Aizpurua and J. J. Baumberg, *Nat. Commun.*, 2020, **11**, 682.
363 J. J. Baumberg, R. Esteban, S. Hu, U. Muniain, I. V. Silkin, J. Aizpurua and V. M. Silkin, *Nano Lett.*, 2023, **23**, 10696–10702.
364 P. Roelli, C. Galland, N. Piro and T. J. Kippenberg, *Nat. Nanotechnol.*, 2016, **11**, 164–169.
365 L. A. Jakob, W. M. Deacon, Y. Zhang, B. de Nijs, E. Pavlenko, S. Hu, C. Carnegie, T. Neuman, R. Esteban, J. Aizpurua and J. J. Baumberg, *Nat. Commun.*, 2023, **14**, 3291.
366 N. C. Lindquist, C. D. L. de Albuquerque, R. G. Sobral-Filho, I. Paci and A. G. Brolo, *Nat. Nanotechnol.*, 2019, **14**, 981–987.
367 N. C. Lindquist and A. G. Brolo, *J. Phys. Chem. C*, 2021, **125**, 7523–7532.
368 J. Lee, K. T. Crampton, N. Tallarida and V. A. Apkarian, *Nature*, 2019, **568**, 78–82.
369 Y. Zhang, B. Yang, A. Ghafoor, Y. Zhang, Y.-F. Zhang, R.-P. Wang, J.-L. Yang, Y. Luo, Z.-C. Dong and J. G. Hou, *Natl. Sci. Rev.*, 2019, **6**, 1169–1175.
370 J. Xu, X. Zhu, S. Tan, Y. Zhang, B. Li, Y. Tian, H. Shan, X. Cui, A. Zhao, Z. Dong, J. Yang, Y. Luo, B. Wang and J. G. Hou, *Science*, 2021, **371**, 818–822.
371 Z.-C. Zeng, S.-C. Huang, D.-Y. Wu, L.-Y. Meng, M.-H. Li, T.-X. Huang, J.-H. Zhong, X. Wang, Z.-L. Yang and B. Ren, *J. Am. Chem. Soc.*, 2015, **137**, 11928–11931.
372 D. Kurouski, M. Mattei and R. P. Van Duyne, *Nano Lett.*, 2015, **15**, 7956–7962.
373 G. Kang, M. Yang, M. S. Mattei, G. C. Schatz and R. P. Van Duyne, *Nano Lett.*, 2019, **19**, 2106–2113.
374 Y.-F. Bao, M.-F. Cao, S.-S. Wu, T.-X. Huang, Z.-C. Zeng, M.-H. Li, X. Wang and B. Ren, *Anal. Chem.*, 2020, **92**, 12548–12555.
375 S.-C. Huang, J.-Z. Ye, X.-R. Shen, Q.-Q. Zhao, Z.-C. Zeng, M.-H. Li, D.-Y. Wu, X. Wang and B. Ren, *Anal. Chem.*, 2019, **91**, 11092–11097.
376 T. Touzalin, S. Joiret, I. T. Lucas and E. Maisonhaute, *Electrochem. Commun.*, 2019, **108**, 106557.
377 J. H. K. Pfisterer, M. Baghernejad, G. Giuzio and K. F. Domke, *Nat. Commun.*, 2019, **10**, 5702.
378 T.-X. Huang, X. Cong, S.-S. Wu, J.-B. Wu, Y.-F. Bao, M.-F. Cao, L. Wu, M.-L. Lin, X. Wang, P.-H. Tan and B. Ren, *Nat. Catal.*, 2024, **7**, 646–654.
379 P. Matousek, I. P. Clark, E. R. C. Draper, M. D. Morris, A. E. Goodship, N. Everall, M. Towrie, W. F. Finney and A. W. Parker, *Appl. Spectrosc.*, 2005, **59**, 393–400.
380 P. Matousek and N. Stone, *J. Biomed. Opt.*, 2007, **12**, 024008.
381 N. Stone, M. Kerssens, G. R. Lloyd, K. Faulds, D. Graham and P. Matousek, *Chem. Sci.*, 2011, **2**, 776–780.
382 N. Stone, K. Faulds, D. Graham and P. Matousek, *Anal. Chem.*, 2010, **82**, 3969–3973.
383 A. V. Baranov and Y. S. Bobovich, *JETP Lett.*, 1982, **36**, 339–343.

384 D. V. Murphy, K. U. Von Raben, R. K. Chang and P. B. Dorain, *Chem. Phys. Lett.*, 1982, **85**, 43–47.
385 K. Kneipp, H. Kneipp and F. Seifert, *Chem. Phys. Lett.*, 1995, **233**, 519–524.
386 J. C. Hulteen, M. A. Young and R. P. Van Duyne, *Langmuir*, 2006, **22**, 10354–10364.
387 J. Kneipp, H. Kneipp and K. Kneipp, *Proc. Natl. Acad. Sci. U. S. A.*, 2006, **103**, 17149–17153.
388 F. Madzharova, Z. Heiner and J. Kneipp, *Chem. Soc. Rev.*, 2017, **46**, 3980–3999.
389 C. B. Milojevich, D. W. Silverstein, L. Jensen and J. P. Camden, *ChemPhysChem*, 2011, **12**, 101–103.
390 P. Matousek, M. Towrie, A. Stanley and A. W. Parker, *Appl. Spectrosc.*, 1999, **53**, 1485–1489.
391 D. V. Voronine, A. M. Sinyukov, X. Hua, K. Wang, P. K. Jha, E. Munusamy, S. E. Wheeler, G. Welch, A. V. Sokolov and M. O. Scully, *Sci. Rep.*, 2012, **2**, 891.
392 S. Yampolsky, D. A. Fishman, S. Dey, E. Hulkko, M. Banik, E. O. Potma and V. A. Apkarian, *Nat. Photonics*, 2014, **8**, 650–656.
393 Z. Sun, J. Lu, D. H. Zhang and S.-Y. Lee, *J. Chem. Phys.*, 2008, **128**, 144114.
394 R. R. Frontiera, A.-I. Henry, N. L. Gruenke and R. P. Van Duyne, *J. Phys. Chem. Lett.*, 2011, **2**, 1199–1203.
395 L. E. Buchanan, N. L. Gruenke, M. O. McAnally, B. Negru, H. E. Mayhew, V. A. Apkarian, G. C. Schatz and R. P. Van Duyne, *J. Phys. Chem. Lett.*, 2016, **7**, 4629–4634.
396 E. L. Keller and R. R. Frontiera, *ACS Nano*, 2018, **12**, 5848–5855.
397 C. L. Warkentin and R. R. Frontiera, *Proc. Natl. Acad. Sci. U. S. A.*, 2023, **120**, e2305932120.
398 T. Ichimura, N. Hayazawa, M. Hashimoto, Y. Inouye and S. Kawata, *Phys. Rev. Lett.*, 2004, **92**, 220801.
399 E. A. Pozzi, M. D. Sonntag, N. Jiang, N. Chiang, T. Seideman, M. C. Hersam and R. P. Van Duyne, *J. Phys. Chem. Lett.*, 2014, **5**, 2657–2661.
400 Y. Luo, A. Martin-Jimenez, R. Gutzler, M. Garg and K. Kern, *Nano Lett.*, 2022, **22**, 5100–5106.
401 J. S. Gao and Z. Q. Tian, *Spectrochim. Acta, Part A*, 1997, **53**, 1595–1600.
402 W. B. Cai, B. Ren, X. Q. Li, C. X. She, F. M. Liu, X. W. Cai and Z. Q. Tian, *Surf. Sci.*, 1998, **406**, 9–22.
403 B. Ren, X.-F. Lin, J.-W. Yan, B.-W. Mao and Z.-Q. Tian, *J. Phys. Chem. B*, 2003, **107**, 899–902.
404 K. A. Willets and R. P. Van Duyne, *Annu. Rev. Phys. Chem.*, 2007, **58**, 267–297.
405 Z.-Q. Tian, Z.-L. Yang, B. Ren and D.-Y. Wu, in *Surface-Enhanced Raman Scattering: Physics and Applications*, ed. K. Kneipp, M. Moskovits and H. Kneipp, Springer Berlin Heidelberg, Berlin, Heidelberg, 2006, pp. 125–146, DOI: 10.1007/3-540-33567-6_7.
406 K. N. Kanipe, P. P. F. Chidester, G. D. Stucky, C. D. Meinhart and M. Moskovits, *J. Phys. Chem. C*, 2017, **121**, 14269–14273.
407 Z.-Q. Tian, Z.-L. Yang, B. Ren, J.-F. Li, Y. Zhang, X.-F. Lin, J.-W. Hu and D.-Y. Wu, *Faraday Discuss.*, 2006, **132**, 159–170.
408 X. Ling, L. Xie, Y. Fang, H. Xu, H. Zhang, J. Kong, M. S. Dresselhaus, J. Zhang and Z. Liu, *Nano Lett.*, 2010, **10**, 553–561.
409 Z. Q. Tian, B. Ren and B. W. Mao, *J. Phys. Chem. B*, 1997, **101**, 1338–1346.
410 J. L. Yao, B. Ren, Z. F. Huang, P. G. Cao, R. A. Gu and Z.-Q. Tian, *Electrochim. Acta*, 2003, **48**, 1263–1271.
411 H. Yamada, Y. Yamamoto and N. Tani, *Chem. Phys. Lett.*, 1982, **86**, 397–400.
412 S. Hayashi, R. Koh, Y. Ichiyama and K. Yamamoto, *Phys. Rev. Lett.*, 1988, **60**, 1085–1088.
413 Y. Wang, J. Zhang, H. Jia, M. Li, J. Zeng, B. Yang, B. Zhao, W. Xu and J. R. Lombardi, *J. Phys. Chem. C*, 2008, **112**, 996–1000.
414 J. R. Lombardi and R. L. Birke, *J. Phys. Chem. C*, 2014, **118**, 11120–11130.
415 X. Wang and L. Guo, *Angew. Chem., Int. Ed.*, 2020, **59**, 4231–4239.
416 X. X. Han, W. Ji, B. Zhao and Y. Ozaki, *Nanoscale*, 2017, **9**, 4847–4861.
417 W. Ji, X. X. Han and B. Zhao, *Recent Developments in Plasmon-Supported Raman Spectroscopy*, 2018, pp. 451–482, DOI: 10.1142/9781786344243_0016.
418 A. Musumeci, D. Gosztola, T. Schiller, N. M. Dimitrijevic, V. Mujica, D. Martin and T. Rajh, *J. Am. Chem. Soc.*, 2009, **131**, 6040–6041.
419 W. Ji, L. Li, W. Song, X. Wang, B. Zhao and Y. Ozaki, *Angew. Chem., Int. Ed.*, 2019, **58**, 14452–14456.
420 W. Ji, L. Li, J. Guan, M. Mu, W. Song, L. Sun, B. Zhao and Y. Ozaki, *Adv. Opt. Mater.*, 2021, **9**, 2101866.
421 P. Li, L. Zhu, C. Ma, L. Zhang, L. Guo, Y. Liu, H. Ma and B. Zhao, *ACS Appl. Mater. Interfaces*, 2020, **12**, 19153–19160.
422 E. Sachet, M. D. Losego, J. T. Guske, S. Franzen and J. P. Maria, *Appl. Phys. Lett.*, 2013, **102**, 051111.
423 Y. Liu, H. Ma, X. X. Han and B. Zhao, *Mater. Horiz.*, 2021, **8**, 370–382.
424 X. Wang, P. Li, X. X. Han, Y. Kitahama, B. Zhao and Y. Ozaki, *Nanoscale*, 2017, **9**, 15303–15313.
425 X. X. Han, C. Köhler, J. Kozuch, U. Kuhlmann, L. Paasche, A. Sivanesan, I. M. Weidinger and P. Hildebrandt, *Small*, 2013, **9**(24), 4175–4181.
426 X. Liu, Z. Ye, Q. Xiang, Z. Xu, W. Yue, C. Li, Y. Xu, L. Wang, X. Cao and J. Zhang, *Chem*, 2023, **9**, 1464–1476.
427 J. Li, Q. Xie, J. Li, L. Sun, Y. Xie, Y. Ozaki and W. Ji, *Adv. Funct. Mater.*, 2024, **34**, 2400523.
428 W. Xu, N. Mao and J. Zhang, *Small*, 2013, **9**, 1206–1224.
429 W. Xu, X. Ling, J. Xiao, M. S. Dresselhaus, J. Kong, H. Xu, Z. Liu and J. Zhang, *Proc. Natl. Acad. Sci. U. S. A.*, 2012, **109**, 9281–9286.
430 X. Ling, W. Fang, Y.-H. Lee, P. T. Araujo, X. Zhang, J. F. Rodriguez-Nieva, Y. Lin, J. Zhang, J. Kong and M. S. Dresselhaus, *Nano Lett.*, 2014, **14**, 3033–3040.
431 S. Zhang, N. Zhang, Y. Zhao, T. Cheng, X. Li, R. Feng, H. Xu, Z. Liu, J. Zhang and L. Tong, *Chem. Soc. Rev.*, 2018, **47**, 3217–3240.

432 H. Kitadai, Q. Tan, L. Ping and X. Ling, *npj 2D Mater. Appl.*, 2024, **8**, 11.
433 H. Xu, L. Xie, H. Zhang and J. Zhang, *ACS Nano*, 2011, **5**, 5338–5344.
434 L. Zhou, L. Pusey-Nazzaro, G. Ren, L. Chen, L. Liu, W. Zhang, L. Yang, J. Zhou and J. Han, *ACS Nano*, 2022, **16**, 577–587.
435 S. Almohammed, A. Fularz, F. Zhang, D. Alvarez-Ruiz, F. Bello, D. D. O'Regan, B. J. Rodriguez and J. H. Rice, *ACS Appl. Mater. Interfaces*, 2020, **12**, 48874–48881.
436 J. Tan, B. Du, C. Ji, M. Shao, X. Zhao, J. Yu, S. Xu, B. Man, C. Zhang and Z. Li, *ACS Photonics*, 2023, **10**, 2216–2225.
437 C. Li, S. Xu, J. Yu, Z. Li, W. Li, J. Wang, A. Liu, B. Man, S. Yang and C. Zhang, *Nano Energy*, 2021, **81**, 105585.
438 M. Shao, C. Ji, J. Tan, B. Du, X. Zhao, J. Yu, B. Man, K. Xu, C. Zhang and Z. Li, *Opto-Electron. Adv.*, 2023, **6**, 230094.
439 D. B. Chase and B. A. Parkinson, *Appl. Spectrosc.*, 1988, **42**, 1186–1187.
440 T. Dörfer, M. Schmitt and J. Popp, *J. Raman Spectrosc.*, 2007, **38**, 1379–1382.
441 B. Ren, X.-F. Lin, Z.-L. Yang, G.-K. Liu, R. F. Aroca, B.-W. Mao and Z.-Q. Tian, *J. Am. Chem. Soc.*, 2003, **125**, 9598–9599.
442 M. W. Knight, N. S. King, L. Liu, H. O. Everitt, P. Nordlander and N. J. Halas, *ACS Nano*, 2014, **8**, 834–840.
443 B. Sharma, M. F. Cardinal, M. B. Ross, A. B. Zrimsek, S. V. Bykov, D. Punihaole, S. A. Asher, G. C. Schatz and R. P. Van Duyne, *Nano Lett.*, 2016, **16**, 7968–7973.
444 M. J. McClain, A. E. Schlather, E. Ringe, N. S. King, L. Liu, A. Manjavacas, M. W. Knight, I. Kumar, K. H. Whitmire, H. O. Everitt, P. Nordlander and N. J. Halas, *Nano Lett.*, 2015, **15**, 2751–2755.
445 S. Tian, O. Neumann, M. J. McClain, X. Yang, L. Zhou, C. Zhang, P. Nordlander and N. J. Halas, *Nano Lett.*, 2017, **17**, 5071–5077.
446 A. Bayles, C. J. Fabiano, C. Shi, L. Yuan, Y. Yuan, N. Craft, C. R. Jacobson, P. Dhindsa, A. Ogundare, Y. Mendez Camacho, B. Chen, H. Robatjazi, Y. Han, G. F. Strouse, P. Nordlander, H. O. Everitt and N. J. Halas, *Proc. Natl. Acad. Sci. U. S. A.*, 2024, **121**, e2321852121.
447 J.-F. Li, S.-Y. Ding, Z.-L. Yang, M.-L. Bai, J. R. Anema, X. Wang, A. Wang, D.-Y. Wu, B. Ren, S.-M. Hou, T. Wandlowski and Z.-Q. Tian, *J. Am. Chem. Soc.*, 2011, **133**, 15922–15925.
448 Y.-P. Huang, S.-C. Huang, X.-J. Wang, N. Bodappa, C.-Y. Li, H. Yin, H.-S. Su, M. Meng, H. Zhang, B. Ren, Z.-L. Yang, R. Zenobi, Z.-Q. Tian and J.-F. Li, *Angew. Chem., Int. Ed.*, 2018, **57**, 7523–7527.
449 J. S. Suh, D. P. DiLella and M. Moskovits, *J. Phys. Chem.*, 1983, **87**, 1540–1544.
450 P. Hildebrandt and M. Stockburger, *J. Phys. Chem.*, 1984, **88**, 5935–5944.
451 E. J. Kiefl, R. F. Kiefl, D. P. dos Santos and A. G. Brolo, *J. Phys. Chem. C*, 2017, **121**, 25487–25493.
452 X. Wang, S.-C. Huang, S. Hu, S. Yan and B. Ren, *Nat. Rev. Phys.*, 2020, **2**, 253–271.
453 T. L. Vasconcelos, B. S. Archanjo, B. S. Oliveira, R. Valaski, R. C. Cordeiro, H. G. Medeiros, C. Rabelo, A. Ribeiro, P. Ercius, C. A. Achete, A. Jorio and L. G. Cançado, *Adv. Opt. Mater.*, 2018, **6**, 1800528.
454 M. Grzelczak, J. Vermant, E. M. Furst and L. M. Liz-Marzán, *ACS Nano*, 2010, **4**, 3591–3605.
455 Z. Ye, C. Li, Q. Chen, Y. Xu and S. E. J. Bell, *Angew. Chem., Int. Ed.*, 2019, **58**, 19054–19059.
456 M. Moskovits, *Phys. Chem. Chem. Phys.*, 2013, **15**, 5301–5311.
457 E. C. Le Ru and B. Auguié, *ACS Nano*, 2024, **18**, 9773–9783.
458 M. Caldarola, P. Albella, E. Cortés, M. Rahmani, T. Roschuk, G. Grinblat, R. F. Oulton, A. V. Bragas and S. A. Maier, *Nat. Commun.*, 2015, **6**, 7915.
459 C. Zhan, B.-W. Liu, Z.-Q. Tian and B. Ren, *J. Am. Chem. Soc.*, 2020, **142**, 10905–10909.
460 D. J. Masiello and G. C. Schatz, *Phys. Rev. A: At., Mol., Opt. Phys.*, 2008, **78**, 042505.
461 T. Neuman, J. Aizpurua and R. Esteban, *Nanophotonics*, 2020, **9**, 295–308.
462 P. J. G. Goulet and R. F. Aroca, *Anal. Chem.*, 2007, **79**, 2728–2734.
463 Y. Sawai, B. Takimoto, H. Nabika, K. Ajito and K. Murakoshi, *J. Am. Chem. Soc.*, 2007, **129**, 1658–1662.
464 J. E. Pemberton and R. P. Buck, *Anal. Chem.*, 1981, **53**, 2263–2267.
465 C. K. Chen, T. F. Heinz, D. Ricard and Y. R. Shen, *Chem. Phys. Lett.*, 1981, **83**, 455–458.
466 C. K. Chen, T. F. Heinz, D. Ricard and Y. R. Shen, *Phys. Rev. Lett.*, 1981, **46**, 1010–1012.
467 J. J. Laserna, E. L. Torres and J. D. Winefordner, *Anal. Chim. Acta*, 1987, **200**, 469–480.
468 G. McAnally, C. McLaughlin, R. Brown, D. C. Robson, K. Faulds, D. R. Tackley, W. E. Smith and D. Graham, *Analyst*, 2002, **127**, 838–841.
469 C. McLaughlin, D. MacMillan, C. McCardle and W. E. Smith, *Anal. Chem.*, 2002, **74**, 3160–3167.
470 K. Faulds, W. E. Smith, D. Graham and R. J. Lacey, *Analyst*, 2002, **127**, 282–286.
471 K. Faulds, W. E. Smith and D. Graham, *Anal. Chem.*, 2004, **76**, 412–417.
472 R. Goodacre, D. Graham and K. Faulds, *TrAC, Trends Anal. Chem.*, 2018, **102**, 359–368.
473 S. E. J. Bell, G. Charron, E. Cortés, J. Kneipp, M. L. de la Chapelle, J. Langer, M. Procházka, V. Tran and S. Schlücker, *Angew. Chem., Int. Ed.*, 2020, **59**, 5454–5462.
474 S. Sloan-Dennison, G. Q. Wallace, W. A. Hassanain, S. Laing, K. Faulds and D. Graham, *Nano Convergence*, 2024, **11**, 33.
475 S. E. J. Bell and N. M. S. Sirimuthu, *Analyst*, 2004, **129**, 1032–1036.
476 D. Zhang, Y. Xie, S. K. Deb, V. J. Davison and D. Ben-Amotz, *Anal. Chem.*, 2005, **77**, 3563–3569.
477 S. E. J. Bell, J. N. Mackle and N. M. S. Sirimuthu, *Analyst*, 2005, **130**, 545–549.
478 K. W. Kho, U. S. Dinish, A. Kumar and M. Olivo, *ACS Nano*, 2012, **6**, 4892–4902.

479 Y. Zhou, R. Ding, P. Joshi and P. Zhang, *Anal. Chim. Acta*, 2015, **874**, 49–53.
480 R. Keir, E. Igata, M. Arundell, W. E. Smith, D. Graham, C. McHugh and J. M. Cooper, *Anal. Chem.*, 2002, **74**, 1503–1508.
481 J.-H. Jung, J.-B. Choo, D.-J. Kim and S.-H. Lee, *Bull. Korean Chem. Soc.*, 2006, **27**, 277–280.
482 D. Lee, S. Lee, G. H. Seong, J. Choo, E. K. Lee, D.-G. Gweon and S. Lee, *Appl. Spectrosc.*, 2006, **60**, 373–377.
483 K. R. Strehle, D. Cialla, P. Rösch, T. Henkel, M. Köhler and J. Popp, *Anal. Chem.*, 2007, **79**, 1542–1547.
484 I. J. Hidi, M. Jahn, M. W. Pletz, K. Weber, D. Cialla-May and J. Popp, *J. Phys. Chem. C*, 2016, **120**, 20613–20623.
485 I. J. Hidi, M. Jahn, K. Weber, T. Bocklitz, M. W. Pletz, D. Cialla-May and J. Popp, *Anal. Chem.*, 2016, **88**, 9173–9180.
486 J. Krajczewski, K. Kołątaj and A. Kudelski, *Chem. Phys. Lett.*, 2015, **625**, 84–90.
487 E. Giorgetti, P. Marsili, F. Giammanco, S. Trigari, C. Gellini and M. Muniz-Miranda, *J. Raman Spectrosc.*, 2015, **46**, 462–469.
488 S.-Y. Ding, E.-M. You, Z.-Q. Tian and M. Moskovits, *Chem. Soc. Rev.*, 2017, **46**, 4042–4076.
489 H.-L. Wang, E.-M. You, R. Panneerselvam, S.-Y. Ding and Z.-Q. Tian, *Light: Sci. Appl.*, 2021, **10**, 161.
490 J. Kneipp, H. Kneipp and K. Kneipp, *Chem. Soc. Rev.*, 2008, **37**, 1052–1060.
491 S. Lal, N. K. Grady, J. Kundu, C. S. Levin, J. B. Lassiter and N. J. Halas, *Chem. Soc. Rev.*, 2008, **37**, 898–911.
492 M. D. Porter, R. J. Lipert, L. M. Siperko, G. Wang and R. Narayanan, *Chem. Soc. Rev.*, 2008, **37**, 1001–1011.
493 N. J. Halas and M. Moskovits, *MRS Bull.*, 2013, **38**, 607–611.
494 B. Sharma, M. Fernanda Cardinal, S. L. Kleinman, N. G. Greeneltch, R. R. Frontiera, M. G. Blaber, G. C. Schatz and R. P. Van Duyne, *MRS Bull.*, 2013, **38**, 615–624.
495 E. A. Pozzi, G. Goubert, N. Chiang, N. Jiang, C. T. Chapman, M. O. McAnally, A.-I. Henry, T. Seideman, G. C. Schatz, M. C. Hersam and R. P. V. Duyne, *Chem. Rev.*, 2017, **117**, 4961–4982.
496 C. L. Brosseau, A. Colina, J. V. Perales-Rondon, A. J. Wilson, P. B. Joshi, B. Ren and X. Wang, *Nat. Rev. Methods Primers*, 2023, **3**, 79.
497 Y.-J. Zhang, H. Ze, P.-P. Fang, Y.-F. Huang, A. Kudelski, J. Fernández-Vidal, L. J. Hardwick, J. Lipkowski, Z.-Q. Tian and J.-F. Li, *Nat. Rev. Methods Primers*, 2023, **3**, 36.
498 E. Bailo and V. Deckert, *Chem. Soc. Rev.*, 2008, **37**, 921–930.
499 T. Deckert-Gaudig, A. Taguchi, S. Kawata and V. Deckert, *Chem. Soc. Rev.*, 2017, **46**, 4077–4110.
500 R. C. Maher, C. M. Galloway, E. C. Le Ru, L. F. Cohen and P. G. Etchegoin, *Chem. Soc. Rev.*, 2008, **37**, 965–979.
501 L. Troncoso-Afonso, G. A. Vinnacombe-Willson, C. García-Astrain and L. M. Liz-Márzan, *Chem. Soc. Rev.*, 2024, **53**, 5118–5148.
502 in *Surface-Enhanced Raman Scattering: Physics and Applications*, ed. M. M. Katrin Kneipp and H. Kneipp, Springer Berlin, Heidelberg, 2006.
503 in *Tip Enhancement*, ed. V. M. S. Satoshi Kawata, Elsevier Science, 2007.
504 in *Surface Enhanced Raman Spectroscopy: Analytical, Biophysical and Life Science Applications*, ed. S. Schlücker, 2010.
505 in *Frontiers of Surface-Enhanced Raman Scattering: Single Nanoparticles and Single Cells*, ed. K. K. Yukihiro Ozaki and R. Aroca, 2014.
506 M. Prochazka, *Surface-Enhanced Raman Spectroscopy: Biological and Medical Physics, Biomedical Engineering*, Springer, Cham, 2016.
507 Y. O. Katrin Kneipp and Z.-Q. Tian, *Recent Developments in Plasmon-Supported Raman Spectroscopy*, 2018.
508 in *Principles and Clinical Diagnostic Applications of Surface-Enhanced Raman Spectroscopy*, ed. Y. Wang, Elsevier, 2021.
509 in *SERS for Point-of-care and Clinical Applications*, ed. A. Fales, Elsevier, 2022.
510 D. A. Long, *Raman Eff.*, 2002, 19–29, DOI: **10.1002/0470845767.ch2**.
511 J.-H. Zhong, X. Jin, L. Meng, X. Wang, H.-S. Su, Z.-L. Yang, C. T. Williams and B. Ren, *Nat. Nanotechnol.*, 2017, **12**, 132–136.
512 J. Lee, N. Tallarida, X. Chen, P. Liu, L. Jensen and V. A. Apkarian, *ACS Nano*, 2017, **11**, 11466–11474.
513 N. Tallarida, J. Lee and V. A. Apkarian, *ACS Nano*, 2017, **11**, 11393–11401.
514 J. Lee, N. Tallarida, X. Chen, L. Jensen and V. A. Apkarian, *Sci. Adv.*, 2018, **4**, eaat5472.
515 K. T. Crampton, J. Lee and V. A. Apkarian, *ACS Nano*, 2019, **13**, 6363–6371.
516 J. Takahara, S. Yamagishi, H. Taki, A. Morimoto and T. Kobayashi, *Opt. Lett.*, 1997, **22**, 475–477.
517 K. V. Nerkararyan, *Phys. Lett. A*, 1997, **237**, 103–105.
518 A. J. Babadjanyan, N. L. Margaryan and K. V. Nerkararyan, *J. Appl. Phys.*, 2000, **87**, 3785–3788.
519 S. Duan, G. Tian and Y. Luo, *Angew. Chem., Int. Ed.*, 2016, **55**, 1041–1045.
520 S. Duan, Z. Xie, G. Tian and Y. Luo, *J. Phys. Chem. Lett.*, 2020, **11**, 407–411.
521 R. B. Jaculbia, H. Imada, K. Miwa, T. Iwasa, M. Takenaka, B. Yang, E. Kazuma, N. Hayazawa, T. Taketsugu and Y. Kim, *Nat. Nanotechnol.*, 2020, **15**, 105–110.
522 N. Agraït, A. L. Yeyati and J. M. van Ruitenbeek, *Phys. Rep.*, 2003, **377**, 81–279.
523 S. Liu, B. Cirera, Y. Sun, I. Hamada, M. Müller, A. Hammud, M. Wolf and T. Kumagai, *Nano Lett.*, 2020, **20**, 5879–5884.
524 S. Liu, A. Hammud, M. Wolf and T. Kumagai, *Nano Lett.*, 2021, **21**, 4057–4061.
525 B. Cirera, Y. Litman, C. Lin, A. Akkoush, A. Hammud, M. Wolf, M. Rossi and T. Kumagai, *Nano Lett.*, 2022, **22**, 2170–2176.
526 R.-P. Wang, C.-R. Hu, Y. Han, B. Yang, G. Chen, Y. Zhang, Y. Zhang and Z.-C. Dong, *J. Phys. Chem. C*, 2022, **126**, 12121–12128.
527 T. Siday, J. Hayes, F. Schiegl, F. Sandner, P. Menden, V. Bergbauer, M. Zizlsperger, S. Nerreter, S. Lingl,

J. Repp, J. Wilhelm, M. A. Huber, Y. A. Gerasimenko and R. Huber, *Nature*, 2024, **629**, 329–334.
528 Y. Luo, A. Martin-Jimenez, M. Pisarra, F. Martin, M. Garg and K. Kern, *Nat. Commun.*, 2023, **14**, 3484.
529 L. Novotny and S. J. Stranick, *Annu. Rev. Phys. Chem.*, 2006, **57**, 303–331.
530 J. Lee and V. A. Apkarian, *Microsc. Microanal.*, 2023, **29**, 622–623.
531 R. Chen and L. Jensen, *J. Chem. Phys.*, 2020, **152**, 024126.
532 R. Chen and L. Jensen, *J. Chem. Phys.*, 2020, **153**, 224704.
533 R. Chen and L. Jensen, *J. Chem. Phys.*, 2022, **157**, 184705.
534 S. Duan, Z. Rinkevicius, G. Tian and Y. Luo, *J. Am. Chem. Soc.*, 2019, **141**, 13795–13798.
535 S. Duan and X. Xu, *J. Phys. Chem. Lett.*, 2023, **14**, 6726–6735.
536 S. Duan, G. Tian and Y. Luo, *Chem. Soc. Rev.*, 2024, **53**, 5083–5117.
537 J. G. Mehtala, D. Y. Zemlyanov, J. P. Max, N. Kadasala, S. Zhao and A. Wei, *Langmuir*, 2014, **30**, 13727–13730.
538 H. He, P. Li, X. Tang, D. Lin, A. Xie, Y. Shen and L. Yang, *Spectrochim. Acta, Part A*, 2019, **212**, 293–299.
539 M. U. Amin, R. Zhang, L. Li, H. You and J. Fang, *Anal. Chem.*, 2021, **93**, 7657–7664.
540 M.-D. Li, Y. Cui, M.-X. Gao, J. Luo, B. Ren and Z.-Q. Tian, *Anal. Chem.*, 2008, **80**, 5118–5125.
541 J.-Y. Huang, C. Zong, L.-J. Xu, Y. Cui and B. Ren, *Chem. Commun.*, 2011, **47**, 5738–5740.
542 S.-Q. Pan, P. Luo, J. Chen, T. Wu, B. Xu, F. Chen, D.-Y. Wu, B. Ren, G.-K. Liu, J. Xie, P. Xu and Z.-Q. Tian, *Anal. Chem.*, 2023, **95**, 13346–13352.
543 P.-S. Wang, H. Ma, X.-H. Xi, X. Yue, S.-Q. Pan, M. Cao, G.-K. Liu, X. Wang and B. Ren, *J. Raman Spectrosc.*, 2023, **54**, 573–579.
544 D. Malyshev, R. Öberg, T. Dahlberg, K. Wiklund, L. Landström, P. O. Andersson and M. Andersson, *Spectrochim. Acta, Part A*, 2022, **265**, 120381.
545 A. I. Pérez-Jiménez, D. Lyu, Z. Lu, G. Liu and B. Ren, *Chem. Sci.*, 2020, **11**, 4563–4577.
546 S. R. Smith and J. Lipkowski, *J. Phys. Chem. C*, 2018, **122**, 7303–7311.
547 Z.-M. Zhou, H. Zheng, T. Liu, Z.-Z. Xie, S.-H. Luo, G.-Y. Chen, Z.-Q. Tian and G.-K. Liu, *Anal. Chem.*, 2021, **93**, 8603–8612.
548 L. He, Y. Liu, J. Liu, Y. Xiong, J. Zheng, Y. Liu and Z. Tang, *Angew. Chem., Int. Ed.*, 2013, **52**, 3741–3745.
549 X. Qiao, B. Su, C. Liu, Q. Song, D. Luo, G. Mo and T. Wang, *Adv. Mater.*, 2018, **30**, 1702275.
550 J. W. M. Osterrieth, D. Wright, H. Noh, C.-W. Kung, D. Vulpe, A. Li, J. E. Park, R. P. Van Duyne, P. Z. Moghadam, J. J. Baumberg, O. K. Farha and D. Fairen-Jimenez, *J. Am. Chem. Soc.*, 2019, **141**, 3893–3900.
551 Q.-Q. Chen, R.-N. Hou, Y.-Z. Zhu, X.-T. Wang, H. Zhang, Y.-J. Zhang, L. Zhang, Z.-Q. Tian and J.-F. Li, *Anal. Chem.*, 2021, **93**, 7188–7195.
552 J. Mosquera, Y. Zhao, H.-J. Jang, N. Xie, C. Xu, N. A. Kotov and L. M. Liz-Marzán, *Adv. Funct. Mater.*, 2020, **30**, 1902082.
553 S. Kasera, F. Biedermann, J. J. Baumberg, O. A. Scherman and S. Mahajan, *Nano Lett.*, 2012, **12**, 5924–5928.
554 D.-W. Li, L.-L. Qu, K. Hu, Y.-T. Long and H. Tian, *Angew. Chem., Int. Ed.*, 2015, **54**, 12758–12761.
555 L. Guerrini, E. Pazos, C. Penas, M. E. Vázquez, J. L. Mascareñas and R. A. Alvarez-Puebla, *J. Am. Chem. Soc.*, 2013, **135**, 10314–10317.
556 J. Liu, Z. Liu, W. Wang and Y. Tian, *Angew. Chem., Int. Ed.*, 2021, **60**, 21351–21359.
557 W. Zhu, E.-L. Cai, H.-Z. Li, P. Wang, A.-G. Shen, J. Popp and J.-M. Hu, *Angew. Chem., Int. Ed.*, 2021, **60**, 21846–21852.
558 Y. Zeng, J.-Q. Ren, A.-G. Shen and J.-M. Hu, *J. Am. Chem. Soc.*, 2018, **140**, 10649–10652.
559 E.-M. You, H.-L. Wang, J.-R. Zheng, Z.-D. Meng, M.-X. Zhang, S.-Y. Ding and Z.-Q. Tian, *J. Raman Spectrosc.*, 2021, **52**, 446–457.
560 S. A. Meyer, E. C. Le Ru and P. G. Etchegoin, *Anal. Chem.*, 2011, **83**, 2337–2344.
561 S. A. Meyer, B. Auguié, E. C. Le Ru and P. G. Etchegoin, *J. Phys. Chem. A*, 2012, **116**, 1000–1007.
562 C.-Y. Li, S. Duan, J. Yi, C. Wang, P. M. Radjenovic, Z.-Q. Tian and J.-F. Li, *Sci. Adv.*, 2020, **6**, eaba6012.
563 C.-Y. Li, J.-B. Le, Y.-H. Wang, S. Chen, Z.-L. Yang, J.-F. Li, J. Cheng and Z.-Q. Tian, *Nat. Mater.*, 2019, **18**, 697–701.
564 J.-C. Dong, X.-G. Zhang, V. Briega-Martos, X. Jin, J. Yang, S. Chen, Z.-L. Yang, D.-Y. Wu, J. M. Feliu, C. T. Williams, Z.-Q. Tian and J.-F. Li, *Nat. Energy*, 2019, **4**, 60–67.
565 Y.-H. Wang, S. Zheng, W.-M. Yang, R.-Y. Zhou, Q.-F. He, P. Radjenovic, J.-C. Dong, S. Li, J. Zheng, Z.-L. Yang, G. Attard, F. Pan, Z.-Q. Tian and J.-F. Li, *Nature*, 2021, **600**, 81–85.
566 X.-M. Lin, X.-T. Wang, Y.-L. Deng, X. Chen, H.-N. Chen, P. M. Radjenovic, X.-G. Zhang, Y.-H. Wang, J.-C. Dong, Z.-Q. Tian and J.-F. Li, *Nano Lett.*, 2022, **22**, 5544–5552.
567 H. Ze, Z.-L. Yang, M.-L. Li, X.-G. Zhang, Y.-L. A, Q.-N. Zheng, Y.-H. Wang, J.-H. Tian, Y.-J. Zhang and J.-F. Li, *J. Am. Chem. Soc.*, 2024, **146**, 12538–12546.
568 Y. Gu, E.-M. You, J.-D. Lin, J.-H. Wang, S.-H. Luo, R.-Y. Zhou, C.-J. Zhang, J.-L. Yao, H.-Y. Li, G. Li, W.-W. Wang, Y. Qiao, J.-W. Yan, D.-Y. Wu, G.-K. Liu, L. Zhang, J.-F. Li, R. Xu, Z.-Q. Tian, Y. Cui and B.-W. Mao, *Nat. Commun.*, 2023, **14**, 3536.
569 H. Ze, X. Chen, X.-T. Wang, Y.-H. Wang, Q.-Q. Chen, J.-S. Lin, Y.-J. Zhang, X.-G. Zhang, Z.-Q. Tian and J.-F. Li, *J. Am. Chem. Soc.*, 2021, **143**, 1318–1322.
570 K. Xu, *J. Power Sources*, 2023, **559**, 232652.
571 Y. Gu, W.-W. Wang, Y.-J. Li, Q.-H. Wu, S. Tang, J.-W. Yan, M.-S. Zheng, D.-Y. Wu, C.-H. Fan, W.-Q. Hu, Z.-B. Chen, Y. Fang, Q.-H. Zhang, Q.-F. Dong and B.-W. Mao, *Nat. Commun.*, 2018, **9**, 1339.
572 Y. Gu, S. Tang, J. Yi, S.-H. Luo, C.-Y. Li, G. Liu, J. Yan, J.-F. Li, B.-W. Mao and Z.-Q. Tian, *J. Phys. Chem. C*, 2023, **127**, 13466–13477.
573 E.-M. You, Y. Gu, J. Yi, D.-Y. Wu, J.-F. Li and Z.-Q. Tian, *Electrochim. Acta*, 2024, **498**, 144689.

574 S. Duan, X. Xu, Y. Luo and Z.-Q. Tian, *Chem. Commun.*, 2011, **47**, 11438–11440.
575 B. Yang, G. Chen, A. Ghafoor, Y.-F. Zhang, X.-B. Zhang, H. Li, X.-R. Dong, R.-P. Wang, Y. Zhang, Y. Zhang and Z.-C. Dong, *Angew. Chem., Int. Ed.*, 2023, **62**, e202218799.
576 Y. Zhang and H. Noji, *Anal. Chem.*, 2017, **89**, 92–101.
577 X. Bi, D. M. Czajkowsky, Z. Shao and J. Ye, *Nature*, 2024, **628**, 771–775.
578 C. D. L. de Albuquerque, R. G. Sobral-Filho, R. J. Poppi and A. G. Brolo, *Anal. Chem.*, 2018, **90**, 1248–1254.
579 J. Li, A. A. I. Sina, F. Antaw, D. Fielding, A. Möller, R. Lobb, A. Wuethrich and M. Trau, *Adv. Sci.*, 2023, **10**, 2204207.
580 H. Zhang, L. Yang, M. Zhang, H. Wei, L. Tong, H. Xu and Z. Li, *Nano Lett.*, 2024, **24**, 11116–11123.
581 A. Tuckmantel Bido and A. G. Brolo, *ACS Appl. Nano Mater.*, 2023, **6**, 15426–15436.
582 H. C. Schorr and Z. D. Schultz, *Analyst*, 2024, **149**, 3711–3715.
583 N. Choi, Y. Zhang, Y. Wang and S. Schlücker, *Chem. Soc. Rev.*, 2024, **53**, 6675–6693.
584 D. Cialla-May, A. Bonifacio, T. Bocklitz, A. Markin, N. Markina, S. Fornasaro, A. Dwivedi, T. Dib, E. Farnesi, C. Liu, A. Ghosh and J. Popp, *Chem. Soc. Rev.*, 2024, **53**, 8957–8979.
585 J. Kneipp, S. Seifert and F. Gärber, *Chem. Soc. Rev.*, 2024, **53**, 7641–7656.
586 S. Lee, H. Dang, J.-I. Moon, K. Kim, Y. Joung, S. Park, Q. Yu, J. Chen, M. Lu, L. Chen, S.-W. Joo and J. Choo, *Chem. Soc. Rev.*, 2024, **53**, 5394–5427.
587 R. Beeram, K. R. Vepa and V. R. Soma, *Biosensors*, 2023, **13**, 328.
588 S. Lee, L. Bi, H. Chen, D. Lin, R. Mei, Y. Wu, L. Chen,
S.-W. Joo and J. Choo, *Chem. Soc. Rev.*, 2023, **52**, 8500–8530.
589 J. H. Granger, N. E. Schlotter, A. C. Crawford and M. D. Porter, *Chem. Soc. Rev.*, 2016, **45**, 3865–3882.
590 S. S. Panikar, D. Cialla-May, E. De la Rosa, P. Salas and J. Popp, *TrAC, Trends Anal. Chem.*, 2021, **134**, 116122.
591 A. Barhoumi, D. Zhang, F. Tam and N. J. Halas, *J. Am. Chem. Soc.*, 2008, **130**, 5523–5529.
592 S. E. J. Bell and N. M. S. Sirimuthu, *J. Am. Chem. Soc.*, 2006, **128**, 15580–15581.
593 L.-J. Xu, Z.-C. Lei, J. Li, C. Zong, C. J. Yang and B. Ren, *J. Am. Chem. Soc.*, 2015, **137**, 5149–5154.
594 K. E. Shafer-Peltier, C. L. Haynes, M. R. Glucksberg and R. P. Van Duyne, *J. Am. Chem. Soc.*, 2003, **125**, 588–593.
595 D. A. Stuart, J. M. Yuen, N. Shah, O. Lyandres, C. R. Yonzon, M. R. Glucksberg, J. T. Walsh and R. P. Van Duyne, *Anal. Chem.*, 2006, **78**, 7211–7215.
596 J. M. Yuen, N. C. Shah, J. T. Walsh, Jr., M. R. Glucksberg and R. P. Van Duyne, *Anal. Chem.*, 2010, **82**, 8382–8385.
597 C. R. Yonzon, C. L. Haynes, X. Zhang, J. T. Walsh and R. P. Van Duyne, *Anal. Chem.*, 2004, **76**, 78–85.
598 K. Ma, J. M. Yuen, N. C. Shah, J. T. Walsh, Jr., M. R. Glucksberg and R. P. Van Duyne, *Anal. Chem.*, 2011, **83**, 9146–9152.
599 X. X. Han, G. G. Huang, B. Zhao and Y. Ozaki, *Anal. Chem.*, 2009, **81**, 3329–3333.
600 G. G. Huang, X. X. Han, M. K. Hossain and Y. Ozaki, *Anal. Chem.*, 2009, **81**, 5881–5888.
601 X. X. Han, H. Y. Jia, Y. F. Wang, Z. C. Lu, C. X. Wang, W. Q. Xu, B. Zhao and Y. Ozaki, *Anal. Chem.*, 2008, **80**, 2799–2804.
602 L.-J. Xu, C. Zong, X.-S. Zheng, P. Hu, J.-M. Feng and B. Ren, *Anal. Chem.*, 2014, **86**, 2238–2245.
603 P.-S. Wang, H. Ma, S. Yan, X. Lu, H. Tang, X.-H. Xi, X.-H. Peng, Y. Huang, Y.-F. Bao, M.-F. Cao, H. Wang, J. Huang, G. Liu, X. Wang and B. Ren, *Chem. Sci.*, 2022, **13**, 13829–13835.
604 A. Barhoumi and N. J. Halas, *J. Am. Chem. Soc.*, 2010, **132**, 12792–12793.
605 J. L. Abell, J. M. Garren, J. D. Driskell, R. A. Tripp and Y. Zhao, *J. Am. Chem. Soc.*, 2012, **134**, 12889–12892.
606 L. Guerrini, Ž. Krpetić, D. van Lierop, R. A. Alvarez-Puebla and D. Graham, *Angew. Chem., Int. Ed.*, 2015, **54**, 1144–1148.
607 E. Garcia-Rico, R. A. Alvarez-Puebla and L. Guerrini, *Chem. Soc. Rev.*, 2018, **47**, 4909–4923.
608 A. Walter, A. März, W. Schumacher, P. Rösch and J. Popp, *Lab Chip*, 2011, **11**, 1013–1021.
609 I. S. Patel, W. R. Premasiri, D. T. Moir and L. D. Ziegler, *J. Raman Spectrosc.*, 2008, **39**, 1660–1672.
610 W. R. Premasiri, J. C. Lee, A. Sauer-Budge, R. Théberge, C. E. Costello and L. D. Ziegler, *Anal. Bioanal. Chem.*, 2016, **408**, 4631–4647.
611 P. Lemler, W. R. Premasiri, A. DelMonaco and L. D. Ziegler, *Anal. Bioanal. Chem.*, 2014, **406**, 193–200.
612 F. Lussier, T. Brulé, M. Vishwakarma, T. Das, J. P. Spatz and J.-F. Masson, *Nano Lett.*, 2016, **16**, 3866–3871.
613 A. Albanese, C. D. Walkey, J. B. Olsen, H. Guo, A. Emili and W. C. W. Chan, *ACS Nano*, 2014, **8**, 5515–5526.
614 W. R. Premasiri, J. C. Lee and L. D. Ziegler, *J. Phys. Chem. B*, 2012, **116**, 9376–9386.
615 X. Bi, J. Wang, B. Xue, C. He, F. Liu, H. Chen, L. L. Lin, B. Dong, B. Li, C. Jin, J. Pan, W. Xue and J. Ye, *Cell Rep. Med.*, 2024, **5**, 101579.
616 H. Ma, S. Yan, X. Lu, Y.-F. Bao, J. Liu, L. Liao, K. Dai, M. Cao, X. Zhao, H. Yan, H.-L. Wang, X. Peng, N. Chen, H. Feng, L. Zhu, G. Yao, C. Fan, D.-Y. Wu, B. Wang, X. Wang and B. Ren, *Sci. Adv.*, 2023, **9**, eadh8362.
617 J. Plou, I. García, M. Charconnet, I. Astobiza, C. García-Astrain, C. Matricardi, A. Mihi, A. Carracedo and L. M. Liz-Marzán, *Adv. Funct. Mater.*, 2020, **30**, 1910335.
618 P. S. Valera, J. Plou, I. García, I. Astobiza, C. Viera, A. M. Aransay, J. E. Martin, I. R. Sasselli, A. Carracedo and L. M. Liz-Marzán, *Proc. Natl. Acad. Sci. U. S. A.*, 2023, **120**, e2311674120.
619 J. Plou, B. Molina-Martínez, C. García-Astrain, J. Langer, I. García, A. Ercilla, G. Perumal, A. Carracedo and L. M. Liz-Marzán, *Nano Lett.*, 2021, **21**, 8785–8793.
620 J.-H. Lee, G.-H. Kim and J.-M. Nam, *J. Am. Chem. Soc.*, 2012, **134**, 5456–5459.

621 J.-H. Lee, M.-H. You, G.-H. Kim and J.-M. Nam, *Nano Lett.*, 2014, **14**, 6217–6225.
622 J.-M. Kim, J. Kim, K. Choi and J.-M. Nam, *Adv. Mater.*, 2023, **35**, 2208250.
623 J. Kim, J.-M. Kim, K. Choi, J.-E. Park and J.-M. Nam, *J. Am. Chem. Soc.*, 2024, **146**, 14012–14021.
624 Y. Zhang, D. Jimenez de Aberasturi, M. Henriksen-Lacey, J. Langer and L. M. Liz-Marzán, *ACS Sens.*, 2020, **5**, 3194–3206.
625 T. E. Rohr, T. Cotton, N. Fan and P. J. Tarcha, *Anal. Biochem.*, 1989, **182**, 388–398.
626 D. S. Grubisha, R. J. Lipert, H.-Y. Park, J. Driskell and M. D. Porter, *Anal. Chem.*, 2003, **75**, 5936–5943.
627 Z. Wang, S. Zong, L. Wu, D. Zhu and Y. Cui, *Chem. Rev.*, 2017, **117**, 7910–7963.
628 T. Park, S. Lee, G. H. Seong, J. Choo, E. K. Lee, Y. S. Kim, W. H. Ji, S. Y. Hwang, D.-G. Gweon and S. Lee, *Lab Chip*, 2005, **5**, 437–442.
629 W. E. Doering, M. E. Piotti, M. J. Natan and R. G. Freeman, *Adv. Mater.*, 2007, **19**, 3100–3108.
630 M. Y. Sha, H. Xu, M. J. Natan and R. Cromer, *J. Am. Chem. Soc.*, 2008, **130**, 17214–17215.
631 P. Dey, *ACS Measure. Sci. Au*, 2023, **3**, 434–443.
632 J. Hwang, S. Lee and J. Choo, *Nanoscale*, 2016, **8**, 11418–11425.
633 S. X. Leong, Y. X. Leong, E. X. Tan, H. Y. F. Sim, C. S. L. Koh, Y. H. Lee, C. Chong, L. S. Ng, J. R. T. Chen, D. W. C. Pang, L. B. T. Nguyen, S. K. Boong, X. Han, Y.-C. Kao, Y. H. Chua, G. C. Phan-Quang, I. Y. Phang, H. K. Lee, M. Y. Abdad, N. S. Tan and X. Y. Ling, *ACS Nano*, 2022, **16**, 2629–2639.
634 J. Prakash, S. Sun, H. C. Swart and R. K. Gupta, *Appl. Mater. Today*, 2018, **11**, 82–135.
635 C. Zhan, X.-J. Chen, Y.-F. Huang, D.-Y. Wu and Z.-Q. Tian, *Acc. Chem. Res.*, 2019, **52**, 2784–2792.
636 L. Cui, D. Zhang, K. Yang, X. Zhang and Y.-G. Zhu, *Anal. Chem.*, 2019, **91**, 15345–15354.
637 M. Vezvaie, C. L. Brosseau and J. Lipkowski, *Electrochim. Acta*, 2013, **110**, 120–132.
638 N. Choi and S. Schlücker, *ACS Nano*, 2024, **18**, 5998–6007.
639 S. Pang, T. Yang and L. He, *TrAC, Trends Anal. Chem.*, 2016, **85**, 73–82.
640 M.-L. Xu, Y. Gao, X. X. Han and B. Zhao, *J. Agric. Food Chem.*, 2017, **65**, 6719–6726.
641 B. Yu, M. Ge, P. Li, Q. Xie and L. Yang, *Talanta*, 2019, **191**, 1–10.
642 M. Fan, G. F. S. Andrade and A. G. Brolo, *Anal. Chim. Acta*, 2020, **1097**, 1–29.
643 A. Hakonen, P. O. Andersson, M. Stenbæk Schmidt, T. Rindzevicius and M. Käll, *Anal. Chim. Acta*, 2015, **893**, 1–13.
644 M. Veneranda, *Appl. Spectrosc. Rev.*, 2023, **59**, 883–907.
645 F. Pozzi and M. Leona, *J. Raman Spectrosc.*, 2016, **47**, 67–77.
646 J. Yi, E.-M. You, G.-K. Liu and Z.-Q. Tian, *Nat. Nanotechnol.*, 2024, **19**, 1748–1762.